Forested Watersheds and Water Supply: Exploring Effects of Wildfires, Silviculture, and Climate Change on Downstream Waters

by

Tyler Barbee Hampton

A thesis

presented to the University of Waterloo

in fulfillment of the

thesis requirement for the degree of

Doctor of Philosophy

in

Earth Sciences - Water

Waterloo, Ontario, Canada, 2023

Examining Committee Membership

The following served on the Examining Committee for this thesis. The decision of the Examining Committee is by majority vote.

External Examiner

Christina Tague

Professor

Bren School of Environmental Science and Management, University of California Santa Barbara

Supervisor

Nandita Basu

Professor

Department of Earth and Environmental Sciences, University of Waterloo

Internal Members

Philippe Van Cappellen

Professor

Department of Earth and Environmental Sciences, University of Waterloo

Andrea Brookfield

Professor

Department of Earth and Environmental Sciences, University of Waterloo

Internal-external Members

Monica Emelko

Professor

Department of Civil and Environmental Engineering, University of Waterloo

Mike Stone

Professor

Department of Geography and Environmental Management, University of Waterloo

Author's Declaration

This thesis consists of material all of which I authored or co-authored. See the Statement of Contributions included in this thesis. This is a true copy of the thesis, including any required final revisions, as accepted by my examiners.

I understand that my thesis may be made electronically available to the public.

Statement of Contributions

Chapter 2 of this thesis consists of a published paper (Hampton & Basu, 2022) co-authored by Dr. Nandita Basu. I lead the analysis and summary of results, with input by Dr. Basu. I wrote the first draft and contributed to most of the manuscript editing and revisions with input by Dr. Basu. I thank Dr. Joslin Goh of the University of Waterloo for assisting with statistical methodology in Chapter 2.

Chapter 3 of this thesis consists of a published paper (Hampton, Lin & Basu, 2022) co-authored by Simon G.M. Lin and Dr. Basu. I lead analysis and summary of results, with input by Dr. Basu. I wrote the first draft and contributed to most of the manuscript editing and revisions with input by Dr. Basu. All co-authors contributed to revising the paper. I thank Simon G.M. Lin and Puvaanah Arrumugam of the University of Waterloo for contributions to data collection and quality-control.

Chapter 4 of this thesis consists of an unpublished paper for which I am the lead author with co-authors Dr. Basu, Dr. Ashley Rust, Dr. Sam Saxe, and Dr. Terri Hogue. Drs. Rust and Saxe contributed the initial data, and I conducted initial analysis. Feedback on results came from all co-authors, and I subsequently wrote the first draft. Dr. Basu contributed to manuscript edits.

Chapter 5 of this thesis will be converted into a manuscript. I was primarily responsible for study design, data synthesis and drafting. Dr. Basu contributed to the model design and analysis and provided feedback during this study. I thank Dr. Jason Leach and Dr. Kara Webster of Natural Resources Canada for providing the measurement data for this study. I thank Simon G.M. Lin and Dr. Ming Han for discussions that contributed to the model in Chapter 5. Dr. Ming Han contributed code and measurements for components of the Robin/3PG model.

Abstract

Drinking water supplies for much of society originate in forests. To preserve the capability of these forests to produce clean and easily treatable water, source water supply and protection strategies focus in particular on potential disturbances to the landscape, which include prescribed forest harvesting and wildfires of varying intensity. While decades of work have revealed relationships between forest harvesting and stream flow response, there is a considerable lack of synthesis disentangling the interactions of climate, wildfires, stream flow, and water quality. Revealing the mechanisms for impacts on downstream waters after disturbances of harvesting and wildfire will greatly improve land and water management. In this dissertation, I combined synthesis of previously published or available data, novel mathematical analyses, and deterministic modeling to disentangle various disturbance effects and further our understanding of processes in forested watersheds. I broadly sought to explore how streamflow and water quality change after forest disturbances, and how new methods and analyses can provide insight into the biogeochemical and ecohydrologic processes changing during disturbances.

First, I examined the effect of wildfire on hydrology, and developed a novel Budyko decomposition method to separate climatic and disturbance effects on streamflow. Using a set of 17 watersheds in southern California, I showed that while traditional metrics like changes in flow or runoff ratio might not detect a disturbance effect from wildfire due to confounding climate signals, the Budyko framework can be used successfully for statistical change detection. The method was used to estimate hydrologic recovery timescales that varied between 5 and 45 years, with an increase of about 4 years of recovery time per 10% of the watershed burned.

Next, in Chapter 3 I used a meta-analysis approach to examine the effect of wildfire on water quality, using data from 121 catchments around the world. Analyzing the changes in concentrations of stream water nutrients, including carbon, nitrogen, and phosphorus, I showed that concentrations generally increased after fire. While a large amount of variability existed in the data, we found concurrent increases in the constituents after fire highlighting tight coupling of the biogeochemical cycles. Most interestingly, we found fire to increase the concentrations of biologically active nutrients like nitrate and phosphate at a greater rate than total nitrogen and phosphorus, with median increases of 40-60% in the nitrate to TN, and SRP to TP ratios.

Next, I conducted an analysis of both water quality and hydrology together after fire in Chapter 4, using a set of 29 wildfire-impacted watersheds in the United States. Concentration-discharge relationships can be used to reveal pathways and sources of elements exported from watersheds, and my overall hypothesis was that these relationships change in post-fire landscapes. I developed a new methodology, using k-means clustering, to classify watersheds as chemostatic, dilution, mobilization and chemodynamic, and explored how their position within the cluster changed in post-fire landscapes. I found that the behavior of nitrate and ammonium was increasingly chemostatic after fire, while behavior of total nitrogen, phosphorus, and organic phosphorus was increasingly mobilizing after fire.

Finally, I developed a coupled hydrology-vegetation-biogeochemistry model to simulate and elucidate processes controlling the impact of harvesting on downstream waters. I focused on the Turkey Lakes watershed where a significant amount of data has been collected on vegetation and soil

nutrient dynamics, in addition to traditional streamflow and water quality metrics, and developed a novel multi-part calibration process that used measured data on stream, forest, and soil characteristics and dynamics. Future work would involve using the model to explore the data driven relationships that have been developed in the earlier chapters of the paper.

The work presented in this dissertation highlights new small and large-scale relationships between disturbances in forested watersheds and effects on downstream waters. With more threats predicted to escalate and overlap in the coming years, the novel results and methodologies that I have presented here should contribute to improving land and water management.

Acknowledgements

This work was supported with funding from the University of Waterloo, the Natural Sciences and Engineering Research Council of Canada (NSERC), the NSERC Network for Forested Drinking Water Source Protection Technologies (*for*Water), the Ontario Trillium Scholarship, and the Vanier Canada Graduate Scholarship.

I am very grateful for the mentorship and guidance of Dr. Nandita Basu during my doctoral studies. It has been a great joy to embark on this research journey together, as we explored topics new to both of us. Her kind and motivating words helped push me over many hurdles. She has helped me grow as a researcher, and I am very proud of what we have accomplished together.

The entire Basu Lab was so supportive of me, and I feel privileged to have studied and grown alongside them. I especially want to thank my longtime colleagues Danyka, Fred, Lamisa, Meghan, and Garima. I also thank the undergraduate co-op students I supervised: Simon, Abigail, and Puvaanah, who contributed to this work. I thank you all for all of our time learning, struggling, and laughing together.

Moving to a new country and building new connections is stressful, and so I am grateful to the many peers and colleagues I was fortunate to make in the Students of the Water Institute Graduate Section and the Graduate Student Association. I thank the faculty and staff in the Department of Earth and Environmental Sciences, and the Office of Graduate Studies and Postdoctoral Affairs for their help and support, especially in navigating a PhD wrenched into the isolation of the COVID pandemic.

Finally, I am grateful to my family, especially my partner Charlie, who has been so supportive as I neared the end of this PhD; and my mother, who lit the spark that started me on this journey in science. I am truly blessed by the love and support of my family, who through visits or just reminders of their love, keep me moving on this journey.

Table of Contents

List of Figures

List of Tables

Chapter 1
Introduction

Ours is a planet of water. Every speck of the planet is shaped by the water that falls from the sky and flows, or by the lack of that water. Processes that have shaped the planet for billions of years are now inextricably influenced by human activity (Abbott et al., 2019; Vörösmarty & Sahagian, 2000). Despite the utter dependence of every living being and human society in all forms on access to water, there are troubling uncertainties pertaining to the fate of water in the Anthropocene (Rockström et al., 2014; Steffen et al., 2015). All water is not the same, and in addition to threats posed by availability (too much water or too little, water too soon or too late), high quality water sources are essential for human society. Much of the world, and about a third of major global cities (Dudley & Stolton, 2003), rely on clean and readily treatable water conveyed from forested areas (T. C. Brown et al., 2008; Davies & Mazumder, 2003; Ernst et al., 2004).

There are myriad anthropogenic pressures threatening source water quality from forested watersheds (Emelko et al., 2011) including global climate change (Creed & van Noordwijk, 2018; Jones et al., 2018), invasive pests (Dhar et al., 2016; Ramsfield et al., 2016), wildfires (Kinoshita et al., 2016; D. A. Martin, 2016; Robinne et al., 2021), and harvesting pressures (Coble et al., 2020; McHale et al., 2008; Melo et al., 2021; Neary et al., 2009). Degraded source water quality increases infrastructure demands and costs of treatment to produce safe drinking water (Delpla et al., 2009; Emelko et al., 2011; Hohner et al., 2016; Writer et al., 2014). These threats to water security have prompted significant investment by municipalities, governments, and the private sector into land management strategies to protect forested areas and source water supplies (Charnley et al., 2017; Emelko et al., 2011; Kinoshita et al., 2016; Medema et al., 2003; Venable et al., 2017). Indeed, the World Health Organization (WHO, 1993) stresses that source water protection strategies should be preferred to treating an already degraded supply. For water and land managers, a key question has been: what are the risks of the aforementioned disturbances for forests and water resources, and how can forest management strategies reduce water treatment expenses and risk to human health?

Among many aspects of water quality, this dissertation will focus on the water quality regimes of nutrients, including carbon (C), nitrogen (N), and phosphorus (P). These three elements and a variety of elemental forms and compounds are of interest for study because of their biological importance, numerous biogeochemical pathways in terrestrial and aquatic environments, and their relevance in

drinking water treatment. Streams draining predominantly forested landscapes rarely have concentrations of C, N, or P that exceed drinking water guidelines (Binkley & Brown, 1993a), however a major problem can arise if these nutrients accumulate in drinking water reservoirs such as those used by many major cities. Even in relatively pristine systems, N and P together can promote algal blooms in reservoirs, producing additional organic matter that requires a greater level of chemical water treatment (H. Bernhardt, 1984), or producing toxins such as microcystin that can contaminate drinking water (Chorus & Welker, 2021; Falconer & Humpage, 2005; Tarczyńska et al., 2001). Organic matter in the treated water, including carbon- and nitrogen-containing dissolved compounds, can sequester residual chlorine that is added to neutralize any pathogens present in water (Crittenden et al., 2012), or can react with chlorine to form potentially harmful disinfection byproducts (DBPs) (Lee et al., 2007; Stevens et al., 1990). These concerns are warranted, as numerous studies have documented increased concentrations in streams draining harvested (Boggs et al., 2016; McBroom et al., 2008; Mupepele & Dormann, 2017; Muwamba et al., 2019; Wynn et al., 2000) and burned watersheds (Rust et al., 2018; Smith et al., 2011). Furthermore, studies have documented higher susceptibility to the formation of DBPs due to the altered nature of carbon from burnt landscapes (Hohner et al., 2016; Writer et al., 2014), and numerous examples from the last decade show increased costs to continue providing clean water in communities impacted by wildfires (Hohner et al., 2016; Sham et al., 2013; Thurton, 2017). A major challenge to managers faced with these multiple potential threats to water security is the inability to predict the magnitude, duration, and character of altered catchment behavior and water degradation following these disturbances. New synthesis is needed to characterize the breadth and variability in post-disturbance catchment behavior.

A major characteristic of environmental behavior, including that of streams and rivers, is change and variability. Variability manifests across years, seasons, days, and hours. In considering the value of environmental data, Emelko et al. (2011) stress that challenges for drinking water treatment often occur during periods of extremes—for example, during storms or the spring freshet, when changes can occur rapidly, and when flows and characteristic measurements like turbidity can spike. The authors also stress that indicators of water "treatability" will be best derived from data contextualizing extreme values. Another aspect of variability in environmental data is spatial variability. Despite many studies summarizing the potential impacts of forest harvesting (Binkley & Brown, 1993a, 1993b; Mupepele & Dormann, 2017; Richardson & Béraud, 2014) and wildfire (Bitner et al., 2001; Rust et al., 2018; Smith et al., 2011) on water quality, there are comparatively fewer synthesis studies

taking temporal water quality variability into account. (Evaristo & McDonnell, 2017) offer meta-analysis as an important tool to synthesize large amounts of data. Such a synthesis could help reveal the "most common" effect after disturbances, but would also characterize the variability in responses and the full range of potentialities. With the goal of characterizing the effects of disturbances on downstream waters, I will focus in this dissertation on how variability can be characterized, and how variability can be parsed to reveal the size and duration of effects from forest disturbances.

In this introductory chapter, I will provide a brief review of the literature (Section 1.1), followed by a summary of gaps in knowledge that this dissertation will seek to address (Section 1.2), and finally specific research objectives and research questions (Section 1.3) that will be addressed in the following chapters.

1.1 Background on the Connection between Forests, Disturbance and Water Quality

The questions of how, where, and when water moves through forested landscapes; and the transport, modification, and removal of elements and compounds along its travels; have been subject to many decades of devoted research (M. G. Anderson & Burt, 1978; Bormann & Likens, 1979; Evaristo et al., 2015; Hinton et al., 1998; Jencso et al., 2009; Likens et al., 1977). Very early in the development of the field of hillslope hydrology and catchment ecohydrology, forest disturbances were included in experiments to measure the effect of these perturbations on streamflows and water quality (Bormann et al., 1968; Helvey, 1980; Hewlett & Hibbert, 1961; Hibbert, 1965; Kusaka et al., 1983). These studies generally focused on small headwater streams, since such localized disturbances might be expected to have an immeasurable effect on a much larger encompassing basin. Now, many decades of streamflow and water quality data—distributed across a vast spatial scale—are available via the internet and open-data government portals, and with these data researchers have documented the effects of widespread landscape disturbances such as forest conversion to urban areas and agriculture, and of anthropogenic climate change (Abbott, Moatar, et al., 2018; Baron et al., 2013; Booij et al., 2019; Falcone et al., 2018; Hallema, Sun, et al., 2018; Jones et al., 2012; Lins & Slack, 1999; Shoda et al., 2019; D. Wang & Hejazi, 2011). The fields of ecohydrology (Guswa et al., 2020; Hannah et al., 2007; Rodriguez-Iturbe, 2000; Yin et al., 2019) and biogeochemistry (Levia et al., 2011; Lohse et al., 2009; McGuire & Likens, 2011) have continued to grow in influence, recognizing the complicated interactions of biological, physical, and chemical processes occurring across the landscape.

These interactions drive how forest disturbances such as wildfire and harvesting impact water quantity and quality in downstream rivers and lakes (Hewlett & Hibbert, 1961, 1967; Hoover & Hursh, 1943; Likens et al., 1970; Likens & Bormann, 1974). Landscape modifications like deforestation and harvesting can dramatically affect downstream water quantity and quality (Alexander et al., 2007; Lowe & Likens, 2005; Neary et al., 2009) and aquatic and terrestrial ecology (Carignan & Steedman, 2000; Kreutzweiser et al., 2005; Tiegs et al., 2008). These findings have led to the adoption of numerous best management practices (BMPs) governing forestry practices with the goal of reducing downstream impacts of harvesting (Ice, 2004), with many examples of success (Binkley & Brown, 1993a, 1993b). Many forested ecosystems have evolved with and depend on fire as an ecological process, but anthropogenic climate change is driving an increase in fire frequency, size, extent, and severity (F. Li et al., 2018; Moritz et al., 2012). The impacts of anthropogenic climate change and altered wildfire regimes threaten our water resources (Creed & van Noordwijk, 2018; Seidl et al., 2017). Forest fires pose a daunting threat to water security, with many documented examples of altered flow regimes (Hallema, Robinne, et al., 2018; Robinne et al., 2018) and degraded water quality (Rhoades, Chow, et al., 2019; Rhoades, Nunes, et al., 2019; Rust et al., 2018; Rust, Saxe, et al., 2019; Smith et al., 2011).

1.1.1 Effects of Wildfire and Harvesting on Stream Flow

There are many ways that disturbances like wildfire and forest harvesting alter watershed hydrology. Vegetation modulates many of the important changes in watershed hydrologic cycling after disturbance. Through transpiration of water from the soil and groundwater into their tissues to fuel photosynthesis, vegetation and trees drive a dominant hydrologic flux in the landscape. After a disturbance, the reduction in plant biomass may result in reduced water loss from the catchment through transpiration (Basso et al., 2020; Maina & Siirila-Woodburn, 2020). There are certainly catchments that break this pattern, with increased evapotranspiration post-disturbance (Goeking & Tarboton, 2022; Tague et al., 2019). Altered evapotranspiration (ET) fluxes may cause changes in other hydrologic pathways, or a change in water routing from the catchment.

Many studies have documented altered and often increased streamflows following forest harvesting and fire (Bosch & Hewlett, 1982; A. E. Brown et al., 2005; Buttle, 2011; Goeking & Tarboton, 2020, 2022; Stednick, 2008) and wildfires (Bart & Hope, 2010; Cerdà, 1998; Ebel et al., 2012; Hallema, Sun, Bladon, et al., 2017; Hallema, Sun, Caldwell, et al., 2017; Hallema, Sun, et al., 2018; Ice, 2004;

Leopardi & Scorzini, 2015; Saxe et al., 2018; Wine & Cadol, 2016). Increased watershed discharge may take subsurface and overland pathways, manifesting in increases in baseflow (Bart & Tague, 2017; Kinoshita & Hogue, 2015; Kreutzweiser et al., 2008; Weis et al., 2006) or storm-flows (Guillemette et al., 2005; Saxe et al., 2018). The loss of a forest canopy also represents a loss in transient storage for incoming precipitation before reaching the ground, and a loss in the damping effect on raindrop velocity and erosive force (Buttle et al., 2000). The process of removing trees during forest harvesting requires access roads to the site, which can concentrate overland flow and result in channelization and faster water routing to the stream (Lang et al., 2018; Tague & Band, 2001). Wildfires can also alter the physio-chemical nature of surface soils, resulting in water-repellent soils and lower infiltration rates, and thus increased overland flow and erosion (Beatty & Smith, 2013; Cerdà, 1998; J. Chen, McGuire, et al., 2020; J. Chen, Pangle, et al., 2020; Ebel & Moody, 2017). Depending on the interplay of over-land and subsurface hydrologic pathways, reduced infiltration after fire could potentially reduce baseflow by routing more water to overland flow during precipitation events, contributing to flash flooding.

In the case of harvesting, the magnitude of changes in streamflow across many experimental harvests and watersheds have been connected to the degree of catchment disturbance (A. E. Brown et al., 2005, 2013). This connection has been more difficult to establish in the case of wildfires, in part due to their unpredictability. Whereas harvesting experiments may be planned ahead, with a harvested catchment co-monitored alongside an unharvested catchment; such an arrangement is often unavailable for burned catchments. This makes the disentangling of effects from the disturbance and changing climatic hydrologic drivers (e.g., precipitation) challenging (Goeking & Tarboton, 2022; Hallema, Sun, et al., 2018). Disentangling these effects is even more complicated when analyzing large numbers of catchments. This problem is explored in Chapter 2 of this dissertation.

1.1.2 Disturbance Effects on Concentrations of C, N and P

Alterations to water quality, including changes in concentrations of total, particulate, dissolved, organic and inorganic forms of N, C, and P have been documented following forest harvesting (Abdelnour et al., 2013; Bormann et al., 1968; Grace III, 2005; Hume et al., 2018; Johnson et al., 1982; Likens et al., 1970; Lynch & Corbett, 1990; C. W. Martin et al., 2000; Mupepele & Dormann, 2017; Rosén & Lundmark-Thelin, 1987; Schelker et al., 2016) and wildfire (Emelko et al., 2016; Rust et al., 2018; Silins et al., 2014; Smith et al., 2011). Fire and harvesting, when following each other in

the same watershed, have also been shown to result in even greater effects on water quality (Carignan et al., 2000; Smith et al., 2012; Wade et al., 2013). Water quality is a manifestation of both physiochemical and biogeochemical processes occurring in the landscape. These processes occur on the land and in the soils, within water bodies like streams and lakes, or along the spatial interface of water and mineral and living things: also known as the critical zone (Wymore et al., 2022).

As discussed in the previous section, the impact of disturbances on vegetation results in a cascade of effects for hydrologic cycles, impacting processes above and below the soil, and in the stream channel itself. Indeed, other physical effects of vegetation loss include decreases in stream shading, resulting in altered stream light, temperature and productivity regimes (E. S. Bernhardt et al., 2022; Pollock et al., 2009). These effects can cascade through the entire stream ecosystem (Wootton, 2012). Disturbance-induced changes to soil moisture regimes have the potential to alter biogeochemical processes, including the decomposition of organic matter, the transformation of N between oxidation states (like ammonium, nitrate, and dinitrogen gas), and the uptake of nutrients like N and P by plant roots (Fairbairn, 2020; Pastor & Post, 1986; Porporato et al., 2003; Rodriguez-Iturbe et al., 1999; Sierra et al., 2015). The harvest or death of trees will impact soil nutrient budgets even more. Suppressed plant N uptake following plant death has been shown to result in increased N exports to the stream (Abdelnour et al., 2013, 2013; Bormann et al., 1968; Hume et al., 2018; Johnson et al., 1982; Likens et al., 1970; C. W. Martin et al., 2000; Mupepele & Dormann, 2017; Rosén & Lundmark-Thelin, 1987; Schelker et al., 2016). Similarly, because of the strong connection of the forest to the soil water and C budgets, exports of dissolved organic carbon (DOC) often also increase after forest harvesting (Clarke et al., 2015; Hume et al., 2018; Lajtha & Jones, 2018; Parolari & Porporato, 2016).

Unlike in forest harvesting, wildfires result in the production of ash from burnt biomass and soil compounds. This ash can accumulate on the landscape, providing readily mobilizable pools of C, N, and P that can be carried to streams, increasing their concentrations in stream water (Brito et al., 2021; Earl & Blinn, 2003; Oliveira-Filho et al., 2018). Exactly how long these ash pools persist on the landscape affects the duration of altered water quality after fire.

Despite the numerous examples cited above showing altered concentrations of C, N, and P after disturbances, there remains a need for synthesis of altered water quality regimes after wildfire. Especially because of potentially greater risk of altered water quality after fire, and event

unpredictability precluding implementation of mitigating landscape BMPs, such a synthesis should also focus on water quality extremes relevant to drinking water treatment. The few existing syntheses (Bitner et al., 2001; Rust et al., 2018; Smith et al., 2011) do not comment on water quality extremes, and mostly summarize changes in mean concentrations. Further these syntheses have not explored the co-variation of elements and element species. While I have discussed each element generally, inorganic species like nitrate (NO_3^-), ammonium (NH_4^+), and phosphate (PO_4^{3-}) are more bioavailable fractions of the total element measurements. Both of these components of post-fire water quality—variability and co-variation—are explored in Chapter 3.

1.1.3 Disturbance Effects on the Relationship between Concentration and Discharge

The previous sections introduced the interactions between watershed ecohydrology and biogeochemistry, including through soil moisture and nutrient cycling. Concentration regimes of nutrients like C, N, and P in stream water are further impacted by streamflow regimes. Regardless of the process that produces or transforms chemicals, their arrival in streams is regulated by the amount of chemical available to be mobilized by water (the "source": a product of the balance of chemical production and removal) and the availability of water to mobilize them ("transport"). Many elements found dissolved in stream water can be derived from the weathering of rocks and soil minerals, meaning their source is ubiquitous. This ubiquity may result in concentrations that do not change between low and high rates of stream flow (Godsey et al., 2009). In contrast, organic and inorganic forms of C, N, and P may be much more impacted by biologic and biogeochemical processes and may not have ubiquitous sources in the watershed (including changes depending on the season). As a result, their concentrations in stream water will be governed by the interactions between source abundance and availability of water for transport (Basu, Destouni, et al., 2010; Dupas et al., 2017; Moatar et al., 2017; Zarnetske et al., 2018). Again, as highlighted above, changes in ecohydrology and biogeochemistry after disturbance can certainly change both source and transport processes for these elements.

Flow (Q) and water quality (C, concentrations) interact through erosion and geomorphology as well. Increased flows alter the pathways of water in the catchment, resulting in greater and flashier flows and more in-channel erosive power (Jones & Grant, 1996; Swanson & Dyrness, 1975). Flow-driven erosion and sediment transport can enhance the export of sediment-bound-phosphorus (P) from the watershed. Vehicle tracks in harvested catchments can be a source for sediment which has been

exposed to erosion, and altered surface water pathways or enhanced surface runoff after harvesting or fires can result in increased in-channel erosion and downstream sediment transport (Carignan et al., 2000; Coombs & Melack, 2013; Grace III, 2005; Johnson et al., 1982; Kreutzweiser & Capell, 2001; Silins et al., 2009; Smith et al., 2010; Wynn et al., 2000). Further sources of sediment could be mobilized during flash flooding and debris flow events, which often occur after extreme rainfall events in fire-impacted watersheds (Cannon et al., 2008; S. F. Murphy et al., 2015, 2018). These extreme events are also likely to increase with climate change in some ecoregions (McGuffie et al., 1999; Nearing, 2001; Segura et al., 2014). Just as P is carried downstream in particle form, organic matter–carrying within it N- and C-rich compounds–can be deposited into the stream, or eroded from soils, and transported by water. All three elements have dissolved forms that can also be released from soils to the stream through subsurface pathways. As discussed above, disturbance driven vegetation mortality results in readily mobilizable soil pools of nutrients that are released from vegetation uptake pressure. How disturbances impact speciation, including particulate versus dissolved, and organic versus inorganic forms of elements has not been studied in any synthesis research.

In addition to a need for new synthesis research on changing concentration variability after disturbance, the co-variation of concentration and flow after disturbance has not been studied across many catchments. Concentration-discharge (CQ) analysis has been used to reveal driving watershed processes in pristine and chronically impacted catchments (Basu, Destouni, et al., 2010; Zarnetske et al., 2018), but its application has only been limited to single catchment analyses in the case of forest disturbances (Emmerton et al., 2020; Silins et al., 2009, 2014; Wilkinson et al., 2006). Research in Chapter 4 of this dissertation examines changes in CQ behavior in multiple fire-impacted catchments to understand how CQ regimes change after fire.

1.1.4 Pan-Ecozone Catchment Responses to Forest Disturbance

I have so far summarized that landscape disturbances like wildfire and harvesting alter streamflows and water quality. While some drivers of the magnitude of change (of flow or concentrations or flux) have been documented, including the percent of the watershed disturbed, along with various watershed characteristics of climate, vegetation, and soils (A. E. Brown et al., 2005; Buma & Livneh, 2017; Rust, Saxe, et al., 2019). As disturbances to forests intensify and spread, including intersecting disturbances of climate change with harvesting and fire, our knowledge and insights about watershed

processes is more vital than ever. To manage potential changes in water quality from these disturbances, it is necessary to be able to Predict responses in Ungauged Basins (PUB). The International Association of Hydrological Sciences announced the Decade on PUB (Sivapalan, Takeuchi, et al., 2003) to spur our application of knowledge and map out where our knowledge falls short. The recognition of the need for PUB led to the proliferation of the idea of "top-down modeling" (Blöschl & Sivapalan, 1995; Sivapalan, Blöschl, et al., 2003), that emphasizes learning from data and hierarchical hypothesis testing and model construction. This approach prioritizes parsimony over complexity, allowing for easier and more reliable extrapolation of models to ungauged basins (Bárdossy, 2007; Besaw et al., 2010; Blöschl et al., 2019; Hrachowitz et al., 2013; Teutschbein et al., 2018; Westerberg et al., 2016). A "top-down" approach to modeling could provide insights into changing soil biogeochemical processes after disturbance, including nutrient retention and export. A modeling exercise and an exploration of interacting processes before and after forest harvesting is presented in Chapter 5 of this dissertation.

1.2 Research Gap

A multi-disciplinary research approach is required to quantify how land management decisions affect watershed ecohydrology and biogeochemistry; water, sediment, and nutrient export; and pose problems for drinking water treatment engineers and infrastructure. For watershed hydrology, the linkage between disturbance (including fire and harvesting) and the hydrologic cycle has been well studied, but usually in one or two catchments per study, and with a single-discipline focus. However, important interactions between ecohydrology and biogeochemistry have been revealed in studies of soil and in-stream element cycles (Bormann & Likens, 1967; Likens & Bormann, 1974; W. H. McDowell & Wood, 1984; Newbold et al., 1981; Vannote et al., 1980). This introductory chapter has so far highlighted a wealth of knowledge about how forest disturbances affect water quality. Two gaps stand out, which my dissertation will seek to address. First, there are a limited number of synthesis studies on how forest disturbances affect water quality and quantity, and more specifically, how alterations in flows and water quality co-occur. This gap calls for new methods of data synthesis and exploration. Second, to ultimately lead to better understanding of the future implications of changing climate and landscape disturbance regimes for drinking water supplies, more process-level understanding is needed. This gap calls for new analysis that can tie water quality effects from disturbances to our knowledge of biogeochemical and ecohydrological processes using a parsimonious modeling approach.

1.3 Research Questions and Objectives

This dissertation aims to characterize the linkage between forest disturbances (here, wildfires and forest harvesting), alterations to water quality and streamflow, and effects of these alterations on hydrochemical variables of relevance to water treatability; with an emphasis on large-scale multi-catchment analysis. The following research questions address both fundamental catchment science as well as water resource management strategies and the broader environmental context within which management decisions are being made:

- How do streamflow regimes change after wildfire? How can we decouple these changes from the influence of changes in climate? Can this decoupled disturbance signal be used to estimate hydrologic recovery times?
- How do water quality regimes change after wildfires? How do changes in elements co-vary? How do mean concentrations change relative to concentration variability, or to extreme concentrations?
- What is the relationship between the disturbance-driven changes in flow (Q) and water quality (C, concentrations)? Do C-Q relationships change after disturbance? How do these changes manifest for different elements?
- What ecohydrological and biogeochemical processes drive forest harvesting impacts on water quantity? Can we use a top-down modeling approach to understand these processes? How can site-measured data be used to inform the modeling approach?

The novelty of my approach includes the simultaneous assessment of wildfire and forest harvesting effects, the assessment of these effects across climatic zones and in various forest ecosystems across North America, and the linkage of watershed ecohydrology to water treatment. As highlighted in my research questions, the disentangling of multiple environmental signals necessitates novel methods of data analysis, which will be detailed in my research objectives. This dissertation aims to occupy a niche that connects watershed hydrologists to water treatment engineers, with the overall goal of increasing the resilience of our drinking water systems, given the rapid climate and land use shifts we are experiencing. My approach is broken down into four research objectives (RO), as listed below:

RO1: Develop a methodology to quantify the effects of wildfires on streamflows and disentangle those effects from changes in climate.

RO2: Perform a meta-analysis on the effects of wildfires on water quality (including compounds of N, P, and C), and develop a methodology to quantify the changes in extreme concentrations relative to mean concentrations.

RO3: Develop a methodology to quantify and characterize changes in concentration-discharge (C-Q) relationships after wildfire.

RO4: Develop a process-based modeling and calibration framework to explore and model the linkage between forest harvesting, soil biogeochemical alterations, and downstream water quality.

To meet my first three objectives, I characterized the scope of current knowledge, through literature review, meta-analysis, and aggregation of existing data. I assessed a large number of studies in each of the research areas of catchment hydrology and disturbance, soil biogeochemistry, and watershed management. I focused on the effects of wildfires on streamflows in RO1, on water quality in RO2, and on concentration-discharge (C-Q) relationships in RO3.

To meet my fourth research objective (RO4), I used top-down modeling techniques to develop a coupled hydrology-biogeochemistry-forest model, with the goal of quantifying how forest management can impact water and solute fluxes, over annual to decadal timescales.

Chapter 2
A novel Budyko-based approach to quantify post-forest-fire streamflow response and recovery timescales

This chapter is a mirror of the following published article. References are unified at the end of the thesis.

Hampton, Tyler B., and Nandita B. Basu. "A Novel Budyko-Based Approach to Quantify Post-Forest-Fire Streamflow Response and Recovery Timescales." *Journal of Hydrology*, March 4, 2022, 127685. https://doi.org/10.1016/j.jhydrol.2022.127685.

All data and codes are publicly available in the online Hydroshare repository: http://www.hydroshare.org/resource/43280a7de6ef48b4b800ab5c12ae58cb

2.1 Abstract

Recent increases in the incidences of wildfires have necessitated the development of methodologies to quantify the effect of these fires on streamflows. Climate variability has been cited as a major challenge in revealing the true contribution of disturbance to streamflow changes. To address this, we developed an annual Budyko "decomposition" method for (1) statistical change detection of hydrologic signatures post-fire, (2) separating climate-driven and fire-driven changes in streamflow, and (3) estimating hydrologic recovery timescales after fire. We demonstrate the use of this methodology for 17 watersheds in Southern California with high interannual variability in precipitation. We show that while traditional metrics like changes in flow or runoff ratio might not detect a disturbance effect due to confounding climate signals, the Budyko framework can be used successfully for statistical change detection. The Budyko approach was also found to be robust in detecting changes in 5 highly burned catchments (>40% burned area ratio), while changes in less burned (2) and unburned catchments (10) were insignificant. We further used the Budyko approach to quantify the contribution of fire-driven versus climate driven changes in streamflow and found that fire contributed to an average increase in streamflow on the order of 80 mm yr^{-1}, though the effect varied greatly between years. Finally, we estimated hydrologic recovery timescales that varied between 5 to 45 years for four burned catchments. We found a significant linear relationship between

recovery time and burned area at medium and high severity for our study catchments, with about 4 years of recovery time per 10% of the watershed burned.

2.2 Introduction

Forested headwaters serve a critical societal function by providing drinking water for large portions of the population in North America and across the globe (T. C. Brown et al., 2008; Ernst, 2004). The protection of these forests and associated ecosystem services is of paramount importance in the face of increased pressures from forest harvesting (C. J. Anderson & Lockaby, 2011), global climate change (Seidl et al., 2016, 2017), and wildfires (DeBano et al., 1998; Hallema, Robinne, et al., 2018; Robinne et al., 2018). Wildfires stand out as an ominous threat to water security (Bladon et al., 2014; Emelko et al., 2011; Nunes et al., 2018; Rockström et al., 2014). By changing streamflows, they can result in increased erosion and decreased hillslope stability (Ryan et al., 2011; Wohl, 2013) , contributing to degraded water quality and aquatic ecosystem health at downstream locations (Basso et al., 2020; Rust, Randell, et al., 2019).

The study of streamflow changes from wildfire is relatively new, but hydrologists have been exploring the response of streamflow to disturbances like forest harvesting for more than half a century using paired catchment studies and before-after-control-impact experiments (BACI) (see reviews by: Bosch & Hewlett, 1982; A. E. Brown et al., 2005; Goeking & Tarboton, 2020). The unpredictability of wildfire occurrence makes it difficult to apply these well-established methodologies to distinguish between climate and fire effects on streamflow responses. This is especially true in semi-arid Mediterranean ecosystems with significant year-to-year variability in climate (McLauchlan et al., 2020). The increasing incidence of extreme wildfires and degraded water quality in these regions (Cannon & DeGraff, 2009; Flannigan et al., 2009; A. Westerling et al., 2014) has spurred numerous studies into how fire alters storm event and baseflow recession dynamics (Bart & Tague, 2017; Soulis et al., 2021), annual water yields (Bart & Hope, 2010; Hallema, Sun, Caldwell, et al., 2017; Hallema, Sun, et al., 2018; Wine & Cadol, 2016), as well as annual runoff ratios (Blount et al., 2019; Kinoshita & Hogue, 2011, 2015). However, there still exists significant uncertainty on how wildfire affects annual water yield. The general assumption is that streamflows increase after wildfire, driven by suppressed evapotranspiration from vegetation mortality (Basso et al., 2020; Ice et al., 2004; Maina & Siirila-Woodburn, 2020), as well as other effects like increase in soil hydrophobicity, decreasing infiltration and increasing overland flow to the stream (Beatty &

Smith, 2013; Robichaud, 2000). However, studies have also found that for low intensity fires that do not result in complete forest mortality, the remaining vegetation may take advantage of either less nutrient or soil-water competition, increasing growth and increasing transpiration, and thus decreasing streamflows (Biederman et al., 2015; Tague et al., 2019). Due to these different factors, and a lack of paired catchment data, decoupling the effects of climate versus wildfire remains challenging.

Two recent large analyses of wildfire-impacted catchments found a wide distribution of increases and decreases in post-fire streamflows (Hallema, Sun, et al., 2018; Saxe et al., 2018). Saxe et al. document intra-annual changes in flows in 82 watersheds in the western U.S. with burned area ratios (BAR) in the range of 9–35% (interquartile range; median 16%; outliers up to 98%). They analyzed several hydrologic metrics (high flows, low flows, runoff ratio, baseflow index, etc.) and found post-fire responses to be highly variable, with trends often difficult to discern. They argue that variability in climate can outweigh any changes in rainfall partitioning to streamflow and evapotranspiration due to wildfire, and this contributes to such apparent confounding effects. Hallema et al. (2018b) analyzed over 150 burned watersheds in the southern and western United States and used climate elasticity models (CEM; Sankarasubramanian et al., 2001) to parse climate and fire effects on streamflow. These authors showed that river flows changed in only 20% of watersheds where BAR exceeded 19%. However, the challenge in their method lies in the detection of a statistically significant changepoint in streamflow prior to CEM analysis. In semi-arid regions, climate variability can be so dominant that a statistically significant change in streamflow might not be apparent immediately after fire. Furthermore, their method focuses solely on evaluating changes in the mean hydrologic responses between the pre-fire and post-fire periods, and thus the findings are sensitive to the number of years of data that is available after the fire. Saxe et al. (2018) found that the effects of fire are greatest in the first few years following fire, and that they dissipate over time. This dissipation timescale, also referred to as hydrologic recovery timescale, is a function of vegetation growth dynamics, and is critical for watershed managers for planning (Buttle et al., 2018; Heath et al., 2014; Kinoshita & Hogue, 2011; Wagenbrenner et al., 2021). No studies to date have developed transferable methodologies that can parse climate and fire effects adequately at the annual timescale and effectively quantify hydrologic recovery timescales.

The overall objective of our study is to address this gap by developing a new method for (1) statistical change detection to quantify the effect of fire on streamflows, (2) parsing the effect of climate versus disturbance from annual streamflows post-wildfire, and (3) quantifying recovery timescales in

wildfire impacted catchments. Our method is based on the Budyko decomposition method, first proposed by D. Wang & Hejazi (2011) and adapted in this paper to the annual timescale for characterizing catchment recovery. We test the robustness of the method by comparing it to more traditional approaches of analyzing effects of wildfire by quantifying changes in the mean annual streamflow and the runoff ratio. Our overall hypothesis is that a change detection methodology rooted in the Budyko framework can be used to distinguish between hydrologic effects in burned and unburned catchments. We provide a case study outlining the application of our method in several watersheds in Southern California impacted by wildfires, and compare them with unburned, reference catchments in the same geographic area. Finally, we conclude with lessons learned and future work.

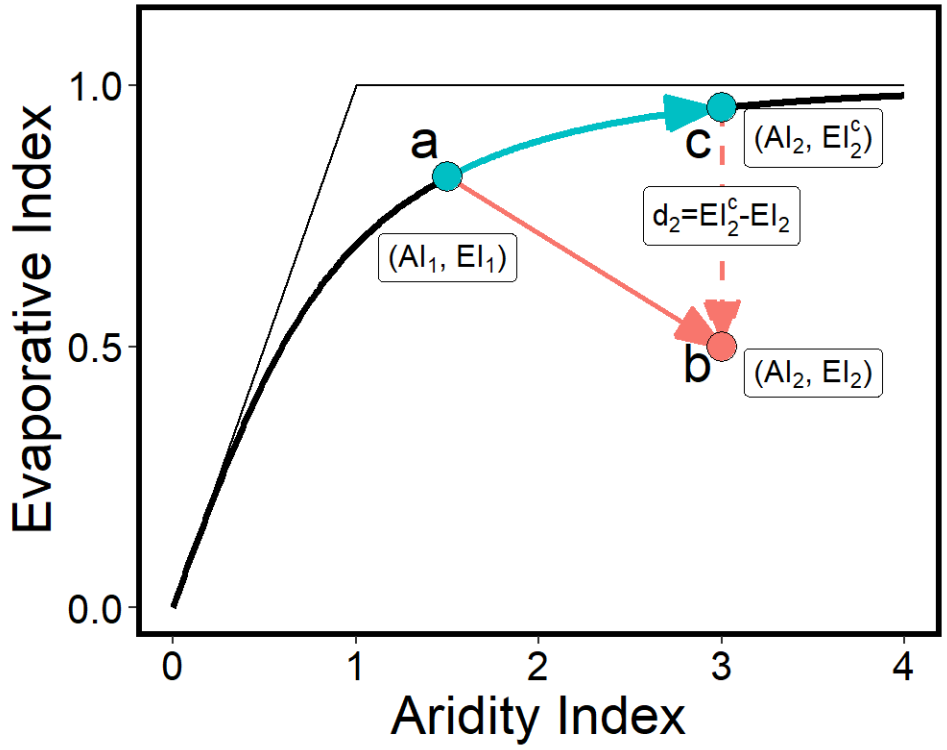

Figure 2-1. Diagram illustrating the Budyko Decomposition method. The black curve is the original Budyko curve. Points represent water-year data. Point "a" in blue represents one year prior to a hypothetical disturbance, and point "c" represents how data would follow the idealized curve if aridity increased the year following a. Point "b" represents how, in the year following the disturbance, while AI did increase relative to a, EI decreased relative to Budyko behavior modelled by c. The dashed red arrow is the magnitude of the disturbance effect, with a magnitude d_2.

2.3 Conceptual Framework and Objectives

2.3.1 Rationale for the Budyko Decomposition Method at the Inter-annual Timescale

Catchments exhibit a strong relationship between climate (energy and precipitation inputs) and water exports (evapotranspiration and streamflow). The Budyko curve (Budyko, 1961, 1974), developed using long term streamflow data from hundreds of catchments, captures this relationship by plotting the water partitioning against the climatic controls (Figure 2-1). Here, climate is characterized by the ratio of energy to water inputs, also known as the Aridity Index (AI), and is calculated as the potential evapotranspiration (PET) over precipitation (P). The water partition is characterized by the Evaporative Index (EI), and is calculated as the ratio of actual evapotranspiration (AET) over P. Figure 2-1 stresses that in the domain of low AI (especially AI less than one), EI responds almost linearly to changing AI, whereas for high AI, EI is almost insensitive to AI.

Recent studies have used the Budyko framework to differentiate between the effects of changing climate and landscape-scale disturbances on streamflow (Jaramillo et al., 2018; C. Li et al., 2018; Mo et al., 2018; Shahid et al., 2018; D. Wang & Hejazi, 2011; H. Wang & Stephenson, 2018; Wu et al., 2018). D. Wang & Hejazi (2011) first presented this "decomposition" method and showed for 413 catchments (from the Model Parameter Estimation Experiment (MOPEX); Duan et al., 2006) in the United States (U.S.) that changes in Q due to climate between two 20-year periods were large (18% ± 0.9% change in mean annual Q), and greater than changes due to human activity. Young et al. (2019) found that the Budyko framework performed similarly in attributing flow changes to disturbance and climate effects when compared against the more traditional paired catchment approach. These studies demonstrate the successful application of the Budyko decomposition method (see also: Creed et al., 2014; Jones et al., 2012); however, they have been limited to examining changes across 10- to 20-year blocks of time and have not examined the response of catchments in the aftermath of single-year disturbances like harvesting or wildfire. Here we expand on this prior work to assess the applicability of the Budyko decomposition method to quantify the immediate response of catchment hydrology to events like wildfire and decouple climate- from fire-effects at the annual timescale.

The first step in this approach is to evaluate the applicability of the Budyko model at the interannual timescale. Indeed, while the traditional Budyko hypothesis was developed at the multi-decadal timescale, a wealth of recent studies have documented the ability of the Budyko curve to capture temporal variations in water balance, demonstrating a remarkable space-time symmetry (Carmona et

al., 2014; X. Chen et al., 2013; Cheng et al., 2011; Donohue et al., 2006; Harman et al., 2011; Milly & Dunne, 2002; Potter & Zhang, 2009; Rice & Emanuel, 2019; Sivapalan et al., 2011; Teng et al., 2012; Troch et al., 2013; Yang et al., 2007). The biggest challenge in application of the Budyko hypothesis at the inter-annual time scale is the assumption of no change in catchment water storage that is fundamental to the original Budyko method. To evaluate the validity of this assumption, Rice & Emanuel (2019) analyzed interannual changes in watershed storage, using ground based and remotely sensed data, in 1000 watersheds across the contiguous U.S. for the 10-year period 2002–2011. They found that in arid catchments with greater evaporative partitioning (high EI), the size of the interannual storage changes were on average quite small relative to the magnitude of annual precipitation (Figure A-1). They further found that watersheds exhibited a positive correlation between the degree of forest cover and the fit to the Budyko-type curve at the interannual scale (see also Roderick & Farquhar, 2011), implying that higher forest cover led to more Budyko-type behavior, indicative of hydrologic steady state. Rice & Emanuel (2019) argue that this occurs because eco-hydrologic feedbacks in forested watersheds reinforce steady state response by downregulating transpiration and decreasing hydrologic connectivity in arid conditions, while increasing evapotranspiration and drainage during wet conditions. Given that the watersheds in our case study have both high EI and significant vegetative cover (Figure 2-2, Tables 1-1 and 1-2), we argue that it is reasonable to use Budyko decomposition at the interannual timescale.

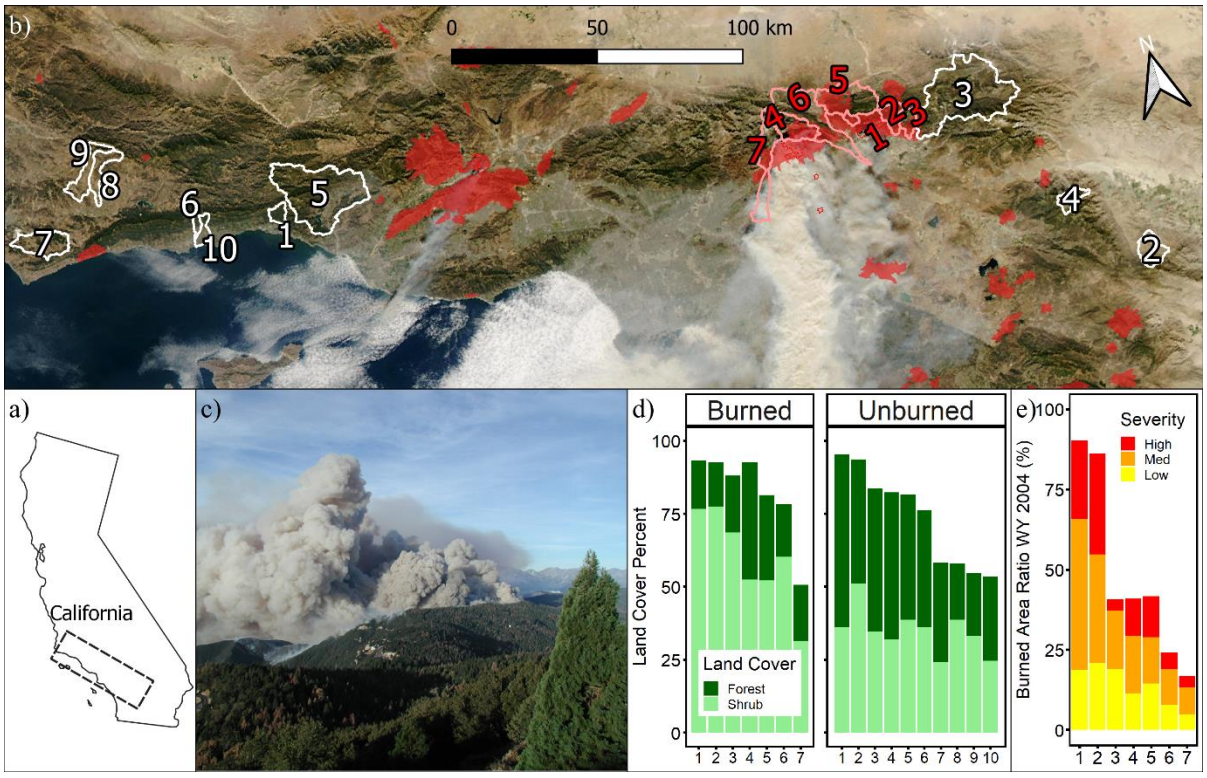

Figure 2-2. Site Map. a) Map of California. Dashed box is the extent of map b. b) Map of sites. Background imagery from NASA Aqua/MODIS, 2003-10-25, showing the Grand Prix Fire, Old Fire, and Piru Fire near Los Angeles (NASA, 2003). Red polygons are fires from 2002–2004 from the MTBS dataset. White polygons are the selected unburned catchments and pink polygons are burned catchments in the San Bernardino Mtns. Sites are numbered as in Table 2-1. c) The Old Fire burning in the San Angeles National Forest on 2003-10-26. Photo by D. Schumaker. d) Land cover percent for the 17 catchments (7 Burned and 10 Unburned), showing total vegetated cover classified as forest or shrub from the GAGES II Dataset. e) Percent of catchment area burned in Water Year 2004 with fire severity class from MTBS.

Table 2-1. Catchments from southern California. Land cover, fire, and topographic characteristics. In the mean, the burned and unburned catchments had a similar range of attributes including elevation, slope, vegetation cover, and catchment area.

id	USGS ID	NAME	Burn % WY2004	Elev. (m)	Slope (%)	Aspect (deg)	Veg (%)	Urban (%)	Area (ha)
B1	11063680	Devil Canyon Ck.	97	1168	39	214	93	6	1440
B2	11055800	City Ck.	93	1197	34	217	93	5	5050
B3	11055500	Plunge Ck.	50	1216	31	217	88	9	4420
B4	11062001	Lytle+Brlne+Cond+Inf	46	1696	44	96	93	2	11970
B5	10260950	West-fork Mojave R.	45	1272	20	22	81	9	17510
B6	11065000	Lytle Ck. @ Colton	28	1250	27	132	78	12	36470
B7	11073360	Chino Ck.	21	1050	27	211	51	45	13230
UB1	11119500	Carpinteria Ck.	0	584	33	208	95	1	3410
UB2	10259200	Deep Ck.	0	1415	25	15	94	1	7910
UB3	11051500	Santa Ana River	2	2071	27	321	84	11	54230
UB4	10258000	Tahquitz Ck.	0	2090	37	110	82	0	4370
UB5	11118500	Ventura River	0	702	29	192	82	9	48570
UB6	11119940	Maria Ygnacio Ck.	0	424	24	214	76	19	1640
UB7	11132500	Salsipuedes Ck.	0	280	17	270	58	4	12210
UB8	11128250	Alamo Pintado Ck.	0	511	19	231	58	9	7380
UB9	11129800	Zaca Ck.	0	444	20	213	55	6	8530
UB10	11120000	Atascadero Ck.	0	311	18	220	54	39	4930

Table 2-2. Hydrologic data for study catchments. Data are averaged between WYs 1982 to WY 2003. Q is discharge (both volume and area-normalized). P is precipitation. PET is potential evaporation (see Equation A-1). Rr is the runoff ratio. EI is evaporative index. AI is aridity index. Fu ω is the fitting parameter for the Budyko curve (see Equation 2-1). fit error is the mean absolute error of the fit points from the fit curve.

id	USGS gage id	Q (mm yr^{-1})	P (mm yr^{-1})	PET (mm yr^{-1})	Rr	EI	AI	Fu ω	Fu fit mean abs error
B1	11063680	195	931	1471	0.18	0.82	1.89	2.62	0.07
B2	11055800	173	760	1601	0.19	0.81	2.57	2.23	0.06
B3	11055500	148	804	1509	0.14	0.86	2.3	2.71	0.05
B4	11062001	285	926	1402	0.29	0.71	1.86	2.05	0.12
B5	10260950	150	578	1563	0.18	0.82	3.34	2.04	0.10
B6	11065000	11	725	1544	0.01	0.99	2.64	25.0	0.01
B7	11073360	115	740	1565	0.16	0.84	2.55	2.27	0.11
UB1	11119500	149	732	1485	0.13	0.87	2.67	2.76	0.05
UB2	10259200	27	327	1617	0.05	0.95	7.05	2.44	0.04
UB3	11051500	56	713	1432	0.06	0.94	2.46	4.44	0.04
UB4	10258000	101	661	1287	0.12	0.88	2.3	3.05	0.06
UB5	11118500	146	763	1683	0.12	0.88	2.93	2.68	0.05
UB6	11119940	132	657	1462	0.14	0.86	2.79	2.44	0.05
UB7	11132500	109	559	1569	0.14	0.86	3.45	2.21	0.06
UB8	11128250	47	596	1729	0.06	0.94	3.83	3.32	0.03
UB9	11129800	26	578	1327	0.03	0.97	2.91	5.19	0.02
UB10	11120000	157	676	1467	0.17	0.83	2.73	2.26	0.04

2.3.2 Objective 1: Statistical Change Detection to Quantify the Effect of Fire on Streamflows

We developed a novel approach for statistical change detection to quantify the effect of fire on streamflows. The first step in this method is the translation of annual catchment data into Budyko-space, given annual values of precipitation (P), streamflow (Q), and potential evapotranspiration (PET) for a watershed. The AET was calculated using the water balance equation (AET = P – Q) which assumes that the carryover of storage between years is negligible compared to the annual fluxes of AET, P, and Q. This assumption has been often used in annual water balance studies (Milly, 1994; Sivapalan et al., 2011; Yang et al., 2007; L. Zhang et al., 2011). However, to minimize the errors introduced by this assumption, we aggregated the monthly values of P and Q over the hydrological rather than the calendar year, as proposed by the U.S. Geological Survey (USGS) and following the approaches by Sivapalan et al. (2011) and Carmona et al. (2014). There should be no major fire or other forest disturbance such as harvesting during this time period to avoid confounding effects.

A Fu-type Budyko curve was then fit using data from the pre-fire period to evaluate the ability of the Budyko curve to capture interannual variability in water partitioning during the non-disturbed period. In Appendix A (Section A2.2) we discuss the choice of the Fu-type curves (Figure A-2) and the robustness to this choice compared to other methods. The Fu curve (Fu, 1981) is characterized by Equation 1:

$$EI_i = 1 + AI_i - (1 + (AI_i)^{\omega})^{1/\omega} \quad (2\text{-}1)$$

The ω parameter was calibrated using nonlinear least squares regression to pre-fire annual data (time series of measured evaporative index EI_i and measured aridity index AI_i) from each watershed using the *stats* and *budyko* packages in R (Hampton, 2020; R Core Team, 2023). The *investr* package (Greenwell & Schubert Kabban, 2014) was used to calculate confidence and prediction intervals from the regression models. The parameter ω is then used to create a timeseries of evaporative index (EI_i^c) as a function of the aridity index AI_i. We then used two different approaches to use the modeled EI_i^c for statistical change detection: a Budyko Deviation Approach, and a Covariate Modelling Approach.

2.3.2.1 Budyko Deviation Approach

In the Budyko Deviation Approach, we assumed that in the absence of landscape disturbance like fire, catchments move back and forth along a Budyko-type curve as a function of temporal variations in climate, as captured by the Aridity Index (AI). Our proposed decomposition method is described in Figure 2-1. If a catchment moves from point "a" (AI_1, EI_1) in the pre-disturbance year to point "b" (AI_2, EI_2) in the post-disturbance year, then this movement can be described as the sum of a climate component and a landscape disturbance component. In the absence of any landscape disturbance, the catchment would have moved from point "a" to point "c" along the Budyko curve. This movement describes the climate component of the change in streamflow, and it has both a horizontal and a vertical component. The effect of the landscape disturbance in the post-disturbance year is then captured by the vertical distance between points "b" and "c". Our change detection method relies on these vertical deviations from the predicted curve. We defined our change metric as the annual vertical Budyko deviation (d_i): the difference between the modelled EI_i^c and measured EI_i values in each year (both pre- and post-fire):

$$d_i = EI_i^c - EI_i \tag{2-2}$$

The d_i is represented in Figure 2-1 as the vertical distance between points "b" and "c". We assessed the statistical significance of the changes in the distribution of d_i using the nonparametric Kolmogorov-Smirnov (K-S) test. The null hypothesis was that the distributions of these deviations were the same in the two equal-length (n-years) periods of time before and after the fire. Our alternative hypothesis was that the deviations were greater post-fire. The analysis was performed in both burned and unburned catchments to help confirm that the lack of an apparent response can be attributed to climatic differences. We argue that the Budyko deviation metric accounts for climatic variability and is thus a more robust detector of the effect of fire than more traditional metrics like the change in streamflow (Q) or runoff ratio (Rr).

2.3.2.2 Covariate Modelling Approach

The Covariate Modelling Approach relies on well-established statistical change detection methodologies using a climate covariate (e.g. Eaton et al., 2010; Zhang and Wei, 2012). To do this, we modelled the time series of EI_i as a function of a climate co-variate (EI_i^c) (as in M. Zhang & Wei, 2012, 2014) and an exponentially decaying intervention effect:

$$EI_i - EI_i^c = d_i = \ m * \exp\,(j * -k) * \begin{cases} if(j \geq 0), 1 \\ if(j < 0), 0 \end{cases} \quad (2\text{-}3)$$

where m and k are constants, i is a counter for years, and j counts years post-fire; exp(x) is the exponential function e^x, where when $j = 0$: $me^{-jk} = m$. For negative values of j the step-function (in brackets) has a value of 0, removing the negative domain of the exponential function. The constant m represents the magnitude of the response in the first post-fire year, while the decay coefficient k describes the rate of recovery. Here, unlike in Equation 1, both pre- and post-fire years are included in the model calibration.

The significance of the post-fire response was assessed by the significance of the parameters m and k. Specifically, we tested a null hypothesis where the climate co-variate EI_i^c adequately predicts the hydrologic response during both the pre-fire and post-fire periods, and the intervention effect (as characterized by m) has a statistically insignificant magnitude; and an alternative hypothesis where the intervention effect has a statistically significant magnitude. This approach was applied to both burned and unburned catchments to confirm whether the m parameter was controlled solely by fire effects. Models were fit using non-linear least squares regression using the *stats* package in R (R Core Team, 2023). The best fit model was determined by minimizing the sum of the squared model residuals. We assessed model appropriateness by comparing the model residuals from the pre- and post-fire time period using 2-sample Kolmogorov-Smirnov (K-S) test with a two-directional alternative hypothesis (*stats* package in R: R Core Team, 2020). An appropriate model confirmed the null hypothesis that the distributions of residuals were not significantly different ($p>0.1$ in all cases). The *investr* package (Greenwell & Schubert Kabban, 2014) was used to calculate confidence and prediction intervals from the regression models. In the Budyko Deviation Approach we relied on a statistical test of the difference between two unordered populations of n years, while in the Covariate Modelling Approach we explicitly considered the ordering of the time series.

2.3.2.3 Benchmarking with Other Change Metrics

We compared our two approaches to more traditional change metrics. As discussed in our review of the literature, many studies apply statistical tests directly to the timeseries of Q and Rr to assess disturbance effects. We averaged data for streamflow (Q), runoff ratio (Rr) and Budyko deviation (d) for 10 years pre-fire and 10 years post-fire . We report the difference in these 10-year averages with the capital letter Δ (e.g. Δd, ΔQ, and ΔRr see Equations 4-6).

$$\Delta d = \frac{1}{n}\sum_{i=1}^{n} d_i - \frac{1}{n}\sum_{j=1}^{n} d_j \quad (2\text{-}4)$$

$$\Delta Q = \frac{1}{10}\sum_{i=1}^{10} Q_i - \frac{1}{10}\sum_{j=1}^{10} Q_j \quad (2\text{-}5)$$

$$\Delta Rr = \frac{1}{10}\sum_{i=1}^{10} Rr_i - \frac{1}{10}\sum_{j=1}^{10} Rr_j \quad (2\text{-}6)$$

In Equations 2-4 to 2-6, the subscript i is used for post-fire years while the subscript j is used for pre-fire years. For these same 10-year periods of data, we tested whether the two samples (pre- and post-fire) were statistically different using a 2-sample K-S test with a one-directional alternative hypothesis (*stats* package in R: R Core Team, 2020).

2.3.3 Objective 2: Parsing the Effect of Climate and Disturbance from Annual Streamflows Post-wildfire

Based on our results from the first objective, we would identify catchments in which fire has had a significant effect. The next step of the analysis is to quantify the magnitudes of the streamflow change due to fire and climate in the fire impacted catchments. To do this, we assume that the Budyko-type curve models how annual evaporative index and thus streamflow would respond to climate in the absence of any catchment disturbance. Thus, in any year i, the climate component of the measured flow (Q_i^c) can be described as a function of modelled evaporative index (EI_i^c) and measured precipitation (P_i):

$$Q_i^c = (1 - EI_i^c)P_i \quad (2\text{-}7)$$

In every year, both pre- and post-fire, there is some deviation between observed annual flow (Q_i) and the modelled flow (Q_i^c). We denote this deviation as Q_i^f, which represents the effect of landscape disturbances like fire.

$$Q_i^f = Q_i^c - Q_i = (EI_i^c - EI_i)P_i \quad (2\text{-}8)$$

which is equivalent to:

$$Q_i^f = d_i P_i \quad (2\text{-}9)$$

We then estimate the average change in streamflow due to climate effects (ΔQ^{c}) and fire effects as (ΔQ^{f}) over two n-year time periods before and after fire (where i is used for post-fire years and j is used for pre-fire years) as:

$$\Delta Q^{\mathrm{c}} = \frac{1}{n}\sum_{i=1}^{n} Q_i^c - \frac{1}{n}\sum_{j=1}^{n} Q_j^c \quad (2\text{-}10)$$

$$\Delta Q^{\mathrm{f}} = \frac{1}{n}\sum_{i=1}^{n} Q_i^f - \frac{1}{n}\sum_{j=1}^{n} Q_j^f \quad (2\text{-}11)$$

such that

$$\Delta Q = \Delta Q^{\mathrm{c}} + \Delta Q^{\mathrm{f}} \quad (2\text{-}12)$$

We use the capital letter Δ to denote change between time periods. We also estimate an annual Q change in each post-fire year relative to the pre-fire average to determine how climate and fire contributed to interannual variability of flow in the post-fire series. Specifically, the climate contribution of the flow change in the post-fire years (δQ_i^c), and the fire contribution of the change (δQ_i^f) are estimated as:

$$\delta Q_i^c = Q_i^c - \frac{1}{n}\sum_{j=1}^{n} Q_j^c \quad (2\text{-}13)$$

$$\delta Q_i^f = Q_i^{\mathrm{f}} - \frac{1}{n}\sum_{j=1}^{n} Q_j^f \quad (2\text{-}14)$$

such that

$$\delta Q_i = \delta Q_i^c + \delta Q_i^f \quad (2\text{-}15)$$

where the lowercase letter δ signifies change in reference to a specific year: the letter i is used for post-fire years and j is used for pre-fire years. Note that the average of the pre-fire (j is used for pre-fire years) flow deviations (Q_j^f) exhibits a similar property as d_j, such that the values ($\frac{1}{n}\sum_{j=1}^{n} d_j$) and ($\frac{1}{n}\sum_{j=1}^{n} Q_j^f$) are small but not necessarily zero.

2.3.4 Objective 3: Quantifying Recovery Timescales in Wildfire-impacted Catchments

Finally, our last objective is to quantify the recovery timescale in wildfire impacted catchments. To do this we use the decay coefficient k that was estimated using the Covariate Modelling Approach in Objective 1. We modelled recovery only catchments in which there is a significant fire effect, as indicated by a significant m parameter. Since we use an exponential model to describe decay which means theoretically recovery time is infinity, we chose an arbitrary threshold beyond which the effect was insignificant in size. We chose a threshold of 90% of the magnitude of m. Catchment recovery (t) was defined by inverting the exponential decay coefficient (k: with units of time^{-1}) and multiplying by a recovery threshold (r), such that $\log(1-r)/k$ provides the 90% recovery time (t_{90}) when $r = 0.9$. The parameter uncertainty (of k) from the nonlinear regression models were used to calculate the uncertainty on t_{90}.

2.4 Methods

2.4.1 Case Study: Southern California

Our proposed method is illustrated in a case study located in the forested areas of southern California, surrounding the San Bernardino area (Figure 2-2a,b). This region stood out as having a high concentration of USGS gaging stations and fires. In particular, water-year (WY) 2004 had a record number of fires (Blackwell & Tuttle, 2003). This large number of fires offers the opportunity to study multiple affected catchments, under the same sequence of climate and disturbance conditions. Criteria for selecting burned catchments were based off those of Rust et al. (2018) and Saxe et al. (2018) and are described in Appendix A (Section A1.1). We began with 112 candidate catchments and selected for those dominated by forested or vegetated cover (minimal urban land cover) and with adequate periods of record, including no large fires during the period of record except for WY 2004. As much of this region is under the management of the USFS, we also confirmed that no harvesting activity took place in these catchments during the period of record (U.S. Forest Service, 2018). This led us to select 7 burned catchments and 10 unburned catchments to analyze (Table 2-1). Two of the catchments in our study, Devil Canyon Creek (B1) and City Creek (B2), have both been studied with respect to streamflow effects after the 2004 water-year fires (Bart, 2016; Bart & Tague, 2017; Kinoshita & Hogue, 2011, 2015).

The mountains of southern California are a diverse geologic and hydroclimatic mosaic. Soils are generally thin and easily erodible (Wells, 1981), and are underlain by heavily faulted assemblages of igneous and metamorphic rocks (Morton & Miller, 2006). A strong orographic effect results in wet windward slopes and dry leeward slopes dropping to the deserts to the east. This gradient results in a chaparral-dominated ecosystem giving way to mixed conifer forest along mountain crests, and Piñon-juniper woodlands in drier climates (Figure 2-2c; Barbour et al., 2007). The fire recurrence period for this ecosystem is around 30–40 years (Keeley & Fotheringham, 2001). The burned and unburned catchments ranged in size from 1,400 ha to 48,000 ha: all have greater than 50% vegetated cover (shrub and forest; Figure 2-2d) and are generally steep (20–40%). For the 7 burned catchments, burned area ratio (BAR) at a moderate or high severity ranged from 12% to 71% (Figure 2-2e). The climate is Mediterranean, with regional rainfall is on average 720 ± 400 mm yr^{-1}, and potential evaporation is 1280 ± 90 mm yr^{-1} (Table 2-2).

2.4.2 Data Sources and Calculations

Streamflow (Q; from USGS) and climatic data (PRISM Climate Group, 2018), including precipitation (P) and temperature (T), were used to calculate the WY hydrologic budget for our catchments. We analyzed data from water years 1982 (beginning of PRISM availability) to 2018. Data from WY 1982 to 2003 were used to calibrate Fu-type Budyko curves, and data from WY 2004 to 2018 were used to calculate the post-fire time series of d_i. Data sources are in Table 2-3. Methods for data retrieval are detailed in Appendix A (Section A1.2). All data and code are provided in an online repository (Hampton, 2022a). PET was calculated using the Hargreaves-Samani equation (Hargreaves & Samani, 1985; see calculations in Appendix A1.3). There are two groups of methods available for estimating PET: temperature-based methods (e.g., Thornthwaite, Hamon, and Hargreaves-Samani) and radiation-based methods (e.g., Turc, Makkink, and Priestley-Taylor). We did not have access to radiation data at our sites and thus used the temperature-based Hargreaves-Samani equation. To ensure that this didn't bring bias into our results, we analyzed the choice of our PET calculation method by assessing agreement between six PET methods (as in Lu et al., 2005; see Appendix A2.1 and Figures A-2,3). Overall, we found no effect of using a temperature- versus radiation-based PET formula in detecting Budyko deviations (Figures A-4,5).

Following retrieval of annual climate and hydrologic data, a single-parameter version of the Budyko curve by Fu (1981) and the ω parameter was fit using nonlinear least squares regression to pre-fire annual data from each watershed using the *nls* and *budyko* packages in R (Hampton, 2020; R Core Team, 2023). Each of the 17 watersheds in our study was fit to a different Fu-type Budyko curve that is a function of the physical properties of the specific watershed, such as soil properties, and vegetation type and coverage (e.g., Milly, 1994; L. Zhang et al., 2001, 2008). All available pre-fire data (WY 1982 – 2003) were used in the curve fitting process. From the Fu fit curves for each watershed, the Budyko deviations (d_i) were then calculated for each year after fire following Equation 2. Annual flow was decomposed into a climate prediction (Equation 7) and fire deviation (Equations 8-9), and "total" effect sizes were calculated following Equations 10–12 and 4-6.

Table 2-3: Descriptions of datasets used in our study

Description	Dataset	Source
Streamflow (Q)	National Water Information System (NWIS)	U.S. Geological Survey (USGS), accessed via *dataRetrieval* package in R (Hirsch & De Cicco, 2015)
Gridded Climate Products (Precipitation P, Temperature T), available monthly at 4 km resolution from 1982 to 2017 WY	PRISM	(PRISM Climate Group, 2018)
Fire perimeters	Monitoring Trends in Burn Severity (MTBS)	(Eidenshink et al., 2007).
Attributes of stream gages and watersheds, geographic shapefiles	GAGES II	(Falcone, 2011)

2.5 Results and Discussion

2.5.1 Statistical Change Detection using the Budyko Framework

We found that all 17 catchments in our study adhered reasonably well to their respective Fu-type Budyko curves in the pre-fire period (1982–2003), with mean absolute error of the Budyko fits generally < 0.1 units of EI (Table 2-2) and the Fu ω values ranging from 2.0–10. In an analysis of 1000 catchments across the U.S., Rice and Emanuel (2019) concluded that catchments with large inter-annual changes in storage deviate below the original Budyko curve (see Appendix A Section A1.4; Figure A-1). Thus, the strong adherence of our data to the Budyko curves in the pre-fire years suggests that the assumption of hydrologic steady state at the annual timescale is appropriate in these catchments. Furthermore, Rice and Emanuel argued that catchments with higher Fu ω values that were closer to the ω of approximately 2.8 for the idealized Budyko curve deviate the least from hydrologic steady state at the inter-annual time scale. Given that our ω values (median ω = 2.6; Table 2-2) were at the higher end of the range of values explored by Rice and Emanuel, it is thus reasonable to also assume steady state in our analysis.

While the pre-fire year EI data strongly conformed to the Budyko curve, strong vertical deviations were apparent in the postfire years in the burned catchments, but not in the unburned catchments (Figure 2-3). The deviations in the burned catchments fell below the Fu-type curves for several years

after fire–indicating an increase in streamflow–possibly due to loss of vegetation and alteration of the surface soils during the fire. We also see that for the two least burned catchments, B6 and B7, there is very little deviation in Budyko space. These were the burned catchments with a burned area ratio (BAR) of < 20%, while the other burned catchments had BAR ranging from 45–97% (Figure 2-2e). These results suggest that the Budyko framework was able to qualitatively distinguish between burned and unburned catchments.

Using the Budyko Deviation Approach (Section 2.1.1), we found statistically significant change in Budyko deviation (Figure 2-4a) for five of the highly burned catchments (B1–B5, BAR >40%), while catchments B6 and B7 (BAR <25%) experienced insignificant deviations. The magnitude of the Budyko deviations Δd ranged from 0.07 for catchment B3 to 0.16 for catchment B1 (average value 0.12). In contrast, for the unburned catchments, there were no significant deviations in Budyko space, and the magnitude of Δd was much smaller (Figure 2-4a).

The significantly larger Δd values in the burned catchments compared to the unburned catchments highlights the ability of this approach to detect the effect of fire. Using the Covariate Modelling Approach (Section 2.1.2), we modelled the EI time series using the climate co-variate and the intervention effect, which was characterized by the parameters m and k, controlling the fire effect size and recovery time, respectively. We found that the m parameter was significant at the 10% confidence level for catchments B1–B5. The magnitude of m was also much higher in the five most highly burned catchments B1–B5 (average 0.21) compared to the two least burned B6–B7 (average -0.02) and unburned catchments (average -0.01; Figure 2-4b). Indeed, where m was small it was also not significantly different from zero in the two less burned and unburned catchments. An increase in the magnitude and significance of the m parameter in the five highly burned catchments highlights the effectiveness of the Budyko framework in statistical change detection post-fire. Having confirmed our hypothesis using two approaches (significance of Δd and m) we sought to test whether more traditional approaches of change detection could parse the same effects.

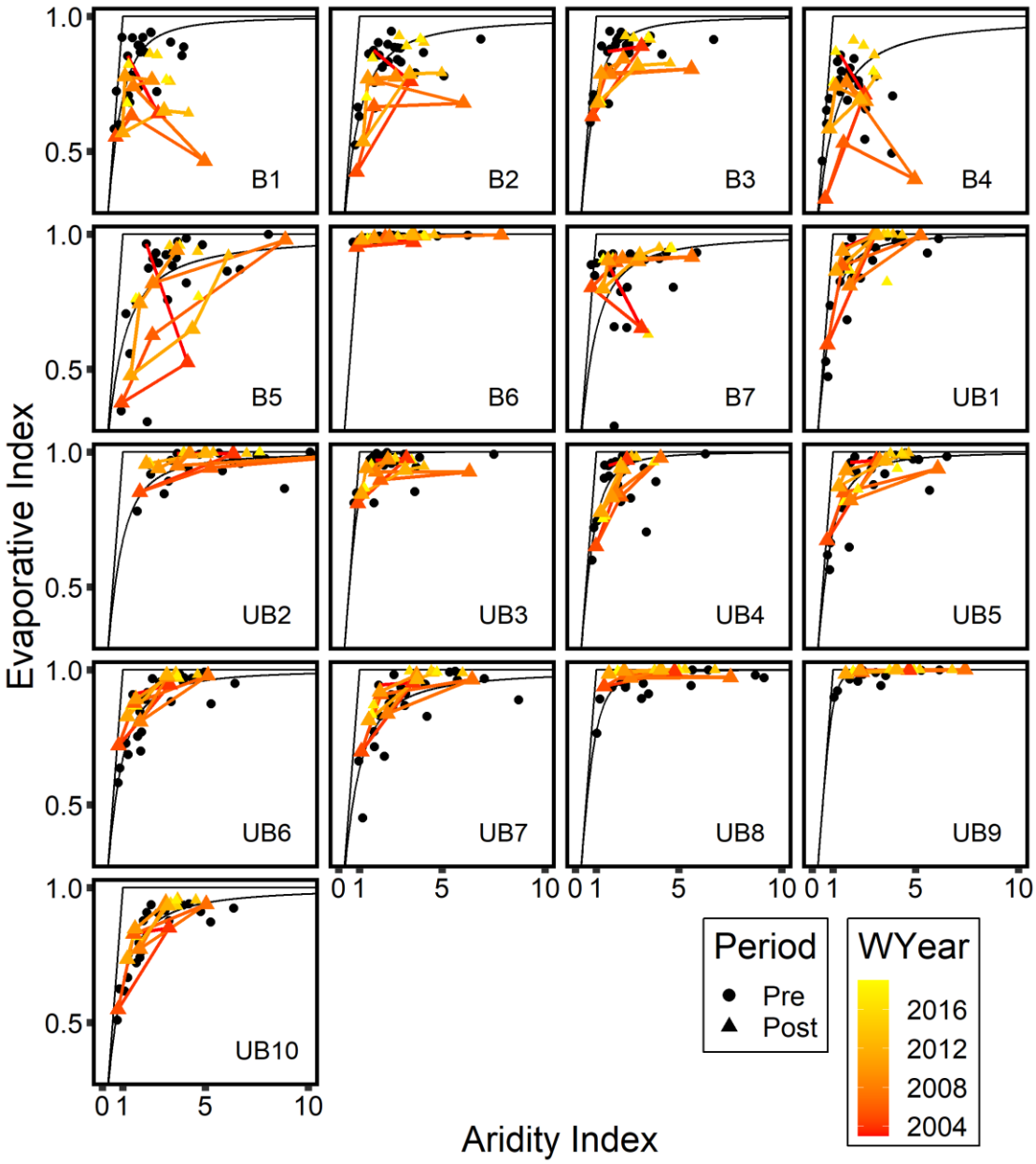

Figure 2-3. Budyko Curves Post-Fire. Time series of pre- and post-fire (pre-/post-WY 2004) evaporative index (EI) versus aridity index (AI) for 8 burned (B) and 10 unburned (UB) catchments. Points from water year (WY) 1982 to WY 2003 are in black, and the Fu curve (solid line) is derived from these data (22 years). Points from WY 2004 to WY 2018 are color coded by year and connected by lines for the first 10 post-fire years. The site id (Table 2-1) is included in the lower right of each plot.

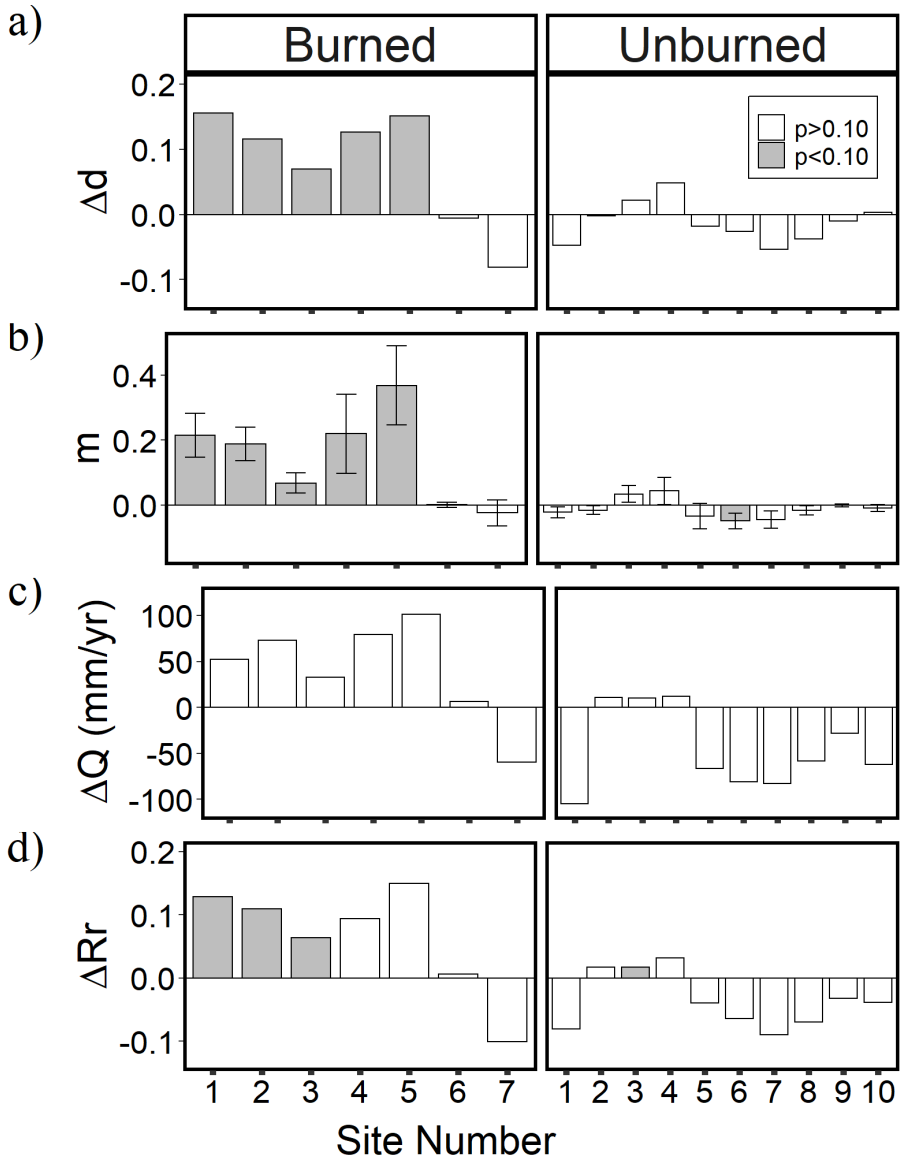

Figure 2-4. Hydrologic changes post-fire. Average change or hydrologic variables between the equal-length pre- (1994-2003) and post-fire periods (2004-2013). a) Change in the vertical Budyko deviation *d* ($\Delta \boldsymbol{d}$; Equation 2-4). Positive $\Delta \boldsymbol{d}$ deviation represents downward movement (lower AI) in Budyko space (see Figure 2-3). b) Parameter m (± std. error) fit to the intervention models described in Section 1.3.3 (Equation 2-3). c) Q change ($\Delta \boldsymbol{Q}$; Equation 2-5). d) Runoff ratio (Rr) change ($\Delta \boldsymbol{Rr}$; Equation 2-6). Box fill is shaded according to p-value. For panels a, c, d, the p-value is from a K-S test indicating a significant difference between the sample distributions, with a one directional alternative hypothesis. In panel b, the p-value is for the parameter provided by the *nls* fit.

2.5.2 Method Comparison to Traditional Approaches

As stated above, the much-preferred BACI approach is difficult to apply in wildfire-impacted catchments due the unpredictability of large fires. Still, many studies have used the wealth of data in the U.S. to analyze pre- and post-fire streamflow data to assess changes in Q and Rr (Blount et al., 2019; Hallema, Sun, Bladon, et al., 2017; Hallema, Sun, et al., 2018; Kinoshita & Hogue, 2011, 2015; Saxe et al., 2018). We observed similar magnitudes of average streamflow changes (ΔQ) between the burned and unburned sites, ranging from -38% to +98% (-60 to +100 mm yr^{-1}) in the burned catchments and ranging from -92% to +120% (-100 to +60 mm yr^{-1}) in the unburned catchments (Figure 2-4c). Furthermore, none of the changes in either the burned or unburned catchments were statistically significant (p-value >0.10; Figure 2-4c). This highlights that the flow changes observed were most likely driven by climatic changes in the post-fire years, and that metrics like the mean streamflow change is not always adequate to isolate the effects of fire driven due to climatic variability. Indeed, annual P was lower in the 10 years after WY 2004, corresponding to increased aridity, for many of the catchments (Figure A-7). This reduced P resulted in lower streamflow that confounded our ability to detect fire-driven increases in streamflow from climate driven decrease. Indeed, the climate and the streamflow are so variable between years in this ecozone that detection of any significant change is difficult. Thus, any change attribution method relying on the detection of a significant Q change point will conclude incorrectly that fire had no effect in these catchments. Possibly the most common metric that has been used for detecting changes following wildfire, or any other disturbance, is the runoff ratio (Rr; e.g. Biederman et al., 2015; Bladon et al., 2019; Blount et al., 2019; Kinoshita & Hogue, 2015). We found the differences in Rr to be somewhat more sensitive for comparison between the pre- and post-fire periods. Rr for Devil Canyon Creek (B1, USGS gage 11063680) experienced a significant increase at the 1% confidence level, while catchments B2 and B3 experienced a significant increase at the 5% level (Figure 2-4d). Notably, in their study of catchment B1, Kinoshita & Hogue (2015) observed increases of Rr of similar magnitudes as ours for Devil Canyon Creek. According to our calculations, all other changes in Rr in burned and unburned catchments were statistically insignificant, except for a small increase of 0.02 units for catchment UB3 (p=0.08). Thus, only three of the seven burned catchments show a statistically significant increase in the distribution of runoff ratios between the pre-fire and the post-fire periods, while almost all of the unburned catchments showed no statistically significant difference. This highlights the challenges in detecting significant changes in this ecozone with high climate variability. The

distribution of streamflow values showed no significant differences between pre-and post-fire periods, while the runoff ratio was only able to detect change in three of the most burned catchments. In contrast, the Budyko metrics Δd and m increased significantly (i.e. decreased EI attributed to disturbance) for the 5 most highly burned sites. Thus, in moving from a series of annual discharge data and runoff ratio to Budyko deviation we increased the detectability of the disturbance effect in the hydrologic time series.

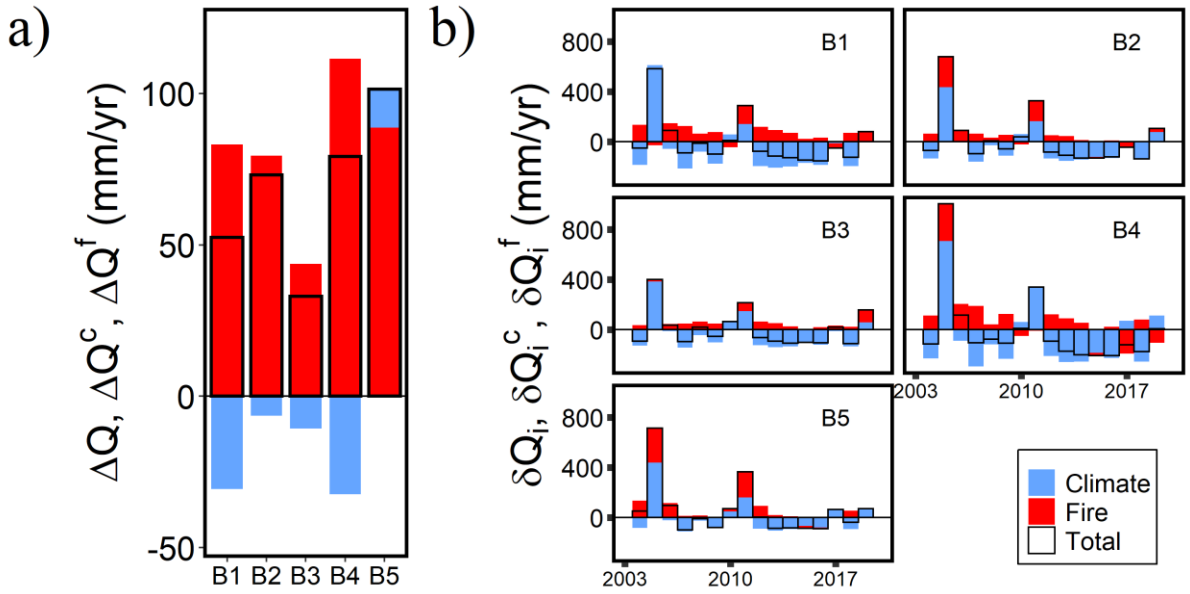

Figure 2-5. Flow changes between pre- and post-fire periods. a) $\Delta \boldsymbol{Q}$ (black bars) broken down into fire ($\Delta \boldsymbol{Q^f}$) and climate ($\Delta \boldsymbol{Q^c}$) components (see Equations 2-7 to 2-9). b) Single-year flow changes in all post-fire years relative to the 10-year pre-fire mean, broken into the total change ($\boldsymbol{\delta Q_i}$, black) and climate and fire components ($\boldsymbol{\delta Q_i^c}$ and $\boldsymbol{\delta Q_i^f}$; Equations 2-13 to 2-15).

2.5.3 Quantifying the Contribution of Fire and Climate to Streamflow Change

Next, we used the Budyko decomposition method to isolate the contributions of fire and climate to the annual Q time series. We focused on catchments B1–B5 since no significant changes were observed in B6 and B7. We used the movement of points along the Budyko-type curves as the climate component (Equation 7), and the vertical Budyko deviations captured by the d values as the fire component (Equations 8–9). Across catchments B1–B5, fire resulted in average increases in flow (ΔQ^{f}) ranging from 43–111 mm yr^{-1} (Figure 2-5a). In catchments B1–B4, the post-fire years were drier than the pre-fire years (P decrease ranged from –35 to –110 mm yr^{-1}; Figure A-7), and thus climate contributed to a decrease in flow in the post-fire years, with ΔQ^{c} ranging from –6 to –30 mm yr^{-1} (Figure 2-5a). The larger values of ΔQ^{f} compared to ΔQ^{c} translated to net flow increases (ΔQ) from 30 to 80 mm yr^{-1} across catchments B1–B4 (Figure 2-5a). In contrast, in catchment B5, mean rainfall was not significantly different between pre- and post-fire years, and thus both climate and fire led to increases in flow (Figure 2-5a). It is important to note that the contribution of fire to streamflow is estimated as the difference between the vertical Budyko deviations between the pre-fire and the post-fire years, and thus the analysis implicitly considers climate and other factors that contribute to deviations in the absence of fire.

The contributions of fire and climate to streamflows varied between wet and dry years (Figure 2-5b). In wetter years (WY 2005; 2 years after fire), climate controlled most of the change in flow. This is possibly because in these very wet years the rain events were so large that soil saturation and overland flow overwhelmed the effect of the reduced evapo-transpiration rates due to vegetation mortality. Coombs & Melack (2013) studied the same region as this study and found that in WY 2005 annual runoff was not dissimilar between burned and unburned catchments. In the two wettest years, WY 2005 and WY 2011, climate amplified the effect of fire (i.e. both fire and climate effects were positive) for most of the catchments. In contrast, for the drier years (WY 2004, WY 2006–2010, WY 2012–2016), we found the effects of climate and fire to be of similar magnitude, with climate often counteracting the effects of fire (Figure 2-5b). In these years, the net change in flow is often negative (dark black bars), and thus not accounting for climate makes it appear that fire has led to a decrease in flow. Herein lies the strength of our method that decouples the climate from the fire signal and allows us to understand how these two components amplify or counteract each other in wet and dry years.

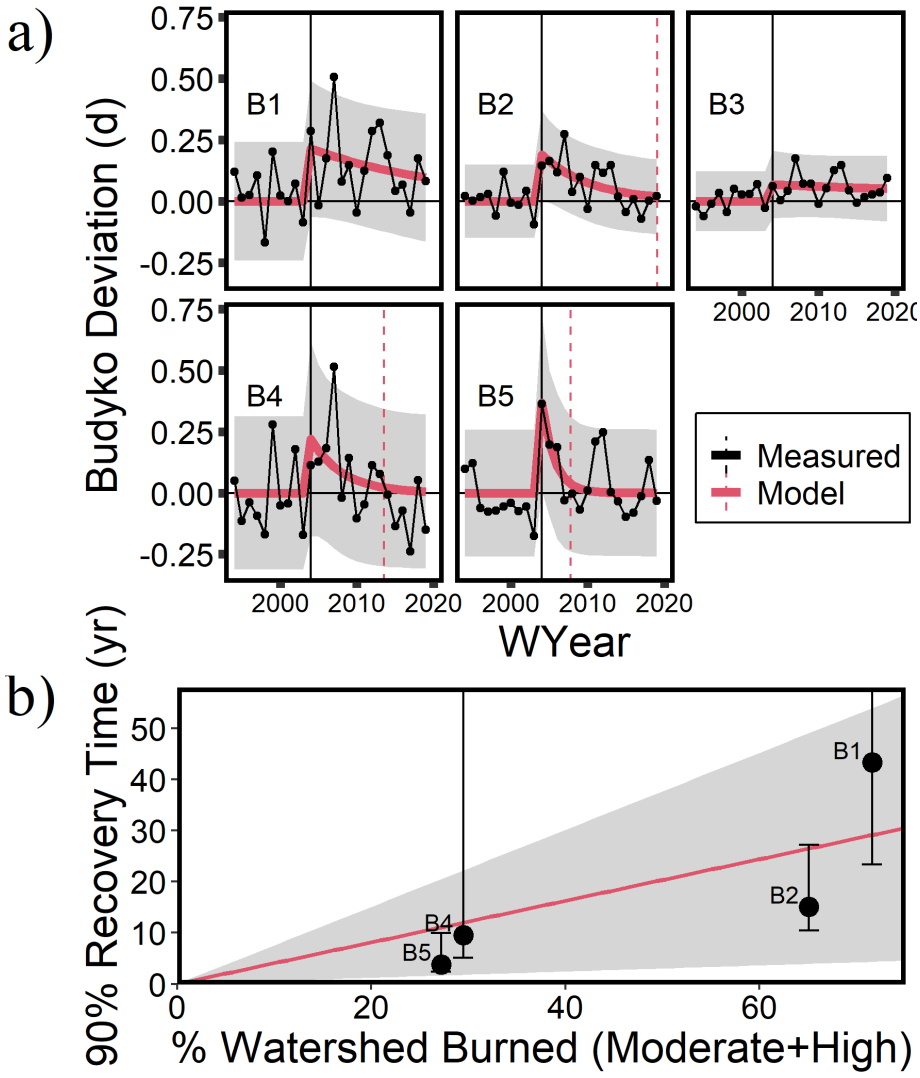

Figure 2-6. Hydrologic recovery. Recovery trends for 5 burned catchments which experienced significant Budyko deviations (see Figure 2-4). a). Annual deviation time series (black points and lines) and modelled $\boldsymbol{d}$ (solid red line; Equation 2-3). Model 95% prediction intervals are shown as a gray shaded area. Vertical red dashed line is the predicted 90% recovery time. b) 90% Recovery time ($\mathbf{log}(\mathbf{0.1})\,/\boldsymbol{k}$) over catchment percent area burned at moderate and high severity. The regression slope (red line) is 4.0 ± 1.1 yr per 10% burned (p-value=0.03, R^2=0.76). B3 is excluded from panel b because the estimate of $\boldsymbol{k}$ was very small (see panel a), and thus the recovery time was extremely large and uncertain.

Of course, while the differences between the wet and dry years are apparent from the results, there are further nuances in the year-to-year relative contributions of fire and climate across the five catchments. These differences are affected by local scale factors such as rainfall seasonality, adjacency of the fire to the stream (e.g.; Bart, 2016; Bart and Tague, 2017), subsurface geology, etc. that is beyond the scope of current work. In the next section, we explore whether we can quantitatively evaluate the recovery of this hydrologic disturbance effect to pre-fire conditions.

2.5.4 Quantifying Hydrologic Recovery Timescales

The annual data from the 5 most burned catchments show significant deviation from pre-fire conditions (Figure 2-4). Figure 2-3 shows that for many of the burned catchments, annual points appear to gravitate back to the pre-fire Budyko curve after several years of strong deviations. Figure 2-6a shows the time series of d for the five most burned catchments, and the modelled values of d (using Equation 3). This decaying effect is apparent in the models for catchments B1–B2 and B4–B5, with varying recovery times back to pre-fire conditions. Catchment B3 did not experience a strong recovery pattern like the others (Figure 2-3,6a), and indeed had the lowest Δd effect size (0.07; Figure 2-4a) of the burned catchments with BAR >40%. The decay coefficients for the B1–B2 and B4–B5 models were transformed into recovery times as described in Section 2.3 ($t_{90} = \log(0.1)\,/k$). We estimated 90% recovery times as 43 years (confidence interval 23-298 years) for catchment B1, 15 (10-27) years for B2, 9.6 (5.1-85) years for B4, and 3.8 (2.3-9.9) years for B5 (Figure 2-6b). We estimated 90% recovery times as 43 years (confidence 23-298 years) for catchment B1, 15 (10-27) years for B2, 9.6 (5.1-85) years for B4, and 3.8 (2.3-9.9) years for B5 (Figure 2-6b). Bart and Tague (2017) used remotely sensed vegetation data to estimate vegetation recovery in catchment B2, and found a 90% recovery timescale of 8.8 years, which is slightly lower than our estimate of 15 years. It is important to remember, however, that vegetation recovery and hydrologic recovery can occur on very different timescales. Note also that B1 has the longest recovery time, and the greatest uncertainty in its estimate, given that we have only 15 years of data. In contrast, recovery time estimates for catchments B4 and B5 are more compatible with the timescales of analysis, and thus uncertainties are lower. While this is a promising approach to estimate recovery times across large scales with varying availability and quality of data, future work needs to focus on validating these estimates with longer timeseries of flow and vegetation data.

Analysis of hydrologic recovery times in post-fire landscapes is often limited by availability of long enough flow time-series after fire. This leaves considerable uncertainty of how long it can take for streamflow to recover after fire. Our longer recovery times are however not inconsistent with other studies using longer timeseries in the same region. A study using 66 years of streamflow data from the San Dimas Experimental Forest in California found that the effects of fire on streamflows can last as many as 20 years (Meixner & Wohlgemuth, 2003). Similarly, a recent study in the Pacific Northwest found no evidence of hydrologic recovery 35 years after fire (Niemeyer et al., 2020). In a recent review of hydrologic recovery after fire in Mediterranean climates, Wagenbrenner et al. (2021) found that among 38 burned study, 42% of sites recovered within 5 years after fire, while 5% of the sites had recovery times between 5-10 years. In contrast, 53% of the sites did not recover during the monitoring period of 4-10 years, making it difficult to estimate recovery times appropriately. In an analysis including catchment B2 from our study, Bart and Tague (2017) showed that the impact of fire on stream baseflow recession rates, and the recovery of this metric post-fire, were correlated with the impact on and recovery of vegetation in the stream riparian zone. These authors found that modelled post-fire vegetation recovery, with a 90% recovery timescale of 8.8 years, adequately predicted recovery of baseflow recession rates. Recovery timescales appear to be a function of type, intensity, and distribution of disturbance, as well as climatic factors, and these factors have not been significantly explored across systems.

2.5.5 Correlation of Effect Sizes and Burn Severity

For the 7 burned sites, we investigated whether BAR correlated with the average Budyko deviation for the 10 years post-fire (Δd). This relationship relatively weak (for B1–B7, p=0.07, R^2=0.41), and appeared to have no strength among the 5 burned catchments with significant changes in Δd (B1–B5, p=0.56). This lack of correlation is similarly found in the results of Saxe et al. (2018) and Hallema et al. (2018b), who also found little to no correlation between BAR and percent changes in flow. We did however see a threshold pattern where sites burned with more than 40% area showed significant Budyko deviations (B1–B5). Further in contrast to the lack of a relationship between BAR and effect size, we found a strong linear relationship between the recovery timescale and the percent of the watershed burned at moderate and high severity (Figure 2-6b, p=0.03). This recovery and burn relationship corresponded to a slope of about 4.1 years of recovery per 10% burned. Note in Figure 2-6b that there is uncertainty around the individual estimates of k and the corresponding recovery times

t_{90}, and there is large uncertainty around the linear regression itself. The longer recovery times of the watershed areas with greater BAR at moderate and high severity most likely arises due to the persistence of detectable effects in the streamflow signal that increases with increasing disturbed area. This pattern should be tested with larger populations of disturbed forested catchments. Further study should explore whether this hydrologic recovery is correlated to ground- or satellite-based measurements of vegetation recovery, or soil infiltration rates.

2.5.6 Limitations and Future Work

Evaluation of the effect of a disturbance like wildfire on hydrologic response is complex because of the significant year-to-year variability in flow, which makes the analysis extremely sensitive to the number of years of post-fire data that is available. Our analysis was based on a 16-year time series of post-fire data, and even though time series like Budyko deviation (d) have less variability than Q, AI, or EI, our statistical tests could still be influenced by the exact choice of years of data available. Our analysis would be increasingly robust to these climatic variations with increased data availability, but for this region of Southern California the high incidences of fire meant that we could isolate only a small timeframe that had only one fire in all the study catchments. Our estimate of hydrologic recovery timescale is limited by the small timeframe of postfire data, and the significant Budyko deviations over this time period. Future work could examine how these Budyko deviations dissipate over time, and whether catchments do indeed return to their pre-fire Budyko curve consistently. Capturing this effect statistically and correlating recovery with satellite products for vegetation indices and soil moisture would add more certainty to such findings.

Since we did not have access to site-measured data including P and radiation, we instead relied on large (4-kilometer) gridded spatial data for P and temperature to satisfy the requirements for the Budyko limiting our ability to capture gradients in climate variables over elevation and with respect to windward and leeward slopes. Further, access only to temperature data limited us in our choice of PET calculation methods. Nonetheless, we performed a comparative analysis in nearby data-rich catchments on whether using a temperature- versus radiation-based PET methods would affect the results of our Budyko analysis and found no significant difference between the two method groups (Appendix A2.1). However, future estimates could be refined with access to radiation data. Additionally, we rely on the assumption of hydrologic steady state at the annual time scale. However, as we have argued in Section 2 of this paper, given that recent studies have provided evidence of the

Budyko curve being applicable at the interannual timescale, this is a reasonable assumption. Furthermore, we find that our catchments have high Fu ω values, and the Budyko curve can capture the interannual variability in data reasonably well across a decadal timescale, proving as per by Rice and Emanuel (2019) that interannual changes in storage is not significant. Of course, there are significant changes that occur both to the vegetation and the soil properties in the post-fire period that might bring into question the validity of the Budyko assumption. However, our finding of the distinctly different responses in the Budyko space between the burned and unburned catchments highlights that the Budyko framework might still be adequate for use in change detection. Indeed, the Budyko Deviation Approach has also been used for change detection in other scenarios involving land use transition, for example conversion of prairies to cropland (D. Wang & Hejazi, 2011; Ye et al., 2012). That said, the thin soils and heavily faulted basement rocks in this area of California may facilitate changes in interactions with deep groundwater following fire, as discussed for Devil Canyon Creek (catchment B1) by Jung et al. (2009). In the future we could use improved satellite-derived ET products (e.g. Poon & Kinoshita, 2018) to specifically estimate any changes in storage, as P minus Q minus AET. All this highlights the need for continued intensive field studies of altered moisture fluxes and water storage at the landscape-scale after fire.

We used satellite-derived fire severity products (MTBS: Eidenshink et al., 2007) to quantify BARin each watershed, following the approaches of two recent large studies in the western U.S. (Hallema, Sun, et al., 2018; Saxe et al., 2018). However, these products have limitations in identifying differences in burn-severity between sites differing in pre-fire forest composition and structure (Harvey et al., 2019; Kolden et al., 2015). Future work would involve the use of more sophisticated satellite products for this purpose.

It is also important to note that the relationship identified between the burn severity and hydrologic recovery is specific to the five catchments analyzed in the study. Future work would involve expanding the analysis across larger geographic scales, similar to the work of Hallema et al. (2018b) and Saxe et al. (2018), to quantify the relative contributions of fire and climate to streamflow. We also acknowledge that many other on-the-ground factors could influence the relationship between fire and hydrologic change, including fire severity, fire proximity to the riparian area, and catchment topography, elevation, and geology (e.g. Feikema et al., 2013; Rust, Saxe, et al., 2019). Again, we stress the need for continued study at the local scale on how we can better characterize “high” or “low” severity, as an ecohydrological effect. Additionally, incorporation of other datasets such as

vegetation indices (e.g. Paci et al., 2017) may help characterize disturbance magnitudes and recovery timescales.

2.6 Conclusions

In this study, we developed a novel methodology based on the Budyko framework to quantify the relative contributions of climate and fire disturbance on annual streamflow time series, and we used this information to characterize hydrologic recovery timescales. This study moves us towards addressing some of the unsolved problems in hydrology summarized by Blöschl et al. (2019): "What are the impacts of land cover change and soil disturbances on water and energy fluxes at the land surface?" and what "causes spatial heterogeneity and homogeneity in runoff, evaporation, subsurface water and material fluxes [and their] sensitivity to their controls (e.g. aridity)?" Our results add to a growing number of studies documenting flow increases following wildfire. Importantly, we have added to a subset of studies that differentiate between climate-related flow changes and those attributed to forest disturbance, with the novel aspect of using the Budyko framework at the annual timescale, and explicitly quantifying the hydrologic recovery time.

In a study region like ours where annual P and AI were highly variable, due in large part to the El Niño-Southern Oscillation (Schonher & Nicholson, 1989), previous methods of comparing either annual streamflow or runoff ratio between pre- and post-fire years can be confounded by climate variability. We argue that while traditional metrics like changes in the mean annual flow and the annual runoff ratio were not statistically different between pre-fire and post-fire years (Figure 2-4c,d), the effect of fire (following water year 2004) manifested as statistically significant differences in the Budyko deviations in five of the most severely burned catchments (Figure 2-4a,b). Importantly, Budyko deviations were not statistically different for the unburned catchments between pre- and post-fire years, lending credence to the hypothesis that it was the fire in the burned catchments that led to the observed deviations. The Budyko Decomposition method, expanded upon in this study, allows us to collapse climate variability and explicitly isolate the effect of fire.

Analyzing 20 years of pre- and post-fire data, we showed that fire on the average increased flow by 80 mm yr^{-1} that was counterbalanced by a general drying over this time period and 10-20 mm yr^{-1} flow decrease due to climate alone. We then modelled the time series of EI and estimated hydrologic recovery timescales which ranged between 3 and 43 years in the study catchments. Although other studies have quantified effects of fires on streamflow, these have primarily focused on average effects

for 10- to 20-year time blocks between pre- and post-fire years. Here, we explicitly captured recovery timescales at an annual resolution. We showed persistence of Budyko deviations (d) out to past ten years post-fire (Figure 2-6a), and hydrologic recovery captured by the deviation series that correlated significantly with catchment burned area (Figure 2-6b). We found that for every 10% burned at moderate and high severity, hydrologic recovery was pushed back approximately 4 years (p=0.03). Thus, we showed that the Budyko framework can be used to decouple fire versus climate effects on streamflow patterns after wildfire, and to effectively quantify hydrologic recovery timescales.

Our finding of increased flow after wildfires, similar to the results of previous studies in the chaparral ecosystems of Southern California (Kinoshita & Hogue, 2011, 2015; Loáiciga et al., 2001; Meixner & Wohlgemuth, 2003), has significant impact with respect to water supplies. This could mean more water available to parched areas of the world, especially California, as noted by Meixner & Wohlgemuth (2003). However, as has been shown in numerous studies, flow increases are often accompanied by changing hydrologic signatures (e.g., flashiness, flood frequency), resulting in increased erosion, suspended sediments (Burke et al., 2013), as well as increased nutrient loads (Smith et al., 2012). All these threaten water security (D. A. Martin, 2016), almost certainly more than increased water supply might alleviate stress. Further, increased flows are generally transient and likely rob down-wind areas of precipitation from local evapotranspiration (Kirchner et al., 2020).

This is the first presentation of results demonstrating that the hydrologic effects and recovery from wildfire can be captured using the Budyko "decomposition" method (D. Wang & Hejazi, 2011). Deforestation studies involving forest harvesting far outnumber wildfire studies despite the hazards involved with fire. This use of open datasets to conduct this analysis could be leveraged to greatly enhance our understanding of the variety of hydrologic effects of forest disturbance including both harvesting and fire; and can be applied across arid to humid regions to differentiate climate forcings from disturbance-related changes in annual streamflow. Given the wealth of streamflow data available in the contiguous United States (Falcone, 2011; Falcone et al., 2010), there are countless opportunities to go "backwards" and reanalyze datasets with respect to nearby and relevant streamflow datasets, coincident with changes in land cover including wildfire, forest harvesting, and urbanization.

Chapter 3
Forest fire effects on stream water quality at continental scales: A meta-analysis

This chapter is a mirror of the following published article. References are unified at the end of the thesis.

Hampton, Tyler B., Lin Simon G.M. and Nandita B. Basu. "Forest fire effects on stream water quality at continental scales: A meta-analysis." *Environmental Research Letters*, May 2022. https://doi.org/10.1088/1748-9326/ac6a6c.

All data and codes are publicly available in the online Hydroshare repository: https://www.hydroshare.org/resource/537dc5206d584625b0fd28ea6b6872de/

3.1 Abstract

Forested watersheds supply over two thirds of the world's drinking water. The last decade has seen an increase in the frequency and intensity of wildfires that is threatening these source watersheds, and necessitating more expensive water treatment to address degrading water quality. Given increasing wildfire frequency in a changing climate, it is important to understand the magnitude of water quality impacts following fire. Here, we conducted a meta-analysis to explore post-fire changes in the concentrations of nitrogen (N) and phosphorus (P) species, dissolved organic carbon (DOC), and total suspended sediments (TSS) in 121 sites around the world. Changes were documented over each study's respective duration, which for 90% of sites was 5 years or fewer. We find concurrent increases in C, N and P species, highlighting a tight coupling between biogeochemical cycles in post-fire landscapes. We find that fire alters N and P speciation, with median increases of 40-60% in the proportion of soluble inorganic N and P relative to total N and P. We also found that fire decreases C:N and C:P ratios, with median decreases ranging from 60-70%. Finally we observe a "hockey stick"-like response in changes to the concentration distribution, where increases in the highest concentration ranges are much greater than increases at lower concentrations. Our study documents strong heterogeneity in responses of water quality to wildfire that have been unreported so far in the literature.

3.2 Introduction

Forested watersheds sustain a significant portion of the world's water supply needs (Dudley & Stolton, 2003; Rockström et al., 2014). The ecological functioning of many forest biomes is sustained by fire (McLauchlan et al., 2020), but fire can also degrade water quality in streams draining forested watersheds, and threaten water-provisioning ecosystem services (Emelko et al., 2011; Kinoshita et al., 2016). These services are under further threat as wildfire regimes across the planet continue to shift in frequency, extent, and severity (F. Li et al., 2018; Moritz et al., 2012; A. L. Westerling, 2006), partly in response to anthropogenic warming and climate change (Abatzoglou & Williams, 2016; Creed & van Noordwijk, 2018; Jain et al., 2021; Khorshidi et al., 2020; Seidl et al., 2017). This dual threat of climate change and unpredictable fire regimes demands greater understanding of the altered landscape processes after fire that can degrade downstream water quality, and impact the ability of water providers to produce safe drinking water (Emelko et al., 2011; Hohner et al., 2019; Robinne et al., 2021).

Decades of wildfire studies have highlighted the effects of wildfires on water resources, including modifications of the hydrologic cycle (Basso et al., 2020; Hallema, Sun, Caldwell, et al., 2017; Hallema, Sun, et al., 2018; Maina & Siirila-Woodburn, 2020), the geomorphic regime (Ice et al., 2004; Shakesby & Doerr, 2006), and element cycling and export (Basso et al., 2020; Bladon et al., 2008; Crandall et al., 2021; Emelko et al., 2016; Hauer & Spencer, 1998; McCullough et al., 2019; Mishra et al., 2021; Rust et al., 2018). While most studies of water quality in post-wildfire landscapes have focused on one or two key variables (e.g., sediments, nitrogen, phosphorus, and carbon), the few that have analyzed the coupling of multiple element cycles have allowed us to gain critical insights. For example, Noske et al. (2010) document how the fluxes of total phosphorus and suspended sediment were strongly linked post-fire in Australian streams. Similarly, in a Canadian Rocky Mountain stream, Emelko et al. (2016) observed how phosphorus speciation shifted after fire towards more bioavailable forms, while nitrogen to phosphorus ratios decreased, likely freeing stream biota from phosphorus limitation and facilitating algal blooms (Bladon et al., 2008; Silins et al., 2014). In an Arctic stream in Siberia, Rodríguez-Cardona et al. (2020) observed that decreasing dissolved organic carbon concentrations post-fire reduced nitrate uptake efficiency by stream biota, thus increasing downstream nitrate export. Another study by (Morales et al., 2013) measured soil and stream export of nitrogen, and showed preferential loss of nitrogen relative to carbon from the studied volcanic soils after fire. Coupled biogeochemical cycles in post-fire landscapes are likely key factors

that control downstream ecosystem responses, such as eutrophication and algal blooms, thus requiring further exploration.

While most studies focus on mean concentration changes after fire, drinking water treatability is often by extremes in precipitation, flow, and water quality. Wilkinson et al. (2006) documented that fire elevates the concentration of suspended sediment and phosphorus during rare high flow events. Indeed, short-term disturbances such as the annual spring flooding in many rivers along with larger post-fire floods and mudslides increase suspended sediment and pose a large and immediate challenge to drinking water treatability (e.g. post-fire flood events; S. F. Murphy et al., 2015, 2018; Writer et al., 2014). Even if the impact on water quality is short lived, extreme events may change the distribution of nutrients across a catchment, for example by creating a reservoir of fine-sediment-associated phosphorus in gravel bedded rivers (Emelko et al., 2016). More needs to be known of the behavior of water quality during extreme events after fire.

Finally, most studies of fire impacts on water quality have been site specific. Multi-site and multi-study analyses include a review paper by Bitner et al. (2001), a review paper (Smith et al., 2011), and a large data synthesis by Rust et al. (2018). Bitner et al. (2001) reviewed how multiple element cycles are altered by fire, including in soils, sediment-associated elements, and exported in streams. Smith et al. (2011) reviewed how fire altered stream water concentrations of suspended sediment, phosphorus, nitrogen, and turbidity across many studies. More recently, a study by Rust et al. (2018) analyzed a post-fire water quality dataset of 73 analytes in 153 burned watersheds in the western US. In a followup study, Rust, Saxe, et al. (2019) analyzed drivers of the post-fire water quality response, and found that the increase in nitrogen and phosphorus loads was related to the increase in the extent of the area burned at a moderate to high severity.

Here, we build on this body of research and use a meta-analysis approach to explore the interactions *between* element cycles in post-fire landscapes, and the effect of fire on the concentration distribution. Our specific objectives are to: (1) quantify the effect of fire on the changes in concentrations of suspended sediments, nitrogen, phosphorus and carbon species, (2) quantify the degree of covariation between the concentrations of these elements in post-fire landscapes, and (3) quantify the effect of fire on concentration distributions.

3.3 Methods

3.3.1 Meta-analyses

All data and code used in this study are provided in an online repository (Hampton, 2022b).We used keyword searches in the Scopus database (Elsevier B.V.), using the following search terms: (‘wildfire’ OR ‘fire’ OR ‘burn) AND (‘water’ OR ‘stream’ OR ‘river’ OR ‘runoff’ OR ‘discharge’ OR ‘export’) AND (‘chemistry’ OR ‘treatment’ OR ‘supply’ OR ‘nutrient’ OR ‘nitrogen’ OR ‘carbon’ OR ‘phosphorus’ OR ‘quantity’ OR ‘water quality’) to isolate publications specific to detecting water quality trends in relation to forest fire. The search was applied to the Title, Abstract, and Keywords of the papers. The search was conducted in August of 2019, and returned 155 publications (Table B1) that were further screened using the following criteria: (1) the study focused on water quality in streams following wildfires (not on soil-water solute concentrations, nor on lakes), (2) the study measured at least one of the following water quality parameters: nitrogen or phosphorus in organic (e.g. dissolved organic nitrogen DON), total (e.g. total nitrogen TN, total phosphorus TP), or inorganic forms (e.g. nitrate NO_3^-, ammonium NH_4^+, phosphate PO_4^{3-}); organic carbon (DOC), or total suspended sediment (TSS), (3) studies that specifically referenced the use of fire suppressants or chemical fertilizers on the landscape were excluded, to remove their possible chemical influence.

The meta-analysis presented in this paper draws data from 34 publications, and includes data from both wildfires and prescribed burns. Locations of the studies are shown on a world map in Figure 3-1, with a total of 121 unique watersheds. The United States has the most studies (20), followed by Australia (6) and Canada (5). Other study locations included Portugal, Spain, and South Africa. It is notable that since August 2019, numerous papers on these topics have been published, representing increased geographic diversity. Future examination of this literature will be able to minimize the bias of studies towards the United States, Australia, and Canada.

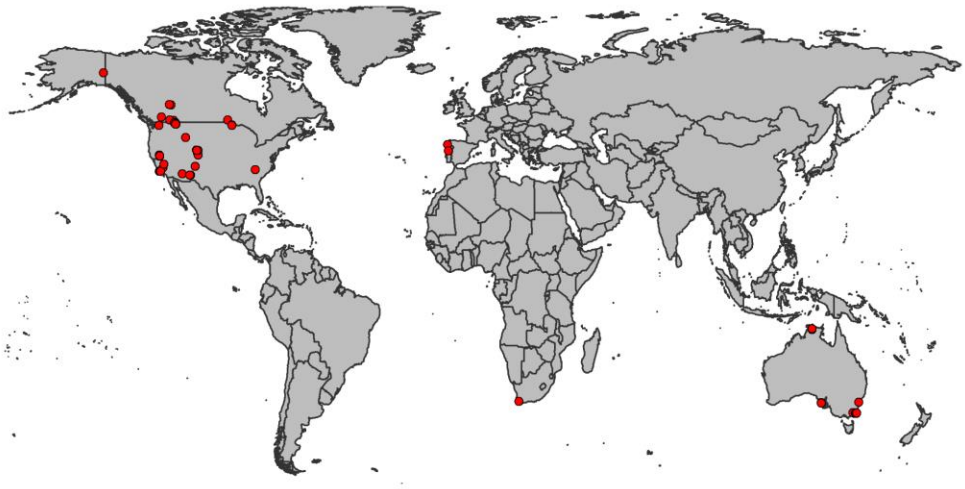

Figure 3-1. Locations of 121 watersheds from 34 studies in the metaanalysis.

3.3.2 Data extraction and Harmonization

Data were either extracted from tables or figures in papers. We used WebPlotDigitizer version 4.2 (Rohatgi, 2019) to extract data from figures. We also recorded study metadata for the dates of fires, so that concentrations can be compared temporally to the fire occurrence. Where graphical data were not included, data were extracted from tables in studies that reported either average pre- and post-fire concentrations of water quality constituents, or annual or monthly values. The majority (19) of studies used data from reference, unburned catchments to compare to data from burned catchments, and these are hereafter referred to as control-impact studies. A smaller group of studies (11) relied exclusively on comparison of pre- and post-fire data, and these are hereafter referred to as before-after studies. In a much smaller subset of studies (4) there was both before-after data, though this was sometimes limited to only certain water quality constituents. When both were present for one variable, we opted to compare fire effects using the control-impact axis. We normalized all concentration units to mg/L (e.g. mg P/L, mg N/L and mg C/L). We assumed "filterable reactive phosphorus", "soluble reactive phosphorus", and "phosphate" to functionally measure the same thing (PO_4^{3-}). Likewise, we assumed that "oxidized nitrogen" was the same as NO_3^-.

3.3.3 Metrics and Statistical Analysis

We used several different metrics and normalization strategies to evaluate the effect of fire on the water quality variables across the 81 burned sites. The change metrics used in this study are the change ratio (CR) of mean concentrations (CR_M; (Hedges et al., 1999; Rosenberg et al., 2013), change ratio of the coefficient of variation (CV) of the concentration distribution (CR_{CV}), Absolute Change (AC), and the decile normalized change (dNC). We used CR instead of more sophisticated metrics like the "Hedge's d" since the latter requires estimates of the variance of water quality concentrations pre- and post-fire, and a large proportion of our sites did not have enough data to reliably estimate a variance (Borenstein et al., 2009).

We define CR_M as the ratio of the mean concentration in the burned to the control catchment for the control-impact studies, or the ratio of the mean concentrations in the post-fire to the pre-fire periods for the before-after studies. This metric was calculated using averaging across all years (CR_M), the first five years (e.g., CR_MYr1-5), and for the first year in the dataset (e.g., CR_MYr1). A CR value of 1 indicates no change, while a value of 10 signifies ten-fold higher concentrations after the fire relative to the average reference concentration. We define CR_{CV} as the ratio of the coefficient of variation (CV) of the concentration in the postfire period to the CV in the prefire period. Here, CV is defined as the ratio of the mean concentration to the standard deviation in the concentration deviation. The CR_{CV} metric was estimated only for sites with more than three samples in each of the reference and burn periods.

We assessed correlation between co-measured change ratios of different parameters. This analysis relied on sites that measured multiple parameters, and on having sufficient data (at least 4 points) to assess the relationship between parameters across sites. We used the non-parametric Kendall's rank correlation to identify significant relationships. KRC allows us to assess the statistical significance of monotonic relationships, and accounts for relationships that may not be strictly linear in shape. KRC also rules out relationships that are heavily biased by large-value outliers, which may cause the linear relationship to be statistically significant, where KRC is not.

The change ratio metric does not capture either the effect of fire on concentration extremes, or the decrease in concentrations in the years post-fire. Ideally, evaluation of the effect of fire should take into account both these factors; however data is often not available at a fine enough temporal

resolution for such analysis. Given that 90% of our sites had data for <5 years, we analyzed the effect of fire on concentration extremes, but did not explore the recovery effect in this study.

To evaluate the effect of fire on concentration extremes, we developed a methodology using concentration decile curves. For this, we isolated a subset of studies where data was available at a higher temporal resolution (at least ten samples in the pre- and post-fire periods). The methodology is illustrated in Figure 3-2 using data from one burned and reference catchment pair (Bladon *et al.*, 2008)(Figure 3-2a). We grouped the two time series into deciles, and estimated the decile specific mean concentration for the reference and burned catchments(Figure 3-2b). We then estimated the decile-specific Absolute Change (dAC; Figure 3-2c) by subtracting the decile-specific mean concentration of the Burned (red line in Figure 3-2b) catchment from the corresponding mean concentration of the reference catchments (blue line in Figure 3-2b). Finally, we divided the dAC for a site by the absolute change (AC) for that site across all concentrations to estimate the decile normalized change (dNC) (Figure 3-2d). The absolute change (AC) is estimated by subtracting the mean concentrations of the reference period from the mean concentration of the burned period. The decile normalized change (Figure 3-2d) showed a distinct "hockey stick" pattern, where at higher deciles (9 or 10) there was the largest increase in concentration. A benefit of our decile-based analysis is that we can accommodate sites with unequal numbers of burned and reference samples. This altered ratio allows us to compare across sites, where total changes range widely in magnitude along with the reference concentrations.

3.3.4 Attribution Analysis

We conducted an analysis of catchment predictor variables and the water quality response variable CR_M. Predictor variables included burn type (natural or prescribed), fire intensity (low, medium, high), percent catchment burned, catchment area, average concentration during the control period, and catchment slope. Studies were unreliable in providing climatic context of their catchments, so we estimated the aridity index for each catchment from a global raster dataset (Trabucco & Zomer, 2018). Relationships were only analyzed if at least 20 catchments had corresponding variables. Correlation between continuous variables was tested using Kendall's rank correlation, while response variables were compared with categorical predictor variables using the Kruskal-Wallis test. Both methods were used from the using the "stats" package in R (R Core Team, 2023). Following the methods of (Rust, Saxe, et al., 2019), conditional inference trees were used to

determine whether any response variables had threshold responses to the predictor variables. We used the ctree function from "partykit" (Hothorn et al., 2006).

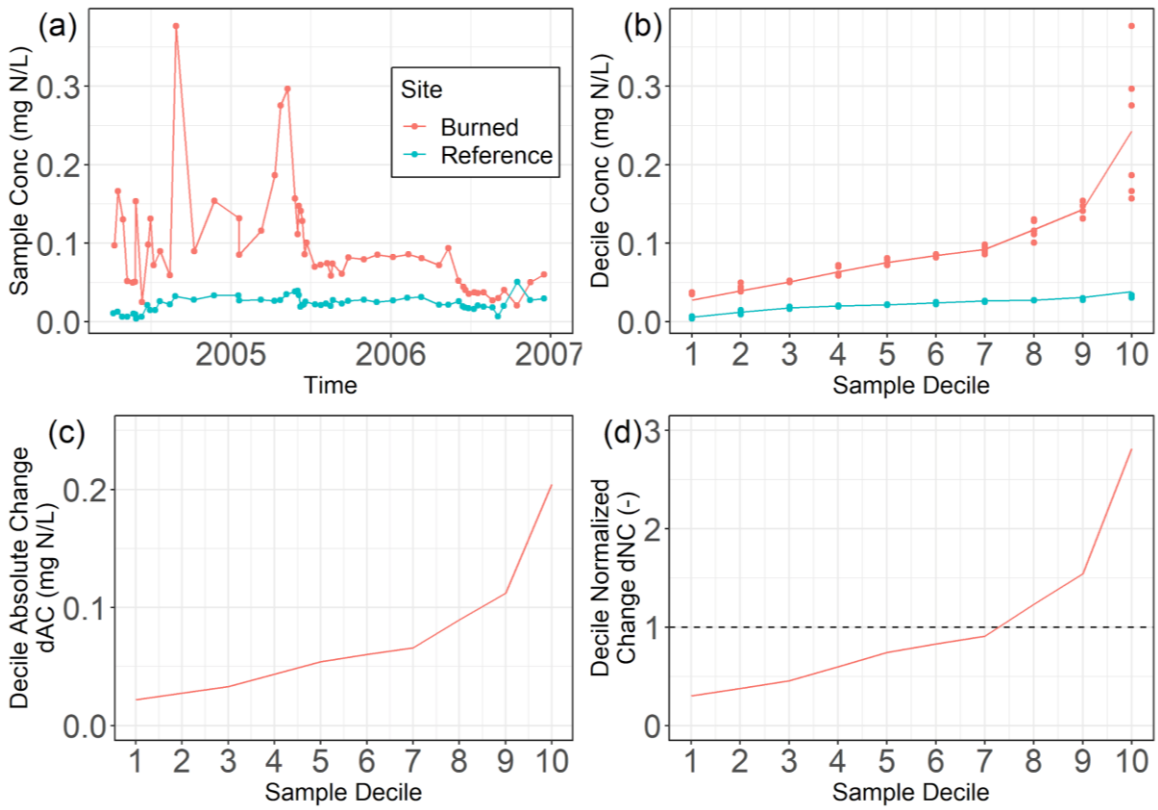

Figure 3-2. Example workflow. Nitrate data from Bladon et al. (2008) was used to calculate the Decile Normalized Change (dNC) Burned site data is in red and reference site data is in blue. The original time series data (a) is sorted by sample rank and then binned into deciles (b). The mean of each decile bin is taken (blue and red lines in b) and the reference is subtracted from the burned value for each of the ten deciles to estimate the absolute decile change (dAC in c). The dAC is then divided by the total average change (here, AC~0.07 mg/L) to calculate the decile normalized change (dNC in d).

3.4 Results and Discussion

3.4.1 Study Metadata

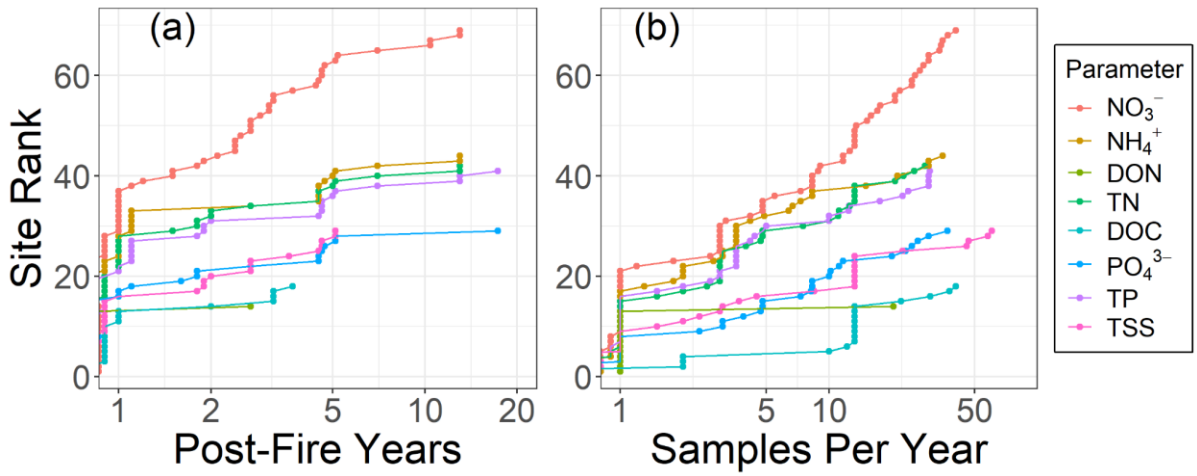

Figure 3-3. Study Metadata. Burned sites (n=81) are rank-ordered based on (a) number of post-fire years of data and (b) samples per year. Nitrate has the most sites with over 5 years of post-fire data, as well as the most sites with over 10 samples per year.

Our meta-analysis identified 34 studies distributed around the world (Figure 3-1; Table B1) that represented data from 121 unique study catchments (of which 81 were burned). Catchment slopes ranged from 0 to 70% (median 20%), catchment area ranged from 0.04 to 10^5 hectares (median 3500 ha), and annual precipitation ranged from 18 mm to 3300 mm (median 820 mm) across our study sites (Table B2). The most commonly sampled parameter was NO_3^- (at 67 of 81 sites; Figure 3-3a; Table B3), followed by TP (41), TN (31), NH_4^+ (30), TSS (26), PO_4^{3-} (20), DOC (17), and DON (14). While not used further in this meta-analysis, the diversity of other parameters was notable: 14 studies sampled for major cations (incl. K, Ca, Na, Mg), 10 for pH, 5 for dissolved O_2, 4 for other dissolved metals (incl. Fe, Mn), and 3 for dissolved organic nitrogen (DON). Only 47% of sites had more than 1-year of data post-fire, with the greatest data density for NO_3^- (Figure 3-3a). Further, only 9% of sites sampled beyond 5 years after the fire. This highlights the propensity of wildfire studies to focus on collecting samples over a short timeframe, making it challenging to evaluate recovery times.

Studies also had a very wide range in the number of samples collected, with sampling frequency ranging from 1 to over 50 samples per year. Figure 3-3b highlights the wide range of sample

numbers, with NO_3^- having by far the most studies and about a quarter of studies having greater than 10 samples per year. For most parameters, about half of sites had a sample density of 10 samples or greater per year , with notable data deficiency for NH_4^+, DON, TN, and TP (Figure 3-3b).

3.4.2 Concentration changes between pre-fire and post-fire periods

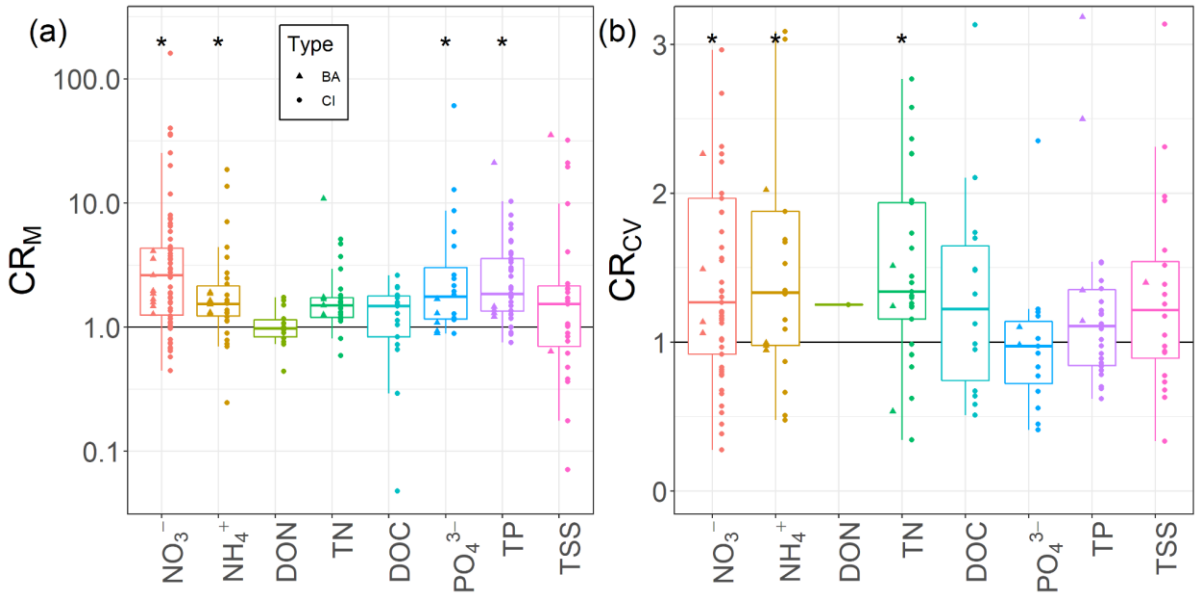

Figure 3-4. Post-fire changes. Change Ratios for (a) mean concentration change (CR_M) and (b) change in CV (CR_{CV}). A change ratio of 1 indicates no change. Each point is one burned catchment site, with study type represented as shapes (before-after as triangle, control-impact as circle). Boxplots are shown for all before-after and control-impact sites combined. The numbers of sites with data per parameter are included in Table B3, with means and medians of the change ratios in Table B4. Stars above each parameter indicate that the population of change ratios has a mean significantly ($p<0.05$) different from 1 (t-test performed on the log of change ratios).

Most sites documented an increase in concentrations across the constituents analyzed, with a median CR_M of 2.1 for NO_3^-, 1.8 for TP, and 1.3 to 1.5 for NH_4^+, PO_4^{3-}, TN, DOC, and TSS (Figure 3-4a). The range of increases across sites was highly variable, with the highest ranges for CRs observed for NO_3^-, PO_4^{3-}, and TSS, while NH_4^+, TN, and DON had smaller ranges (Figure 3-4a). We found $CR_M < 1$ for about 38% of sites for TSS and 18% of sites for NO_3^-, indicating that for those sites post-fire concentrations were lower than pre-fire concentrations. Our documented CR_M values are similar to

those found by Rust et al. (2018) who synthesized data from a large number of wildfire-impacted catchments in the western US (Table B4).We tested whether study duration influenced CR_M by comparing the all-time CR_M (Figure 3-4) with CR_M based on the first five post-fire years of data (CR_MYr1-5). For all parameters, the distribution of the two values were indistinguishable ($p>0.8$, Wilcoxon Rank Sum test), and they were highly correlated (Pearson's $R^2>0.99$) (Figure B1).

We also tested whether the variability in the concentration distributions changed after fire by using the CR_{CV}. This analysis focused on a smaller subset of the data (Table B3) since all sites did not have adequate data to reliably estimate variance. The variability in concentrations increased for ~60-70% of the sites for NO_3^-, NH_4^+ and TN, but increased for 40-60% of sites for DOC, PO_4^{3-}, TP, and TSS. For NO_3^-, NH_4^+, and TN, there was a median 1.2 to 1.3-fold increase in CV post-fire, while PO_4^{3-} was the only parameter with CR_{CV} approximately 1 (Figure 3-4b). We tested whether CR_{CV} and CR_M for each parameter were correlated (Figure B2). In log-space, the correlation was positive and significant for NO_3^- ($p=0.05$, $R^2=0.08$), NH_4^+ ($p=0.003$, $R^2=0.38$), and DOC ($p=0.03$, $R^2=0.33$), suggesting increases in mean concentration also corresponded to increases in concentration variability.

3.4.3 Co-variation between elemental cycles in burned watersheds

We then analyzed relationships between the CR_M values of the various elements to understand how biogeochemical cycles interact post fire. Here, we focused only on a subset of the total dataset where data from multiple constituents was available (63 burned sites). The most data existed for sites co-measuring NO_3^--TP (30), then by NO_3^--TN (27), NO_3^--NH_4^+ (26), TN-TP (23), NO_3^--TSS (22), and TN-TSS (21). We found that constituents generally increased together after fire (Figure 3-5), and the CR_M values of multiple parameters were significantly correlated (Figure 3-5, Table B5). The most significant positive correlations (assessed by Kendall's rank correlation (KRC) and τ) were observed between TP and PO_4^{3-} CRs (slope = 0.30, KRC $p = 0.07$, $\tau=0.62$), and TN and NO_3^- CRs (slope = 0.36, KRC $p = 0.01$, $\tau=0.36$). The positive relationship between the dissolved and total N and P species suggests that similar source and flow pathways impact both dissolved and particulate elemental species. We also observed significant relationships between change ratio pairs DOC-TN (KRC $p<0.01$, $\tau=0.69$) and DOC-PO_4^{3-} (KRC $p=0.06$, $\tau=0.73$), highlighting the coupling between the C, N and P cycles. Finally, TSS showed insignificant correlation to all N, P and C species, except DOC (Figure 3-5; Table B3). No significant relationship was observed between TSS and TP, contrary

to other studies that have documented significant TP-TSS relationships (Froelich, 1988; Reddy et al., 1999; Romanya et al., 1994); (Noske et al., 2010)).

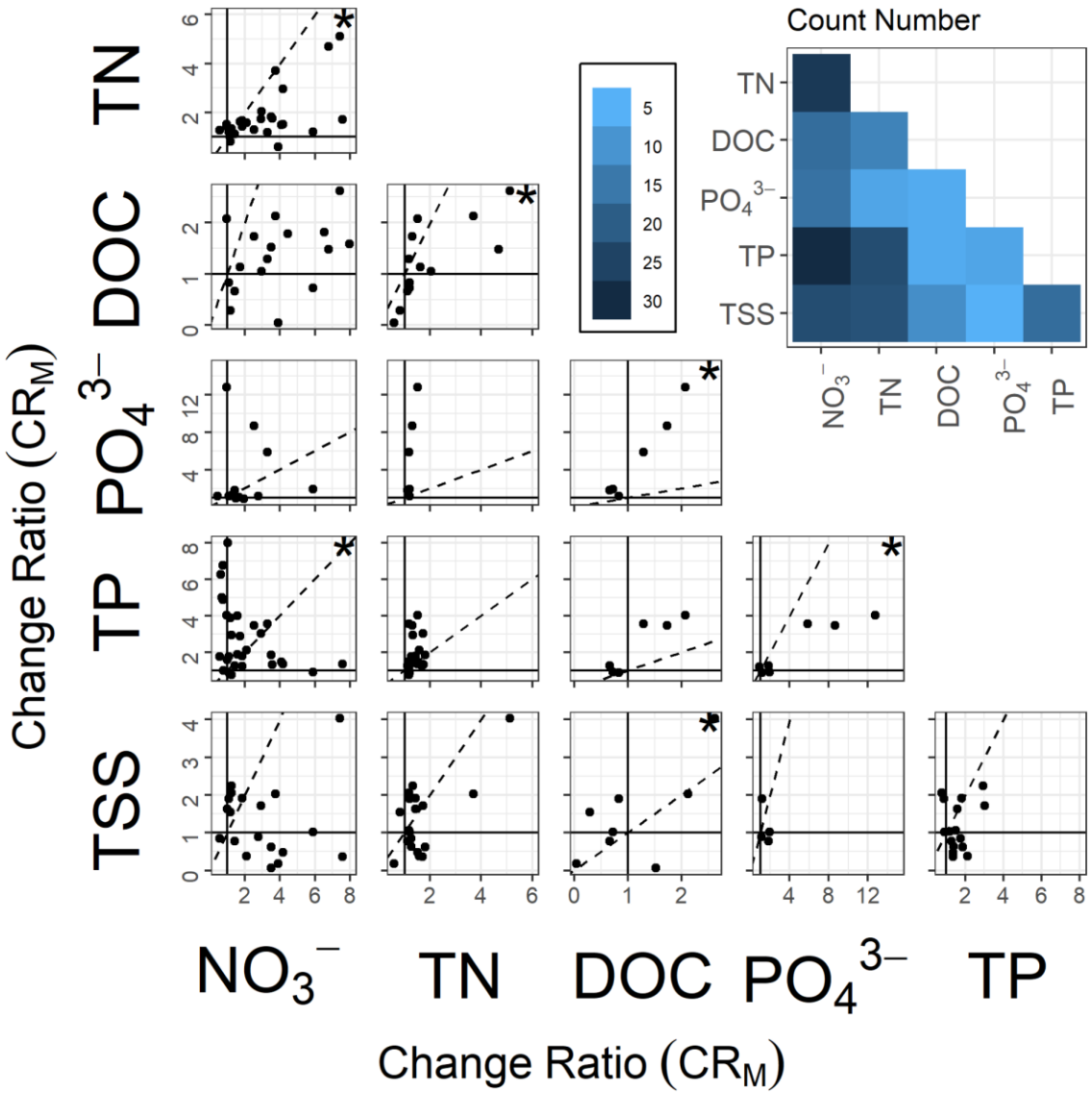

Figure 3-5. Comparison of CR_M for pairs of constituents between burned and reference conditions. There is one point for each burned-reference pair. CR_M=1 indicates no change. In each subplot, the black dashed 1-to-1 line is drawn. Kendall's rank correlation was measured for each relationship, and significant relationships ($p<0.10$; Table B5) are shown with a star in the upper right of each subplot. For all data (including NH_4^+ and DON) see Table B5. The upper right inset shows data availability for pairs of parameters.

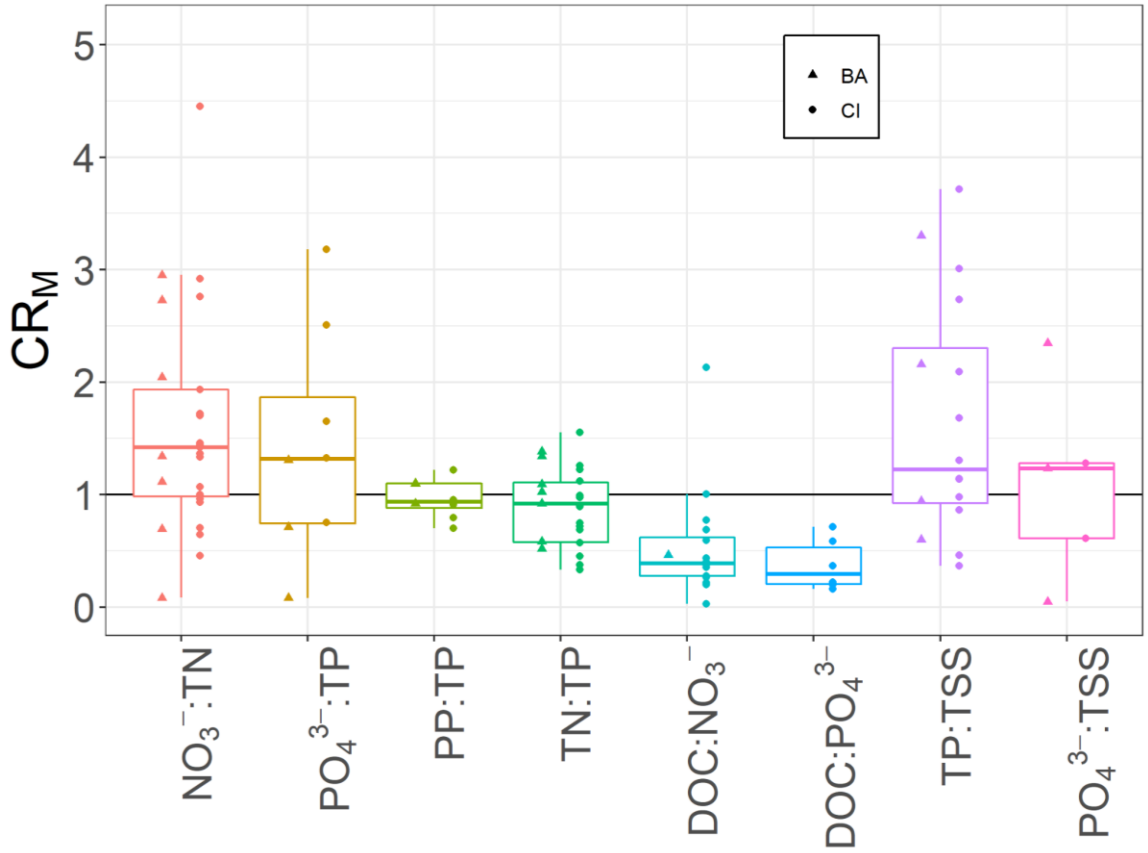

Figure 3-6. Change ratios (CR_M) for the nutrient ratios. A value greater than 1 indicates that the ratio of the two elements has increased post-fire compared to the reference. Data is presented as in Figure 3-4.

While significant correlations between the CR_M values highlight the coupling of the biogeochemical cycles, the slope of the relationship captures the relative proportions of the changes post-fire. For example, most points in the PO_4^{3-}-TP relationships (Figure 3-5) lie below the 1:1 line, implying that PO_4^{3-}-TP ratio increases after fire, with a median CR_M value of 1.3 post-fire (Figure 3-6). The results are similar for the NO_3^-:TN ratio where ~75% of the sites document a value of CR_M>1 after fire, with over 4-fold increases at one site, and a median value for CR_M of 1.4 increase across all sites (Figure 3-6).

Fire contributed to both increases and decreases in the TN:TP ratio across the sites analyzed, with a median CR_M of approximately 1 (IQR 0.57-1.1) (Figure 3-6). The TP:TSS ratio increased after fire, with a median CR_M of 1.3, which we attribute to an increase in the PO_4^{3-}-TP ratio (median CR_M=1.3)

and decrease in the PP-TP ratio (CR_M=0.93) post-fire (Figure 3-6). Finally, we found consistent patterns in the ratios of DOC-NO_3^- and DOC-PO_4^{3-} post-fire, with all sites exhibiting decreases in carbon to nutrient ratios post-fire.

3.4.4 Effect of fire on concentration extremes

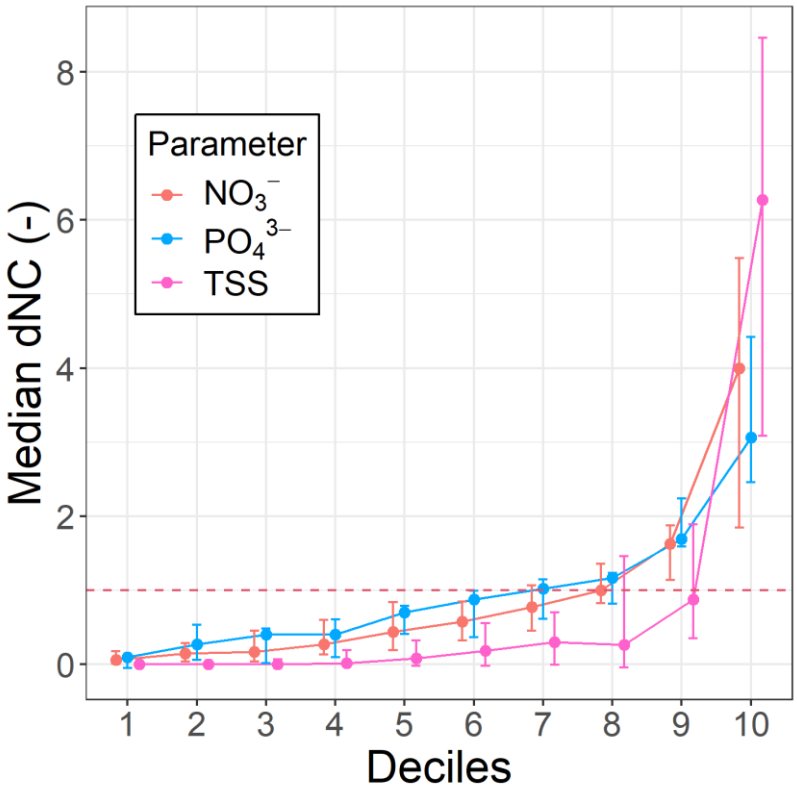

Figure 3-7. Decile changes. Following the example in Figure 3-2, for each burned site with sufficient data to calculate deciles, the decile normalized change (dNC) was calculated as the ratio of decile change (dAC) over total change (AC). For each parameter, the median value of dNC is shown with error bars representing the interquartile range. For all data, see Figure B3.

While the above analysis focused only on the mean change across the post-fire period, fire can potentially impact concentration extremes and this was visualized using concentration-decile curves. For this analysis we used a subset of the studies that had enough samples: 33 burned sites for NO_3^-, and 10-18 for TSS, TN, TP, DOC, NH_4^+, and PO_4^{3-}. The decile normalized changes (dNC) were aggregated across all sites to evaluate the effect of fire on concentration extremes (Figure 3-7). We find the "hockey stick" pattern that was apparent at a single site (Figure 3-2) to be apparent for almost

all parameters, and across all sites (Figure B3 for all sites). We find TSS to have the most dramatic effect, with the tenth decile concentrations increasing six times more than the mean increase across all sites, while the deciles lower than eight all recorded increases less than the mean increase. Again, this suggests that for all parameters the vast majority of the time, absolute changes (dAC) at high deciles (7-10) drive the magnitude of the site-specific change in the mean concentrations (AC). Looking at low-decile changes, values are either very close to zero or sometimes negative. This suggests that during periods when an unburned catchment would experience low concentrations, little change is seen during the same periods in burned catchments. More extreme behavior is observed at the higher deciles where the median 10th decile change for TSS is 6 times the average increase in TSS concentration, highlighting that the extremes in the concentration distribution show greater change in burned catchments. Finally, it is important to note that there is significant spatial variability between the sites, but the "hockey stick" persists across almost all sites (Figure B3). These documented increases in concentration extremes are important for drinking water treatment operators that have to plan for extremes in flow and concentrations after fire (Hohner et al., 2019).

One challenge in analyzing these data was the wide range in effect sizes, characterized as either dAC or decile Change Ratios (dCR; Figure B4). The normalized metric dNC significantly compressed variability, highlighting the importance of changes at high concentrations. That said, the use of Change Ratios throughout the rest of this study highlights benefits and some limitations of these metrics. CR can be highly influenced by small denominators in the fraction, thus inflating the metrics. For example, dCR values show indiscernible patterns across deciles (Figure B4), because as you decrease in decile, the concentration decreases and the dCR metric inflates. While different metric certainly have different uses, we are confident that the dNC provides a useful comparison of the magnitude of decile changes relative to total changes.

3.4.5 Attribution Analysis

The results of the attribution analysis were challenging to interpret, given the limited information available at the individual sites, and the high variability between the sites. CR_M for NO_3^- was negatively correlated with catchment area (Kendall's rank correlation tau Krct, $p<0.01$, $n=55$), possibly indicating dilution effects at larger catchment sizes. While CR_M for NO_3^- did not have a significant relationship with percent burned, catchment size was negatively correlated with areal burn percent (Krct, $p=0.04$; Figure B5). Smaller catchments have more prescribed fires (Kruskal-Wallis

test (KWt), $p<0.001$), which possibly contributes to the higher burn percent. In contrast to the individual correlations, the conditional inference tree analysis highlighted a breakpoint predicted by burn type for CR_M for NO_3^- (prescribed, n=7, mean 29.5; natural, n=64, mean 4.7; p=0.015). The relationships were also not consistent across the spectrum of solutes, with CR_M for TP being positively correlated with catchment area (Krct, p=0.03, n=29), while CR_M for TSS had a significant correlation with areal burn percent (Krct, p=0.02, n=23). Overall, our attribution analysis (Figure B6) was not able to identify any common trends among variables. Part of the challenge in identifying drivers of nutrient changes are the confounding effects of single perturbation events from long-term nutrient budget alterations. A recent analysis by (Crandall et al., 2021) compared pristine and anthropogenically impacted burned watersheds in Utah, USA. They conclude that "direct human impact, not megafire, is the primary threat to aquatic ecosystems in semiarid ecosystems." A recent isotope-tracing study (Abbott et al., 2021) in burned Arctic watersheds highlighted that the isotopic signature of exported nitrate was similar to that in unburned watersheds, highlighting the ability of fire to mobilize existing nutrient stocks. Other analyses have focused on a wider range of variables, such as stream temperature, that have been affected by fire (Kichigina & Bilichenko, 2019; Rhoades et al., 2011; Subiza et al., 2018). These kinds of analyses will be improved in the future as more high temporal and spatial resolution water quality data are combined with detailed catchment characteristics from satellites and other sources.

3.5 Summary and Conclusions

In the present work, we have used a meta-analyses approach to quantify the effect of fire on nitrogen, phosphorus, carbon species, as well as suspended sediments in streams draining burned watersheds. We identified 34 studies, including data from 81 burned and 40 reference catchments. We found that while 31 studies measured flow, almost none had data in an accessible format for use in our metaanalysis. We acknowledge that our sites and findings are primarily relevant to North America, and future extensions of this work should include a broader geographical distribution of sites. With increasing incidences of wildfires across the world, the number of studies exploring wildfire effects are increasing which will allow future meta-analysis studies to be more geographically diverse. For water quality parameters, the most data were available for nitrogen (67 as NO_3^-, 30 as NH_4^+), followed by phosphorus (41 as PO_4^{3-}, 20 as TP) and suspended sediments (26 sites). Studies that looked at DOC and DON were more limited. Most studies focused on one or two elements, thus

making it challenging to understand the coupling of elemental cycles. For example, only ~40% of NO_3^- sites were also sampled for TSS or TP. Finally, we found that most sites (>92%) recorded data for 5 years or fewer, severely limiting our ability in this study to evaluate recovery of streams post-fire.

Overall, we found that concentrations of nutrients and sediments increased after fire (measured as the change ratio of mean concentration CR_M), with the largest increases observed for NO_3^- (median CR_M=2.1), TP (CR_M=1.9), and NH_4^+ (CR_M=1.5), with smaller increases for PO_4^{3-}, TN, DOC, and TSS. When exploring the coupling of nutrient cycles, we found that increases in one parameter generally predicted an increase in another parameter. The proportion of inorganic nitrogen and phosphorus (NO_3^--TN and PO_4^{3-}-TP) increased in 74% and 62% of sites post-fire, with median CR_M values of 1.4 and 1.3, respectively. We also found that DOC-NO_3^- and DOC-PO_4^{3-} ratios decreased post fire at almost all sites. Increase in dissolved inorganic nutrients in the immediate aftermath of the fire can be attributed to a variety of reasons, including: (1) subsurface release due to suppressed nutrient uptake by terrestrial biota (Certini, 2005; Hauer & Spencer, 1998; Ranalli, 2004), (2) ash deposits from the fire as a source of dissolved organic and inorganic nutrients (Brito et al., 2021; Cawley et al., 2016, 2018; Earl & Blinn, 2003; Revchuk & Suffet, 2014; Rhoades et al., 2011; Spencer et al., 2003), and (3) inhibition of in-stream processes, such as NO_3^- uptake, due to lower DOC export and a more aromatic DOC signature from burned watersheds (Rodríguez-Cardona et al., 2020). Indeed, we find a decrease in DOC-NO_3^- and DOC-PO_4^{3-} ratios after fire, which possibly inhibits NO_3^- uptake in the streams draining the forested watersheds. D. M. Anderson et al. (2002) have suggested that shifts in nutrient ratios including N:P and DOC:DON caused shifts in freshwater plankton species composition. The changes in these ratios are important to the downstream ecosystem and potential for algal growth. Dissolved forms of the nutrients are more bioavailable, and thus might pose greater eutrophication risk downstream. Much is yet to be learned about these altered ratios in post-fire landscapes.

Finally, we explored the effect of fire on concentration extremes, and found that concentration increases were greater at the higher concentration deciles, compared to the lower concentration deciles, creating a hockey-stick-like response. The increase in concentration extremes in the post-fire period has significant implications with respect to water treatability for downgradient communities that might be using the river as a water source. It is thus recommended that studies place special emphasis on capturing high concentration events that often co-occur with high flow events. Our meta-

analysis highlights the need for continued long term monitoring of water quality in post-fire landscapes, along with the exploration of covariation between multiple elemental cycles and storm driven responses in concentration extremes. Increased data-sharing of existing and future datasets will greatly aid future analyses of fire effects on water quality, especially as more studies from around the globe are published on this topic. Such advances in the field will help managers plan for water treatment challenges arising from fires in forested source waters. Stream corridors are complex ecohydrological systems, and disturbance regimes add even more complexity as we seek to understand the effects of short- and long-term changes across the landscape. Fire has been a natural part of these systems for millenia, and there is much work left to do to understand the impacts of fire to both natural systems and our human infrastructure.

Chapter 4
Wildfire alters stream nutrient concentration-discharge relationships.

4.1 Abstract

Numerous studies have documented changes to both flow and water quality in streams following wildfires. While documenting changes in nutrient and sediment fluxes after fire is of great relevance to land and water managers, less attention has been paid to changing concentration-discharge (CQ) relationships. CQ analysis has been used extensively in the study of catchments across a wide range of sizes, land cover, and disturbance regime to parse relevant processes driving catchment export of solutes and suspended matter. With flow data and nutrient concentrations (nitrogen, phosphorus, carbon) from fire-impacted watersheds across the conterminous United States, we modeled daily concentration using the WRTDS model (Weighted Regression over Time, Discharge, and Season) with the "Wall" feature to analyze the sharp discontinuity in the pre- and post-fire CQ relationships. To document the changes in CQ relationships after fire, we used standard metrics such as concentration (C), discharge (Q), and flux; as well as the CQ slope (*b*), the ratio of the coefficients of variation of the C and Q timeseries (CV_C/CV_Q), and the regression fit of the log-linear CQ relationship. Some of these metrics also allow us to characterize CQ behavior as generally chemostatic versus chemodynamic (dilution- or enrichment-type). We use clustering techniques to understand the magnitude and direction of changes in CQ characteristics. Our results will help reveal in what circumstances (when and where) certain altered landscape processes drive the changes in stream nutrient CQ relationships after fire.

4.2 Introduction

The effects of fire on stream water quality have been subject to intense study (Emelko et al., 2011; Rust et al., 2018). From a land management perspective, forested watersheds are often managed to provide multiple ecosystem services, including provision of ecosystem services, commercial silviculture, and water supply (Ernst, 2004). Fire is well documented to result in altered flows and concentration regimes in streams (Hallema, Sun, et al., 2018; Hampton et al., 2022; Hampton & Basu, 2022; Kinoshita & Hogue, 2015; Rhoades, Nunes, et al., 2019; Rust et al., 2018; Rust, Saxe, et al., 2019; Saxe et al., 2018), which poses challenges for water treatment and provision (Bladon et al.,

2014; Emelko et al., 2011; Hohner et al., 2019; Nunes et al., 2018). With the observable increase in fire frequency and intensity across many areas of the globe (Cannon & DeGraff, 2009; A. L. Westerling, 2016), there is also interest in understanding the underlying mechanisms of how fire impacts hydrologic and biogeochemical watershed processes. Incorporating fire effects into modeling frameworks is one way to test our understanding (Basso et al., 2020; Maina & Siirila-Woodburn, 2020), as well as develop predictive tools that then inform watershed and land managers. Still, syntheses of possible effects are sorely needed to supplement the numerous site-based studies that have been published so far.

Moving towards a broad accounting of the effects of fires on stream water quality will further inform both watershed management strategies and mechanistic understanding. It is perhaps most important to recognize that we are seeking to understand the effects of fires overlain across a deep body of knowledge on the hydrogeochemical functioning of headwater and forested catchments (S. P. Anderson et al., 1997; Godsey et al., 2009, 2019; Thompson et al., 2011). Recent literature has documented that in the majority of cases, when aggregating across large numbers of fires and catchments, that stream discharge and concentrations of nutrients and suspended solids increase after fire (Bitner et al., 2001; Hallema, Sun, et al., 2018; Hampton et al., 2022; Hampton & Basu, 2022; Rust et al., 2018; Smith et al., 2011). As expected with a large number of samples, there is variability in response direction, significance, and magnitude. There are examples of decreases in flow after fire (including after attempts to normalize for climatic variability (Hallema, Sun, et al., 2018; Hampton & Basu, 2022); along with decreases in concentrations of nutrients, suspended solids, and various dissolved species (Hampton et al., 2022; Rust et al., 2018). With the large amount of data available, it is now possible to begin exploring possible mechanistic explanations for fire effects on streams. Foremost to explore is the fact that cycles and fluxes of water and elements are intrinsically linked. In the literature of post-fire stream water quality effects, there have been few attempts to link in the hydrologic behavior of catchments through concentration-discharge (CQ) analysis (Bladon et al., 2008; Emmerton et al., 2020; Silins et al., 2014; Wilkinson et al., 2007). While effects on total fluxes (concentration multiplied by discharge) have been examined, the more complicated interrelations of concentration and discharge have not yet been analyzed across many catchments.

Catchment moisture regime, hydrologic pathways, and residence times (influenced by all manner of variables: soils properties, topography, etc.) are inseparable from our understanding of the cycling and transport of elements in a watershed (Godsey et al., 2009, 2019; Musolff et al., 2015, 2021;

Winter et al., 2021). Structural heterogeneity plays a key role in governing what pattern of water quality concentrations we observe at a catchment over time, including spatial distribution of element pools within a catchment (Abbott, Gruau, et al., 2018), and the distribution of these pools across soil depth (Thompson et al., 2011; Zhi & Li, 2020). Hydrologic residence time tends to correlate negatively with soil depth, such that "deep flow" that has percolated through the soil and traveled through deeper regolith or bedrock has a slow and fairly constant contribution to total streamflow. "Shallow flow" is generally "fast flow", traveling overland during rain events or through shallow soil pathways (including soil pipes; (van Meerveld & McDonnell, 2006; van Meerveld & Weiler, 2008). Element distribution is also highly heterogeneous with soil depth (Inamdar et al., 2004, 2008), and thus transport from these pools to the stream is subject to the total amount of water flow, its speed, and spatial distribution within the catchment.

In a very simplified conceptual model of watershed element cycles, the streamflow between storm events (i.e., base flow) consists mostly of deeper groundwater that has longer residence times. Here, slow mineral weathering may contribute to the chemical profile of this water, with higher concentrations of silica and elemental cations. In addition, any highly mobilizable species (for example nitrates) may have been mobilized as water initially percolated down through soils, and is then carried along these deeper flowpaths. When rain falls, water will access numerous shallower and faster flow paths (e.g. because of soil saturation, increased hydraulic head, infiltration exceedance, etc.). While reduced soil-water residence times may result in decreased concentrations of mobilizable species (e.g. weathering products, nitrate), increased erosive power in streams will increase concentrations of solids including sediments and organic particulates (containing particulate carbon, phosphorus, nitrogen, etc.). In addition, "fill-and-spill" behavior (van Meerveld & McDonnell, 2006) can be activated when landscape features like wetlands reach a threshold where organic-rich waters flood the stream network (see also: "pulse-shunt" concept, (Raymond et al., 2016). With this conceptual model in mind, we can next explore how fire would change elemental and hydrologic cycles and fluxes.

As described above, there are a wealth of studies summarizing fire effects on hydrology and water quality across hundreds of catchments. Numerous studies have individually explored the mechanisms behind these changes in great detail, from erosive effects (Abney & Berhe, 2018; Blake et al., 2010; Crandall et al., 2021; S. F. Murphy et al., 2012; Silins et al., 2009; Stone et al., 2011) to ash chemistry and transport (Bodí et al., 2014; Brito et al., 2021; Cawley et al., 2018; Earl & Blinn, 2003) to soil

hydrophobicity and overland flow (Certini, 2005; J. Chen, McGuire, et al., 2020; J. Chen, Pangle, et al., 2020; Delač et al., 2022; Robichaud, 2000). Natural disturbances are crucial to many ecosystems (N. G. McDowell et al., 2020; Turner, 2010), with fire-dependent (co-evolved with fire) ecosystems covering 53% of global terrestrial area (Shlisky et al., 2007, 2009). Of course, there will be immense variability across ecozones of the impacts of fires on vegetation, soils, hydrology, and biogeochemical cycles. On top of this, there is bias in historical studies of fires to North America and Australia (Hampton et al., 2022). Nonetheless, no study to date has synthesized the interplay between altered concentration regimes and post-fire discharge, putting fire effects in context of our understanding of the drivers of concentration regimes (Moatar et al., 2017; Zhi & Li, 2020). We have gathered concentration and discharge time series data from 29 catchments from the U.S. Geological Survey database to analyze CQ behaviors pre- and post-fire.

4.3 Methods

This study took advantage of the enormous amount of publicly-available satellite imagery and water conditions data from the United States. We used previously published analysis by (Rust et al., 2018) intersecting wildfire extent data with available watershed data on discharge and water quality.

4.3.1 Data Acquisition

The Monitoring Trends in Burn Severity (MTBS) program uses 30-meter-resolution Landsat data to map the extent of fires and classify severity based on ground reflectance (Eidenshink et al., 2007). These data were overlaid with the geographic extent of the U.S. Geological Survey (USGS) monitored watersheds to determine which watersheds experienced fires, in which years, and which parameters (streamflow and water quality) are available in the preceding and following 10 years after each fire.

After identifying fire-affected watersheds to be examined, streamflow and water quality data were downloaded from the USGS National Water Information System (NWIS) via the package *dataRetrieval* (De Cicco et al., 2022) in the software R (R Core Team, 2023). The package *USGSreadR* (Hampton, 2022c) was used to manipulate and sort NWIS data. Compared to the study by Rust et al., this study focused narrowly on common nutrients, including nitrogen (N) as total N (TN), ammonium (NH_4^+), organic N (ON), nitrate (NO_3^-), and nitrite (NO_2^-); phosphorus (P) as total P

(TP), phosphate (PO_4^{3-}), and organic P (OrgP); and carbon (C) as organic C (OrgC). A full list of the USGS parameter codes used in data gathering can be found in Appendix C.

4.3.2 WRTDS

Next, the concentration and flow data were input into the Weighted Regression against Time Discharge and Season (WRTDS) model (Hirsch et al., 2010). WRTDS was chosen to process the input data because of variation in the number of samples between site-fire-parameter sets. With this variation, comparison of variables like coefficient of variation and R^2 of regressions might be compromised by different sample numbers. A uniform number of daily modeled data points in the pre- and post-fire time series should allow for appropriate comparison. The model was implemented in the *EGRET* package in R (Hirsch & De Cicco, 2015). The WRTDS model allows sparse water quality data to be paired with continuous flow data to interpolate a fully continuous water quality timeseries. Data from 10-year pre- and post-fire intervals were input into the model, and additional screening ensured that at minimum 25 water quality measurements were taken in each interval. The expansion to 10 years of data pre- and post-fire served to allow the WRTDS model to have ample calibration data to capture CQ dynamics during each interval, and to accommodate 7-year windows across the model domain (windowY and windowSide). In our implementation, we used the "wall" feature (EGRET 3.0 enhancements; (Hirsch & De Cicco, 2018) to differentiate between the pre- and post-fire timeseries. As discussed in their commentary on the model enhancements, Hirsch & De Cicco lay out the utility of WRTDS for hypothesis testing of altered CQ regimes. This study is to our knowledge the first application of the "wall" feature in the examination of disturbance effects on water quality.

4.3.3 Number of Sites

From the approximately 150 sites used by Rust et al. (2018) accessible via the NWIS, 47 sites measured the hydrochemical variables of interest for this study (Appendix C Table C1). Inclusion criteria for the study by Rust et al. (2018) were a minimum of 10 water quality measurements in each of the 5-year-long pre- and post-fire periods, and a watershed burned percent greater or equal to 5%. Our criteria narrowed their list of sites from 47 to 32 by further expanding the sample requirements to 25 water quality measurements in each of the 10-year-long pre- and post-fire periods. We filtered out sites where greater than 40% of water quality measurements appeared to be at or near method detection limits (with non-unique single-significant-digit values: e.g. 0.01, 0.001 mg/L). After

running the WRTDS model, model-runs were excluded from the study if the flux bias statistic (Hirsch & De Cicco, 2015) exceeded 10%. These final filters reduced our site count to 29. Accounting for multiple parameters measured at each site, and sometimes multiple fires documented at the same site (at minimum 10 years apart), our analysis is conducted on 186 site-fire-parameter sets.

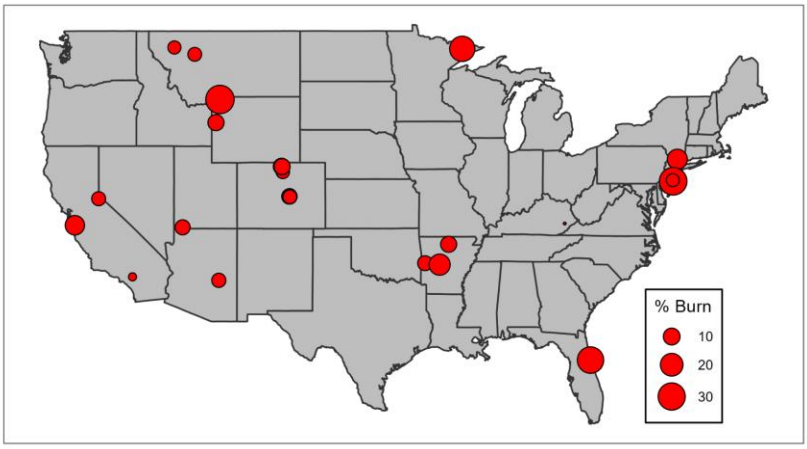

Figure 4-1: Map of study sites in the United States. The percentage of watershed burned is represented by point size.

4.3.4 CQ Analysis

After using WRTDS to generate 10-year pre- and post-fire daily discharge and concentration time series, we fit both intervals to the linearized power-law CQ model:

$$ln(C) = b * ln(Q) + ln(a) \quad (4\text{-}1)$$

where *a* and *b* are the calibrated intercept and slope coefficients, respectively. Calculations were performed using the *stats* package in R. The linear model was fit for the 10-year pre-fire data, as well as for the first post-fire year, and the first 5 post-fire years. The regression R^2 was recorded.

The metric CV_C/CV_Q (Thompson et al., 2011) was calculated as the coefficient of variation of concentration divided by the coefficient of variation of discharge (Q).

4.3.5 Linear Regression

Using standardized multiple linear regression, we performed linear regression between changes in concentration (crC, all change ratios were log-transformed) and changes in flow (crQ), concentration

variability ($crCV_C$), *b* slope (absolute change), and *a* intercept (absolute change). We performed multiple linear regression of crC against the four other metrics, along with 1-on-1 comparisons, and "leave one out" analysis to measure the improved contribution of each metric to the linear models.

4.3.6 CQ Clustering

Past studies have used CQ analysis to examine slopes and variability in CQ-space. Choosing which metrics and variables to examine, and how to interpret these is inevitably arbitrary. We point out that the commonly used *b* slope parameter has frequently had bins of $-0.2 < b < +0.2$ regarded as a working definition of "chemostatic" (Meybeck & Moatar, 2012; Moatar et al., 2017). Indeed, this threshold decently bounds data for geogenic solutes that in behavior should be chemostatic (Godsey et al., 2009). In commentary on the exclusive-use of power-law CQ slopes, (Thompson et al., 2011) said "the absence of a dependence of concentration on discharge (as indicated by, e.g., $b \approx 0$) is not evidence that the variability in concentration is small." They reference the variability in concentration relative to the variability in discharge (specifically, the coefficients of variation divided, as in CV_C/CV_Q) as another characteristic of concentration regime. There is a weakness in the CVC/CVQ metric to assess variation around a power-law CQ fit. As shown in Figure 4-2, two time series may have almost the same slope and CV_C/CV_Q metric, but the degree of correlation (as R^2 of the linear regression, Equation 4-1) between C and Q could be very different. Thompson et al. (2011) noted the same phenomenon, that the variables *b*, CV_C/CV_Q, and R^2 can vary fairly independently.

We employed a k-means clustering technique to sort CQ relationships according to three characteristics: the *b* slope, CV_C/CV_Q, and the linear regression R^2. Numerous studies have used k-means clustering for the analysis of hydrologic and watershed data (McManamay et al., 2014; Olden et al., 2012). We calculated the three clustering metrics for the 10-year pre-fire period with WRTDS-interpolated data, so that each time series would have an equal number of data points. As mentioned above, we filtered for appropriately performing WRTDS models. We used the *factoextra* (Kassambara & Mundt, 2020) package in R to determine the optimal number of clusters. The average silhouette width method (Rousseeuw, 1987) was used to determine the number of clusters. In addition to clustering based on the pre-fire data, we clustered all CQ relationships together, across different chemical parameters. This allowed for increased sample numbers and for us to put individual CQ relationships in context of the broader range of potential behavior.

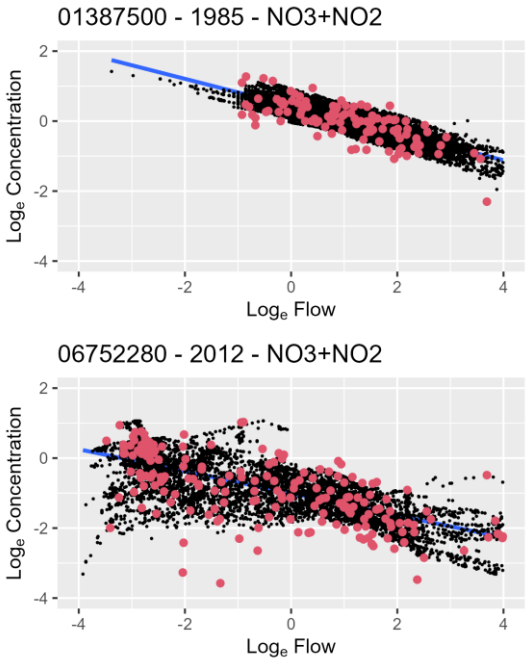

Figure 4-2: Example of CQ metrics. The two plots shown above represent 10-year pre-fire periods of data (red) and WRTDS interpolation (black). CQ characteristics of the WRTDS output is similar, with ***b*** values of about -0.35 and CV_C/CV_Q values of about 0.27. In contrast, the upper data have a linear regression R^2 of 0.88, and the lower data have an R^2 of 0.41. Plot titles include USGS site number, year of the fire, and water quality parameter.

4.4 Results and Discussion

4.4.1 Pre-fire CQ Relationships

Our cluster analysis was able to identify four distinct clusters in CQ relationships as a function of *b*, CV_C/CV_Q and R^2 values: Chemostatic (#1, n=102), Dilution (#2, n=22), Mobilization (#3, n=55), and Chemodynamic (#4, n=7) (Figure 4-3a-e). The chemostatic, dilution and mobilization clusters are differentiated by differences in the *b* and R^2 values, where chemostatic clusters are characterized by *b* values close to zero (median b = 0.03, Figure 4-3c), and low R^2 (median R^2 = 0.09; Figure 4-3e), while dilution clusters are characterized by negative b values (median *b* = -0.44, Figure 4-3c), and higher R^2 (median = 0.62, Figure 4-3e) and mobilization clusters are characterized by positive *b* values (median = 0.32, Figure 4-3c), and higher R^2 (median = 0.50, Figure 4-3e). The chemodynamic cluster has a wide range of *b* values (median = 0.38) with a median similar to the mobilization cluster,

but stands apart due to its high CV_C/CV_Q (median = 2.0) and low R^2 (median = 0.1) (Figure 4-3a and d). Note that while there is overlap between the cluster boundaries in Figure 4-3a, specifically between the chemostatic and the mobilization and dilution clusters, inclusion of the R^2 metric allows us to define the boundaries of the clusters better, as shown in Figure 4-3b. Thus, two watersheds can have similar CV_C/CV_Q and *b* values, but might be differentiated into the mobilization cluster if there is a tight relationship between C and Q, as captured by the R^2 metric (Figure 4-2). Indeed, the variable R^2 strongly differentiates the Mobilization and Dilution clusters (high R^2, >0.25) from Chemostatic and Chemodynamic clusters (low R^2, <0.25).

While the cluster analysis used data from all elements and all sites, we next analyzed element specific membership in the different clusters: nitrogen as total N (TN, n=24), ammonium and organic N (NH_4^++OrgN, n=61), nitrate and nitrite (NO_3^-+NO_2^-, n=31); phosphorus as total P or total inorganic phosphate (P, n=25), and organic P (OrgP, n=28); and carbon as organic C (OrgC, n=14). Across 5 of the 6 element groups, >50% of the sites' pre-fire behavior was chemostatic (Figure 4-4), with the exception of NO_3^-+NO_2^-, where only 19% of NO_3^-+NO_2^- sites are chemostatic, and the plurality (46%) of NO_3^-+NO_2^- sites were in the Dilution cluster. In contrast, TN shows a dominant chemostatic behavior (62% of TN sites), with some mobilization behavior (19% of TN sites), while TP and OrgC shows a mix of chemostatic and mobilization behavior. Our result for OrgC mirrors that of (Zarnetske et al., 2018), who found that OrgC *b* slopes strongly cluster around values of 1, representing chemostatic behavior. We echo their hypothesis that OrgC will exhibit CQ mobilization when OrgC concentrates in shallow soils, and in low-lying topography like wetlands that can be rapidly "shunted" into the stream network during high flow events (Raymond et al., 2016). While our study had a broader definition of chemostatic behavior, capturing most OrgC sites in our analysis, (Zarnetske et al., 2018) found that OrgC rarely displays dilution behavior, and that *b* slopes are greater than 1 for about 80% of watersheds they examined across the continental US. Similarly, we found that 85% of OrgC sites had *b*>1, and 50% of sites were classified in the Mobilization or Chemodynamic clusters.

Phosphorus will often exhibit mobilization behavior because its movement in rivers is largely driven by sediment export (Jarvie et al., 2005; Withers & Jarvie, 2008). At the lowest of flows, while erosion is minimal, fine-sediment-associated-P is easily transported. At higher flows, as the stream network expands and new P is transported overland to the streambed, increased velocities allow for erosion and re-mobilization of P (Silins et al., 2009; Stone et al., 2011). Depending on the spatial homogeneity of P sources in the watershed, mobilization or chemostatic behavior is likely compared

to dilution. While total N and P and organic N and P are likely to be associated with eroded organic debris and transported with or dissolved from organic-laden sediments in the shallow soil, inorganic N in the form of NO_3^- should have a different response (Bladon et al., 2008). Because NO_3^- has weak associations with sediment and organic matter, it moves downwards through soil profiles, accumulating in deeper soil pools or groundwater, and this can lead to dilution behavior where low flows are associated with high groundwater concentrations.

It is important to note, however, that our sample size is relatively small and thus not representative of all forested watersheds. There are other continental scale papers that focus on more representative behaviors as a function of land use. Instead we are focused here on wildfire impacted watersheds, and thus focus only on catchments with adequate pre- and post-fire data to answer our question. However, the methodology of classifying CQ typologies by clustering allows for a binary yes/no change metric to compare pre- and post-fire behavior, to accompany other CQ metrics such as slope and CV_C/CV_Q.

The differences between CQ typologies expressed by different element groups provides a window into watershed processes. CQ typologies are strongly influenced by size and heterogeneity of distribution of element mass stored across the landscape (Abbott, Gruau, et al., 2018, 2018; Basu, Destouni, et al., 2010; Basu et al., 2011; Moatar et al., 2017; Musolff et al., 2016, 2017; Thompson et al., 2011). The classic mechanistic explanation for the predominance of chemostatic behavior for geogenic solutes (Godsey et al., 2009, 2019) is a homogeneously-distributed source pool (x-y spatial distribution; and z direction, shallow and deep soils) that is readily mobilized through multiple flow paths, including fast overland flow, shallow subsurface flow, and slow groundwater flow. (Zhi & Li, 2020) highlight that differences in element stores in the soil profile (z direction) will manifest in changing *b* slope of the CQ relationship.

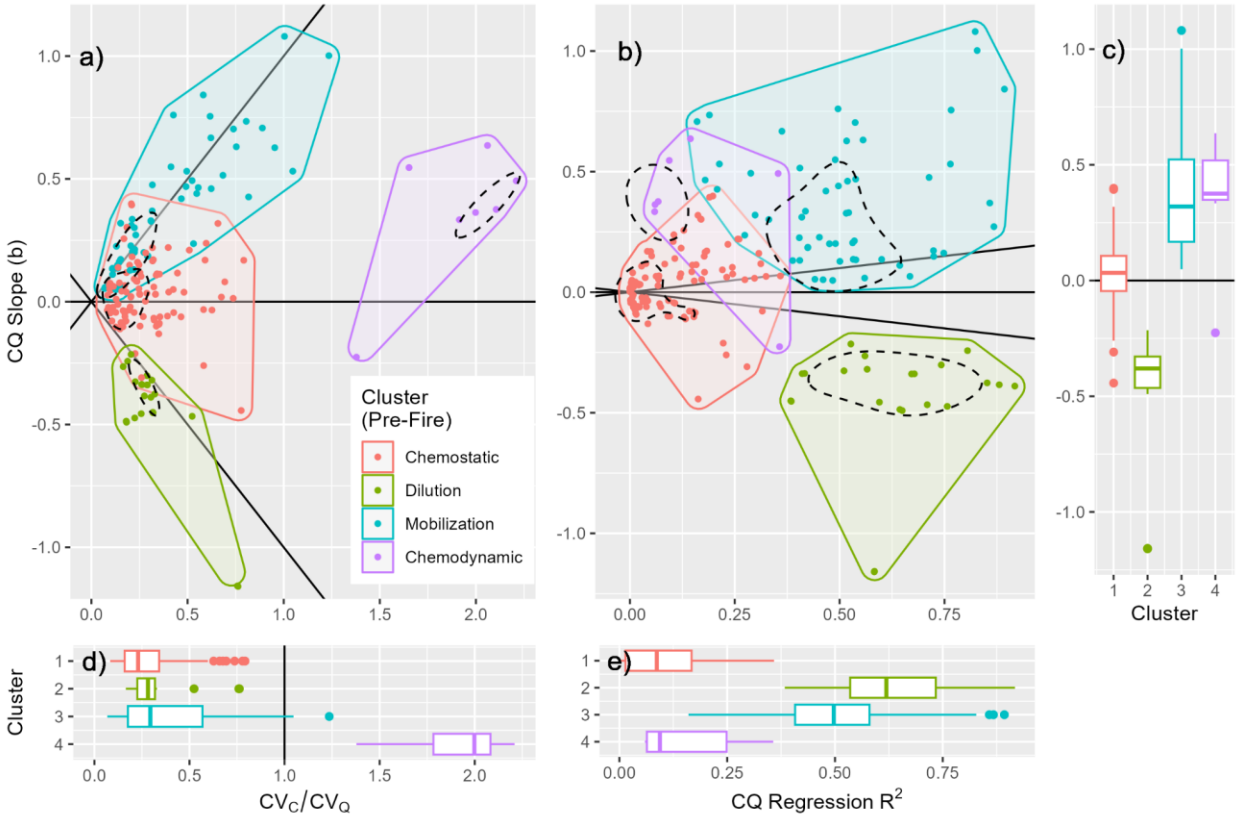

Figure 4-3. Clusters of CQ behavior. Clusters calculated from pre-fire CQ characteristics for the all 6 hydrochemical variables combined (TN, NH_4^++OrgN, NO_3^-+NO_2^-, OrgC, OrgP, P) and all 186 site-fire-parameter sets. Axes are shared across panels. Panel a) shows variables ***b*** slope and CV_C/CV_Q. Panel b) shows variables ***b*** slope and R^2. Kernel density 50th percentile contours for each cluster are drawn with black dashed lines. Convex hulls are drawn with colored backgrounds and perimeters around the clusters. Panels c), d), and e) show boxplots of the variables (***b***, CV_C/CV_Q, R^2) by cluster, and are oriented to their corresponding axis in a) and b).

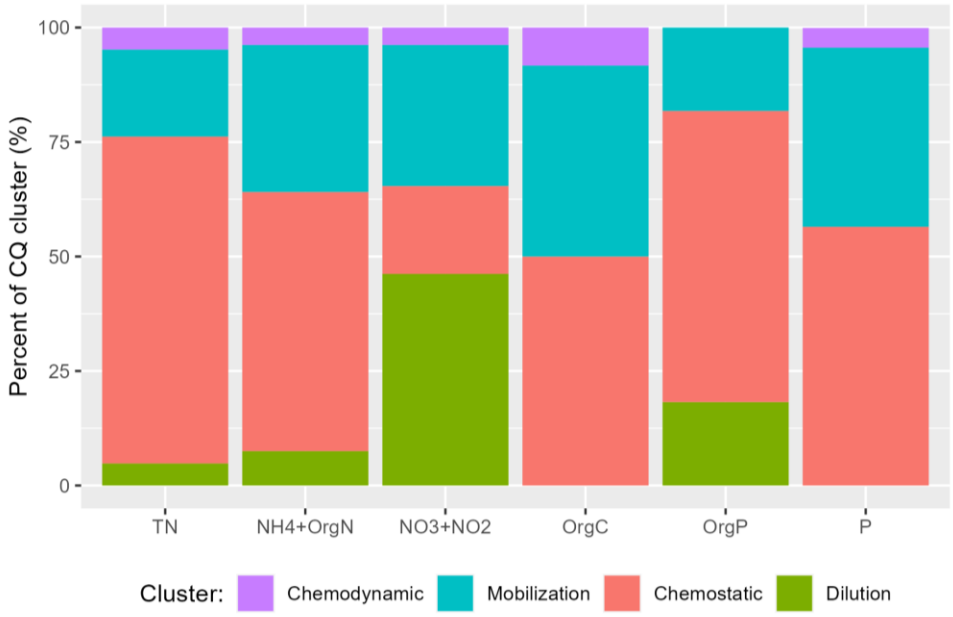

Figure 4-4. Percent of element-fire-site pre-fire CQ behavior represented by each cluster.

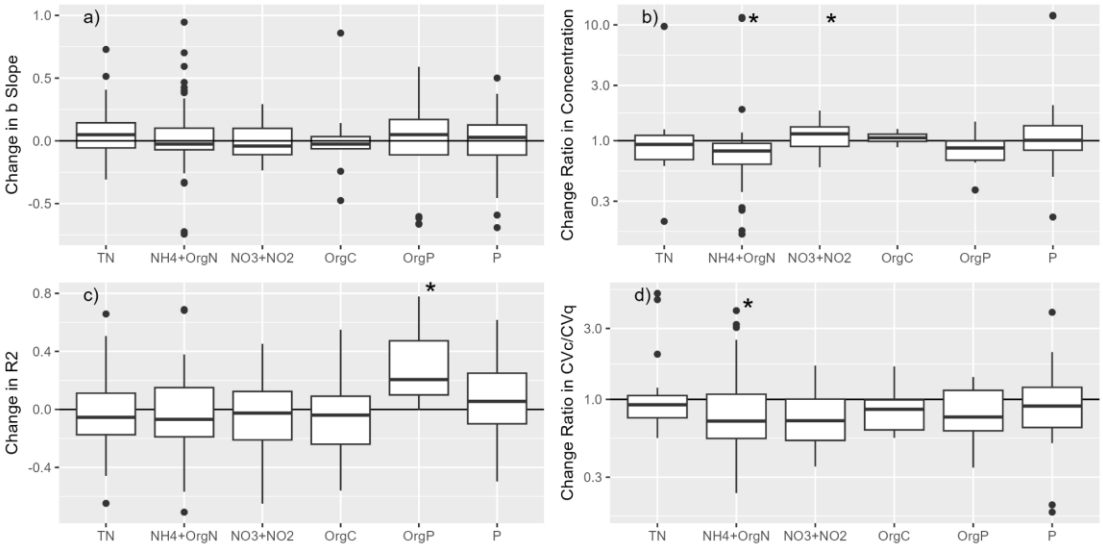

Figure 4-5. Traditional change analysis across elements. Change in *b* slope (a), the change ratio of Concentration (b, note log scale), change in R^2 (c), and change ratio of CVc/CVq (d, log scale). Above and to the right of each boxplot, an asterisk indicates if the distribution of points is significant (using a one-sample Wilcoxon test, $p<0.05$).

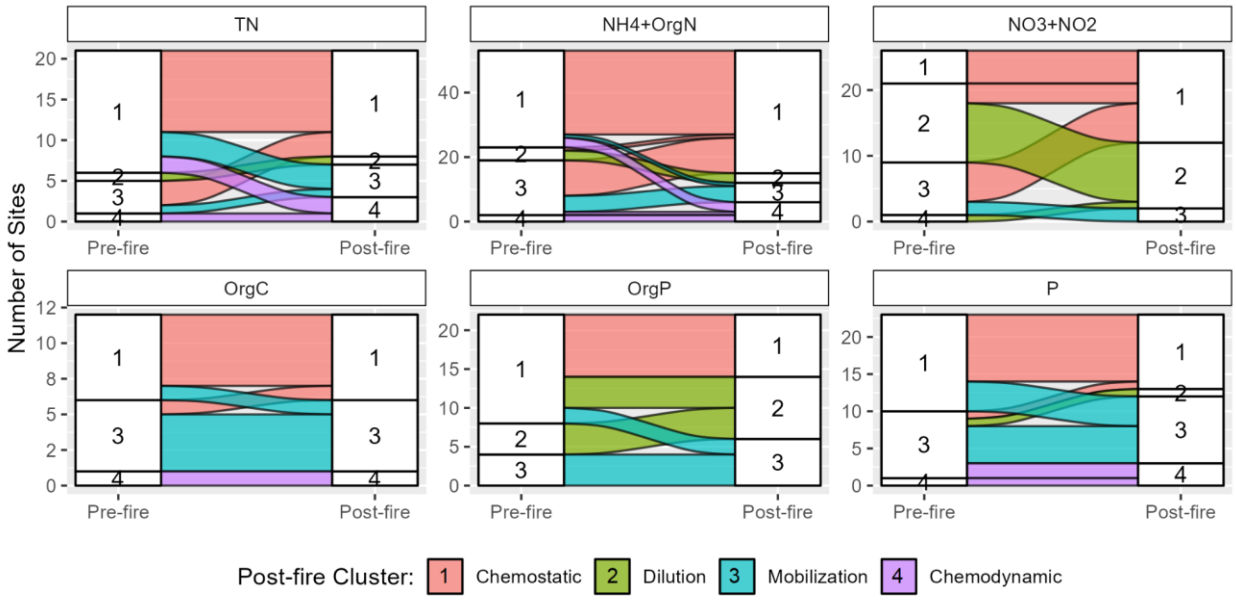

Figure 4-6. Alluvial diagram for six hydrochemical variables. "Flows" of sites from pre-fire clusters (left side) to post-fire clusters (right side). Flows are colored by post-fire clusters. Y axes indicate the number of sites.

4.4.2 Post-fire CQ Relationships

4.4.2.1 Post Fire Response evaluated using Traditional Change Metrics

We found that, besides variability in other change metrics, fire resulted in decreasing CV_C/CV_Q for all elements (Figure 4-5d). This change was significant at a level of $p<0.05$ for NH_4^++OrgN (using a one-sample Wilcoxon test). The decrease in CV_C/CV_Q was driven by decreases in CV_C for all nitrogen species and carbon (significant for nitrogen species at $p<0.05$) as well as increases in CV_Q for all variables except for TN (significant for NH_4^++OrgN, NO_3^-+NO_2^-, OrgP, P at $p<0.05$). As will be discussed later in attribution analysis, changes in Q also corresponded with CQ changes post-fire. For the sites where NO_3^-+NO_2^-, OrgP, and P were measured after fire, there were significant increases in flow, while for other parameters changes in flow were not significant.

Examining post-fire change in CQ behavior, we found relatively small median changes in *b* slopes (-0.04 to +0.05; Figure 4-5a). While none of the changes in *b* slopes were significant across element groups (Figure 4-5a), we observed median decreases in slope for NO_3^-+NO_2^- and NH_4^++OrgN, while

slopes increased for TN. This contrast within the N species seems contradictory, especially since OrgP and P showed mirrored median increases in *b* slopes.

Previous multi-site synthesis of fire effects on water quality has shown increases in dissolved NO_3^-, NO_4^+, TN, phosphate, and TP concentrations across 121 watersheds (Hampton et al., 2022). This study has been able to collect a similar number of site-fire-parameter sets (Appendix C Table C1) measuring both water quality and discharge, compared to only water quality. Analysis of many sites could characterize change of mean concentrations. We found median decreases in mean concentrations of TN, NH_4^++OrgN, and OrgP (Figure 4-5). Median increases in concentrations of NO_3^-+NO_2^-, OrgC, and P were small (7-14% median increases), compared to 30-110% increases found by Hampton et al. (2022). These findings suggest that different numbers of studies and sites could sample different degrees of altered water quality, however, given the accompaniment of flow data in this study, we can also attempt to disentangle changes in flow from changes in concentrations.

We performed analysis to try to explain changes in concentration (C) using different CQ metrics. Using standardized multiple linear regression, we analyzed correlation between other CQ metrics and the change ratio of concentration (crC). We found that overall, flow was a poor predictor of changes in concentration. Initially looking at the change ratio of Q (crQ), we only identified a single weak relationship for OrgC ($p=0.04$; R^2 regression=0.27; Figure C4) between crC and crQ. Given that pre-fire CQ behavior for OrgC showed a dominance in the Mobilization cluster, this suggests increasing post-fire flows correlated to increasing post-fire concentrations, and vice versa. While there was an almost ubiquitous lack of correlation of crC to crQ, we found a very prominent correlation of crC to the change in the CQ *a* parameter (d*a*). All elements except OrgC showed significant linear correlation ($p<0.05$; Figure C4) between crC and d*a*, with a mean regression R^2 of 0.38 (not incl. OrgC). In the "leave one out" analysis, inclusion of d*a* lead to mean improvements of regression R^2 of 0.31 (not incl. OrgC). Since the parameter *a* simply defines the intercept of the CQ relationship, it makes sense that it would have a strong predictive ability on change in C. No matter how the distribution of Q changes (i.e. "left to right" on CQ diagram, Figure 4-2), a shift upward in *a* could result in an increase in C even with a decrease in Q. For TN, NH_4^++OrgN, and OrgP, crC was also significantly correlated to the change in concentration variability (change ratio of coefficient of variation: $crCV_C$), with a mean regression R^2 of 0.41 and mean R^2 improvement after inclusion of 0.20 (Figure C4). For TN and NH_4^++OrgN, $crCV_C$ was the most important variable in the multiple linear regression, and for these elements along with OrgP, $crCV_C$ showed the largest R^2 alone against

crC. From the meta-analysis by Hampton et al. (2022), we see that concentration variability (i.e. changes in concentration at upper deciles) was implicated in total concentration change. Our analysis confirms a positive correlation between $crCV_C$ and crC for several elements. In contrast, for $NO_3^- + NO_2^-$ we identified significant and negative correlation between $crCV_C$ and crC ("alone", R^2=0.21). When all elements are analyzed together, correlating crC to the 4 other metrics, the linear model has an R^2 of 0.48. This demonstrates a large amount of unexplained variability, and a limitation of analyzing different aspects of CQ behavior after fire without a broader picture that can be provided by our CQ typologies.

One interesting element store present in wildfire-impacted watersheds that is absent in undisturbed watersheds is ash. The hydrogeochemical properties of ash (e.g. elemental makeup, particle size, hydrophobicity, solubility) vary widely, and may be affected by burn temperature (Bodí et al., 2014; Qian et al., 2009). Depending on the elemental makeup, there are usually soluble nutrients (e.g. PO_4^{3-}, NO_3^-, NH_4^+) that readily leach out of the ash upon contact with water (Brito et al., 2021; Earl & Blinn, 2003). The dichotomy between ash's erodibility (compare to "mobilization" CQ) and exhaustible soluble components (compare to "dilution" CQ) could potentially contribute to unique elemental CQ relationships depending on local conditions. How long ash persists in the landscape and the residence time of other fire-impacted elemental pools has been documented to lead to detectable effects of fire on water quality over 5 years after fire (Hauer & Spencer, 1998; Spencer et al., 2003). The spatial heterogeneity of ash distribution after fire may explain some of the highly variable changes in water quality that we observed after fire.

4.4.2.2 **Evaluating Post-fire Response using Clusters**

As discussed in the previous section, traditional methods of measuring change in water quality after fire presented problems, including a wide distribution of changes (Figure 4-5), and multiple concurrent changes in CQ relationships that makes explaining changes difficult (Figure C4). The clustering technique that we used to classify CQ typologies allows us to compare pre- and post-fire classifications and changes across all of the variables used for clustering. Figure 4-6 shows an Alluvial diagram, with the pre- and post-fire distributions of sites (broken out by element group) connected by "flows" of sites, showing the number of sites moving between each cluster.

Across the entire dataset we find that the proportion of the sites in the chemostatic cluster decreases for TN (71% to 62%), OrgP (64% to 36%) and TP (57% to 43%), while it increases for $NO_3^- + NO_2^-$

(19% to 54%) and NH_4^++OrgN (57% to 72%), and does not change for OrgC. Decrease in chemostatic response for TN and TP arises primarily from movement of sites from chemostatic to the mobilization and chemodynamic clusters, and this can be attributed to erosion and particulate transport in post-fire landscapes that correspond to increasing concentrations at higher flows. The opposite behavior is apparent for NO_3^-+NO_2^- and NH_4^++OrgN where movement occurs from both dilution and mobilization clusters to the chemostatic cluster. It's possible that this chemostatic behavior results from homogenization of source areas of soluble nitrogen (organic and inorganic) with depth in the catchment (Thompson et al., 2011; Zhi & Li, 2020), as biologic uptake is suppressed after fire. With accumulation in the subsurface, subsurface sources and surface sources like ash might result in more homogenous export regardless of flow pathway.

In Section 4.4.2.1., we compared pre- and post-fire conditions using change metrics of the continuous nature, while in this section we compared conditions with binary change between clusters. While the changes between clusters capture multiple variables at once (the variables used in the cluster formation), it can be useful to validate that our binary change metrics is not too sensitive: meaning, that very small changes are less likely to be represented by cluster change than larger changes. We show that changes in cluster behavior post-fire correspond to larger movements in the CQ parameter space. Because of the unique characteristics of these clusters, and the benefit that they map onto more classical CQ typologies (Figure C2), we can visualize post-fire movement according to the same characteristics. An example of a logical and expected result would be to examine movement from the Mobilization to Chemostatic cluster (Figure C5: upper-left of panels (a) and (b); blue empty circles to red circles). As we could imagine looking at Figure 4-3, we see that real movement from Mobilization to Chemostatic corresponds to decreases in *b* slope and Regression R^2, as well as mostly decreases in CV_C/CV_Q. Based on the three input variables into our clustering methodology, we calculated Euclidean distances in "cluster space" (Figure C6), to reconcile the pairings of variables in Figure 4-3 (also Figure C5). Figure 4-6 shows that a large number of sites remain in the same cluster post-fire, and our Euclidean distances tell us that while there is movement in cluster-space for unchanged sites (Figure C6: "like" colors), movement between clusters correlates to larger distances. Indeed, Euclidean distances moved from the Mobilization to Chemostatic cluster (Figure C6: blue box on red background) is greater than within-cluster movement, but movement from Dilution to Chemostatic clusters is even greater. This is largely due to the large movements along the R^2 axis, despite smaller movements on the *b* axis (Figure C5b). One eye-catching part of Figure C6 are the

large Euclidean distances moved *within* the Chemodynamic cluster, between pre- and post-fire. Indeed, movement within the Chemodynamic cluster appears to represent increases in *b*, as well as R^2, setting a new domain for the cluster (Figure C7) in the post-fire period. Due to the low number of sites in this cluster, we cautiously speculate that the movement towards the domain of "threshold dominated transport" (Figure C2; Musolff et al., 2015) will have implications for concentration regimes and fluxes of elements from fire-impacted landscapes.

4.4.2.3 Change in Flux Post-Fire

We next explored how change in the CQ dynamics can lead to a change in solute fluxes. Our initial hypothesis in this research was that the CQ *b* slope would be the most important predictor of changes in CQ behavior, which would logically translate to the product of C and Q: Flux. We found that changes in flux were better described by either grouping by clusters (Figure 4-7), or multiple linear regression of multiple variables (Figure 4-8). Of those variables, *b* slope was among the least important predictors.

We found that the change in flux post-fire (comparing the 5 years post-fire to the pre-fire period) varied with clustering behavior pre- and post-fire (Figure 4-7). Our results are mostly logical: movement from dilution to chemostatic behavior results in increasing fluxes, as does movement from chemostatic to mobilization or chemodynamic behavior. We've seen that there can be changes in CQ characteristics within clusters (Figure C6), and so too are there changes in fluxes where the cluster classification does not change pre- to post-fire (Figure 4-7). An oddity in our results includes relatively little change in flux for sites moving from the Mobilization cluster to Chemostatic, despite seeing from Figure C5 that this corresponds with decreases in the *b* slope.

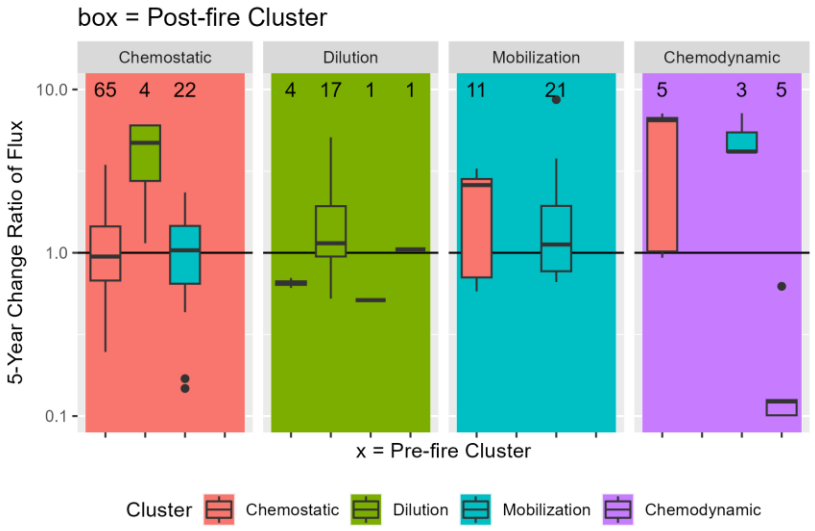

Figure 4-7. Change ratio of Flux. Comparing average of daily fluxes 0-5 years post-fire to the pre-fire period. The plot is separated into 4 panels, indicating the post-fire cluster, and each of 4 divisions on the x axis indicates the pre-fire cluster. Boxplot fill color indicates pre-fire cluster, while larger panel color indicates post-fire cluster. Like-colors indicate no change in cluster. Mis-matched color indicates the "to" and "from" of changing clusters. Above each boxplot is the number of points for each group (refers to "flows" in Figure 4-6).

In our initial examination of changes in concentration (crC), we found that the change ratio for flow (crQ) was very weakly correlated, compared to stronger correlations with CQ metrics like change in intercept parameter *a* or with the change ratio in concentration variability ($crCV_C$). We conducted the same correlation analysis for the post-fire change ratio for flux (crF, calculated from the WRTDS models), with an additional variable test against change in concentration. Daily flux is calculated from daily measured flow and either measured or modeled daily concentration, so it would be unsurprising that flux is highly correlated to both variables. Given that the majority of our sites were classified in the Chemostatic cluster both pre- and post-fire, we would expect that variation in changes in flux post-fire could be mostly explained by changes in flow post-fire (Thompson et al., 2011). Instead, we see that change in concentration is a more important variable by several aspects. In a single-variable comparison (for all elements), the R^2 of the model of crF against crC was 0.45, compared to R^2 of crF against crQ of 0.37.

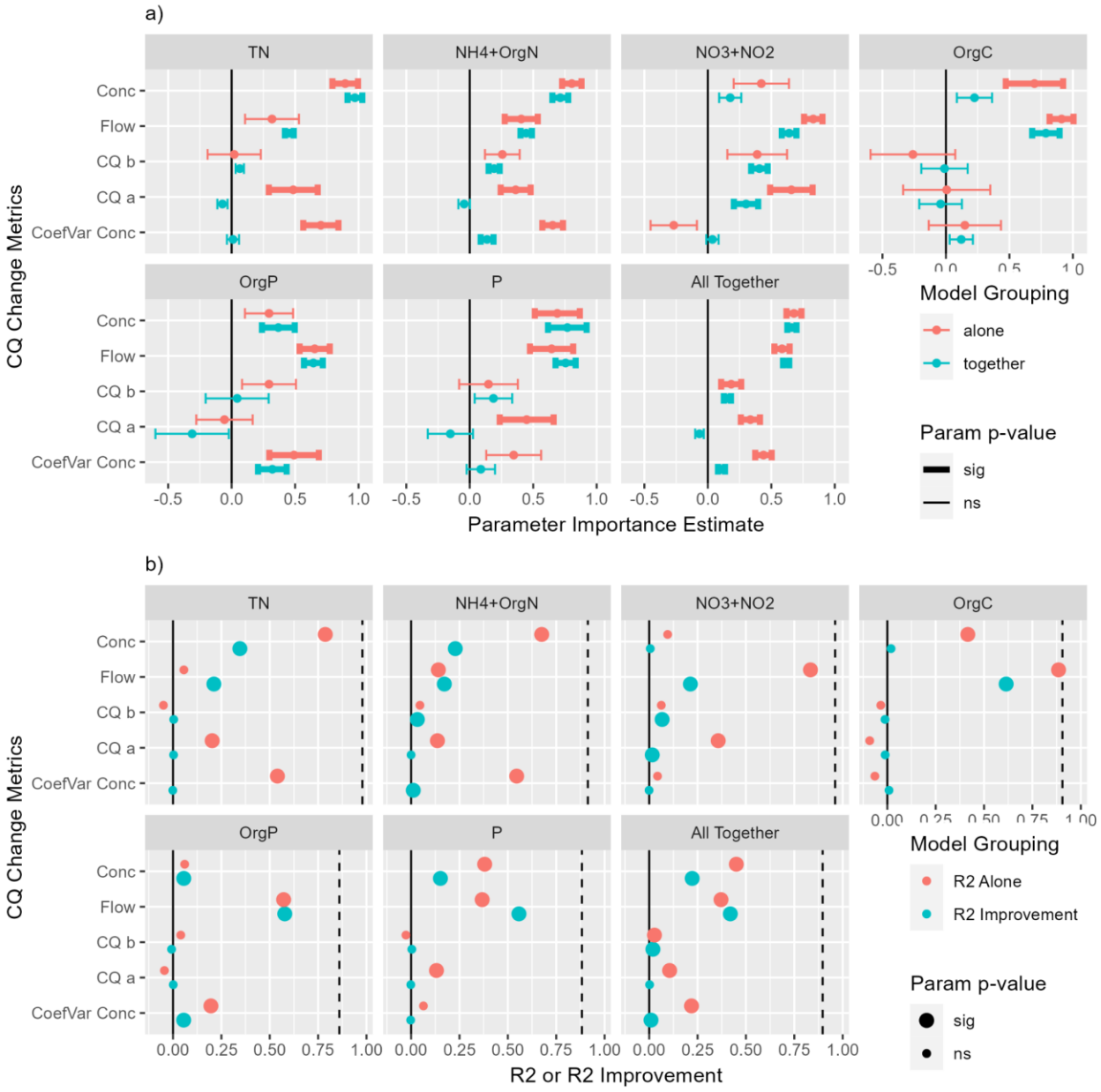

Figure 4-8. Standardized multiple linear regression output. Model metric is the change ratio of flux (crF). Change ratios (cr) were log transformed, and then all variables were divided by their respective standard deviations. Regression variables were changes in flow (crQ), concentration (crC), concentration variability (coefficient of variation; $crCV_C$), *b* slope (absolute change, d*b*), and intercept parameter *a* (absolute change, d*a*). Significance was measured with an alpha of 0.05. Model "alone" (solid lines or circles) was each variable independently against crF. Model "together" (dashed lines) was crC against all four variables. R^2 gain (triangles) was measured during "leave one out" analysis as the R^2 improvement after the inclusion of each variable back into the model against crC and the remaining not "left out".

In a joint model of crF against crC+crQ, model R^2 increased to 0.85, with variable importance estimates of 0.69 for crC and 0.60 for crQ. Adding the other variables (difference d*a*, d*b*; change ratio $crCV_C$) improved model R^2 slightly to 0.90. Breaking out by element group, we see differences, where for TN, NH_4^++OrgN, and P, crC remains the largest variable importance and R^2 (Figure 4-8). In contrast, for NO_3^-+NO_2^-, OrgC, and OrgP, crQ supersedes with the largest variable importance and R^2. When we previously examined correlation to crC, for OrgC the only significant correlation was crQ. Examining correlations for change in flux of OrgC, we again see that the only significant correlation is between crF and crQ. The other element groups have multiple significant correlations, noting the most important ones we just laid out. The change in variation of concentration ($crCV_C$) correlated to crF for the same elements for which it was correlated to crC, including TN, NH_4^++OrgN, and OrgP. For TN and NH_4^++OrgN, the variable importance estimates and R^2 for $crCV_C$ and d*a* were all higher than those values for crQ. For each element group, in the "leave one out" analysis, crC and crQ were the only two metrics to see substantial improvement in R^2 after inclusion. This highlights the interplay between change in flux and CQ relationships. Our cluster analysis roughly grouped change after fire into two behaviors: increasing chemostatic behavior (decreasing mobilization) for NO_3^-+NO_2^- and NH_4^++OrgN, and decreasing chemostatic behavior (generally increasing mobilization) for TN, OrgP, and P. Our study has shown the importance of considering multiple aspects of concentration and flow regimes and CQ behavior. Especially important is the role of variability in concentration. Differences between our cluster groupings and behavioral changes post fire, compared to flow- versus concentration-dominated flux changes, highlights the potential for future work in large synthesis analysis.

Changes in post-fire water quality have implications for both our understanding of catchment biogeochemical function, and the usability of water downstream by humans. Our clustering analysis has shown that variability is an important characteristic for water quality regimes, in headwater catchments, and in catchments susceptible to wildfires. In our clustering technique, 2 of the 3 input variables captured an aspect of water quality variability. Many prior CQ analyses have exclusively used *b* slopes (and variations such as segmented slopes) to characterize CQ typologies, including attempts to correlate catchment characteristics with *b* slopes (Godsey et al., 2009; Moatar et al., 2017; Zarnetske et al., 2018). While these analyses along with others (Zhi & Li, 2020) make reasoned arguments to mechanistically explain the emergence of different CQ typologies (namely chemostasis,

dilution, mobilization), variability in concentration *around* a modeled CQ relationship should receive more focus. So far, prior studies of CQ relationships with a focus on CV_C/CV_Q as a metric have found that across gradients of increasing land cover alteration or increasing anthropogenic nutrient inputs, CV_C/CV_Q decreases as element fluxes increase (Basu, Destouni, et al., 2010; Musolff et al., 2015, 2017; Thompson et al., 2011). Our study has shown that dramatic changes in water quality variability are possible after fire.

4.4.3 Limitations and Future Work

The work presented here presents a novel method of classifying CQ typologies. Because we used all 186 site-fire-parameter sets from all element groups (including species of N, P, and C), the cluster groupings aggregate behavior from water quality constituents. Our results showed a dominance of chemostatic behavior for all elements except for $NO_3^-+NO_2^-$, but this conclusion might change if we had performed the k-means clustering on CQ behavior of each element or specie independently. Ultimately, despite an impressive number of 186-site-fire-parameter sets, our work was limited by the number of sites available for all of the studied elements. This was mostly apparent in analysis of the Chemodynamic cluster, which had only n=7 members. The Dilution cluster was also poorly represented, at n=22 members, most of which were from $NO_3^-+NO_2^-$ sites. With this context, we suggest that our interpretation of results might be slightly biased–for instance, the switching of some sites towards the Dilution cluster for OrgP and P post-fire. If our classification of dilution behavior is informed mostly by $NO_3^-+NO_2^-$ sites, are the parameters for that classification (as determined by the pre-fire k-means groupings) appropriate for the observed post-fire behavior of OrgP and P? This could be answered in future work, where more sites and more data could better characterize the boundaries of CQ behavior, in undisturbed systems, and in post-disturbance water quality regimes.

The number of sites in this study is the primary limitation to conducting analysis on catchment characteristics (e.g., slope, geology, soils, vegetation, nutrient budgets) with respect to CQ behavior. While numerous studies (see the previous section) have performed such analyses for systems ranging from pristine to heavily human-impacted, no study has compared CQ behavior from pre- and post-disturbance as we have done, and no study has yet to examine how CQ behavior change correlates to other catchment characteristics. Notably, the work of (Rust, Saxe, et al., 2019) found that wildfire severity (as percent of watershed as moderate or high burn intensity) was correlated to elevated post-fire total N and P loading. If further use of these CQ typologies intend to target whether source or

sink areas in watersheds are altered by fire, then analysis on disturbance characteristics will be important.

In addition to limitation by the number of sites, our analysis may also be limited by the data availability at those sites. Our sample threshold is quite low (25 measurements in each 10-year interval), and while the processing of data through WRTDS allowed us to analyze daily modeled concentrations for each site, the validity of those daily WRTDS estimates should be further interrogated. While the flux bias statistic threshold of 10% enforces some quality control on the WRTDS estimates, further screening could ensure that water quality concentration samples come from across the flow regime (sampling both low and high flows). This could highlight bias in both low and high temporal resolution timeseries.

4.5 Conclusions

This analysis presents what is to our knowledge some of the first cross-site synthesis in changes in concentration-discharge (CQ) behavior in disturbed watersheds: here specifically in wildfire-impacted watersheds. Numerous studies have used CQ plotting and analysis to represent the impact of fire on water quality (Bladon et al., 2008; Emmerton et al., 2020; Silins et al., 2014; Wilkinson et al., 2006), and generally showed increases in the *b* slope of the CQ relationship. We approached this work assuming we would see this finding of increased *b* slope across many sites. In our synthesis of 29 watersheds (Figure 4-1) and 186 site-fire-parameter sites, examining the post-fire response of nutrients including nitrogen (as NO_3^-+NO_2^-, NH_4^++OrgN, TN), phosphorus (OrgP and TP), and carbon (OrgC), we observed complicated relationships between changes in C, Q, and Flux.

We analyzed several aspects of CQ behavior pre-fire, including the variables *b* slope, CV_C/CV_Q (coefficient of variation of concentration over CV of flow), and the CQ regression R^2, and generated several CQ typologies (Figure 4-3) mapping to characteristics we called Chemostatic, Dilution, Mobilization, and Chemodynamic (following descriptions by (Musolff et al., 2015). We found that chemostatic behavior dominated all of the hydrochemical variables, except for NO_3^-+NO_2^- (Figure 4-4). We then analyzed the classification of these clusters post-fire, compared to pre-fire, and found that for NO_3^-+NO_2^- and NH_4^++OrgN, the proportion of sites with chemostatic behavior increased after fire, while the proportion decreased when measuring TN, TP, and OrgP (Figure 4-6).

In addition to our novel cluster typology method, we analyzed metrics of CQ behavior after fire to detect change (Figure 4-5). Overall, we did not observe universal increases or decreases in

concentration or flux, similar to our previous findings in a meta-analysis of post-fire water quality response (Hampton et al., 2022). This lack of universal response led us to return to our cluster analysis and examine how water quality changed relative to the cluster classifications. We found that changes in flux were well predicted by the corresponding changes in cluster classifications. Notably, movement from the Dilution cluster to Chemostatic corresponded with increases in flux, as did movement from Chemostatic to Mobilization and all movement to the Chemodynamic cluster. This clustering technique is a novel way to reconcile changes occurring in multiple characteristics of the CQ relationship after a disturbance.

While our study benefited from abundant data from different fires and hydrochemical variables, the limited number of unique watersheds prevented analysis of catchment attributes. With the abundant characteristics of CQ relationships, however, we were able to conduct correlation analysis to understand the roles of concentration (C) and flow (Q) in controlling changes in flux after fire. Surprisingly, we found that change in concentration was the strongest predictor of change in flux (Figure 4-8). For individual hydrochemical variables, change in flow was the most important predictor for change in flux in the case of OrgC, NO_3^-+NO_2^-, and OrgP. As discussed above, there was no universal direction of change for the CQ *b* slope, and the change in *b* slope after fire was the least important predictor of change in flux, despite our initial assumption otherwise. In fact, the change in variability in concentration was the third most important predictor overall, after concentration and flow, and was the second most important for NH_4^++OrgN. This analysis points back to our clustering typologies and suggests that analysis and grouping of multiple CQ characteristics can be beneficial to disentangling the large amount of variability in water quality changes after disturbance.

Chapter 5
Development of a coupled hydrologic, vegetation, and biogeochemical model to simulate disturbance effects on stream nutrient export regimes

5.1 Introduction

Forested watersheds have served as a focal point of intense interest from watershed managers and hydrologic and biogeochemical modelers investigating how water, vegetation, and soils interact (Blöschl et al., 2019). Finding a balance between multiple uses for and pressures on forests requires detailed study of the hydrologic, biotic, and biogeochemical processes that manifest in the forest behaviors we observe. Further study under "undisturbed", recovering, and disturbed conditions can reveal which processes are important where and when on the landscape. From harvesting disturbances in particular, there are concerns that increases in concentrations of dissolved organic carbon and nutrient forms of nitrogen or phosphorus could lead to challenges in water treatment (Mistick & Johnson, 2020; Mupepele & Dormann, 2017; Neary & Koestner, 2012), whether those challenges come from treatability or cost of treatment.

From many decades of individual studies of forest harvesting effects, it has become clear that the response of hydrology and water quality is highly dependent on the magnitude of disturbance and the climatic context. In the United States, one of the preeminent research experiments in the northeastern hardwood forest ecosystem has been conducted at the Hubbard Brook Experimental Forest (Campbell et al., 2021; Fahey et al., 2015; Likens et al., 2021). One key insight from over 5 decades of work there is the role of intersecting disturbances, where the water quality and ecosystem effects of experimental harvests are influenced by disturbances many decades prior, including historic acid deposition, extreme weather events, climate change, and prior harvests. In Canada, the Turkey Lakes Watershed Study (TLW; (Foster et al., 2005; Jeffries & Foster, 2001; Webster, Leach, Hazlett, et al., 2021) has also served as an important long-term benchmark of forest health and recovery from multiple disturbances. Experimental harvests of differing magnitudes showed that while clearcut harvesting has the largest effect on post-harvest water quality, other industry standard harvesting procedures had smaller effects (Webster et al., 2022). Large synthesis reviews by (Bosch & Hewlett, 1982; A. E. Brown et al., 2005) found rough correlation between disturbance magnitude (percent

watershed harvested) and the response of streamflow, however work by Goeking (Goeking & Tarboton, 2020, 2022) suggests that the specific disturbance-response relationship is governed by climate, with wetter climates exhibiting a larger increase in flow after disturbance. While forests in dryer climates may defy the traditional hypothesis of increased flow after harvest, for wetter forests the hypothesis generally predicts that a reduction in vegetation leads to less transpiration, increased soil moisture, and increased streamflow, at least until vegetation recovers from the disturbance. This soil moisture effect has a large impact on the cycling of carbon and nitrogen in the forest post-harvest. Important work remains to translate the intersecting effects of harvesting on hydrologic, biotic, and biogeochemical processes to accurate explanations of post-harvest water quality.

Mathematical models representing the cycling of water, carbon, and nitrogen in forests have long been used to apply the extent of our knowledge of forest processes to try to explain or predict real-world behaviors. These models stem from influential predecessors (Aber et al., 1982; Aber & Federer, 1992; Band et al., 1991, 1993, 2001; Creed & Band, 1998; Pastor & Post, 1986; Running & Coughlan, 1988; Running & Gower, 1991; Tague & Band, 2001, 2004). Significant contributions to knowledge of these cycles have also come from models of non-forested systems (Comins & McMurtrie, 1993; D'Odorico et al., 2003; Kelly et al., 1997; Laio et al., 2001; Parton et al., 1987, 1988; Porporato et al., 2001, 2003; Rodriguez-Iturbe et al., 1999, 1999, 2001). In addition to modeling catchments in "undisturbed" conditions, these coupled models have proven effective in reproducing the effects of disturbance on stream flow and water quality (Gbondo-Tugbawa et al., 2001; Valipour et al., 2018). Applications of models in silviculture and managing forests for water supply have greatly increased in recent years, but the scales of study are often limited to single watersheds at a time (Beckers et al., 2009; Johnsen et al., 2001; X. Li et al., 2008; Loucks & Van Beek, 2017; Mäkelä et al., 2000, 2000; Monserud, 2003; Taylor et al., 2009). Models such as the Regional Hydro-Ecological Simulation System (RHESSys) (Band et al., 1991) and the Soil and Water Assessment Tool (SWAT) (Gassman et al., 2007) have been very successful in simulating climate change and disturbance effects on water quality at a process-level (Beckers et al., 2009; Hanan et al., 2017; Kennedy et al., 2017; Krysanova & Arnold, 2008; McKenzie & Perera, 2015). Despite this, the complex nature of these models makes understanding the broader processes leading to degraded water quality prohibitively expensive and time consuming. In addition, there is a trade-off between cross-site applicability and an intense site-specific calibration process for each model. In this effort, emphasis will be placed on model simplicity or parsimony, such that important patterns

can be replicated with minimal computational effort (Basu, Rao, et al., 2010; Sivapalan, Blöschl, et al., 2003; Sivapalan et al., 2011).

Studies have already shown that "simple" box models with as few as six parameters can appropriately model the regime and flow duration curves of approximately 200 catchments across the conterminous USA (Ye et al., 2012). Similarly, the study by Parolari and Porporato (2016) showed that complicated soil C and N dynamics can be modeled with closer to 20 parameters, such that modeled aboveground plant biomass trajectories can match observed values following disturbances. These results are a strong argument for prioritizing model parsimony. To capture both water and forest dynamics, the combination of these two models should be able to show the effect of vegetation on soil moisture and streamflow and altered soil moisture regimes on nutrient cycling and export. Valipour et al. (2018) show the application of a similar non-distributed hydrology and soil biogeochemistry model (PnET-BGC) to a clearcut site at the Hubbard Brook Experimental Forest. They show strong fits for total plant biomass recovery as well as several elements in soil and soil water solution. Streamwater DOC is poorly modeled however, requiring further investigation. Simple one or two-layer soil pools such as those used in the Parolari and Porporato (2016) model can house important processes like organic matter decomposition, nitrification, denitrification, and sorption; appropriately capturing trends of element fluxes through time. This "top-down" modeling approach is the best way to ensure model parsimony and will illustrate important universal processes needed to replicate streamflow and water quality timeseries at multiple forest sites.

The goal of this study is to elucidate the processes in a forested watershed that drive the hydrologic and biogeochemical response after harvesting and other disturbances. In this work, I developed a modeling framework emphasizing simplicity and cross-site applicability and drawing on principles used in simpler models of carbon and nitrogen dynamics in forest soils (Gbondo-Tugbawa et al., 2001; Parolari & Porporato, 2016; Porporato et al., 2003). My modeling approach was characterized by the following principles:

- parsimony: the model should strive to have as few as possible parameters, processes, and variables (Atkinson et al., 2002; Basu, Rao, et al., 2010; Sivapalan, 2003)
- downward approach (Sivapalan, Blöschl, et al., 2003; Ye et al., 2012): the model construction will have an iterative and cyclical process where justifications are made to increase model complexity

The model results can elucidate the most important soil biogeochemical and ecohydrological processes altered by forest disturbances, and the sensitivity of these models and their predictions in different ecozones/climates. I compare model performance to multiple parameters including mean concentrations and fluxes, how the model captures variability in water quality after disturbance, post-disturbance C-Q relationships, and timescales of water quality recovery.

5.2 Model Design

The design of this model features a novel combination of model components including hydrology and soil moisture dynamics, vegetation, and soil biogeochemistry. The construction of this model, while drawing heavily on equations and components from other models, focussed on simplicity while also calibrating/validating the model against real-world data.

Numerous bottom-up models exist that have modeled one to all three of these components with varying spatial complexity. For example, RHESSys (Band et al., 1996, 2001; Tague & Band, 2004) can model all three of these components, spatially distributed and varying in characteristics throughout a watershed, but the model features numerous complicated physically-based processes and a very large number of parameters. The Physiological Principles Predicting Growth model (3PG: (Landsberg & Waring, 1997) features complicated vegetation processes and behaviors, but generally ignores subsurface processes, whereas the work of Porporato et al. (2003) focuses on parsimonious soil moisture and soil biogeochemical interactions, while ignoring dynamic vegetation behavior. In contrast, S. Ye et al. (2012) developed a parsimonious lumped hydrology model applicable to catchments varying in size and in climate, with additions of vegetation influence on hydrology. Parolari & Porporato (2016) developed a simplified version of the subsurface model by Porporato et al., to better model steady-state and regrowth vegetation dynamics and impacts of soil nutrition on growth.

Our goal is to follow in the footsteps of these authors and solidify linkages between all three of these components (Figure 5-1a, Table 5-1). First the lumped hydrologic model (see Section 5.2.1.), is linked with vegetation and canopy dynamics (Section 5.2.2.), incorporating interception of precipitation. The evapotranspiration flux also varies with seasonal and multi-year changes in vegetation. Inversely, vegetation growth is limited in low-moisture conditions. All biogeochemical processes in the subsurface (Section 5.2.3.) are influenced by soil moisture. This in turn impacts the availability of nitrogen for uptake by vegetation, imposing nutrition limitations on growth. Nitrogen

and carbon from the vegetation biomass is returned to the soil through turnover, governing the nutrients available for decomposition and later uptake, and also influencing the C/N ratios in the soil. The details of all model components are summarized in the sections below. The full model set of model equations and parameters are included in Appendix D to this dissertation. This model is tailored to the small experimental watersheds at the Turkey Lakes Watershed Study (TLW), but the application of parsimony can make it applicable to other catchments. Details about the TLW site are in Section 5.3.1.

Table 5-1. Summary of model components. Numbers of state variables/pools, processes, and parameters. The state variables may be referred to as pools throughout this Chapter.

Model Component	State Variables	Processes/Functions	Total Parameters
Hydrology	3	10	17
Soil Biogeochemistry	12	12	22
Vegetation	4	14	30

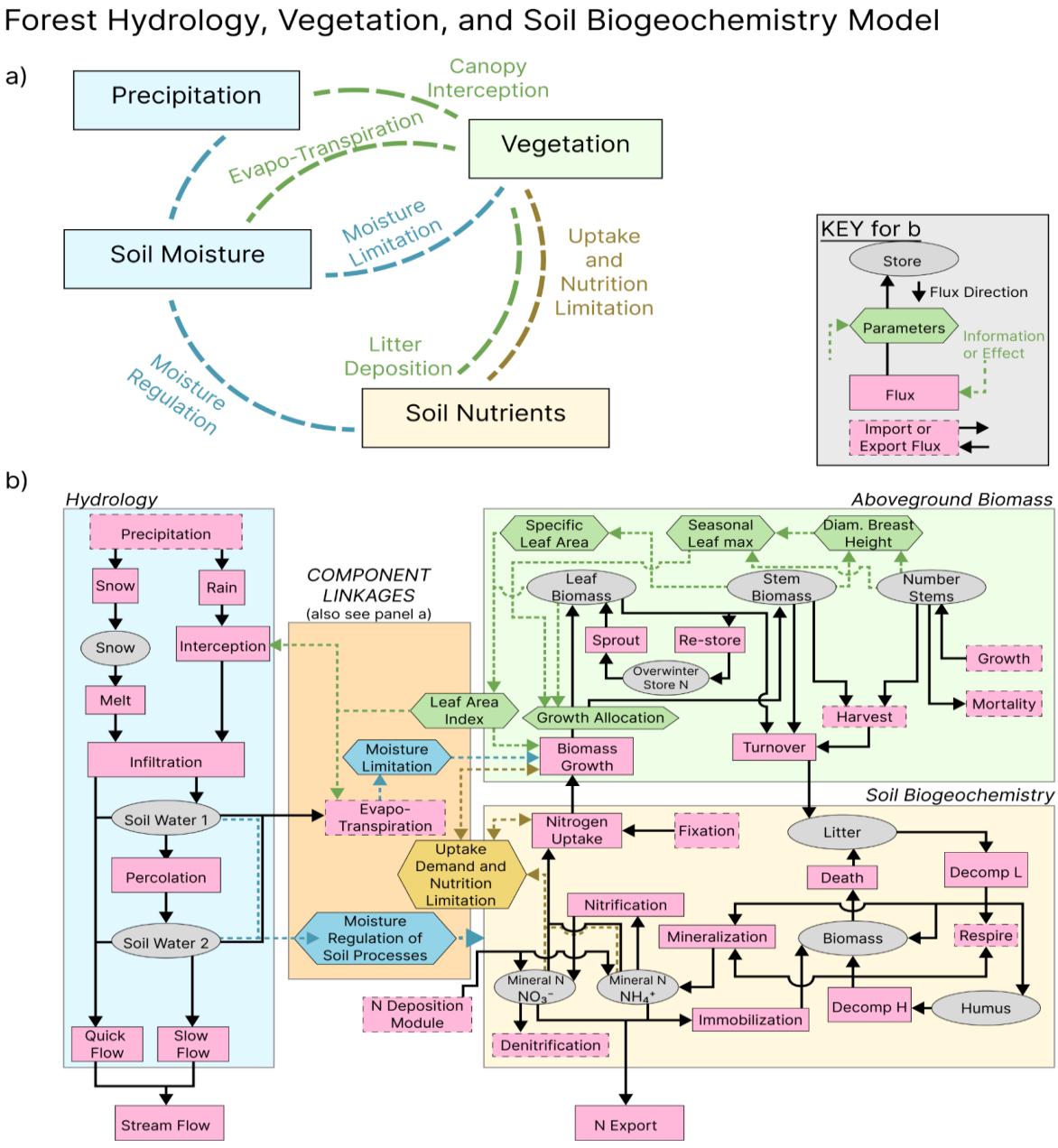

Figure 5-1. Forest hydrology and growth model schematic. (a) Schematic of the model and influences (dashed lines with labels) between model components (boxes). Each component has influence on at least one other, with a cyclical behavior resulting from the relationships. (b) Detailed organizational chart of the main model components (summarized in Table 5-1, italicized text). Model stores with gray ellipses are connected by black flux arrows (labeled with text in pink rectangles) indicating material movement direction. Important parameters driving the component linkages are labeled with colored hexagons. Information feeding each parameter and influence direction of each parameter is indicated with dashed colored arrows. The important component linkages in the center

box correspond with those labeled in panel a. The Nitrogen Deposition Module follows the form of the hydrology stores and fluxes, with details provided in Section 5.2.3.1.

5.2.1 Hydrology and Soil Moisture Dynamics

The hydrology model is affected by the vegetation model (see Figure 5-1) and specifically by the leaf area index (LAI) which modulates the interception and evapotranspiration fluxes. Soil moisture calculated from the hydrology model in turn affects soil biogeochemical processes and plant growth. Hydrology is modeled with a lumped 'leaky bucket' model (Atkinson et al., 2002; Milly, 1994; Ye et al., 2012), with two vertically stacked boxes to represent soil moisture dynamics (Eq. D2-8,9), and a separate snow compartment to capture snowmelt dynamics (Eq. D2-7). While the general structure of the hydrology model follows the approach by S. Ye et al. (2012), slightly more complex and nonlinear model equations are used to describe the coupling between the soil moisture and vegetation dynamics, incorporated from Porporato et al. (2003) and the HBV model (Bergström, 1995). The model equations are included in Appendix D2.2.

5.2.1.1 Snow and Interception

The snow component of the model follows the formulation by S. Ye et al. (2012). A transition temperature governs whether precipitation fell as rain or snow (Eq. D2-10,11). Precipitation as snow is added to the snowpack store. Snow melt follows the degree-day formulation, as used by S. Ye et al. (2012) and (Eder et al., 2003). Melt rate is proportional to the calibrated degree-day factor and the amount that air temperature exceeds the melting threshold temperature (Eq. D2-12,13).

Interception (See Figure 5-1a; Eq. D2-14,15) of the rainfall by the tree canopy is calculated following the formulation used in the HYDRUS model (Šimůnek et al., 2005, 2013), as used by (Sutanto et al., 2012). Interception increases with the static parameter α (alpha), the daily LAI, and with an exponential extinction coefficient. I assume that interception can result in instantaneous evaporation of water, up to the daily potential evapotranspiration (PET) amount. Since the model ran on a daily timescale, I assume that if PET is met, the remainder of water would find its way through stemflow to the soil surface over the course of a single day.

5.2.1.2 Hydrologic Fluxes

The water arriving at the soil surface includes rainfall that is not intercepted and snowmelt (Eq. D2-16). A portion of this water infiltrates into box 1, with infiltration (Eq. D2-17) modeled using the HBV formulation (Bergström, 1995), while the remaining is directed to streamflow as infiltration-excess runoff (Eq. D2-18). Percolation moves water from box 1 to 2 (Eq. D2-19) and this is modeled as a threshold-based exponential process, as in (Porporato et al., 2003)). Two lateral fluxes route water from box 2 to the stream: a baseflow component that uses an exponential formulation (Eq. D2-20), and a subsurface fast flow component that is triggered when box 2 is fully saturated (Eq. D2-21).

5.2.1.3 Evapotranspiration

Potential evapotranspiration (PET) is modeled using the Hargreaves-Samani method (Hargreaves & Samani, 1985), following (Buttle et al., 2019) (Eq. D2-1 to Eq. D2-6). Following Sutanto et al. (2012), Beer's law is used to partition potential evapotranspiration to plant transpiration or soil evaporation, according to the canopy cover fraction (b, Eq. D2-22,23,24). Following Porporato et al. (2003), transpiration (Eq. D2-26) occurred when soil moisture is above the wilting point. Plant transpiration has a scaled regime for soil moisture between the wilting point and a stress point (s*). At and above the stress point, total transpiration can equal the daily PET. Between the 2 soil water boxes, transpiration is allocated according to the fraction of evaporate-able water (calculated as soil moisture above the hygroscopic or wilting points, Eq. D2-25). Soil evaporation (Eq. D2-27) only had one threshold at the hygroscopic point (as in Porporato et al., 2003), below which no evaporation took place, and above which, evaporation occurred according to the allocated PET (adjusted by b, as above) up to a capped maximum evaporation rate.

5.2.2 Vegetation Model

The vegetation model is connected to the hydrology model (Figure 5-1) through the evapotranspiration flux that is limited by available soil moisture and by the leaf area index (LAI), and through the interception flux that is related to LAI. The vegetation model is also connected with the soil nutrient model through nutrient uptake and availability in the subsurface and litter contribution; all of which heavily influence the subsurface CN biogeochemistry and stream water quality. Four state variables are modeled: the biomass (in mass of carbon per unit area) of leaves and stems, the number of stems (per unit area), and an overwinter nitrogen store (mass of N per area) that facilitates leaf growth in spring (Figure 5-1).

The vegetation model incorporates modules or equations from (Parolari & Porporato, 2016), Porporato et al. (2003), 3PG ((Landsberg & Waring, 1997) and the Canadian Terrestrial Ecosystem Model (CTEM, (Arora & Boer, 2005). Section 5.2.2.1. describes the calculation of biomass growth, addition of growth to the leaf and stem biomass pools, and seasonal variation in growth. Section 5.2.2.2. describes biomass turnover and turnover seasonality, litter contribution to the soil, and contributions to the overwinter N pool. Section 5.2.2.3. describes how N uptake demand is calculated, allocation of N demand to withdrawals from the overwinter N pool or to soil mineral N (described in more detail in Section 5.2.3.), and how biomass growth rates are limited by insufficient N uptake. Section 5.2.2.4. describes the dynamics of the "number of stems" state variable and how it contributes to several allometric equations (see dashed green lines in Figure 5-1b) that ultimately feed back to the vegetation model's influence (through the canopy) on the combined model system.

5.2.2.1 Vegetation Growth and Phenology

Vegetation growth is modeled as net primary productivity (NPP), and is related to N uptake (Figure 5-1) through C to N ratios specific to each of the biomass pools. NPP is modeled at the daily scale as a function of the solar radiation, temperature, soil moisture and Leaf Area Index (LAI). Just as in the 3PG and RHESSys models, NPP increases with solar radiation (Eq. D2-32), with factors related to radiation interception by the canopy (Eq. D2-22,24); and is inhibited due to low moisture (Eq. D2-26) and low nutrition availability (Eq. D2-53).

For simplicity, the daily maximum possible rate of NPP is tied through the constant calibrated parameter (g) to daily transpiration (Eq. D2-32), which, through the dependence on daily potential evapotranspiration (PET), already incorporated radiation (modeled, see Appendix D2.1), daily temperature (measured, see Section 5.3.2); and also already accounts for water availability (moisture) stressors. The maximum rate of NPP is allocated to leaves and stems (Eq. D2-33) following the approach used in the 3PG model, with potential limitation of growth by nutrition stress calculated later (detailed in Section 5.2.2.3). The phenology of growth allocation is classified into four seasons (based on CTEM, (Arora & Boer, 2005):

1. the maximum growth stage (we will call "leaf-out", most growth goes to leaves),
2. the normal growth stage (we will call "summer"),
3. the senescence stage (we will call "leaf-fall", no leaf growth occurs), and
4. the dormancy stage (no growth occurs).

At a given timestep, biomass growth (accounting for both carbon and nitrogen allocation) can contribute to growth of stems or leaves. This allocation (Eq. D2-33) is largely governed by a preference to allocate growth to leaf biomass during the leaf-out period, until the leaf biomass approaches some fraction of the seasonal maximum leaf biomass (Eq. D2-34, for more detail see Figure 5-1b and Section 5.2.2.4.). This allocation leads to different N demands from the soil mineral nitrogen pool (see Section 5.2.2.3.). During the leaf-out period, 100% of growth is allocated to leaves. Because of the necessity to model both carbon and nitrogen, we explicitly modeled C/N allocation from the stems to the leaves at the beginning at the leaf-out period, which we called "sprouting" (Eq. D2-35, Figure 5-1b). The physical basis for this process is supported by general literature (Millard, 1996; Millard & Grelet, 2010; Pregitzer et al., 2010) and studies of sugar maple at TLW specifically (Morrison, 1991). The dates of summer growth are determined by the end of leaf-out and the beginning of leaf-fall. During summer growth, growth is allocated to leaves and stem, according to how close the leaf biomass is to the potential seasonal maximum biomass (Eq. D2-33). After the beginning of the leaf-fall stage, growth allocated to leaves is manually set to zero, and leaf turnover begins (see Section 5.2.2.2.). While any leaves remain during the leaf-fall stage, and whenever PET and transpiration are above zero, 100% of NPP is allocated to stems. The dormancy stage follows the leaf fall stage. Because the canopy leaf biomass approaches zero, no growth can occur. This period of fall and winter is characterized by low PET, due to low temperatures and solar radiation.

5.2.2.2 Plant Biomass Turnover

The leaf biomass pool only experiences turnover during the leaf-fall stage (Eq. D2-57), while the stem biomass pool experiences a small rate of turnover year-round (Eq. D2-59). During leaf-fall, a constant fraction of leaf biomass nitrogen is conserved on a daily timestep, contributing to the overwinter store that will contribute to sprouting in the spring (Eq. D2-58).

5.2.2.3 Nitrogen Uptake and Limitation

As discussed in Section 5.2.2.1, the rate of maximum daily growth can be from a combination of NPP (of leaf and/or stem) and sprouting (Eq. D2-36,37). While the daily maximum rate of NPP is tied to moisture availability through the transpiration rate, the maximum sprouting rate is only modulated to calculate the true sprouting rate by nitrogen availability. As discussed above, leaf growth through sprouting or NPP will require a different C/N ratio than NPP allocated to stem growth. After accounting for N withdrawal from overwinter stem storage (Eq. D2-39), and "free" N at the C/N ratio

of stems (Eq. D2-38), the daily maximum N demand from uptake (sprouting and NPP) is calculated (Eq. D2-41).

Following the methods of Porporato et al. (2003), N uptake is divided into passive and active processes, with different characteristics for the two N species ammonium (NH_4^+) and nitrate (NO_3^-). While NO_3^- is assumed to be readily soluble in water, NH_4^+ is assumed to be strongly bound to soil, and thus resistant to solubility. Passive uptake is assumed to be uncontrolled, as in, the trees cannot throttle down passive uptake if demand is low. Passive uptake represents incorporation of soil solution and any accompanying minerals through transpiration. Uptake of the soluble minerals from each of the two water boxes is proportional to the mineral pool size, its associated solubility, and the fraction of water taken up by transpiration in each timestep (Eq. D2-42,43). Excess passive uptake contributes to N storage in plant tissues (Eq. D2-44), although it is not expected that this is a large contributor to the N budget during the growing season.

If the maximum daily N demand is not met by total passive uptake (of the two N species, from each of the two water boxes), then the plants engage in active uptake (Eq. D2-46). Active N uptake is also related to soil moisture (Eq. D2-45). Following the methods of Porporato et al. (2003), the moisture dependency of active uptake for each pool decreases with the total moisture, due to dilution of the existing N within the soil pool, but increases relative to the fractional moisture due to nonlinear poor connectivity, and increased diffusion through the soil.

Finally, if the maximum daily N demand is not met by total active and passive uptake, nitrogen fixation by soil microbes is also considered to contribute to plant N (Eq. D2-47). Studies of northern hardwood forests, including sugar maple dominated forests, have documented surprisingly large N fixation budgets, either through mass balance approaches or explicit measurement of fixation (Benoist et al., 2022; Bormann et al., 1970, 1977; Johnson & Turner, 2014; Roskoski, 1980; Vitousek et al., 2013). A maximum daily N fixation rate is specified.

The total N available for growth is the sum of N store withdrawal and passive, active, and fixation uptake (Eq. D2-48). Sprouting is given first priority in terms of growth and N allocation (Eq. D2-49,50). The final daily sprouting rate is calculated as the available N allocation to sprouting times the leaf C/N ratio (Eq. D2-51). The remaining N is allocated to NPP (Eq. D2-52). The timestep NPP allocation to leaves and stem is calculated as in Section 5.2.2.1 (Eq. D2-55,56), and because the N

demand from that allocation is already calculated according to the leaf and stem C/N ratios, any deficit in N uptake can be fractionally distributed between the two (Eq. D2-53,54).

5.2.2.4 Stem Modelling and Allometric Equations

As shown in Figure 5-1, the "number of stems" state variable experiences its own growth and mortality rates (with units of stems per unit area, rather than carbon per unit area). The modeling of stems followed the form of the 3PG model (Landsberg & Waring, 1997). At a given timestep, the number of stems provides information to several allometric equations including the diameter at breast height (DBH, Eq. D2-60), and the seasonal maximum leaf biomass (Eq. D2-34, as discussed in Section 5.2.2.1.), connecting the stem module to drivers of the vegetation biomass module.

Because the leaf biomass pool asymptotically approaches the seasonal maximum biomass each year, the variation in LAI (Eq. D2-62) seasonally and between years is thus dependent on the dynamics in the number of stems pool (Figure 5-1). After harvest, the number of stems will increase from a small number to a larger number, and likewise the maximum possible amount of leaf biomass will increase considerably as the forest ages. LAI is also proportional to the specific leaf area (SLA, units of m^2 kg^{-1}, Eq. D2-61). The SLA changes also as a function of forest age, such that young trees have a higher SLA, and thus a higher LAI, for a given leaf biomass.

The variation in the number of stems is governed by a simple set of growth and mortality equations. Both growth and mortality have different regimes as the forest ages. The timestep stem growth has two regimes (based on (W. J. Wang et al., 2013); Eq. D2-64):

- If the number of stems is less than a "canopy closer" threshold (Eq. D2-65), growth in the number of stems will occur at its maximum rate
- If the number of stems is greater than the closer threshold, then growth scales down asymptotically to zero as the number of stems approaches a maximum stem threshold (Eq. D2-66).

The timestep stem mortality from the 3PG model has three regimes:

- If the number of stems exceeds a thinning threshold (Eq. D2-64, itself calculated according to the total forest biomass), then thinning or "crowding" induced mortality occurs (Eq. D2-68)
- When total forest biomass is low, age-induced stem mortality (Eq. D2-69,70) is low
- When total forest biomass is large, age-induced stem mortality is high

When harvesting occurs in the model, both plant biomass and the number of stems are reduced.

5.2.3 Soil Biogeochemistry Model

I modeled twelve state variables in the soil, following the approach of Porporato et al. (2003): organic carbon storage (in mass C per unit area) in the litter, humus, and soil biomass pools (Eq. D2-72,74,75); organic nitrogen storage (in mass N per unit area) in the litter pool (Eq. D2-73), and mineral nitrogen (in mass N per unit area) as both NO_3^- and NH_4^+ in snow (Eq. D2-76,77) and each of the two vertically stacked soil boxes (Eq. D2-78,79,80,81), and the storage of dissolved organic carbon (in mass C per unit area) in each of the two vertically stacked soil boxes (Eq. D2-82,83).

The soil biogeochemistry model is influenced in almost every process by soil moisture dynamics, provided from the hydrology model (Figure 5-1). In addition to material removal through hydrologic export, contribution of nitrogen through atmospheric deposition is closely linked to hydrologic pathways (see Section 5.2.3.1.). Similarly, the vegetation model contributes material to the soil through litter deposition, and removes material through vegetation uptake. The soil biogeochemistry model is derived in almost complete form from the work of Porporato et al. (2003) (see also (D'Odorico et al., 2003), and follows a similar form to well-used models such as FOREST-BGC (Running & Coughlan, 1988). The interactions between soil nutrients and vegetation are derived from the work of Parolari & Porporato et al. (2016). The implementation of this soil biogeochemistry model assumes that of the two hydrologic boxes described in Section 5.2.1, soil processes occur in the upper box. The second box lower has more limited functionality, but does serve as a store of mineral N that is subject to leaching, plant root uptake, or denitrification.

5.2.3.1 Nitrogen Deposition

Nitrogen deposition arrives at the soil surface as dry or wet deposition. In the case of dry deposition, N is added directly to the box 1 mineral N pools, and in the case of wet deposition, N follows hydrologic pathways into and through the soil. Section 5.3.2.2 describes the calculation of annual nitrogen deposition, and downscaling to the daily scale. Deposition is allocated as both ammonium (NH_4^+) and nitrate (NO_3^-). Deposition is assumed to not interact with the tree canopy, but is assumed to interact with the snowpack. If there is snow, then deposition is allocated entirely to the snowpack N pool . If there is no snow, then deposition arrived at the soil surface. Wet deposition arriving at the soil surface is allocated according to hydrologic pathways. If any fast water flow is generated on a

day with wet deposition (with no snowpack), then wet N deposition is allocated proportionally between quickflow and infiltration.

5.2.3.2 Litter Input and Decomposition

Plant turnover and litter production (Figure 5-1) is one of the main carbon (Eq. D2-87) and nitrogen (Eq. D2-88) sources to the plant litter pool. Soil biomass death (Eq. D2-89) is also added to the litter pool. The material added to the litter pool from turnover has a varying C/N ratio, according to the mixture of leaf, stem, and soil biomass components.

The decomposition processes are governed by biotic activity, moisture, soil temperature, and carbon to nitrogen ratios. The term φ (phi, Eq. D2-90,91,92,93) was developed by Porporato et al. (2003) to regulate decomposition, such that an optimal ratio of carbon to nitrogen is available for biotic uptake (C/N_b). Ultimately, two scenarios take place:

- if the C/N ratio from all decomposition is greater (more carbon rich) than C/N_b, then biomass is N-deficient, and the decomposition rate will be reduced while N must be immobilized (Eq. D2-102,103) from the mineral pool to supplement biotic uptake;
- if the C/N ratio from all decomposition is less than C/N_b, then N is produced in excess, and excess N will be mineralized to NH_4^+ (Eq. D2-100,101).

Mineralized N is added to the NH_4^+ pool, whereas immobilization of N can draw from both NH_4^+ and NO_3^-, proportion to their relative abundance in the total soil nitrogen pool.

The decomposition rates (Eq. D2-97,98) are scaled by φ (Eq. D2-93), soil moisture (Eq. D2-94), and soil temperature (Eq. D2-95). Following Porporato et al. (2003), maximum decomposition takes place at field capacity and decreases linearly as moisture decreases. Above field capacity, decomposition decreases at a slower rate. Decomposition of the litter and humus are assumed to be governed by the soil moisture in box 1. The impact of soil temperature on decomposition followed the implementation in RHESSys (Tague & Band, 2004), where soil temperature is calculated as a muted signal of air temperature (Eq. D2-96). The model added a calibrated parameter that could regulate the degree of thermal control on decomposition, with two possible endmembers: isothermal behavior (as in Porporato et al., 2003), or thermal control as in RHESSys.

5.2.3.3 Nitrification and Denitrification

Studies of nitrogen cycling at TLW highlight the importance of NH_4^+ and nitrification in total N export from the catchments. Spoelstra et al. (2001) used isotopes to determine that the majority of NO_3^- exported originally underwent nitrification from NH_4^+. While the N deposition module assumes a fraction of both NO_3^- and NH_4^+ in deposition, once within the soil, the nitrification process is modeled according to Porporato et al. (2003). Nitrification (Eq. D2-105) converts NH_4^+ to NO_3^-, and the process is limited by moisture (Eq. D2-104) assumed to take place in box 1) similar to decomposition. Nitrification is at its maximum at field capacity and decreases linearly as moisture decreases. Above field capacity, nitrification also decreases linearly to zero as moisture approaches 100%.

Denitrification (Eq. D2-107), in contrast, is favored at high moisture levels (Eq. D2-106). Denitrification is inhibited below a threshold soil moisture, above which denitrification increases exponentially to its maximum as moisture approaches 100%. Unlike the other biologic processes, denitrification is assumed to occur in both soil water boxes. Mineral N that leaches into box 2 (Section 5.2.3.4.) can be subject to denitrification, governed then by the box 2 soil moisture.

Both nitrification and denitrification have a governing rate constant, and are proportional to the pool size of the reactant (e.g., soil NH_4^+ in the case of nitrification) and the soil biomass pool, which can be thought of as facilitating the processes.

5.2.3.4 Subsurface N and C Leaching

All subsurface hydrologic flows of mineral N are proportional to the pool size, the solubility factor, and the fractional water flux relative to the water store (Eq. D2-109,110). Just as in transpiration, percolation of N from box 1 to box 2 will be proportional to the timestep percolation rate divided by the timestep pool size. In this way, when N is abundant, it will be more likely to flow with water, and when flows are large, the N pool will be more readily mobilized. Like with N, dissolved organic carbon (DOC) moved through the subsurface with water, with a solubility factor of 1. DOC is produced by a dissolution process (Eq. D2-108) that is assumed to be regulated by a calibrated fraction of the litter pool. No uptake or modification of DOC took place in the subsurface after its production.

5.3 Methods

Most watershed models are calibrated only on streamflow and water quality fluxes at the catchment outlet, giving rise to equifinality issues. The Turkey Lakes Watersheds (description in Section 5.3.1.) are unique with respect to the richness of the datasets on hydrology, vegetation, and soil nutrient pools that have been collected over the years. Calibration of the coupled model presented in this Chapter therefore used a combination of more traditional calibration, as well as more soft calibration techniques (Gharari et al., 2014; Seibert & McDonnell, 2002; Shafii et al., 2017) to increase the robustness of our model. Time series data used for calibration are described in Section 5.3.2. Additional data from the site which are used to "increase realism" in parameter ranges (Gharari et al., 2014) and limit the amount of calibration needed are described in Section 5.3.3. Methodology for calibration is described in Section 5.3.4.

5.3.1 Site Description

The Turkey Lakes Watersheds (TLW) are among the longest running and most data-dense hydrologic and ecosystem study sites in North America. Like the Hubbard Brook Ecosystem Study (Campbell et al., 2021; Fahey et al., 2015; Likens et al., 2021), the measurements from TLW have provided an important multi-decadal signal of change in climate, pollution, and ecosystems (Creed et al., 2014, 2015; Foster et al., 2005; Webster et al., 2022; Webster, Leach, Hazlett, et al., 2021; Webster, Leach, Houle, et al., 2021; Webster & Hazlett, 2015).

The TLW were chosen for model exploration because of partnerships with Jason Leach and Kara Webster of the Natural Resources Canada (NRCAN) Great Lakes Forestry Centre in Sault Ste. Marie, Ontario. This partnership provided access to data and a site visit to provide context for the forests and hydrology at the site.The characteristics of TLW are provided by (Buttle et al., 2018; Jeffries et al., 1988; Webster, Leach, Hazlett, et al., 2021), and are summarized below. The total TLW has an area of 10.5 km^2 (Figure 5-2). Norberg Creek drains the catchment, which also includes a string of lakes, and several experimental gaged headwater catchments (Figure 5-2). This study focuses on catchments c32 (size of 6.74 ha, control catchment) and c31 (size of 4.62 ha, harvested catchment). Harvesting was conducted in the fall of 1997 (beginning of water-year 1998) along the south-facing slope of the TLW valley in catchments including c31. Pre-harvest forest characteristics were likely very similar between catchments c31 and c32 (Figure 5-2; Buttle et al., 2018). Catchment c32 had no harvesting, and served as a reference catchment. Catchment c31 was "clearcut", where all trees with DBH greater

than 10 cm were felled, but trees with DBH greater than 20 cm were removed from the site (limbs and crowns were removed on site and left on site). Time series of pre- and post-harvest forest dimensions are provided by Buttle et al. (2018) and reported in Appendix D Table D4.

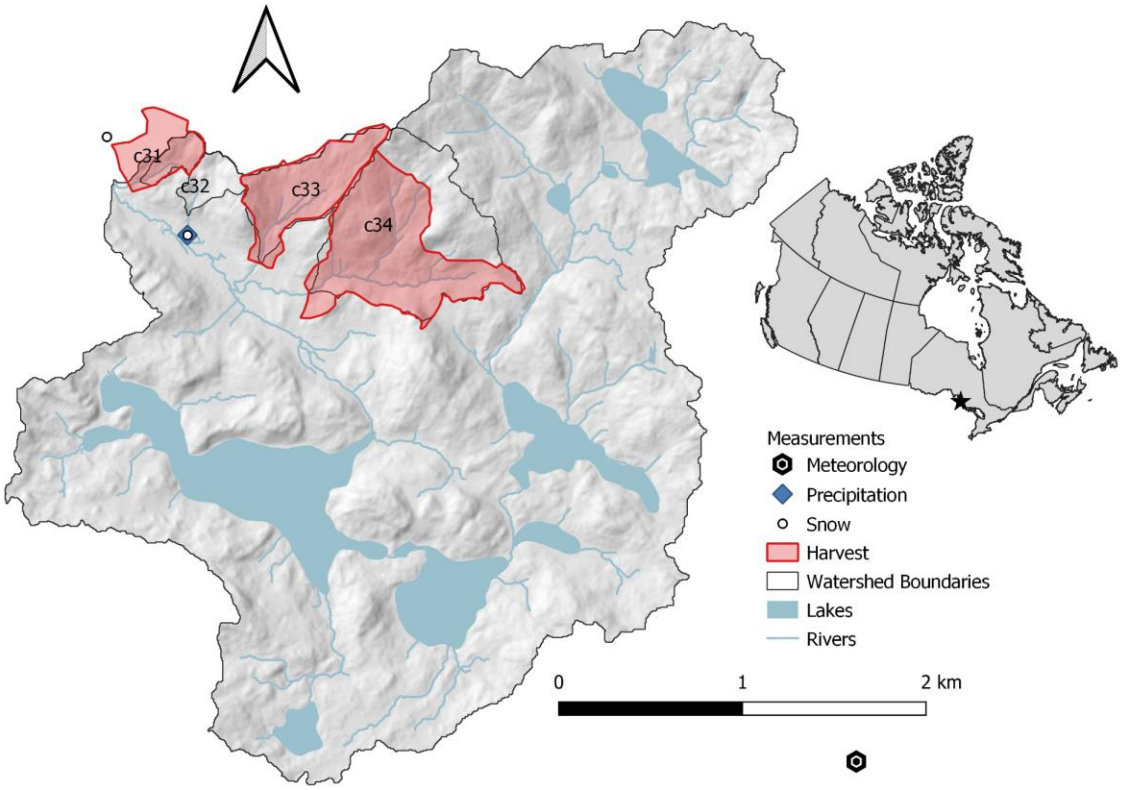

Figure 5-2. Site map of the Turkey Lakes Watershed (TLW) and subcatchments. Red opaque area shows experimental harvests above labeled sub-catchments. Symbols show different measurement stations. The black star shows the TLW in the inset map of Canada.

5.3.1.1 Site Geology and Soils

The TLW basin is underlain by silicate greenstone bedrock (metamorphosed basalt) of Precambrian age. This rock type would usually have low porosity and permeability, and thus would play little role in hydrologic storage or conveyance. While regional faulting manifests on the surface as predominant patterns in the stream drainage network, the landscape is also heavily scoured by glacial activity. The soils at the site are primarily glacial in origin. The soil parent materials suggest a more felsic (granitic) origin, which Jeffries et al. (1988) suggest to mean that the materials are derived from

bedrock farther to the north. The materials were also deposited in two different glacial contexts. The bottommost glacial material is a basal till, which was deposited underneath the glacier at its base during advancement.

Figure 5-3. Photograph of TLW forest. Photograph by Tyler Hampton from October 25, 2018, of the weir, stream, and vegetation at the outlet of catchment c31, which was clear cut in 1997. The image captures a bouldery streambed, bedrock outcrops or large glacial erratics, deadwood on the forest floor, and small saplings regrowing since the harvest.

The basal till is compact, sandy loam in texture, and has low hydraulic permeability ($1x10^{-7}$ cm s^{-1}), which often results in a perched water table above this layer (Hazlett et al., 2001; Murray & Buttle, 2005; Nicolson, 1988). Above the basal till is an ablation till, which was deposited during the glacial retreat. The ablation till is silt loam in texture, and has two orders of magnitude higher hydraulic

permeability ($1x10^{-5}$ cm s^{-1}). Generally, till depth is 1–2 m, and decreases to <1 m upslope at higher elevations.

The soils formed in the glacial tills are podzols. With the accumulation of an organic rich forest floor, acids from the decomposition of organic matter and abundant rainfall create conditions to leach cations like iron and aluminum from the upper soil to deeper layers. This process also results in the breakdown of clay minerals, leaving behind a white-coloured eluviated horizon beneath the forest floor, and deeper organic rich (~10%) soils coloured by the oxidized iron and aluminum (Hazlett et al., 2001; Retallack, 2021).

5.3.1.2 Site Climate and Hydrology

The TLW receives an annual precipitation of about 1200 mm (1980–2017 period). About a third of precipitation falls as snow (Semkin et al., 2012). The winter snowpack usually peaks at between 200 and 400 mm of snow-water equivalent (SWE; (Leach et al., 2020)). Annual average air temperature over the same period was 4.5°C. Monthly average temperatures range from -10.7°C in January to 17.9°C in July. Runoff ratios measured at the small subcatchments range from 0.3 to 0.6, resulting in 360 to 720 mm of annual streamflow on average. Due to the long record of data monitoring, long-term trends have been observed in temperature (0.3°C increase per decade) and growing conditions (degree days, later fall senescence: (Creed et al., 2015). As is typical for snow-dominated catchments, the highest streamflow is usually during the snowmelt period. Summer baseflow is quite low, and some of the smaller experimental watersheds experience no-flow days. As soils wet up in the fall, large rainstorms can rarely generate flows comparable in size to the freshet.

5.3.1.3 Site Vegetation

The forests at TLW (Figure 5-3) are dominated by sugar maple (*Acer saccharum*), making up over 80% of basal area in some areas (Morrison, 1990). Smaller components of the forest include yellow birch (*Betula alleghaniensis*; 9.5%), red maple (*Acer rubrum*; 3.7%), ironwood (*Ostrya virginiana*; 3.4%), white spruce (*Picea glauca*; 1%) and white pine (*Pinus strobus*). According to Morrison (1990), the forest is at a steady state in terms of aboveground biomass, with natural mortality compensated by new growth. Throughout this work, the description of “steady state” will be used to reference this characteristic of the forest; that aboveground biomass does not change substantially year-to-year. The same assumption is applied to carbon and nitrogen pools in the subsurface. The

most common stem-class (as measured in 1980 by Morrison, 1990) is 5–20-cm diameter at breast height (DBH), and the largest amount of phytomass is stored in the 20–40-cm DBH class. Trees with DBH of 50 cm were observed with the smallest frequency, and generally made up less phytomass than trees smaller than 20 cm DBH.

5.3.2 Site Data

Data measured at TLW was summarized by (Webster, Leach, Hazlett, et al., 2021), including meteorology, atmospheric deposition, precipitation, snow and snowpack, streamflow and stream chemistry, and forest and soil characteristics.

5.3.2.1 Meteorological Inputs

Meteorological data was measured at TLW at the Algoma CAPMoN (Canadian Air and Precipitation Monitoring Network) site (47.033 °N, 84.379 °W), which is about 4 km southeast of the experimental catchments (Figure 5-2). The CAPMoN site data included wind speed, air temperature (daily mean, minimum, and maximum), relative humidity, and incoming solar radiation. Precipitation was measured at a smaller meteorological station 300 m from the TLW outlet on Norberg Creek and from the outlet of catchment c31. Meteorological data was available daily from 1980, however the first full year of precipitation data was available from 1981. Notably, hydrologic data is summarized in the results according to Water Years (defined here as October 1 to September 30, aligned with usage by Leach et al., 2020), in contrast with previous studies which used different definitions (Buttle et al., 2018 used June 1 to May 31).

5.3.2.2 Nitrogen Deposition

Atmospheric deposition was modeled at a daily timestep. Measured annual atmospheric nitrogen deposition was available from (Sirois et al., 2001) for the Turkey Lakes watershed for the years 1981 to 1997 (Table D6). They differentiated N deposition into wet and dry deposition. Annual wet deposition (annual average 0.47 g m^{-2} yr^{-1}) was very well correlated to annual precipitation (R^2 of 0.99, slope: 0.37 g m^{-2}/1000 mm precip). This relationship was used to estimate wet deposition for the years 1998 to 2011. The percentage of deposition as wet (wet/wet+dry) was also well correlated to annual precipitation (p=0.002, R^2 of 0.43, 36% + 24% per 1000 mm). This relationship was used to extract total and dry deposition. Nitrogen deposition was differentiated between NH_4^+ and NO_3^-, which were assumed to each represent 50% of deposition, based on measurements reported by Beall

et al. (2001). Dry deposition was constant daily, and the yearly deposition was divided by 365. The annual wet deposition was also divided by 365 and allocated as potential deposition. Wet deposition occurred on days with precipitation. For each day without precipitation, it was assumed that the potential deposition accumulated, and was all released on the next precipitation day.

5.3.2.3 Stream Flow and Water Quality Measurements

Daily streamflow data was available at both catchments c31 and c32 beginning in the year 1980. Quality controlled streamflow records were available through 2012 for this study. Details on streamflow measurement are provided by (Hazlett et al., 2001; Leach et al., 2020). At the outlet of each catchment, the streambed was excavated down into the basal till, and a v-notch weir was installed to capture streamflow. Water level loggers placed in stilling wells were used to record stream stage, and rating curves were developed to calculate volumetric flow. As discussed by Leach et al. (2020), due to an incomplete seal between the weirs and the bedrock beneath the basal till, some subsurface flow likely bypasses the weirs.

Water quality samples were collected (since 1981) at catchment outlets at varying intervals. During the spring freshet, samples were collected every 1-2 days. For the remainder of the year, samples were collected weekly or biweekly. Concentrations of NO_3^-, NH_4^+ and DOC were measured from samples. For catchments c31 and c32, annual stream NO_3^- export (1982-1996 average) was approximately 0.47 g NO_3^--N m^{-2} $year^{-1}$, and NH_4^+ export was approximately 0.008 g NH_4^+-N m^{-2} $year^{-1}$ (P. N. C. Murphy et al., 2009). This suggests that NH_4^+ export makes up less than 2% of annual TN flux.

5.3.3 Parameter Constraints

Many characteristics of the TLW were used for parameter definition or constraining parameter calibration. The wealth of studies in these forests covered the snowpack, climate, precipitation, canopy characteristics, vegetation dimensions and element makeup, and the soils hydrology and element distribution. Ranges used in parameter calibration, and values chosen for parameters are included in Appendix D1.4.

5.3.3.1 Snowpack Model and Measurements

Leach et al. (2020) performed hydrologic modeling of travel times in TLW catchments. Their model incorporated snow water equivalent (SWE, mm of water) to capture catchment hydrology, providing

a benchmark to my model performance. More information about snow survey data is provided by Semkin et al. (2012). Since 1980, snow surveys have been conducted throughout the winter months, measuring snow depth, water equivalent, and density. As seen in Appendix D1.4, the transition temperatures were calibrated with a range between -1.5°C and +1°C, to possibly reflect errors in the reported temperatures from the meteorological station, or to reflect a role that solar radiation might play. For example, intense radiation on a cold (<0°C) day may still result in melt. The degree day factor, as discussed by (Braun, 1984; Eder et al., 2003; Ye et al., 2012), was calibrated to a range of 1–4.5 mm day^{-1} $°K^{-1}$ (Appendix D1.4).

5.3.3.2 Canopy Measurements

As described in Section 5.3.1.3., all indications point to the forests at TLW existing in a "steady state", having likely peaked in total aboveground biomass, and now with growth balanced equally by mortality. For the purposes of this model, I assume that other allometric characteristics of the forest, including of the canopy, are also at steady state, and will stay so except for disturbance by harvest.

Leaf Area Index (LAI) has been measured at the TLW in the reference (c32) and clearcut (c31) catchments in the years 1998, 1999, 2002, 2006, 2007 and 2015. The data are as of yet unpublished (source RL Fleming), but the measurement methods are described by (Leach et al., 2022). Estimates for similar sugar maple stands measured by Buttle & Farnsworth (2012) and reported by Leach et al. (2022) constrain summertime maximum LAI to between 4 and 6. Han (2022) presents additional LAI data measured using the Landsat satellite interpolated monthly for the years 1986-2012. Estimates by Han and subsequent annual modeling with the Robin model converge at summertime maximum LAI of 4.5.

(Buttle & Farnsworth, 2012) measured properties of a mature (>70 years old) sugar maple stand in southern Ontario, including canopy cover fractions (b, equivalent to the inverse of the soil cover fraction used in HYDRUS) of approximately 0.9. For deciduous forests including significant components of sugar maple, estimates for maximum canopy interception range between roughly 0.1–2.0 mm day^{-1} (Buttle & Farnsworth, 2012). The Hydrological Simulation Program Fortran (HSPF) watershed model estimates maximum canopy interception of 3.8–5.0 mm day^{-1} for light and heavy (respectively) forest (EPA Office of Water, 2000).

Estimates of the canopy cover and leaf area index were used to constrain parameters related to canopy cover fraction (b) and precipitation interception. When LAI is zero, b will also be zero. For an LAI of

4.5, a value of the exponent $K_{Ie} = 0.512$ will return $b = 0.9$. A larger value of K_{Ie} will increase interception. The parameter α scales up interception, but in this model it does not represent the maximum daily interception rate. For K_{Ie} of 1 and α of 0.1, 0.4, 0.7, 1.0, interception asymptotes towards 0.45, 1.77, 3.05, 4.30 mm day^{-1}, respectively.

LAI in the model was a factor of total leaf biomass. Measurements of the foliage carbon pool at TLW (Morrison et al., 1993; see also Appendix D3) estimated about 180 g C m^{-2}. The season maximum leaf biomass itself was an allometric equation, which governed how much leaf biomass would accumulate in a given year. Knowing the pre-harvest forest stem stocking of between 900–1000 stems and DBH of about 20 cm (Buttle et al., 2018), the model parameters should be fit to produce a leaf max of about 180 g C m^{-2}. The specific leaf area (SLA) function, which shifts between two values as the forest ages, is multiplied by leaf biomass to calculate the LAI. Knowing the pre-harvest forest leaf biomass and LAI of about 4.5, SLA for the steady-state forest can be calculated. Data from the regrowing forest can be used to infer the other SLA value. Data from 2013 presented by Buttle et al. (2018) indicate a full re-population of stems (1085 stems per hectare) and a decreased DBH (calculated to be 10.6 cm). Despite full stem-repopulation to pre-harvest numbers, the tree biomass only increased by 13% above the immediate post-harvest biomass. For our function that shifts SLA based on forest age, which we instead substituted as forest biomass relative to the carrying capacity (review Section 5.2.2.1. and Appendix D2.3.3.), it can be assumed that the SLA in 2013 would be almost the same as immediately post-harvest in 1997. Satellite measurements presented by Han (2022), supported by field measurement of LAI (unpublished, RL Fleming, see Leach et al., 2022) also suggest full LAI recovery by 2013. Knowing the desired LAI, the maximum leaf allometric equation and regrowth forest SLA can be back calculated (See Section 5.3.5 and Appendix D1.4).

Other characteristics of the canopy phenology include the timing of leaf-on and leaf-off. Data (from years 1983 to 2009) from (Creed et al., 2015) were used to calculate average Julian dates for the beginning and end of the leaf-out (dates 115 to 135) and leaf-fall periods (dates 280 to 300). The duration of the greening and senescing periods allowed for soft calibration to determine the daily rates of sprouting and leaf death, and the threshold of seasonal maximum leaf biomass where NPP should begin allocation to stems.

5.3.3.3 Soil Physical Properties

As described in Section 5.3.1, the soils of the TLW are well studied, with numerous hydrology and biogeochemical studies reporting characteristics.

Murray & Buttle (2005) provide several physical soil characteristics, measured at soil pits. Ablation till characteristics include an average porosity of about 0.65, thicknesses of 0.5 to 0.8 m, and 240 to 330 mm of water storage capacity. While estimates did not exist for basal till water capacity, it was assumed that box 2 water storage capacity would not exceed 100 mm. These values informed the range of values for the water storage pools (Appendix D1.4).

Values of soil characteristics for a sandy loam to silt loam texture came from a literature review conducted by Laio et al. (2001). This constrained the ranges for field capacity (0.5–0.65 of water capacity), plant stress threshold (0.25–0.45), and hygroscopic point (0.11–0.25; wilting point and hygroscopic point were assumed to be the same).

Buttle et al. (2018) conducted a water balance approach to estimate seasonal root zone water storage capacity. While they used a temporally varying approach, to try to parse the effects of the harvesting disturbance on the water balance, they found average capacity of 100 mm, ranging up to 300 mm, for the undisturbed catchment c32, and average capacity of closer to 50 mm, ranging up to 200 mm, for the disturbed catchment c31. For plant-available water capacity to range up to 300 mm, that requires equivalent water at moisture levels above the hygroscopic point. With an estimated upper limit of box 1 water capacity of 350 mm, and an upper limit hygroscopic point of 0.25, box 1 might provide in that scenario 262 mm of plant available water. Thus, box 2 would need to be accessible to plant roots. An additional 75 mm of plant available water could come from a box 2 of maximum size 100 mm.

Soil pit measurements by Murray & Buttle (2005) constrained potential infiltration rates with hydraulic conductivity measurements up to 10^{-6} m s^{-1} (~86 mm day^{-1}, Guelph permeameter test), and percolation rates on the order of 40–60 mm day^{-1}. Some constraints existed for maximum percolation rates through the ablation till. Hydraulic conductivity of the basal till was estimated to be at least an order of magnitude smaller (10^{-7} m s^{-1} =~8.6 mm day^{-1}; (Nicolson, 1988). Ranges for exponential flow shape parameters were provided by (Laio et al., 2001) for the corresponding sandy loam soil type.

5.3.3.4 Vegetation Carbon and Nitrogen Storage and Fluxes

To constrain my model to the vegetation characteristics of TLW, several measurements were used as initial conditions to the model, and to validate annual element fluxes. Appendix D3 has tabulated measurements reported from several papers.

As discussed by (Morrison, 1990), the forest at TLW is likely in equilibrium, with some trees exceeding 250 years in age. The forest is unevenly aged in composition. Total vegetation carbon content was about 11,180 g C m^{-2}, with 180 g C m^{-2} as foliage and about 10,980 g C m^{-2} as woody material (including branches, stem, stump, and roots; dead and alive), with 9,280 g C m^{-2} as living woody material (Morrison et al., 1993). Estimates of nitrogen content varied between two forest sites at TLW studied by Morrison (1990). The average foliage nitrogen content was 9.4 g N m^{-2}, resulting in a carbon to nitrogen (C/N) ratio of 19. Woody material nitrogen content estimates ranged from 400–470 g N m^{-2} (Mitchell et al., 1992; Morrison, 1990; Morrison et al., 1992), resulting in C/N ratios of 270 and 230, respectively. If only carbon pools of living material were used (which excluded root carbon), the materials C/N ratio could be 196 (Table D2). Although root nitrogen estimates did not exist (only lumped green vs woody), it is difficult to understand what role roots play in plant C/N ratio, if they are not explicitly modeled. Estimates for sugar maples place root C/N ratios as similar to foliage (Pregitzer et al., 2010). I interpret my model to assume that the lumped plant stem pool also includes roots, and I therefore assign the plant stem pool (no leaves) C/N ratio is close to 200 (balanced between N-rich roots and C-rich woody material).

Assuming that the TLW forests remain at steady state, in that no net biomass is added to the forest, the annual fluxes of carbon and nitrogen can be back calculated. As for magnitude of gross growth, (Morrison et al., 1993) estimate that annual gross growth includes about 120 g C m^{-2} $year^{-1}$ in stem carbon allocation, and 175 g C m^{-2} $year^{-1}$ in leaf carbon allocation. Notably, annual leaf carbon flux should be roughly equal to the season-maximum leaf biomass, which Morrison (1990) estimated to be 180 g C m^{-2}. As discussed in Section 5.2.2., some N from leaves is reabsorbed back into trees before leaf-fall. Morrison (1991) estimated that 63% of N was reabsorbed. This also results in a C/N ratio of leaf litter fall of 65 (Table D3), significantly more N-depleted than the leaf C/N ratio of 20 (Mitchell et al., 1992).

5.3.3.5 Soil Carbon and Nitrogen Storage

Soil organic matter is distributed across soils in multiple vertical locations and degrees of chemical and biological degradation. Descriptions of the soils as humo-ferric podzols (Creed et al., 2002) implies the large amount of carbon stored. The forest floor has the greatest variety of organic matter degradation, and the largest per-weight carbon content. Within the forest floor, organic matter is classified as LFH: Litter (fresh), Fermented (still identifiable in origin), and Humus (well decomposed) (B.C. Ministry of Forests, 1997). Progressing from L to H, the carbon content decreases sharply, resulting in progressive enrichment in N (Morrison, 1990). Mitchell et al. (1992) provide estimates for the total forest floor carbon and nitrogen (See Appendix D3 Table D2). Despite being the smallest carbon pool in areal mass, the forest floor is expected to have a very high turnover rate, as will be discussed. As organic matter undergoes decomposition and humification, leachate carries organic matter, acids, and geogenic solutes from the forest floor and upper few centimetres of mineral soil (the A and E horizons) to the deeper soil. Much of this material is deposited in the soil B horizons. In this model, the forest floor is modeled as a vertically-distributed and homogeneous pool, as discussed in Sections 5.3.1. and 5.2.3.2. Because of thousands of years of organic matter translocation, and the relatively slower decomposition rate of humified matter, the mineral-soil-associated pool represents the largest store of organic carbon and nitrogen at the TLW (Table D2), at almost 10 times the store size of the forest floor (Creed et al., 2002; Foster et al., 1986; Mitchell et al., 1992; Morrison, 1990). In translating the Porporato et al. (2003) model to this site, we assumed that this mineral-soil-associated carbon would represent the long-residence-time pool in their model, called “humus”.

The Porporato et al. (2003) model makes several assumptions about the decomposition of organic matter that should be addressed. The steady state behavior of the plant-litter-humus-biomass system (See Figure 5-1, Table 5-5) depends on two key parameters: the percent of decomposed carbon (respiration ratio) that becomes carbon dioxide, and the percent of decomposed litter that becomes humified (humification ratio). D’Odorico et al. (2003) and Parolari & Porporato (2016) assume respiration ratios of 60% and 75% (respectively) and humification ratios of 25% and 20% (respectively). (Brady & Weil, 2016) definitively assert that the respiration ratio is two thirds (66%), but other work highlights the large documented variability in microbial carbon use efficiency (CUE: defined as 1 minus respiration ratio). (Manzoni et al., 2012) show in a meta-analysis that soil

microbial CUE may vary (interquartile range) between about 40–70 percent (implied respiration ratios of 30–60%).

I present an analytical solution that can be used to solve for the value of the respiration ratio, providing that I assume that the plant-litter-humus-biomass system exists in a multi-year steady state equilibrium. While intra-annual decomposition rates vary with soil moisture as discussed in Section 5.2.3.2, observations of steady-state conditions in TLW forests provide justification that the underlying soil system is also at steady state. The solution for the respiration ratio requires that I know the annual rates of carbon turnover in the leaf and stem pools, and carbon to nitrogen ratios (C/N) of the plant leaf and stem pools, along with the litter, humus, and biomass pools in the soil. Measured data exists to inform many of these values, as seen in Table 5-5 and D2. I had to assume a pool size for soil biomass and a C/N ratio, for which I used values of 300 g C m^{-2} and 10, respectively (Manzoni & Porporato, 2007; Parolari & Porporato, 2016; Xu et al., 2013). I also had to assume a value for the humification ratio. A humification ratio of 20% resulted in a humus pool residence time of about 280 years. Without knowing annual humus decomposition rates from TLW, I assumed that a humification ratio of 10% (0.1) would produce more realistic residence times at least closer to 500 years (Gaudinski et al., 2000; Wattel- Koekkoek et al., 2003). A value of 66% for leaf-fall nitrogen reintegration was also used from the literature (Morrison, 1991). Given these values, I used Equation 5-1 to solve for a respiration ratio (rr) of 47%, given the measured value of the litter C/N ratio of 18.

$$CN_l = \frac{LFp+LFl}{1-\epsilon} \times \left[\frac{LFp+fN\times LFl}{CNp} + \frac{LFp+LFl}{CNb}\left(\frac{\epsilon}{1-\epsilon}\right)\right]^{-1} \quad (5\text{-}1)$$

where

LFp and LFl are the annual litter fall (carbon) fluxes from plant stem and leaf biomass turnover,

$CNp, CNpl, CNb$ are the C/N ratios for plant stem, leaf, and soil biomass,

fN is a factor accounting for C/N ratio differences between stem and leaf, such that

$$fN = CNp \times CNpl^{-1} \times (1 - Nstore) \quad (5\text{-}2)$$

where $Nstore$ is the fraction of reintegrated leaf nitrogen during leaf-fall.

$$\epsilon = rh(1 - rr) + (1 - rr - rh) \quad (5\text{-}3)$$

where rh is the humification ratio and rr is the respired carbon ratio.

A derivation of Equation 5-1 is presented in Appendix D5, along with a mathematical proof showing the equivalence of Equation 5-1 to the steady state equation provided by Parolari & Porporato (2016).

5.3.3.6 Nitrogen Export

The sorptive properties of NH_4^+ in the subsurface are dependent on a "protection" parameter. I used the value from Porporato et al. (2003), which assumed that NH_4^+ experienced 95% "protection" from leaching and uptake (e.g. Eq. D2-42,46,109,110).

5.3.3.7 Forest Dimensions and Stocking

In results presented by Han (2022), yearly maximum leaf area index returns to pre-harvest values after about 12 years (validated with Landsat satellite measurements). Similarly, the number of stems recovers quickly after harvest, taking about 16 years to exceed the pre-harvest values (Buttle et al., 2018; Table D5). Values of post-harvest yearly maximum LAI (from Han) and number of stems (from Buttle) were used to calibrate model parameters (see Section 5.3.4.2., Table 5-2), while pre-harvest values were used as initial conditions for the model.

5.3.3.8 Post-harvest Effects

The effect of harvesting in the model primarily impacted the plant stem pool and the stem stocking. As in the experiments at TLW, harvesting took place in the fall of 1997 (modeled on year-day 320) after the conclusion of leaf senescence. After harvesting, the stem carbon pool and stem stocking were set to values of 2460 g C m^{-2} and 200 stems $hectare^{-1}$, respectively, following measurements reported by Buttle et al. (2018). The harvesting event was assumed to result in a pulse of fresh biological material to the litter pool. The size and C/N stoichiometry of this pulse were calibrated (See Appendix D1.4.3). Although the root carbon component (from 3PG) was removed from the model structure (Section 5.3.2), it could be assumed that the harvesting event would lead to some dieback of the root network. As such, this "pulse" of material could represent material added as slash (branches and crowns) from the harvested trees, as well as dieback of roots in the subsurface. It was assumed that the lower limit of the C/N ratio of this pulse was 10, or the same as living soil biomass. Root C/N ratios are rare in the literature, and are likely different between different structures (fine vs coarse), but for maple species might be around or less than 20 (Ferlian et al., 2017).

5.3.4 Model Calibration

The models in this study were written in R Version 4.2.2. (R Core Team, 2023). The model was solved with the forward Euler method using a sub-daily (0.25 d) timestep. The "data.table" package in R (Dowle & Srinivasan, 2022) was used with a "fast aggregation" method (Slowikowski, 2015) to speed up post-run aggregation of model results to the daily or yearly timestep for calibration.

Section 5.3.4.1. describes formulations of evaluation metrics that we used to achieve specific calibration goals, which are outlined in Section 5.3.4.2. Section 5.3.4.3. describes the software and algorithms used to perform calibration.

5.3.4.1 Evaluation Metrics

The Kling-Gupta Efficiency (KGE, Equation 5-4, (Gupta et al., 2009) has become one of the preferred hydrologic model evaluation metrics, due to its incorporation of evaluation of the mean, variation, and correlation of simulated versus observed time series data.

$$KGE = 1 - \sqrt{(1-r)^2 + (\frac{\sigma_{sim}}{\sigma_{obs}} - 1)^2 + (\frac{\mu_{sim}}{\mu_{obs}} - 1)^2} \quad (5\text{-}4)$$

where r is the linear correlation coefficient, σ_{sim} and σ_{obs} are the standard deviation of simulated and observed data, and μ_{sim} and μ_{obs} are the mean value of simulated and observed data.

The KGE has an optimal value of 1, and poor performance trends downwards towards negative infinity.

Many calibration efforts used the absolute percent error (Equation 5-5) to evaluate deviation from a desired value. We define the function absolute percent error as PER.

$$PER = \frac{|obs_i - sim_i|}{obs_i} \quad (5\text{-}5)$$

where sim_i and obs_i are the ith simulated and observed values, respectively.

For multiple observations, the mean absolute percent error is used, and is defined as $MAPE$

$$MAPE = \frac{1}{n}\sum_{i=1}^{n} \quad \frac{|obs_i - sim_i|}{obs_i} \quad (5\text{-}6)$$

where n is the number of observations.

Alternatively, the root mean square error ($RMSE$) may be used as opposed to $MAPE$.

$$RMSE = \sqrt{\frac{1}{n}\sum_{i=1}^{n} (obs_i - sim_i)^2} \quad (5\text{-}7)$$

A multi-metric objective function could use several different benchmarks. For instance, if m_1 is PER of the plant pool from the steady state value, m_2 is PER of the litter pool, and m_3 is PER of annual stream nitrogen flux, then one evaluation metric can be calculated that results in the minimization of all three metrics:

$$obj = max(w_1 m_1, w_2 m_2, w_3 m_3, \dots) \quad (5\text{-}8)$$

where w is the weight applied to each metric.

By using the maximum function (Eq. 5-8) as the calibrated objective function, calibration can preferentially target each metric and the parameters influencing it. Other approaches might use the mean function to aggregate metrics, however this can result in one metric being minimized, at the cost of another increasing, just as long as the mean of the two decreases slightly.

5.3.4.2 Calibration Strategy

Due to the large number of parameters and processes in the coupled model (Table 5-1), calibration of parameters took place in several stages. During each stage, a segment of the fully coupled model was isolated, and a subsetted group of parameters specific to that segment were calibrated, with calibration metrics targeting outputs of the model segment against measured data from the TLW. After the calibration of the model segment, the best parameters were selected and "locked in", and would not be calibrated during later calibrations of other model segments or the fully coupled model. Table 5-2 describes the model segments and the number of corresponding parameters in each group, as well as which input data were used and which model outputs were targeted in calibration. Appendix D1.4. has a complete list of all model parameters, with indicators of the grouping with which they were calibrated. The remainder of this section outlines calibration targets, objective functions, and function weights (e.g. Eq. 5-8) for each of the 6 calibration groupings.

Table 5-2. Parameter calibration groupings. Each grouping of parameters was solved in order of this table. Parameters calibrated in each grouping (second column) were "locked in" for subsequent calibrations using other targets. The Calibration Target describes the measured data used for calibration of the model outputs. In Appendix D1.4, the "Symbol" (in parentheses) in this table corresponds to the "Calibr." column describing the Calibration Grouping of every parameter. The subset of equations used for the calibrated model segment are listed.

Calibration Grouping and Symbol	No. Params	Measured Data as Inputs	Calibration Targets (comparison of model vs. measured)	Model Eq. (See Appx. D)
Hydrology (CalH)	12	Precipitation (daily), Temperature (daily), Leaf Area Index (yearly, from Han, 2022)	Streamflow (daily)	Eq, D2-1 to D2-27
Allometric (CalA)	6	Number of Stems and Stem Biomass (at 2 points, see Table D4)	Leaf biomass carbon (at one point, see Table D2); Leaf Area Index (at 2 points, see Table D4); Diameter at Breast Height (at 5 points, see Table D4)	Eq. D2-34 and D2-60 to D2-63
Regrowth (CalR)	6	Stem Biomass (at 5 points, Table D4)	Number of Stems (at 5 points, see Table D4)	Eq. D2-31 and Eq. D2-64 to D2-71
Steady-State Soil Carbon (CalSS)	2	Pool sizes (steady state assumption)	Carbon to Nitrogen Ratio of Litter	Eq. 5-1 to 5-3
Coupled Model Pre-Harvest (CalPre)	14	Precipitation (daily), Temperature (daily)	**Pool Sizes (five carbon pools):** Plant stem biomass; litter, humus, and soil carbon (see Table 5-5) **Model Rates** Plant stem growth (Table 5-5), Nitrogen Export (flux and concentration) Dissolved Organic Carbon Export (concentration)	All Equations
Coupled Model Post-Harvest (CalPost)	2	Precipitation (daily), Temperature (daily)	Post-harvest stream NO_3^- concentrations.	All Equations

Briefly, we first calibrated the hydrology module (CalH) to predict streamflow and substituted the dynamically modeled Leaf Area Index (LAI, see Figure 5-1) for measured LAI as a model input. We then calibrated four allometric equations that predict the leaf biomass carbon, LAI and the diameter at breast height (DBH) as a function of measured data on the number of stems and stem biomass (CalA). This step allowed us to connect how post harvest dynamics in the number of stems and stem biomass impacts allocation of carbon to leaves, and ultimately impacts post-harvest LAI. We then solved the differential equation for calculating the number of stems as a function of growth and mortality rates that are controlled by measured values of stem biomass (CalR). Finally, we calibrated the fully coupled model for the pre-harvest period and used the plant and leaf biomass, as well as the soil carbon pools, plant stem growth as well as nitrogen and carbon export fluxes as calibration targets. When the calibrated model was run in the post harvest period, we found that while hydrology was adequately captured, the model underestimated post-harvest nitrogen fluxes. A perturbation was added to the model, occurring directly at the time of the harvest, and having the characteristics of a pulse of fresh organic material to the litter pool. This pulse had parameters for size (total amount of organic material, and the C/N ratio of that material). This multi-step top down calibration process allowed us to appropriately integrate soft calibration data, and address some of the equifinality issues that are key issues with coupled modeling.

The specific process used for calibration is as follows:

[1] Hydrology Calibration: The hydrology model was isolated from the coupled model and initially calibrated alone. The vegetation linkage with hydrology (LAI effect on interception and evapotranspiration) was preserved through substitution of measured maximum pre-harvest LAI data (see Table D4). Measured LAI was input into a trapezoidal time series which fluctuated between zero and the maximum LAI (4.5), corresponding with the timing of the leaf-on and leaf-off periods (See Section 5.3.3.2.). Climate and streamflow data from the control catchment c32 were used as model inputs and calibration data, respectively. The Kling Gupta Efficiency (KGE, see Section 5.3.4.1) of daily streamflow for the 13-year period of 1982 to 1995 was used as the evaluation metric. KGE of water-year summed streamflow, and root mean square error (RMSE) of snow water equivalent (SWE) was recorded, but not used in calibration. Of the hydrology model parameters, 12 were

calibrated. Ranges for parameters are summarized in Appendix D1.4. These ranges were determined based on site characteristics, as discussed in Section 5.3.3.

[2] Allometric Calibration: The key linkage between the vegetation and hydrology model is the LAI, however the hydrology was only calibrated in the pre-harvest period, and using LAI values not calculated from the characteristics of the vegetation model. To capture the behavior of LAI in the post-harvest period, the behavior of LAI with varying vegetation characteristics had to be calibrated. This calibration *did not* involve solving differential equations, and instead optimized 6 parameters (see Appendix D1.4) governing 3 key allometric equations (Eq. D2-34,60,61) to match 8 data points. Evaluation metrics for each of the 8 data points were (1) the percent error (PER) of reported pre-harvest growing season plant leaf biomass (see Table 5-5, Table D2, from Morrison et al., 1992; given a weight of 4), (2-3) PER of the growing season LAI in years 1997 (pre-harvest) and 2013 (see Table D4, data from Han, 2022; given weights of 4 and 2, respectively), and (4-8) the $MAPE$ of DBH for all measured years 1997 (pre- and post-harvest) to 2013 (see Table D4, data calculated from Buttle et al., 2018; given weights of 1). The objective function (obj_A) used the maximum function to collectively reduce the values of all the data

$$obj_A = max(4 \times PER_{Leaf-97}, 4 \times PER_{LAI-97}, 2 \times PER_{LAI-13}, 1 \times MAPE_{DBH}) \quad (5\text{-}9)$$

[3] Regrowth Calibration: Following calibration and "locking in" of the allometric equation parameters, the dynamics of the Number of Stems pool needed to be calibrated using the full differential equations in Eq. D2-31. Given measured data on the regrowth of plant stem biomass overtime, the dynamics of the Number of Stems pool needed to be tuned to achieve quasi-steady state (a balance of growth and mortality) in the pre-harvest period, as well as a net growth rate (more growth, less mortality) matching the measured data in the post-harvest period. Calibration of 6 parameters (See Appendix D1.4) used in Equations D2-64 to D2-71 targeted 5 measured values for Number of Stems provided by Buttle et al. (2018, see Table D4). The objective function minimized the mean absolute percent error ($MAPE$) of Number of Stems.

[4] Steady State Soil Carbon Pools: The multiyear steady state behavior of the soil carbon pools (litter, humus, biomass) depends largely on two parameters: the humification ratio and the respiration ratio. The calibration of these parameters is described in Section 5.3.3.5. and Appendix D5. The value of the humification ratio was selected based on the assumption of a residence time of the humus pool of approximately 500 years, and given the value of the humification ratio, the value of the respiration

ratio can be analytically calculated. Calibration metrics are not reported for this grouping because of the presence of the analytical solution.

[5] Coupled Model Calibration (Pre-Harvest): By isolating several model components, and using the wealth of data available at TLW to ground truth behaviors of those components through time, a total of 24 parameters were calibrated all before ever running the fully coupled model. With that complete, the next task was to tune the growth and turnover rates of the vegetation and soil biogeochemical pools such that they achieved a quasi-steady-state on a multi-year timescale (see Section 5.3.1.3.). The ten calibrated parameters were all involved in regulating pool growth or turnover. Four objective functions were created to target either quasi-steady-state of pool sizes, or to target streamflow export of nitrogen and carbon:

(1) quasi-steady-state of the plant pool: PER of simulation-end stem biomass from a value of 11,0000 g C m^{-2} and PER of average annual gross stem growth at 110 g C m^{-2} $year^{-1}$ (see Table 5-5),

$$obj_{Plant} = max(20 \times PER_{Cp}, 20 \times PER_{NPPstem}) \quad (5\text{-}10)$$

(2) steady state of the litter, humus, and biomass pools (PER of simulation end pool size from values of 1600, 21400, and 300 g C m^{-2}, respectively; see Table 5-5),

$$obj_{Soil} = max(10 \times PER_{Cl}, 10 \times PER_{Ch}, 10 \times PER_{Cb}) \quad (5\text{-}11)$$

(3) Nitrogen export was calibrated using (1) percent error in prediction of annual NO_3^- flux PER_{Flux}, (2) percent error in predicting the ratio of NO_3^- to total nitrogen flux (NO_3^- plus NH_4^+) $PER_{\%NO3}$, and (3) KGE of daily measured concentrations of NO_3^- in stream water KGE_{Nconc}. Dissolved organic carbon export was calibrated using KGE of daily DOC concentration. (PER of average annual flux from a value of 0.47 g N m^{-2} $year^{-1}$, PER of percent of N flux as NO_3^- >90%: both values from Murphy et al., 2009).

$$obj_{NFlux} = max(3 \times PER_{Flux}, 3 \times PER_{\%NO3}, 1 \times (1 - KGE_{Nconc})) \quad (5\text{-}12)$$

$$obj_{DOC} = 1 \times (1 - KGE_{Cconc}) \quad (5\text{-}13)$$

[6] Post-harvest Water Quality Calibration: With the implementation of the harvest disturbance to the forest (see Section 5.3.3.8), accurate modeling of NO_3^- concentrations was the primary interest for calibration. My assumption was that the pulse of nitrogen from the subsurface post harvest would be

best captured by the decomposition of organic material in the subsurface. A one-time pulse of material was added to the litter pool, and its characteristics (pool size in units of carbon, and its carbon to nitrogen ratio) were calibrated. The $RMSE$ of measured versus modeled NO_3^- concentrations for the first 5 post-harvest years served as the objective function. $RMSE$ was used instead of KGE because of the non-stationarity of the mean and variability of concentrations year-to-year after harvest, as well as the gradual shift in the concentration regime from elevated post-harvest to lower than pre-harvest levels.

5.3.4.3 Calibration Software and Algorithms

The Ostrich software (Matott, 2017) was used to automatically explore the pre-defined parameter space and optimize the model according to the provided objective function(s). Ostrich was run with multi-core parallel execution, using Microsoft Message Passing Interface (MPI, Version 10.1.1, Microsoft Corporation). Given an objective function, the Dynamically Dimensioned Search (DDS) algorithm (Tolson & Shoemaker, 2007) was used within Ostrich to identify optimal parameter sets. The DDS algorithm has been shown to appropriately explore the provided parameter range for many parameters and rapidly converge on global optimal solutions. Notably, DDS has been shown to not get stuck in local optima. The Ostrich software used the General Purpose Constrained Optimization Platform (GCOP) and the Additive Penalty Method (APM) to handle objective function values. When using the KGE metric as an objective function, the value of one minus the KGE had to be handed to the GCOP, because it is only equipped to minimize the value of an objective function.

At times in early model calibration, the Pareto Achieved DDS (PADDS) algorithm (Asadzadeh & Tolson, 2013) was used within Ostrich to balance two different objective functions. The Exact HyperVolume Contribution ((Knowles et al., 2003) was used as a selection metric.

5.4 Results and Discussion

This section presents results from the calibration, performance, and scenario behavior of the coupled model. Section 5.4.1. presents the best results for objective functions and model fits from the 6 Calibration Groupings (Section 5.3.4.2.) of various model parameters. Section 5.4.2. presents the final model configuration to describe various aspects of the model behavior, with scenarios including unharvested and harvested. Section 5.4.3. describes potential model improvements and how they might apply specifically to the study site at TLW or to the model's applicability to other sites.

5.4.1 Model Calibration and Validation

This section is ordered following the Calibration Groups (Section 5.3.4.2., Table 5-2). Each subsection describes the lowest achieved objective function values (see also, Table 5-3), and how they compared to expected values (either from literature or other site observations). Behavior of model fit in relation to calibrated parameters is described, along with tradeoffs between parameters or choice of objective function.

5.4.1.1 Snow Model

The snow model was initially calibrated as an even smaller isolated subset of the hydrology model. The calibration of three snow parameters attempted to match measurements of snow water equivalent (SWE), which were taken outside the experimental catchments, as seen in the map in Figure 5-2. In their hydrologic model, Leach et al. (2020) report root mean square error (RMSE) of 44 mm in SWE. Equations from the HBV model were used for both models by Leach et al. (2020) and myself. By calibrating the three parameters of the snow model, I was first able to achieve RMSE of 43.5 mm SWE for the 30 year period of 1982 to 2011. As is discussed in the next section, it was found that calibrating the snow to measured data had negative effects on the fit of streamflow data from the hydrologic model. As such, calibration of the hydrologic model allowed for varying the snow parameters to optimize streamflow, at the expense of SWE fit.

Table 5-3. Calibration Results. Calibration Groupings match Table 5-2. Calibrated metrics have an asterisk*. Validation metrics are included for information but did not guide calibration. PER is percent error. MAPE is mean absolute percent error. MAE is mean absolute error.

Calibration Grouping	Calibration Targets (comparison of model vs. measured)	Calibration* and Validation Metrics
Hydrology (CalH)	Streamflow (Q) Catchment c32, period: water years 1982–1994	Daily Q KGE = 0.677*
		Water-Year Sum Q KGE = 0.708
		Q Balance = +5.1%
		SWE RMSE = 61 mm
Allometric (CalA)	Leaf Area Index (LAI): LAI 1997 pre-harvest LAI 2013 LAI all 5 points	 PER = -4%* PER = -2%* MAPE = 23%*, MAE = 0.64
	Diameter Breast Height (DBH): DBH all 5 points	 MAPE = 8%*, MAE = 1.1 cm
	Leaf Biomass Carbon 1997:	PER 0.3%*
Regrowth (CalR)	Number of Stems, 5 points	MAPE = 13%*, MAE = 51 stems/ha
Coupled Model Pre-Harvest (CalPre)	**Pool Sizes (carbon):** Plant stem biomass Litter Humus Soil biomass	 PER = 0.8%* PER = 1.4%* PER = 0.07%* PER = 1.0%*
	Model Rates: Mean Plant stem growth Mean NO_3^- Flux Mean % TN Flux as NO_3^-	 PER = 1.0%* PER = 5.7%* PER = 5.9%*
	Water Quality Timeseries: Stream NO_3^- Conc Dissolved Org Carbon Conc	 KGE = 0.70* KGE = 0.50*
	Hydrology Validation:	Daily Q KGE = 0.681
Coupled Model Post-Harvest (CalPost)	**Stream NO_3^- Conc:** c31: first 5 years post-harvest c32: first 5 years post-harvest c31: 30-year 1982-2011 c32: 30 year 1982-2011	 RMSE = 2.34 mg/L* RMSE = 0.64 mg/L RMSE = 1.1 mg/L RMSE = 0.61 mg/L

The snow model was recalibrated alongside the hydrology model. While the isolated calibration of the snow model produced optimal parameter fits of about 2.8 for the degree day factor and close to 0 for the snow transition temperature (Appendix D1.4), the optimal melt transition temperature was about 0.9. The fit of the hydrology model was influenced by the melt temperature (Figure D1), favoring a temperature less than negative 1. By optimizing for best daily streamflow fit, the snow data fit was RMSE of 61 mm SWE (Table 5-3). On average, the hydrology model underestimated the measured SWE by 21%, with a mean absolute error of 29% (MAE 44.9 mm SWE). It's possible that the data available for calibration for Snow Pit #8 (Figure 5-2) is not representative of the snow behavior across the modeled catchments. While Snow Pit #8 rests in a small valley near the outlet of Norberg Creek at an elevation of 340 m above mean sea level (MSL), the elevations of both catchments c31 and c32 range from about 355–437 m MSL. There may be significantly different snow and melt dynamics 100 m above the snow and precipitation station.

5.4.1.2 Hydrologic Model

The hydrologic model was first run in Calibration Group 1 (see Table 5-2). A total of 12 parameters were calibrated, including the "bucket sizes" for the two water pools, as well as process rate constants. Optimal parameter values are shared in Appendix D1.4. Inputs to the model included daily climatological data including precipitation and temperature, along with summertime maximum LAI (from Han, 2022) which were used to create a trapezoidal LAI function as a substitution for the dynamically modeled LAI that in the fully coupled model is dependent on plant leaf carbon and stem carbon.

The calibration resulted in very good fits for daily streamflow (Figure 5-4). For the calibrated period (using catchment c32 streamflow for water-years 1982–1994), the modeled daily Q Kling-Gupta efficiency (KGE) was 0.677 (Table 5-3, 5-4). While daily Q KGE was the calibration metric, the water-year summed Q KGE was also quite good, at 0.708, and the total Q balance was 5.1% (modeled having 5% more streamflow than measured for the 13-year period). Modeled flow captured the timing of storm events and high flows well, including the spring freshet (Figure 5-4, left panel). The model struggled however to capture the magnitudes of very low flows, but captured well the distribution of flow above the median flow (Figure 5-4, right panel).

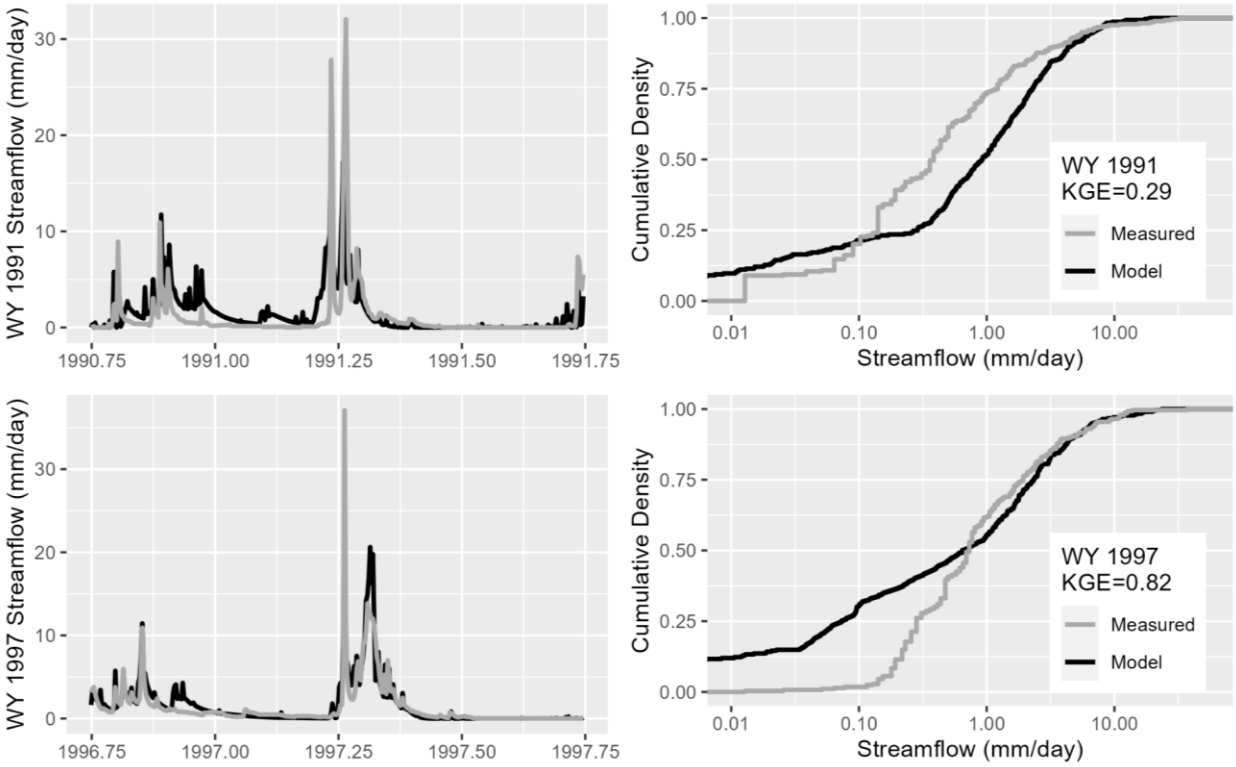

Figure 5-4. Hydrology calibration results. Hydrographs (left column) and cumulative distribution functions (right column) for water years 1991 (top row) and 1997 (bottom row). KGE for WY 1991 is 0.29 and KGE for WY 1997 is 0.82. Gray lines are measured streamflow and black lines are modeled. The X axis is the calendar year, not the water year.

Table 5-4. Performance of the isolated hydrologic model against measured streamflow. The first row with the asterisk* is the calibrated scenario and evaluation metric (Daily KGE), and the other rows serve as model validation. A positive Q balance implies model over-estimation.

Model	Daily Q KGE	WYear Q KGE	% Q Balance
c32, 13 years pre*	0.677*	0.708	+5.1%
c32, 13 years post	0.521	0.683	+27%
c32, 30 years	0.617	0.812	+13%
c31, 13 years pre	0.710	0.940	+1.5%
c31, 13 years post	0.539	0.638	-9.6%
c31, 30 years	0.610	0.872	-6%

I conducted validation of the hydrology model for different time periods (the 13 years pre-harvest, the 13 years post-harvest, and a 30-year period spanning the harvest), and validated against measured streamflow from either catchment c32 (control, not harvested) or c31 (harvested in 1997). The model performed well, especially in the pre-harvest period, and similar to other studies, pre-harvest calibration resulted in poorer representation of post-harvest streamflow (Lin, 2022). During the 13-year pre-harvest period in catchment c31, the hydrology model achieved a KGE of 0.71, higher than the calibrated value for catchment c32. Similarly, the water-year summed KGE was 0.9 (and only 1.5% difference in Q balance). For both catchments, the worst fit was for the 13 years from 1998 to 2010. For c31, which was harvested in the fall of 1997, the trapezoidal simulated LAI (as discussed in Section 5.3.4.2) was altered to reduce the maximum summertime LAI after harvest, and slowly increase over the following years (using the summertime LAI values in Han, 2022). Despite better performance of c31 relative to c32 during the post-harvest period, daily KGE values were lower than pre-harvest: 0.539 and 0.521, respectively. The Q balance went in opposite directions for this post-harvest period, with c32 modeling a 27% overestimate, and c31 a 9.6% underestimate.

While whole-period daily KGE was 0.677 (13-year calibration, Table 5-4), within-water-year KGE ranged from -0.1 (2007) to 0.83 (1985) between water years (WY) 1983–2011. Figure 5-4 shows water year hydrographs for the years 1991 and 1997. For both years, the timing of snowmelt and spring freshet (around year decimal 0.35), and the baseflow recession coming into the summer were quite well matched. The large difference in within-water-year KGE for these two years was reflected at all times of year. The freshet periods (year decimal 0.25–0.5) for 1991 and 1997 had daily KGE of 0.23 and 0.85 respectively: almost indistinguishable from the annual KGE. For some reason, at the end of 1990 into 1991, soil moisture must have been replenished, resulting in higher base flow through the winter that was not successfully modeled (Figure 5-4). In contrast, in 1997, modeled and measured streamflow were close, and much lower than in 1991. The cumulative distributions also show that in 1997, modeled very low flows make up a much larger portion of flows than the measured data suggests. Despite this, the median flow (cumulative density = 50%) for 1997 was very close, while for 1991 the model over-estimated median flow.

5.4.1.3 Forest Allometry and Stem Growth Calibration

Calibration Groups 2 & 3 calibrated the stem components to measured data provided by Buttle et al. (2018; Appendix D Tables D2 & D4). Measured stem biomass (Figure 5-5a) was used as input to the allometric equation calibration. This calibration resulted in good fits for diameter at breast height (DBH, fits of MAPE 8.4% and MAE 1.1 cm, Figure 5-5b). Leaf Area Index (LAI) was a function of DBH, leaf biomass, and the specific leaf area (SLA, itself a function of plant biomass). Having calibrated the former values (Table 5-3), a good LAI fit was achieved (MAPE 23% and MAE 0.64, Figure 5-5c). In Calibration Group 3 the dynamics of the stem pool were calibrated, resulting in model mean absolute percent error (MAPE) in stem stocking was 13% (MAE 51 stems ha^{-1}) (Figure 5-5d, Table 5-3).

The most important aspects of the stem modeling component included the pre- and post-harvest characteristics, the rate of change post-harvest, and "the overshoot" during recovery. This "overshoot" refers to the fact that measured data showed the number of stems post-harvest exceed the pre-harvest value. This likewise causes an overshoot in LAI, which will increase net primary productivity and transpiration in the coupled model post-harvest. The sparse measured data provided some difficulty for calibration. While the harvesting activity could reduce the number of stems and amount of tree biomass by a desired precise amount, the rate of growth to target was not consistent in measured data. For example, as seen for stem biomass (Figure 5-5a), the second post-harvest measurement suggested a slower rate of growth than the third measurement, and the fourth measurement showed a smaller rate again. This problem is discussed for calibration of the fully coupled model (Section 5.3.4.2, with results in 5.4.1.4). In contrast, the measured stem stocking seemed to have a more dramatic exponential increase than what the model could achieve, although the model matched the third and fourth post-harvest targets very well. The recovery data for LAI (from Han, 2022) presents a somewhat paradoxical contrast with basal area, where LAI recovery appears to be very fast. While the model captured the fourth post-harvest measurement well, it is unclear how modeled and measured post-harvest plant growth might differ, given that the second and third LAI measurements were underestimated by 43% and 30%, respectively. Again, this seems paradoxical because the growth rates suggested by measured basal area seem to vary significantly over this 16 year post-harvest period.

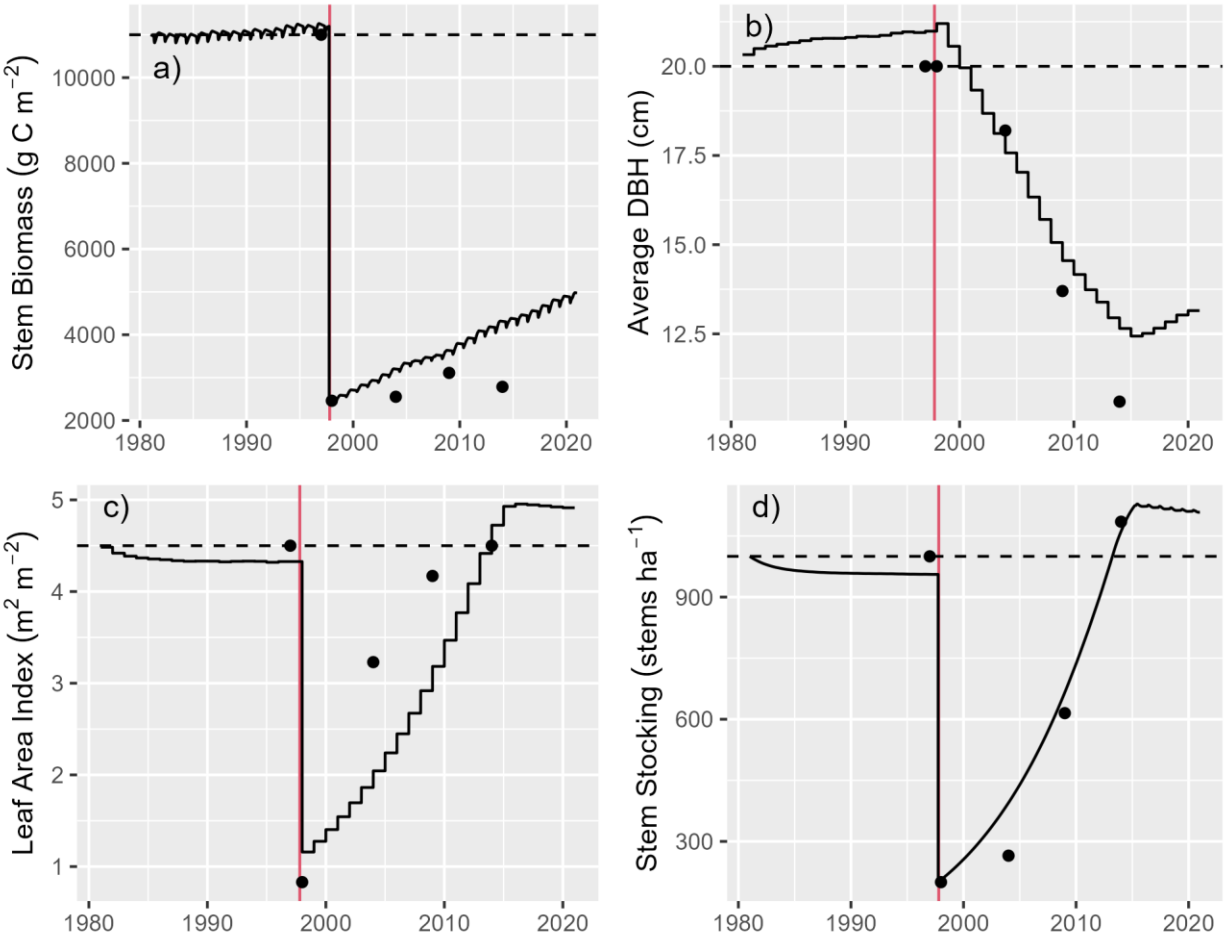

Figure 5-5. Comparison of measured and modeled forest geometries. Points represent measured data (described in Table 5-2 and Table D4). Lines represent modeled data. The horizontal dashed line represents the pre-harvest condition and the vertical red line represents the timing of the harvest.

5.4.1.4 Fully Coupled Model Pre-Harvest Calibration

The fully coupled model was first run in Calibration Group 5. With the soil moisture regimes locked in by the calibration of soil parameters (Section 5.4.1.2.), allometric equations calibrated (Section 5.4.1.3.), and final parameters governing soil carbon allocation analytically solved (see discussion in Section 5.3.4.2., and Appendix D5), achieving a steady state of the carbon budget required balancing pool volumes and turnover rates at appropriate levels on a multi-year basis. As discussed in Section 5.3.1.3., work by Morrison (1990) suggests that the forests at TLW exist in steady state, leading to the

assumption that aboveground biomass and soil carbon stocks should be generally unchanging over time in the unharvested scenario. Calibration for Group 5 used the full 30 years of climate for catchment c32 to demonstrate steady state of the forest biogeochemical cycle. From the best model results, average pool sizes and average water-year summed fluxes are presented in Table 5-5 in parentheses accompanying the calculated values. Absolute percent error (PER) of pool stability was 0.8% for Cp, 1.4% for Cl, 0.07% for Ch, 1.0% for Cb, and 1.0% for annual stem NPP (average 112 g C m^{-2}). Initial validation of the model also showed that assumptions made during earlier phases of calibration were reasonable. Namely, switching out the trapezoidal LAI for dynamically modeled LAI resulted in no meaningful change in hydrologic fit, ultimately resulting in a daily flow KGE of 0.681.

All modeled carbon pools are interdependent, and so stability is achieved when each has a balance of inputs and outputs (Table 5-5). For litter, humus, and soil biomass, calibration only affects a single turnover rate applied to each pool. While the soil temperature influence on soil processes was applied equally, the "switch" parameter determined the amount of influence. Calibration appeared to show little sensitivity in pool calibration to the temperature influence, however the water quality metrics showed preference to the isothermic equations (Figure D2).

Table 5-5. Carbon and nitrogen pools and fluxes at Turkey Lakes Forest. Values without annotation (parentheses, asterisks) are approximations of values measured at the TLW site, including pool sizes for plant stem, plant leaf, litter, and humus (see also, Table D2). Values with asterisks* are calculated according to equations in Appendix D5. Values in parentheses are averages from a 30-year steady-state model run. Values with a hat^ are completely dependent on the carbon value divided by the Pool C/N ratio.

Pool	Carbon Pool (g C m^{-2})	Nitrogen Pool (g N m^{-2})	C Turnover (g C m^{-2} y^{-1})	N Turnover (g N m^{-2} y^{-1})	Pool C/N Ratio
Plant Leaf Biomass	180 (174)	9^	180 (173)	9^ Uptake 3^ (2.95) Fall	20
Plant Stem Biomass	11,000 (10958)	55^	110 (112)	0.55^	200
Soil Biomass	300 (302)	30^	271* (274)	27.1^	10
Litter Pool	1600 (1554)	87.4^ (84.4)	560.9* (560.6)	30.7^ (30.38)	18.3 (18.44)
Humus Pool	21400 (21236)	972^	56.09* (62.9)	2.55^	22

Table 5-6. Modeled nitrogen fluxes for ammonium (NH_4^+) and nitrate (NO_3^-). Values in parentheses are averages from 30-year steady-state model run. Calculated mineralization has an asterisk* (from Table 5-5, subtract soil biomass N turnover from litter pool N turnover).

	NH_4^+ Flux	Flux Name or Internal Flux	NO_3^- Flux
Inputs ($g\ N\ m^2\ year^{-1}$)	0.34	Deposition	0.34
	3.61* (3.868)	Mineralization	-
		Atmospheric N Fixation (1.2)	
Internal Flux ($g\ N\ m^2\ year^{-1}$)		Nitrification (NH_4^+ to NO_3^-) → (4.13) →	
Outputs ($g\ N\ m^2\ year^{-1}$)	-	Denitrification	(1.91)
	(0.03)	Plant Uptake	(2.08)
	(0.052)	Leaching	(0.48)
	0.08	Stream Concentration (mg/L)	0.94

Table 5-7. Residence times of model stores. Residence times were calculated as pool size over the sum of outgoing fluxes (e.g. turnover or withdrawal).

Pool	Residence Time Long → Short
Plant Leaf C	1 year
Plant Stem C	45 year
Soil Litter C	2.73 year
Soil Humus C	337 year
Soil Biomass C	1.11 year
Mineral N - NH_4^+	47 days
Mineral N - NO_3^-	3.9 days

The final parameter affecting the plant pool was the stem turnover rate ($mp2$). Because the calibration metric emphasized both pool stability and a specific pool gross growth rate (Equation 5-9), the turnover rate targeted a specific turnover rate to match the growth rate. Had the growth rate not been a calibration target, it is conceivable that the calibration could have favored both growth and turnover rates close to zero, such that no change occurs in the pool, achieving "stability" in that way instead. Constraining the potential range of the growth and turnover parameters also prevented this equifinality problem. Given the steady state calculations in Appendix D5, the achievement of model stability in the litter, humus, and soil biomass pools was entirely dependent on turnover rates, and calibration found optimal values for these rates (Figure D2).

Calibration of the fully-coupled forest model simultaneously targeted steady-state behavior of the carbon and nitrogen pools, and appropriate export of nitrogen. Over the 30-year timeframe for catchment c32, modeled annual NO_3^- flux averaged 0.44 g N m^2 $year^{-1}$ (Table 5-6; PER of 5.6%), with 89% of total N flux as NO_3^- (target was 95% of flux). For calibration of daily measured NO_3^- concentrations (available 1981–2018), a KGE of 0.7 was achieved (Figure 5-6a). The components of NO_3^- concentration KGE incorporated the mean (PER of -14%), standard deviation (PER of 6%), and the correlation (R^2 = 0.75), which all indicated a good fit of the model to measured data. Calibration of daily measured dissolved organic resulted in a KGE of 0.5 (Figure 5-6). The components of DOC concentration KGE incorporated the mean (PER of -27%), standard deviation (PER of 22%), and the correlation (R^2 = 0.72).

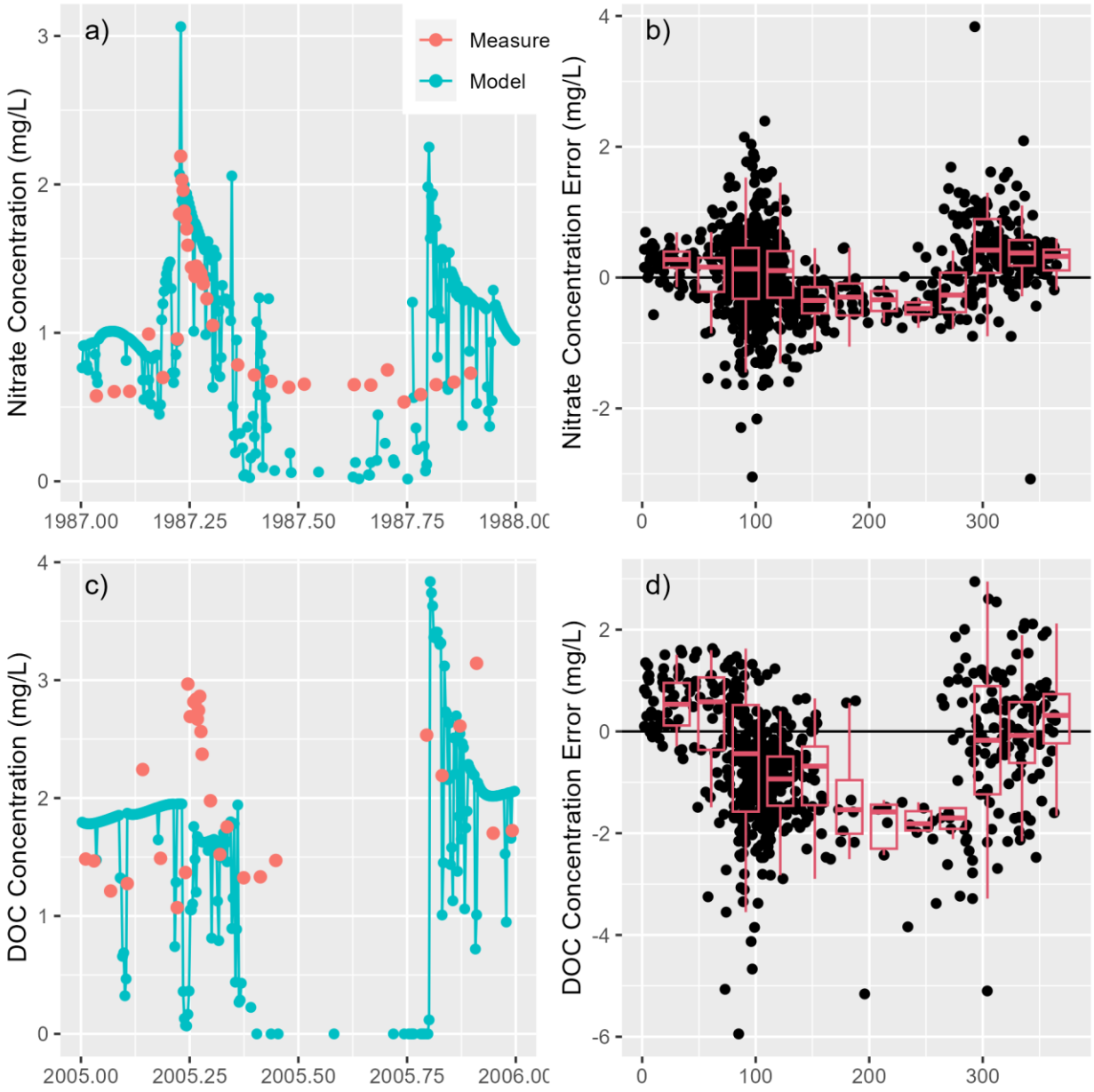

Figure 5-6. Comparison of model concentrations to measured data. Modeled NO_3^- (a) dissolved organic carbon (c) concentrations (blue) compared to measured data (red) for the years 1987 and 2005 (respectively). Absolute error (model minus measured) over year-day (black points) and month (red boxplots) for NO_3^- (b) and DOC (d).

Overall fit for NO_3^- concentrations was good, but seasonal fit for modeled NO_3^- concentrations varied significantly. Modeled NO_3^- concentrations routinely underpredicted summertime concentrations by 50–75% (Figure 5-6a,b). Notably, though, the summer period also had the least measured concentration data. I suspect that the model behavior during the leaf-out period of the model, characterized by a strong drawdown of the soil N pool, manifested in very low modeled stream NO_3^- concentrations. During initial calibration, I increased the maximum N fixation rate (Figure D2), resulting in more N uptake during leaf-out being derived from fixation, leading to less drawdown of the soil N pool and improving modeled concentration in the early spring. The majority of measured concentrations were in the spring and fall. Despite a wide range of single-day under- or over-predictions, median error was close to zero during the spring and fall (Figure 5-6b). During periods of higher measurement frequency, some modeled years showed very low error during the spring freshet period. In the fall, modeled data sometimes overpredicted the measured concentrations by over a factor of 2. The difficulty in calibration for NO_3^- concentration stemmed in part from the model design oriented around distinct climatological and biological periods (Section 5.2.2.1): winter dormancy, leaf-out, summer, and leaf-fall. As discussed above, the largest modification to the soil N pool takes place during leaf-out, where soil N that accumulated during the dormant period and high-moisture high-decomposition high-N-production conditions. The increase in transpiration driven by canopy growth and warmer temperatures then draws down soil moisture, resulting in a low-decomposition low-N-production regime into the summer. While NO_3^- concentrations during the spring freshet are modeled quite well (Figure 5-6a), the same high moisture regime that arrives in the leaf-fall period appears to be more difficult to model than the freshet. The amount of soil N accumulated at the end of the summer is governed by the summertime N uptake, pulses of decomposition during periodic soil-wetting events, and enrichment of the litter pool in N (decreased C/N ratios), which results in more N production per unit litter decomposition. On the median, fall model NO_3^- concentrations fit measured data about as well as the rest of the dormant period, however there appears to be some mechanism that drives very high concentrations during storm events that are not observed in the measured data.

The comparison of model fit for NO_3^- versus DOC concentrations gives useful insights into the model processes. While NO_3^- and NH_4^+ are subject to a myriad of production, removal, and modification processes in the soil, in this model, DOC is modeled mostly as a conservative tracer, with a variable input dependent on decomposition. Generally, median monthly behavior for DOC concentration was

a good match except in June through September (Figure 5-6c,d). These months had the most modeled no-flow days and the most low-flow days $0<Q<0.1$, where estimation of concentration would be extremely sensitive to flow. These months also had the most days where modeled flow was 100% derived from overland fast flow, where no model mechanism existed for DOC transport or production. Because the model assumes that all DOC comes from subsurface pathways, surface pathways for production and transport (e.g., surface ponded water, particulate organic matter) are unrepresented in the model.

5.4.1.5 Water Quality Calibration Post-Harvest

The behavior of the model following harvesting was modified from the control scenario by two disturbances: the removal of plant biomass and stems (setting up a long-term cascade of effects from the growth of new vegetation), and the "pulse" addition of fresh biotic material to the litter pool (setting up a short-term cascade of effects from decomposition and mineralization). The only calibrated parameters for the post-harvest period were for the "pulse". Specifically, both the size and stoichiometry (C/N ratio) of the pulse were calibrated. Calibration was most sensitive to the C/N ratio of the pulse, strongly favoring the minimum value of 10 (Figure D3). I observed that the pulse led to a spike in decomposition, however at higher C/N ratio of the pulse (especially at higher C/N than the average litter C/N of 18), the spike in decomposition and reduction in the average litter pool C/N led to a switch from mineralization to immobilization behavior. Contrary to the observed spike in NO_3^- concentrations (Figure 5-7a), calibration scenarios with higher C/N and the subsequent immobilization led to suppressed NO_3^- leaching and concentrations.

For the final optimally calibrated harvested model, modeled and measured concentrations showed strong agreement (Figure 5-7). The calibrated objective function of RMSE of the first 5 years of post-harvest NO_3^- concentrations was 2.34 mg/L. The 30-year (1982-2011) RMSE was 1.1 mg/L. For comparison, for the control scenario, the 5-year (1998-2002) and 30-year RMSE of NO_3^- concentrations was 0.64 and 0.61 mg/L, respectively. While the model behavior replicated the rise-and-fall shape of NO_3^- concentrations, the model underpredicted the very high concentrations in the second year post-harvest (WY 1999). Then, by WY 2002, the model overestimates concentrations, whereas measured concentrations for the harvested catchment on average fell below the control catchment for the next 10 years (and presumably more).

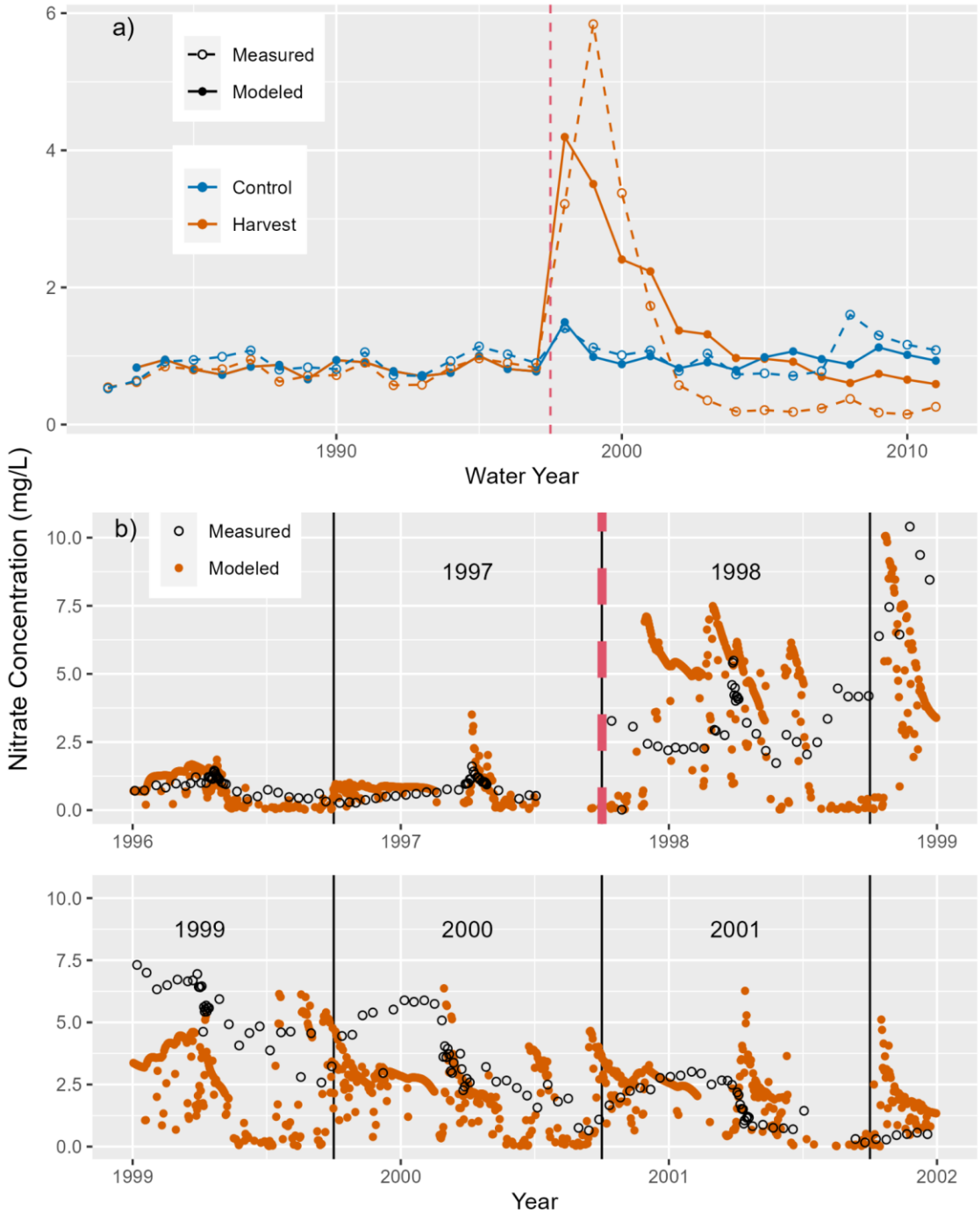

Figure 5-7. Comparison of stream NO_3^- concentration for modeled versus measured data. a) Water-year-averaged concentrations, comparing the harvested and control scenarios. Vertical dashed red line shows modeled date of harvest. b) Discrete daily concentration for six years (1996-2001, x-axis), showing pre- and post-harvest behavior for harvested scenarios (modeled and measured). Water-years (mid-panel labels) are separated by vertical black lines.

5.4.2 Model Behavior

The goal of this modeling exercise was to gain insight into which biological, hydrologic, and biogeochemical processes are important in driving the water quality and streamflow response to harvesting. In the previous section, I used several data to calibrate and validate that this model can replicate real world behavior of the forest at TLW, including hydrology and the concentration and export regime of dissolved nitrogen.

5.4.2.1 Effect of Harvesting on Flow and Hydrology

The effect of forest harvesting on streamflow at the TLW has been previously summarized in work by Buttle et al. (2018), Leach et al. (2020), Lin (2022), and Han (2022). A key challenge highlighted by all these authors is the correlation in time between a shift from wetter to drier conditions (10 years pre- and post-harvest comparison: 170 mm/year, 13% reduction in precipitation; 47 mm/year, 7% increase in potential evapotranspiration) at the same time that harvesting took place (in the fall of 1997). As discussed previously, a general hypothesis for post-harvest behavior would be that the loss of vegetation would decrease transpiration and increase runoff. The observed climatic shift instead decreased runoff across the TLW. At the simplest level, the effect of harvesting can be described as relatively little change in runoff in the harvested catchments (c31, c33, c34) between the pre- and post-harvest periods, while runoff decreased in an assemblage of control catchments (c32, c35, c46): the implication being that runoff *would have* decreased if not for the harvest. In the same 10 year period comparison (Figure 5-8), measured water-year flow in c31 decreased by 71.4 mm/year (-12%), while flow in c32 decreased by 149 mm/year (-25%).

The harvest scenario in the model was clearly able to replicate a small increase in streamflow relative to the control scenario (Figure 5-8a,b). The model replicated the decrease in streamflow in the control catchment due to the drier weather, and the magnitude of streamflow increase in the harvest scenario was similar to measured data, except for a very large measured streamflow in c31 in WY 2004. Despite efforts to use linear regression to isolate the climatic effect of the drier post-harvest period, there was no significant difference in the effect size in measured data (Figure 5-8b) between the pre-harvest (WY 1982-1997: 39 mm/year) and post-harvest (WY 1998-2011: 41 mm/year) periods. This stands in contrast to the clearer trend in modeled effect size, which increased to about 100 mm/year in WY 2000 and then around 50 mm/year after that, until receding by WY 2006.

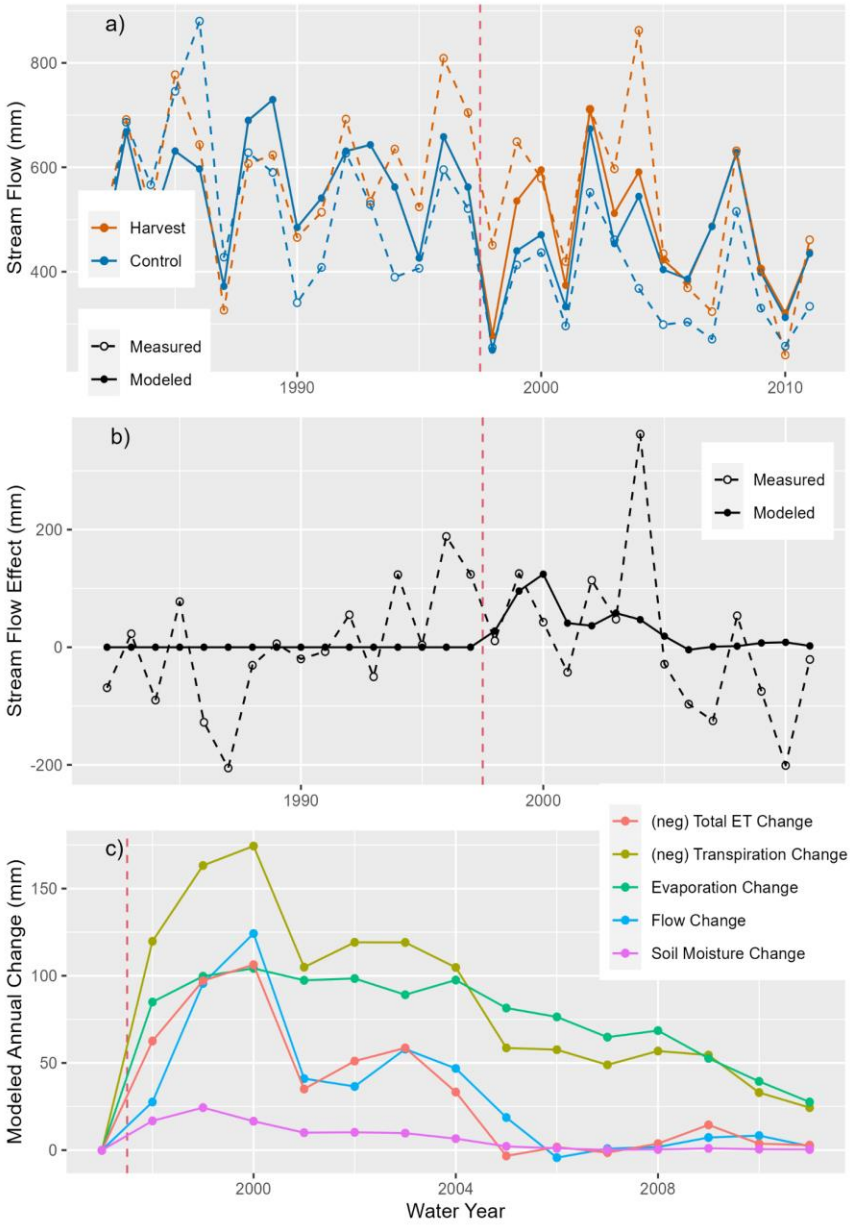

Figure 5-8. Hydrologic effects of harvesting. a) Measured (dashes and open circles) and modeled (solid lines and circles) water-year streamflow in the control (c32) and harvested (c31) catchments. b) Effect size in measured and modeled streamflow for the harvested scenario. "Expected" values for streamflow in the clearcut harvested catchment c31 were calculated from streamflow in the control catchment 32 from linear regression. The regression (for water-years 1982–1997) resulted in a significant relationship ($p=0.012$, adjusted $R^2=0.33$) with water-year streamflow (in mm): $Q_{31} = 0.53 * Q_{32} + 305$. The regression was then used to calculate expected values for c31 for water-years 1998–2011. Effect size was calculated as measured minus expected. c) Absolute value of modeled changes in hydrologic fluxes contributing to the change in streamflow. "neg" means the effect size was negative.

The cause of the streamflow change after harvesting was almost exclusively driven by the net change in evapotranspiration (Figure 5-8c). While transpiration decreased by up to 175 mm/year, a compensatory increase in soil evaporation (driven in part by the reduced tree canopy and more solar radiation reaching the soil surface, and in part by increased soil moisture) resulted in a peak modeled effect size of 124 mm/year in WY 2000 (average 44.5 mm/year for the post-harvest period). By WY 2005, the regrowth of the canopy balanced the rebounding transpiration effect with a slowly decreasing evaporation effect, resulting in little divergence in modeled streamflow.

5.4.2.2 Effect of Harvesting on NO_3^- Export

Beginning this work, my hypothesis was that export of nitrogen would be governed according to the seasons. In winter, nitrogen mineralization, nitrification, and subsequent export would be governed by soil moisture, itself affected by precipitation and snowpack dynamics. Denitrification would be a major sink of NO_3^-, preventing its export. In summer, soil moisture levels are drawn down by plant transpiration, thus preventing export due to the lack of flow.

The effect of the harvest was immediately seen in measured concentrations (Figure 5-7b). Concentrations of NO_3^- in catchment c31 exceeded 3 mg N/L in the fall of 1997—the highest level in the period 1982–1997. For WY 1998 (starting October 1997), the average modeled NO_3^- concentration slightly exceeded measured concentrations (Figure 5-7a), and while measured concentrations rose on average in the next WY 1999, modeled concentrations fell slightly. The averaging effect conflated two problems with the modeled concentrations: first, dormant period concentrations (including immediately after the harvest in October 1997) should have risen immediately (Figure 5-7), but immediately after the harvest the model concentrations were similar values to immediately before the harvest. This is likely due to the fact that little flow was generated in the model at these times, and the only nitrogen pathway for overland flow would be precipitation wet deposition or transport of the snowpack N store. The second problem is in the non-dormant period of 1998, where modeled concentrations appear to be twice as high as measured. While the impact of the freshet is clear in both modeled and measured concentrations, the constantly elevated model values likely stems from the decomposition of the large N-rich dead root pulse. The mismatch in the second post-harvest WY suggests that perhaps some decomposition of the pulse should have been delayed,

such that more N would be released later and not earlier. With that said, the fall of 1998 showed good agreement in the magnitude of the N concentrations, peaking around 10 mg N/L.

Following the increase in NO_3^- concentrations, measured concentrations dropped from WY 1999 to 2000 and 2001, and in WY 2002 concentrations for the harvested catchment c31 dropped below those of the control catchment c32. As discussed above, the modeled concentrations peaked in WY 1998, but fell slower than measured concentrations, and did not fall below those of the control catchment until about 2005–2007. The WY-averaged modeled concentrations mirrored the rise and fall of modeled soil NO_3^- pool (boxes 1 and 2), suggesting that the mismatch between modeled and measured from WY 2000 onwards was due to too much addition to the soil, or too little removal of NO_3^- from the soil (either via denitrification, or vegetation uptake). After the harvest, denitrification increased from a rate of 2 g N m^{-2} $year^{-1}$ to about 8 g N m^{-2} $year^{-1}$, and declined along the same pattern of soil NO_3^-. In contrast, plant N uptake (of which about 90% is of NO_3^-) decreased from a rate of about 3 g N m^{-2} $year^{-1}$ pre-harvest to less than 1.5 g N m^{-2} $year^{-1}$ for a period of 11 years. Total plant N uptake returned to pre-harvest levels in WY 2011. Interestingly, NH_4^+ uptake exceeded pre-harvest levels by a factor of 2 in 2008, 2009, and 2011, but was otherwise about the same post-harvest as pre-harvest. These high-NH_4^+-uptake years corresponded to very low soil NO_3^- years, whereas 2010 had slightly higher soil NO_3^-. Similar patterns of increase in the immediate post-harvest years (usually 1998–1999) and then subsequent decreases were seen for soil biomass, the litter and humus pools themselves, and consequently the processes of mineralization and nitrification.

5.4.2.3 Concentration-Discharge Behavior

Measured NO_3^- concentrations for catchment c32 showed a generally chemostatic behavior at low flows, with concentrations ranging between 0.5 and 0.75 mg N L^{-1}, and mobilization behavior during high flows like the spring freshet. Concentration-discharge (C-Q) analysis of measured data shows a slight positive slope (b=0.16) of the total log-concentration log-discharge regression. Breakpoint analysis at the median measured discharge (0.436 mm day^{-1}) showed an insignificant slope less than the median (p=0.5) and a significant and positive slope greater than the median (b=0.21). Freshet measured NO_3^- concentrations ranged up to above 3 mg N L^{-1}.

C-Q analysis for daily modeled NO_3^- concentration reflected some of the seasonal trends. Examining the entire 30-year daily model time series, NO_3^- concentration showed a significant breakpoint C-Q

pattern, with a positive slope (b=0.18) for the lower quantile (below measured median discharge) and a negative slope (b=-0.04) for the upper quantile. This stands in contrast to the pattern seen in measured data. If instead, the modeled daily data was subsetted to only days corresponding to measured data, the modeled data C-Q pattern switches to an insignificant lower quantile slope (p=0.4) and a slightly positive upper quantile slope (b=0.11). Kendall's rank correlation test deemed both the lower and upper quantile correlations as insignificant (p=0.35, p=0.98, respectively). This difference highlights some of the challenges in assessing CQ relationships when there are significant differences in data resolution, as discussed in Chapter 4.

5.5 Conclusions and Future Work

The work presented in this chapter comprised the development and calibration of a coupled hydrologic-vegetation-biogeochemistry model, and discussion of the processes driving the downstream effect of forest harvesting. While several complicated spatially distributed models with such capabilities have been developed such as RHESSys and SWAT (Band et al., 1991; Gassman et al., 2007), no model has been developed with the top-down and parsimonious approach undertaken here, with the capabilities to capture behavior in all three process categories of hydrology and rainfall-runoff dynamics; vegetation influence on hydrology and nutrient budgets; and soil biogeochemistry and element cycling.

5.5.1 Major Drivers of Nitrogen Export

Applied to the Turkey Lakes Watersheds (TLW), my coupled model revealed several surprising relationships between environmental processes and downstream water quality. Firstly, with regard to the behavior of vegetation, I found that appropriate modeling of nitrogen export relied heavily on provision of biological nitrogen fixation (BNF). The close proximity in time of the spring freshet and flushing of the subsurface with maximum nitrogen demand during leaf-out created a challenge in modeling, such that an external N source was necessary to supply enough N for leaf-out and N export in stream water. This conclusion is supported by large forest-scale nitrogen budgets that conclude that BNF contributes to the N budget of northern hardwood forests. Like the addition of this external source, I also found that modeling the process of denitrification was critical to water quality calibration. Over the summer, as soil drainage subsided and N accumulated, a major portion of the N budget (about 40%) had to be removed from the system before complete flushing in the subsurface during the fall soil wet-up. Finally, I found that in calibration of nitrogen export, isothermic soil

decomposition was favored over temperature-dependency. This contrasts with behavior from models such as RHESSys, which assume that decomposition in winter is suppressed due to low soil temperatures. Instead, I found that buildup of N from soil decomposition over the winter was important for appropriately capturing peak stream NO_3^- concentrations during the freshet and soil flushing.

5.5.2 Future Model Improvements and Applications

While my model achieved quite good calibration metrics for NO_3^- concentrations in stream water after harvest, my model underestimated the peak concentrations in the second water-year post-harvest, and underestimated the post-harvest decline in concentrations to below the non-harvested regime. I suggest that the post-harvest behavior could be better modeled if the N-rich "pulse" addition to the litter pool (thought to represent fine root death) had a decomposition term different from that of normal litter additions, delaying the increase in mineralization to match the post-harvest stream NO_3^- peak. If plant regrowth resulted in more growth of N-expensive leaves earlier after harvest (as demonstrated by the underestimate of early post-harvest leaf area index), the soil mineral N pools could have been depleted faster, matching the measured data. Finally, my model might not appropriately capture the compensatory balance between post-harvest reduction in transpiration (which was about 40% lower than pre-harvest for about 10 years after harvest) and an increase in soil evaporation (due to reduced canopy cover). Given the high dependency of my model on soil moisture regimes, the relatively small effect of harvesting on soil moisture might suggest that the effect was not well modeled.

Future application of the model will include other climate and disturbance scenarios. Possibilities include potentially changing precipitation, temperature, and nitrogen deposition trends or seasonalities. Other experiments possibly include a suite of disturbance magnitudes, like the experiments at TLW with differing degrees of vegetation removal.

Finally, the top-down nature of this model makes it especially adaptable to other landscapes and forest types. While the work presented in this chapter details a complicated sequence of calibrations of various sets of parameters, lessons learned could improve the efficiency of calibration while not compromising on model fit.

Chapter 6
Conclusions

6.1 Contributions of this Dissertation

This dissertation presented new results on the effects of forest disturbances on downstream waters, including alterations to flows and flow regimes; water quality (including concentrations of nutrients like nitrogen, phosphorus, and carbon); and changes in the co-variation of concentrations and flow (CQ). Working with data from hundreds of catchments, I developed multiple novel methodologies to disentangle the effects of climate variation from disturbance effects on flows, concentrations, as well as CQ behavior.

In research presented in Chapter 2, I sought to answer the following questions: How do streamflow regimes change after wildfire? How can we decouple these changes from the influence of changes in climate? Can this decoupled disturbance signal be used to estimate hydrologic recovery times? I developed a novel climate decomposition method based on the Budyko framework that allowed me to isolate the effect of disturbance from climate. I found that the wildfire effect on streamflow in seven burned watersheds in Southern California (USA) was statistically detectable in five watersheds, where the effect size was approximately 80 mm yr^{-1}. Using a deviation term derived from the Budyko decomposition, I estimated that hydrologic recovery from fire to the pre-fire climate-flow relationship ranged between 5 to 45 years, and was significantly correlated with the burn extent in the watersheds. The simplicity of the method developed allows for future expansion beyond the seven catchments to isolate the effect of fires on catchment response at regional and continental scales.

In research presented in Chapter 3, I sought to answer the following questions: How do water quality regimes change after wildfires? How do changes in elements co-vary? How do mean concentrations change relative to concentration variability, or to extreme concentrations? I conducted a meta-analysis to explore post-fire changes in concentrations of nitrogen (N) and phosphorus (P) species, dissolved organic carbon (C), and total suspended sediments from 121 watersheds around the world. I found concurrent increases in concentrations of C, N, and P species after forest fire. I found that fire alters N and P speciation, with median increases of 40%–60% in the proportion of soluble inorganic N and P relative to total N and P. I also found that fire decreases C:N and C:P ratios, with median decreases ranging from 60% to 70%. Further, I developed a methodology to identify how extreme

concentrations changed after fire. I showed that the highest concentration percentiles increased at a greater rate after fire than the median and lowest concentration percentiles. This validates many studies showing that rare events often associated with extreme precipitation make up an important part of the wildfire effect in watersheds.

In research presented in Chapter 4, I sought to answer the following questions: What is the relationship between the disturbance-driven changes in flow (Q) and water quality (C, concentrations)? Do C-Q relationships change after disturbance? How do these changes manifest for different elements? I analyzed co-measured water quality and flow data from 29 watersheds across the continental United States and with 186 site-fire-parameter sets. Given the high temporal and spatial variability in the data, it was challenging to find a consistent pattern in changes of various CQ metrics. To address this, I developed a novel clustering methodology to create CQ "typologies" that mapped well onto traditional classifications of chemostasis, mobilization, dilution, and chemodynamic behavior. These typologies captured aspects of the CQ relationships like CQ slope, but also multiple metrics related to variability. I then explored how individual elements and sites changed their cluster membership after fire. Interestingly, I found that CQ relationships following disturbance moved towards chemostasis for dissolved nitrogen species (between 15 and 35% more sites), and moved towards more mobilization for total nitrogen and phosphorus species (about 10% more sites). This clustering method showed promise for explaining the varied responses of flux (the product of C and Q) after fire, with flux increasing after fire when sites' CQ behavior shifted from dilution to chemostatic or chemostatic to mobilization or chemodynamic. I used multiple linear regression to show that post-fire change in C was actually a more important predictor of change in flux than was change in Q. This varied somewhat by element, where change in Q was more important than change in C for explaining nitrate and organic carbon fluxes . In addition to presenting a unique synthesis of post-disturbance changes in CQ relationships, I developed methodologies that could be applied to other CQ analyses.

In research presented in Chapter 5, I sought to answer the following questions: What ecohydrological and biogeochemical processes drive forest harvesting impacts on water quantity? Can we use a top-down modeling approach to understand these processes? How can site-measured data be used to inform the modeling approach? I developed a coupled hydrologic-vegetation-biogeochemistry model to reveal the dominant processes shaping the downstream export of nitrogen and carbon in a forested watershed. The model development favored parsimony, and used a top-down approach to incorporate

components from several models previously applied to forested watersheds. I used an exhaustive multi-step calibration approach to make use of the wealth of information available from the Turkey Lakes study site, and to calibrate against multiple characteristics of hydrology, vegetation behavior, and water quality in the unharvested and harvested scenarios. Short residence times of nitrogen in soil means that seasonal shifts in N sources or sinks is the primary driver of stream water nitrate concentration regimes. The overlapping effects of short-term climatic variation, including a dry post-harvest period, and the removal of vegetation during the harvest, demonstrated some of the challenges in modeling the behavior of a steady-state old-growth forest with an aggrading regrowth forest.

6.2 Future Research Directions

Forests are undoubtedly crucially important ecosystems. Numerous ecosystem services from forests may be under threat, yet significant uncertainty remains in how exactly different ecosystems and hydroclimatic regions will respond to changes at the region, continental, or global scales. Those seeking to incorporate forests as part of "nature based solutions" should heed these concerns, and encourage research into the following areas:

6.2.1 Interacting hydrologic effects of climate and disturbance

The research presented in this dissertation, including in Chapters 2 and 5, have great applicability to disentangling the effects of climatic variability and landscape disturbance on downstream waters. Alongside attempts to review and synthesize hydrological data from forested watersheds and obtain predictive relationships of forest cover alteration and streamflow, researchers have debated the ethics of considering tradeoffs between sacrificing forest cover for potentially more human-available water. With the methodology for Budyko climate decomposition presented in Chapter 2, a continental-scale analysis could be conducted to determine the appropriateness of the methodology across a wider range of climatic diversity, and determine the potential differences in the disturbance flow response.

The Budyko curve and subsequent derivations or alterations can themselves be considered top-down models, used to predict either long-term or annual streamflow from incoming water and energy. From its elegance and simplicity, more can be learned by comparing it to the wealth of measured streamflow and climatic variables from across the continental US and the world, and by comparing its predictions to those of other simple top-down models, which have already been applied at similar spatial scales.

6.2.2 Altered element cycles after disturbance

Our novel finding from Chapter 3 that dissolved bio-active forms of nitrogen and phosphorus increase relative to total export has significant implications for this field of study. Future work will investigate the prevalence of this finding to other disturbances, and analyze the conditions that lead to this outcome. We might ask, is the role of fire and ash-driven water quality change important to this outcome, or do we see similar outcomes after forest harvesting? How might element cycling in the watershed—for example, in-stream processing—alter these element ratios as water travels farther away from the solute source or disturbed area? Research in Chapter 4 produced novel classifications of concentration-discharge (CQ) relationships, and there are many more opportunities to apply these classifications to undisturbed and post-disturbance CQ regimes.

6.3 Closing Message

The work on wildfires presented in this dissertation is among a large upswing in research on the topic, with particular interest in the effects on water quality. In fact, as I finish writing this dissertation, massive plumes of wildfire smoke have spread from northern Ontario and Quebec Ontario throughout much of eastern North America. This serves as a stark reminder that wildfire is here on our landscape, and its effects will be felt. Research should continue to constrain how climate and wildfire conditions will change, as land managers balance these changes with the existing activities (e.g., harvesting) taking place in forests. With that knowledge, our research on the post-disturbance changes of water quality will serve to inform water users and protect the public and public resources.

References

Abatzoglou, J. T., & Williams, A. P. (2016). Impact of anthropogenic climate change on wildfire across western US forests. *Proceedings of the National Academy of Sciences*, *113*(42), 11770–11775.

Abbott, B. W., Moatar, F., Gauthier, O., Fovet, O., Antoine, V., & Ragueneau, O. (2018). Trends and seasonality of river nutrients in agricultural catchments: 18years of weekly citizen science in France. *Science of The Total Environment*, *624*, 845–858. https://doi.org/10.1016/j.scitotenv.2017.12.176

Abbott, B. W., Gruau, G., Zarnetske, J. P., Moatar, F., Barbe, L., Thomas, Z., et al. (2018). Unexpected spatial stability of water chemistry in headwater stream networks. *Ecology Letters*, *21*(2), 296–308. https://doi.org/10.1016/j.earscirev.2016.06.014

Abbott, B. W., Bishop, K., Zarnetske, J. P., Hannah, D. M., Frei, R. J., Minaudo, C., et al. (2019). A water cycle for the Anthropocene. *Hydrological Processes*, *0*. https://doi.org/10.1002/hyp.13544

Abbott, B. W., Rocha, A. V., Shogren, A., Zarnetske, J. P., Iannucci, F., Bowden, W. B., et al. (2021). Tundra wildfire triggers sustained lateral nutrient loss in Alaskan Arctic. *Global Change Biology*, *n/a*(n/a). https://doi.org/10.1111/gcb.15507

Abdelnour, A., McKane, R. B., Stieglitz, M., Pan, F., & Cheng, Y. (2013). Effects of harvest on carbon and nitrogen dynamics in a Pacific Northwest forest catchment. *Water Resources Research*, *49*(3), 1292–1313. https://doi.org/10.1029/2012WR012994

Aber, J. D., & Federer, C. A. (1992). A Generalized, Lumped-Parameter Model of Photosynthesis, Evapotranspiration and Net Primary Production in Temperate and Boreal Forest Ecosystems. *Oecologia*, *92*(4), 463–474. https://doi.org/10.1007/bf00317837

Aber, J. D., Melillo, J. M., & Federer, C. A. (1982). Predicting the effects of rotation length, harvest intensity, and fertilization on fiber yield from northern hardwood forests in New England. *Forest Science*, *28*(1), 31–45.

Abney, R. B., & Berhe, A. A. (2018). Pyrogenic Carbon Erosion: Implications for Stock and Persistence of Pyrogenic Carbon in Soil. *Frontiers in Earth Science*, *6*. https://doi.org/10.3389/feart.2018.00026

Addor, N., Newman, A. J., Mizukami, N., & Clark, M. P. (2017). The CAMELS data set: catchment attributes and meteorology for large-sample studies. *Hydrology and Earth System Sciences*, 21. https://doi.org/10.5194/hess-21-5293-2017

Alexander, R. B., Boyer, E. W., Smith, R. A., Schwarz, G. E., & Moore, R. B. (2007). The Role of Headwater Streams in Downstream Water Quality. *JAWRA Journal of the American Water Resources Association*, *43*(1), 41–59. https://doi.org/10.1111/j.1752-1688.2007.00005.x

Allen, R. G., Pereira, L. S., Raes, D., & Smith, M. (1998). *Crop evapotranspiration-Guidelines for computing crop water requirements* (No. FAO Irrigation and drainage paper 56). Rome: Food and Agriculture Organization of the United Nations.

Anderson, C. J., & Lockaby, B. G. (2011). Research Gaps Related to Forest Management and Stream Sediment in the United States. *Environmental Management*, *47*(2), 303–313. https://doi.org/10.1007/s00267-010-9604-1

Anderson, D. M., Glibert, P. M., & Burkholder, J. M. (2002). Harmful algal blooms and eutrophication: Nutrient sources, composition, and consequences. *Estuaries*, *25*(4), 704–726. https://doi.org/10.1007/BF02804901

Anderson, M. G., & Burt, T. P. (1978). The role of topography in controlling throughflow generation. *Earth Surface Processes and Landforms*, *3*(4), 331–344.

Anderson, S. P., Dietrich, W. E., Torres, R., Montgomery, D. R., & Loague, K. (1997). Concentration-discharge relationships in runoff from a steep, unchanneled catchment. *Water Resources Research*, *33*(1), 211–225. https://doi.org/10.1029/96WR02715

Arora, V. K., & Boer, G. J. (2005). A parameterization of leaf phenology for the terrestrial ecosystem component of climate models. *Global Change Biology*, *11*(1), 39–59. https://doi.org/10.1111/j.1365-2486.2004.00890.x

Asadzadeh, M., & Tolson, B. (2013). Pareto archived dynamically dimensioned search with hypervolume-based selection for multi-objective optimization. *Engineering Optimization*, *45*(12), 1489–1509. https://doi.org/10.1080/0305215X.2012.748046

Atkinson, S. E., Woods, R. A., & Sivapalan, M. (2002). Climate and landscape controls on water balance model complexity over changing timescales. *Water Resources Research*, *38*(12), 50-1-50–17. https://doi.org/10.1029/2002WR001487

Band, L. E., Peterson, D. L., Running, S. W., Coughlan, J., Lammers, R., Dungan, J., & Nemani, R. (1991). Forest ecosystem processes at the watershed scale: basis for distributed simulation. *Ecological Modelling*, *56*, 171–196. https://doi.org/10.1016/0304-3800(91)90199-B

Band, L. E., Patterson, P., Nemani, R., & Running, S. W. (1993). Forest ecosystem processes at the watershed scale: incorporating hillslope hydrology. *Agricultural and Forest Meteorology*, *63*(1–2), 93–126. https://doi.org/10.1016/0168-1923(93)90024-C

Band, L. E., Mackay, D. S., Creed, I. F., Semkin, R., & Jeffries, D. (1996). Ecosystem processes at the watershed scale: sensitivity to potential climate change. *Limnology and Oceanography*, *41*(5), 928–938.

Band, L. E., Tague, C. L., Groffman, P., & Belt, K. (2001). Forest ecosystem processes at the watershed scale: hydrological and ecological controls of nitrogen export. *Hydrological Processes*, *15*(10), 2013–2028. https://doi.org/10.1002/hyp.253

Barbour, M., Keeler-Wolf, T., & Schoenherr, A. A. (Eds.). (2007). *Terrestrial vegetation of California* (Vol. 3rd edition). Berkely, California, USA: Univ of California Press.

Bárdossy, A. (2007). Calibration of hydrological model parameters for ungauged catchments. *Hydrol. Earth Syst. Sci.*, 9.

Baron, J. S., Hall, E. K., Nolan, B. T., Finlay, J. C., Bernhardt, E. S., Harrison, J. A., et al. (2013). The interactive effects of excess reactive nitrogen and climate change on aquatic ecosystems and water resources of the United States. *Biogeochemistry*, *114*(1–3), 71–92.

Bart, R. R. (2016). A regional estimate of postfire streamflow change in California. *Water Resources Research*, *52*(2), 1465–1478. https://doi.org/10.1002/2014WR016553

Bart, R. R., & Hope, A. (2010). Streamflow response to fire in large catchments of a Mediterranean-climate region using paired-catchment experiments. *Journal of Hydrology*, *388*(3), 370–378.

https://doi.org/10.1016/j.jhydrol.2010.05.016

Bart, R. R., & Tague, C. L. (2017). The impact of wildfire on baseflow recession rates in California. *Hydrological Processes*, *31*(8), 1662–1673. https://doi.org/10.1002/hyp.11141

Basso, M., Vieira, D. C. S., Ramos, T. B., & Mateus, M. (2020). Assessing the adequacy of SWAT model to simulate postfire effects on the watershed hydrological regime and water quality. *Land Degradation & Development*, *31*(5), 619–631. https://doi.org/10.1002/ldr.3476

Basu, N. B., Destouni, G., Jawitz, J. W., Thompson, S. E., Loukinova, N. V., Darracq, A., et al. (2010). Nutrient loads exported from managed catchments reveal emergent biogeochemical stationarity. *Geophysical Research Letters*, *37*(23). https://doi.org/10.1029/2010GL045168

Basu, N. B., Rao, P. S. C., Winzeler, H. E., Kumar, S., Owens, P., & Merwade, V. (2010). Parsimonious modeling of hydrologic responses in engineered watersheds: Structural heterogeneity versus functional homogeneity. *Water Resources Research*, *46*(4).

Basu, N. B., Thompson, S. E., & Rao, P. S. C. (2011). Hydrologic and biogeochemical functioning of intensively managed catchments: A synthesis of top-down analyses. *Water Resources Research*, *47*(10).

B.C. Ministry of Forests. (1997). *Silviculture Prescriptions Field Methods Book* (No. No. SIL411). Victoria, B.C., Canada: B.C. Ministry of Forests Forestry Division Services Branch. Retrieved from https://www.for.gov.bc.ca/hfd/pubs/docs/sil/sil411/A411.htm#E9E1

Beatty, S. M., & Smith, J. E. (2013). Dynamic soil water repellency and infiltration in post-wildfire soils. *Geoderma*, *192*, 160–172. https://doi.org/10.1016/j.geoderma.2012.08.012

Beckers, J., Smerdon, B., & Wilson, M. (2009). Review of hydrologic models for forest management and climate change applications in British Columbia and Alberta. *Forrex Series*, (25).

Benoist, A., Houle, D., Bradley, R. L., & Bellenger, J.-P. (2022). Evaluation of biological nitrogen fixation in coarse woody debris from Eastern Canadian boreal forests. *Soil Biology and Biochemistry*, *165*, 108531. https://doi.org/10.1016/j.soilbio.2021.108531

Bergström, S. (1995). The HBV model. In V. P. Singh (Ed.), *Computer models of watershed hydrology* (pp. 443–476). Water Resources Publications.

Bernhardt, E. S., Savoy, P., Vlah, M. J., Appling, A. P., Koenig, L. E., Hall, R. O., et al. (2022). Light and flow regimes regulate the metabolism of rivers. *Proceedings of the National Academy of Sciences*, *119*(8), e2121976119. https://doi.org/10.1073/pnas.2121976119

Bernhardt, H. (1984). Treatment disturbances with water out of eutrophic reservoirs as a consequence of extensive algal development. *Water Supply*, *2*, SS4-7.

Besaw, L. E., Rizzo, D. M., Bierman, P. R., & Hackett, W. R. (2010). Advances in ungauged streamflow prediction using artificial neural networks. *Journal of Hydrology*, *386*(1), 27–37.

Biederman, J. A., Somor, A. J., Harpold, A. A., Gutmann, E. D., Breshears, D. D., Troch, P. A., et al. (2015). Recent tree die-off has little effect on streamflow in contrast to expected increases from historical studies. *Water Resources Research*, 9775–9789. https://doi.org/10.1002/2015WR017401

Binkley, D., & Brown, T. C. (1993a). Forest practices as nonpoint sources of pollution in North America. *JAWRA Journal of the American Water Resources Association*, *29*(5), 729–740.

Binkley, D., & Brown, T. C. (1993b). *Management impacts on water quality of forests and rangelands* (General Technical Report No. RM-239). Fort Collins, CO, USA: USDA Forest Service.

Bitner, K., Gallaher, B., & Mullen, K. (2001). *Review of wildfire effects on chemical water quality*. Los Alamos National Lab., NM (US).

Blackwell, J. A., & Tuttle, A. (2003). *California Fire Siege 2003: The Story*. Sacramento, CA: California Dept. of Forestry and Fire Protection. Retrieved from http://www.fire.ca.gov/downloads/2003FireStoryInternet.pdf

Bladon, K. D., Silins, U., Wagner, M. J., Stone, M., Emelko, M. B., Mendoza, C. A., et al. (2008). Wildfire impacts on nitrogen concentration and production from headwater streams in southern Alberta's Rocky Mountains. *Canadian Journal of Forest Research*, *38*(9), 2359–2371. https://doi.org/10.1139/X08-071

Bladon, K. D., Emelko, M. B., Silins, U., & Stone, M. (2014). Wildfire and the future of water supply. *Environmental Science & Technology*, *48*, 8936–8943. https://doi.org/10.1021/es500130g

Bladon, K. D., Bywater-Reyes, S., LeBoldus, J. M., Keriö, S., Segura, C., Ritóková, G., & Shaw, D. C. (2019). Increased streamflow in catchments affected by a forest disease epidemic. *Science of The Total Environment*, *691*, 112–123. https://doi.org/10.1016/j.scitotenv.2019.07.127

Blake, W. H., Theocharopoulos, S. P., Skoulikidis, N., Clark, P., Tountas, P., Hartley, R., & Amaxidis, Y. (2010). Wildfire impacts on hillslope sediment and phosphorus yields. *Journal of Soils and Sediments*, *10*(4), 671–682. https://doi.org/10.1007/s11368-010-0201-y

Blöschl, G., & Sivapalan, M. (1995). Scale issues in hydrological modelling: A review. *Hydrological Processes*, *9*(3–4), 251–290. https://doi.org/10.1002/hyp.3360090305

Blöschl, G., Bierkens, M. F. P., Chambel, A., Cudennec, C., Destouni, G., Fiori, A., et al. (2019). Twenty-three Unsolved Problems in Hydrology (UPH) – a community perspective. *Hydrological Sciences Journal*, *64*(10), 1141–1158. https://doi.org/10.1080/02626667.2019.1620507

Blount, K., Ruybal, C. J., Franz, K. J., & Hogue, T. S. (2019). Increased water yield and altered water partitioning follow wildfire in a forested catchment in the western United States. *Ecohydrology*, *n/a*(n/a), e2170. https://doi.org/10.1002/eco.2170

Bodí, M. B., Martin, D. A., Balfour, V. N., Santín, C., Doerr, S. H., Pereira, P., et al. (2014). Wildland fire ash: Production, composition and eco-hydro-geomorphic effects. *Earth-Science Reviews*, *130*, 103–127. https://doi.org/10.1016/j.earscirev.2013.12.007

Boggs, J., Sun, G., & McNulty, S. G. (2016). Effects of Timber Harvest on Water Quantity and Quality in Small Watersheds in the Piedmont of North Carolina. *Journal of Forestry*, *114*(1), 27–40. https://doi.org/10.5849/jof.14-102

Booij, M. J., Schipper, T. C., & Marhaento, H. (2019). Attributing Changes in Streamflow to Land Use and Climate Change for 472 Catchments in Australia and the United States. *Water*, *11*(5), 1059. https://doi.org/10.3390/w11051059

Borenstein, M., Hedges, L. V., Higgins, J. P. T., & Rothstein, H. R. (2009). *Introduction to Meta-Analysis*. New York, NY, USA: JohnWiley & Sons.

Bormann, F. H., & Likens, G. E. (1967). Nutrient Cycling. *Science*, *155*(3761), 424–429.

Bormann, F. H., & Likens, G. E. (1979). *Pattern and Process in a Forested Ecosystem*. New York, NY, USA: Springer-Verlag.

Bormann, F. H., Likens, G. E., Fisher, D. W., & Pierce, R. S. (1968). Nutrient Loss Accelerated by Clear-Cutting of a Forest Ecosystem. *Science*, *159*(3817), 882–884. https://doi.org/10.1126/science.159.3817.882

Bormann, F. H., Siccama, T. G., Likens, G. E., & Whittaker, R. H. (1970). The Hubbard Brook Ecosystem Study: Composition and Dynamics of the Tree Stratum. *Ecological Monographs*, *40*(4), 373–388. https://doi.org/10.2307/1942336

Bormann, F. H., Likens, G. E., & Melillo, J. M. (1977). Nitrogen budget for an aggrading northern hardwood forest ecosystem. *Science*, *196*(4293), 981–983.

Bosch, J. M., & Hewlett, J. D. (1982). A review of catchment experiments to determine the effect of vegetation changes on water yield and evapotranspiration. *Journal of Hydrology*, *55*(1), 3–23. https://doi.org/10.1016/0022-1694(82)90117-2

Brady, N. C., & Weil, R. R. (2016). *The nature and properties of soils* (15th ed.). Columbus, OH, USA: Pearson.

Braun, L. N. (1984). *Simulation of snowmelt-runoff in lowland and lower alpine regions of Switzerland* [Application/pdf,XVII, 166 p.]. ETH Zurich. https://doi.org/10.3929/ETHZ-A-000334295

Brito, D. Q., Santos, L. H. G., Passos, C. J. S., & Oliveira-Filho, E. C. (2021). Short-Term Effects of Wildfire Ash on Water Quality Parameters: A Laboratory Approach. *Bulletin of Environmental Contamination and Toxicology*, *107*(3), 500–505. https://doi.org/10.1007/s00128-021-03220-9

Brown, A. E., Zhang, L., McMahon, T. A., Western, A. W., & Vertessy, R. A. (2005). A review of paired catchment studies for determining changes in water yield resulting from alterations in vegetation. *Journal of Hydrology*, *310*(1), 28–61. https://doi.org/10.1016/j.jhydrol.2004.12.010

Brown, A. E., Western, A. W., McMahon, T. A., & Zhang, L. (2013). Impact of forest cover changes on annual streamflow and flow duration curves. *Journal of Hydrology*, *483*, 39–50. https://doi.org/10.1016/j.jhydrol.2012.12.031

Brown, T. C., Hobbins, M. T., & Ramirez, J. A. (2008). Spatial Distribution of Water Supply in the Conterminous United States. *JAWRA Journal of the American Water Resources Association*, *44*(6), 1474–1487. https://doi.org/10.1111/j.1752-1688.2008.00252.x

Budyko, M. I. (1961). The Heat Balance of the Earth's Surface. *Soviet Geography*, *2:4*, 3–13. https://doi.org/10.1080/00385417.1961.10770761

Budyko, M. I. (1974). *Climate and life*. New York, Academic Press.

Buma, B., & Livneh, B. (2017). Key landscape and biotic indicators of watersheds sensitivity to forest disturbance identified using remote sensing and historical hydrography data. *Environmental Research Letters*, *12*(7), 074028. https://doi.org/10.1088/1748-9326/aa7091

Burke, M. P., Hogue, T. S., Kinoshita, A. M., Barco, J., Wessel, C., & Stein, E. D. (2013). Pre- and

post-fire pollutant loads in an urban fringe watershed in Southern California. *Environmental Monitoring and Assessment*, *185*(12), 10131–10145. https://doi.org/10.1007/s10661-013-3318-9

Buttle, J. M. (2011). The Effects of Forest Harvesting on Forest Hydrology and Biogeochemistry. In D. F. Levia, D. Carlyle-Moses, & T. Tanaka (Eds.), *Forest Hydrology and Biogeochemistry: Synthesis of Past Research and Future Directions* (pp. 659–677). Dordrecht, Netherlands: Springer. https://doi.org/10.1007/978-94-007-1363-5_33

Buttle, J. M., & Farnsworth, A. G. (2012). Measurement and modeling of canopy water partitioning in a reforested landscape: The Ganaraska Forest, southern Ontario, Canada. *Journal of Hydrology*, *466–467*, 103–114. https://doi.org/10.1016/j.jhydrol.2012.08.021

Buttle, J. M., Creed, I. F., & Pomeroy, J. W. (2000). Advances in Canadian forest hydrology, 1995–1998. *Hydrological Processes*, *14*(9), 1551–1578. https://doi.org/10.1002/1099-1085(20000630)14:9<1551::AID-HYP74>3.0.CO;2-J

Buttle, J. M., Beall, F. D., Webster, K. L., Hazlett, P. W., Creed, I. F., Semkin, R. G., & Jeffries, D. S. (2018). Hydrologic response to and recovery from differing silvicultural systems in a deciduous forest landscape with seasonal snow cover. *Journal of Hydrology*, *557*, 805–825. https://doi.org/10.1016/j.jhydrol.2018.01.006

Buttle, J. M., Webster, K. L., Hazlett, P. W., & Jeffries, D. S. (2019). Quickflow response to forest harvesting and recovery in a northern hardwood forest landscape. *Hydrological Processes*, *33*(1), 47–65. https://doi.org/10.1002/hyp.13310

Campbell, J. L., Rustad, L. E., Bailey, S. W., Bernhardt, E. S., Driscoll, C. T., Green, M. B., et al. (2021). Watershed studies at the Hubbard Brook Experimental Forest: Building on a long legacy of research with new approaches and sources of data. *Hydrological Processes*, *35*(1), e14016. https://doi.org/10.1002/hyp.14016

Cannon, S. H., & DeGraff, J. (2009). The Increasing Wildfire and Post-Fire Debris-Flow Threat in Western USA, and Implications for Consequences of Climate Change. In K. Sassa & P. Canuti (Eds.), *Landslides – Disaster Risk Reduction* (pp. 177–190). Berlin, Heidelberg: Springer. https://doi.org/10.1007/978-3-540-69970-5_9

Cannon, S. H., Gartner, J. E., Wilson, R. C., Bowers, J. C., & Laber, J. L. (2008). Storm rainfall conditions for floods and debris flows from recently burned areas in southwestern Colorado and southern California. *Geomorphology*, *96*(3), 250–269. https://doi.org/10.1016/j.geomorph.2007.03.019

Carignan, R., & Steedman, R. J. (2000). Impacts of major watershed perturbations on aquatic ecosystems. *Canadian Journal of Fisheries and Aquatic Sciences*, *57*(S2), 1–4.

Carignan, R., D'Arcy, P., & Lamontagne, S. (2000). Comparative impacts of fire and forest harvesting on water quality in Boreal Shield lakes, 13. https://doi.org/10.1139/f00-125

Carmona, A. M., Sivapalan, M., Yaeger, M. A., & Poveda, G. (2014). Regional patterns of interannual variability of catchment water balances across the continental US: A Budyko framework. *Water Resources Research*, *50*(12), 9177–9193. https://doi.org/10.1002/2014WR016013

Cawley, K. M., Hohner, A. K., Podgorski, D. C., Cooper, W. T., Korak, J. A., & Rosario-Ortiz, F. L.

(2016). Molecular and Spectroscopic Characterization of Water Extractable Organic Matter from Thermally Altered Soils Reveal Insight into Disinfection Byproduct Precursors. *Environmental Science & Technology*, *51*(2), 771–779.

Cawley, K. M., Hohner, A. K., McKee, G. A., Borch, T., Omur-Ozbek, P., Oropeza, J., & Rosario-Ortiz, F. L. (2018). Characterization and spatial distribution of particulate and soluble carbon and nitrogen from wildfire-impacted sediments. *Journal of Soils and Sediments*, *18*(4), 1314–1326.

Cerdà, A. (1998). Changes in overland flow and infiltration after a rangeland fire in a Mediterranean scrubland. *Hydrological Processes*, *12*(7), 1031–1042.

Certini, G. (2005). Effects of fire on properties of forest soils: A review. *Oecologia*, *143*(1), 1–10. https://doi.org/10.1007/s00442-004-1788-8

Charnley, S., Spies, T. A., Barros, A. M., White, E. M., & Olsen, K. A. (2017). Diversity in forest management to reduce wildfire losses: implications for resilience. *Ecology and Society*, *22*(1).

Chen, J., McGuire, K. J., & Stewart, R. D. (2020). Effect of soil water-repellent layer depth on post-wildfire hydrological processes. *Hydrological Processes*, *34*(2), 270–283. https://doi.org/10.1002/hyp.13583

Chen, J., Pangle, L. A., Gannon, J. P., & Stewart, R. D. (2020). Soil water repellency after wildfires in the Blue Ridge Mountains, United States. *International Journal of Wildland Fire*. https://doi.org/10.1071/WF20055

Chen, X., Alimohammadi, N., & Wang, D. (2013). Modeling interannual variability of seasonal evaporation and storage change based on the extended Budyko framework. *Water Resources Research*, *49*(9), 6067–6078. https://doi.org/10.1002/wrcr.20493

Cheng, L., Xu, Z., Wang, D., & Cai, X. (2011). Assessing interannual variability of evapotranspiration at the catchment scale using satellite-based evapotranspiration data sets. *Water Resources Research*, *47*(9). https://doi.org/10.1029/2011WR010636

Chorus, I., & Welker, M. (Eds.). (2021). *Toxic Cyanobacteria in Water: A Guide to Their Public Health Consequences, Monitoring and Management* (2nd Edition). London, UK: Taylor & Francis. Retrieved from https://www.taylorfrancis.com/books/oa-edit/10.1201/9781003081449/toxic-cyanobacteria-water-ingrid-chorus-martin-welker

Clarke, N., Gundersen, P., Jönsson-Belyazid, U., Kjønaas, O. J., Persson, T., Sigurdsson, B. D., et al. (2015). Influence of different tree-harvesting intensities on forest soil carbon stocks in boreal and northern temperate forest ecosystems. *Forest Ecology and Management*, *351*, 9–19. https://doi.org/10.1016/j.foreco.2015.04.034

Coble, A. A., Barnard, H., Du, E., Johnson, S., Jones, J., Keppeler, E., et al. (2020). Long-term hydrological response to forest harvest during seasonal low flow: Potential implications for current forest practices. *Science of The Total Environment*, 138926.

Comins, H. N., & McMurtrie, R. E. (1993). Long-Term Response of Nutrient-Limited Forests to CO2 Enrichment; Equilibrium Behavior of Plant-Soil Models. *Ecological Applications*, *3*(4), 666–681. https://doi.org/10.2307/1942099

Coombs, J. S., & Melack, J. M. (2013). Initial impacts of a wildfire on hydrology and suspended

sediment and nutrient export in California chaparral watersheds. *Hydrological Processes*, *27*(26), 3842–3851. https://doi.org/10.1002/hyp.9508

Crandall, T., Jones, E., Greenhalgh, M., Frei, R. J., Griffin, N., Severe, E., et al. (2021). Megafire affects stream sediment flux and dissolved organic matter reactivity, but land use dominates nutrient dynamics in semiarid watersheds. *PLOS ONE*, *16*(9), e0257733. https://doi.org/10.1371/journal.pone.0257733

Creed, I. F., & Band, L. E. (1998). Exploring functional similarity in the export of Nitrate-N from forested catchments: A mechanistic modeling approach. *Water Resources Research*, *34*(11), 3079–3093. https://doi.org/10.1029/98WR02102

Creed, I. F., & van Noordwijk, M. (2018). *Forest and Water on a Changing Planet: Vulnerability, Adaptation and Governance Opportunities. A Global Assessment Report.* (Vol. Volume 38). Vienna, Austria: International Union of Forest Research Organizations (IUFRO).

Creed, I. F., Trick, C. G., Band, L. E., & Morrison, I. K. (2002). Characterizing the spatial pattern of soil carbon and nitrogen pools in the Turkey Lakes Watershed: a comparison of regression techniques. *Water, Air and Soil Pollution: Focus*, *2*(1), 81–102.

Creed, I. F., Spargo, A. T., Jones, J. A., Buttle, J. M., Adams, M. B., Beall, F. D., et al. (2014). Changing forest water yields in response to climate warming: results from long-term experimental watershed sites across North America. *Global Change Biology*, *20*(10), 3191–3208. https://doi.org/10.1111/gcb.12615

Creed, I. F., Hwang, T., Lutz, B., & Way, D. (2015). Climate warming causes intensification of the hydrological cycle, resulting in changes to the vernal and autumnal windows in a northern temperate forest. *Hydrological Processes*, *29*(16), 3519–3534. https://doi.org/10.1002/hyp.10450

Crittenden, J. C., Trussell, R. R., Hand, D. W., Howe, K. J., & Tchobanoglous, G. (2012). *MWH's Water Treatment: Principles and Design* (3rd ed.). Hoboken, NJ, USA: John Wiley & Sons Inc. Retrieved from https://doi.org/10.1002/9781118131473

Davies, J.-M., & Mazumder, A. (2003). Health and environmental policy issues in Canada: the role of watershed management in sustaining clean drinking water quality at surface sources. *Journal of Environmental Management*, *68*(3), 273–286. https://doi.org/10.1016/S0301-4797(03)00070-7

De Cicco, L. A., Hirsch, R. M., Lorenz, D., & Watkins, W. D. (2022). dataRetrieval: R packages for discovering and retrieving water data available from Federal hydrologic web services (Version v.2.7.11). Retrieved from doi:10.5066/P9X4L3GE

DeBano, L. F., Neary, D. G., & Folliott, P. F. (1998). *Fire's Effects on Ecosystems*. New York, NY, USA: John Wiley and Sons, Inc.

Delač, D., Carrà, B. G., Esteban Lucas-Borja, M., & Zema, D. A. (2022). Hydrological Drivers and Effects of Wildfire in Mediterranean Rural and Forest Ecosystems: A Mini Review. In F. Calabrò, L. Della Spina, & M. J. Piñeira Mantiñán (Eds.), *New Metropolitan Perspectives* (pp. 47–55). Cham: Springer International Publishing. https://doi.org/10.1007/978-3-031-06825-6_5

Delpla, I., Jung, A.-V., Baures, E., Clement, M., & Thomas, O. (2009). Impacts of climate change on

surface water quality in relation to drinking water production. *Environment International*, *35*(8), 1225–1233. https://doi.org/10.1016/j.envint.2009.07.001

Dhar, A., Parrott, L., & Heckbert, S. (2016). Consequences of mountain pine beetle outbreak on forest ecosystem services in western Canada. *Canadian Journal of Forest Research*, *46*(8), 987–999. https://doi.org/10.1139/cjfr-2016-0137

D'Odorico, P., Laio, F., Porporato, A., & Rodriguez-Iturbe, I. (2003). Hydrologic controls on soil carbon and nitrogen cycles. II. A case study. *Advances in Water Resources*, *26*(1), 59–70. https://doi.org/10.1016/S0309-1708(02)00095-7

Donohue, R. J., Roderick, M. L., & McVicar, T. R. (2006). On the importance of including vegetation dynamics in Budyko? s hydrological model. *Hydrology and Earth System Sciences Discussions*, *3*(4), 1517–1551. https://doi.org/10.5194/hessd-3-1517-2006

Dowle, M., & Srinivasan, A. (2022). _data.table: Extension of `data.frame`_ (Version 1.14.6). Retrieved from https://CRAN.R-project.org/package=data.table

Duan, Q., Schaake, J., Andréassian, V., Franks, S., Goteti, G., Gupta, H. V., et al. (2006). Model Parameter Estimation Experiment (MOPEX): An overview of science strategy and major results from the second and third workshops. *Journal of Hydrology*, *320*(1), 3–17. https://doi.org/10.1016/j.jhydrol.2005.07.031

Dudley, N., & Stolton, S. (2003). *Running pure: the importance of forest protected areas to drinking water: a research report*. Gland, Switzerland; Washington, D.C.: WWF International; World Bank. Retrieved from http://wwf.panda.org/?8443/Running-Pure-The-importance-of-forest-protected-areas-to-drinking-water

Dupas, R., Musolff, A., Jawitz, J. W., Rao, P. S. C., Jäger, C. G., Fleckenstein, J. H., et al. (2017). Carbon and nutrient export regimes from headwater catchments to downstream reaches. *Biogeosciences Discuss.*, *2017*, 1–30. https://doi.org/10.5194/bg-2017-82

Earl, S. R., & Blinn, D. W. (2003). Effects of wildfire ash on water chemistry and biota in south-western U.S.A. streams. *Freshwater Biology*, *48*(6), 1015–1030. https://10.1046/j.1365-2427.2003.01066.x

Eaton, B. C., Moore, R. D., & Giles, T. R. (2010). Forest fire, bank strength and channel instability: the 'unusual' response of Fishtrap Creek, British Columbia. *Earth Surface Processes and Landforms*, *35*(10), 1167–1183. https://doi.org/10.1002/esp.1946

Ebel, B. A., & Moody, J. A. (2017). Synthesis of soil-hydraulic properties and infiltration timescales in wildfire-affected soils. *Hydrological Processes*, *31*(2), 324–340.

Ebel, B. A., Moody, J. A., & Martin, D. A. (2012). Hydrologic conditions controlling runoff generation immediately after wildfire. *Water Resources Research*, *48*(3).

Eder, G., Sivapalan, M., & Nachtnebel, H. P. (2003). Modelling water balances in an Alpine catchment through exploitation of emergent properties over changing time scales. *Hydrological Processes*, *17*(11), 2125–2149. https://doi.org/10.1002/hyp.1325

Eidenshink, J., Schwind, B., Brewer, K., Zhu, Z.-L., Quayle, B., & Howard, S. (2007). A Project for Monitoring Trends in Burn Severity. *Fire Ecology*, *3*(1), 3–21. https://doi.org/10.4996/fireecology.0301003

Emelko, M. B., Silins, U., Bladon, K. D., & Stone, M. (2011). Implications of land disturbance on drinking water treatability in a changing climate: Demonstrating the need for "source water supply and protection" strategies. *Water Research*, *45*(2), 461–472. https://doi.org/10.1016/j.watres.2010.08.051

Emelko, M. B., Stone, M., Silins, U., Allin, D., Collins, A. L., Williams, C. H. S., et al. (2016). Sediment-phosphorus dynamics can shift aquatic ecology and cause downstream legacy effects after wildfire in large river systems. *Global Change Biology*, *22*(3), 1168–1184. https://doi.org/10.1111/gcb.13073

Emmerton, C. A., Cooke, C. A., Hustins, S., Silins, U., Emelko, M. B., Lewis, T., et al. (2020). Severe western Canadian wildfire affects water quality even at large basin scales. *Water Research*, *183*, 116071. https://doi.org/10.1016/j.watres.2020.116071

EPA Office of Water. (2000). *BASINS Technical Note 6 Estimating Hydrology and Hydraulic Parameters for HSPF* (No. EPA-823-R00-012). U.S.A. Environmental Protection Agency. Retrieved from https://www.epa.gov/sites/default/files/2015-08/documents/2000_08_14_basins_tecnote6.pdf

Ernst, C. (2004). *Land Conservation and the Future of America's Drinking Water: Protecting the Source* (Water Protection Series). The Trust for Public Land and American Water Works Association. Retrieved from https://www.tpl.org/sites/default/files/cloud.tpl.org/pubs/water-protecting_the_source_final.pdf

Ernst, C., Gullick, R., & Nixon, K. (2004). Conserving Forests to Protect Water. *Opflow*, *30*(5), 1–7. https://doi.org/10.1002/j.1551-8701.2004.tb01752.x

Evaristo, J., & McDonnell, J. J. (2017). A role for meta-analysis in hydrology. *Hydrological Processes*, *31*(20), 3588–3591. https://doi.org/10.1002/hyp.11253

Evaristo, J., Jasechko, S., & McDonnell, J. J. (2015). Global separation of plant transpiration from groundwater and streamflow. *Nature*, *525*(7567), 91–94.

Fahey, T. J., Templer, P. H., Anderson, B. T., Battles, J. J., Campbell, J. L., Driscoll Jr., C. T., et al. (2015). The promise and peril of intensive-site-based ecological research: insights from the Hubbard Brook ecosystem study. *Ecology*, *96*(4), 885–901. https://doi.org/10.1890/14-1043.1

Fairbairn, L. G. (2020, February 19). *Linking soil moisture content and carbon dioxide fluxes: From batch experiments to process-based modelling* (Master Thesis). University of Waterloo. Retrieved from https://uwspace.uwaterloo.ca/handle/10012/15660

Falcone, J. A. (2011). *GAGES-II: Geospatial attributes of gages for evaluating streamflow* (USGS Unnumbered Series). Reston, VA: US Geological Survey. Retrieved from https://pubs.er.usgs.gov/publication/70046617

Falcone, J. A., Carlisle, D. M., Wolock, D. M., & Meador, M. R. (2010). GAGES: A stream gage database for evaluating natural and altered flow conditions in the conterminous United States. *Ecology*, *91*(2), 621–621. https://doi.org/10.1890/09-0889.1

Falcone, J. A., Murphy, J. C., & Sprague, L. A. (2018). Regional patterns of anthropogenic influences on streams and rivers in the conterminous United States, from the early 1970s to 2012. *Journal of Land Use Science*, *13*(6), 585–614. https://doi.org/10.1080/1747423X.2019.1590473

Falconer, I. R., & Humpage, A. R. (2005). Health Risk Assessment of Cyanobacterial (Blue-green Algal) Toxins in Drinking Water. *International Journal of Environmental Research and Public Health*, *2*(1), 43–50. https://doi.org/10.3390/ijerph2005010043

Feikema, P. M., Sherwin, C. B., & Lane, P. N. J. (2013). Influence of climate, fire severity and forest mortality on predictions of long term streamflow: Potential effect of the 2009 wildfire on Melbourne's water supply catchments. *Journal of Hydrology*, *488*, 1–16. https://doi.org/10.1016/j.jhydrol.2013.02.001

Ferlian, O., Wirth, C., & Eisenhauer, N. (2017). Leaf and root C-to-N ratios are poor predictors of soil microbial biomass C and respiration across 32 tree species. *Pedobiologia*, *65*, 16–23. https://doi.org/10.1016/j.pedobi.2017.06.005

Flannigan, M. D., Krawchuk, M. A., Groot, W. J. de, Wotton, B. M., & Gowman, L. M. (2009). Implications of changing climate for global wildland fire. *International Journal of Wildland Fire*, *18*(5), 483–507. https://doi.org/10.1071/WF08187

Foster, N. W., Morrison, I. K., & Nicolson, J. A., J. A. (1986). Acid deposition and ion leaching from a podzolic soil under hardwood forest, 11.

Foster, N. W., Mitchell, M. J., Morrison, I. K., & Shepard, J. P. (1992). Cycling of acid and base cations in deciduous stands of Huntington Forest, New York, and Turkey Lakes, Ontario. *Canadian Journal of Forest Research*, *22*(2), 167–174.

Foster, N. W., Beall, F. D., & Kreutzweiser, D. P. (2005). The role of forests in regulating water: The Turkey Lakes Watershed case study. *The Forestry Chronicle*, *81*(1), 142–148.

Froelich, P. N. (1988). Kinetic control of dissolved phosphate in natural rivers and estuaries: a primer on the phosphate buffer mechanism 1. *Limnology and Oceanography*, *33*(4part2), 649–668.

Fu, B. P. (1981). On the calculation of the evaporation from land surface. *Sci. Atmos. Sin*, *5*(1), 23–31.

Gassman, P. W., Reyes, M. R., Green, C. H., & Arnold, J. G. (2007). The Soil and Water Assessment Tool: Historical Development, Applications, and Future Research Directions. *Transactions of the ASABE*, *50*(4), 1211–1250. https://doi.org/10.13031/2013.23637

Gaudinski, J. B., Trumbore, S. E., & Zheng, S. (2000). Soil carbon cycling in a temperate forest: radiocarbon-based estimates of residence times, sequestration rates and partitioning of fluxes. *Biogeochemistry*, *51*, 33–69.

Gbondo-Tugbawa, S. S., Driscoll, C. T., Aber, J. D., & Likens, G. E. (2001). Evaluation of an integrated biogeochemical model (PnET-BGC) at a northern hardwood forest ecosystem. *Water Resources Research*, *37*(4), 1057–1070. https://doi.org/10.1029/2000WR900375

Gharari, S., Hrachowitz, M., Fenicia, F., Gao, H., & Savenije, H. H. G. (2014). Using expert knowledge to increase realism in environmental system models can dramatically reduce the need for calibration. *Hydrology and Earth System Sciences*, *18*(12), 4839–4859. https://doi.org/10.5194/hess-18-4839-2014

Godsey, S. E., Kirchner, J. W., & Clow, D. W. (2009). Concentration–discharge relationships reflect chemostatic characteristics of US catchments. *Hydrological Processes: An International Journal*, *23*(13), 1844–1864.

Godsey, S. E., Hartmann, J., & Kirchner, J. W. (2019). Catchment chemostasis revisited: Water quality responds differently to variations in weather and climate. *Hydrological Processes*, *33*(24), 3056–3069. https://doi.org/10.1002/hyp.13554

Goeking, S. A., & Tarboton, D. G. (2020). Forests and Water Yield: A Synthesis of Disturbance Effects on Streamflow and Snowpack in Western Coniferous Forests. *Journal of Forestry*, *118*(2), 172–192. https://doi.org/10.1093/jofore/fvz069

Goeking, S. A., & Tarboton, D. G. (2022). Variable Streamflow Response to Forest Disturbance in the Western US: A Large-Sample Hydrology Approach. *Water Resources Research*, *58*(6), e2021WR031575. https://doi.org/10.1029/2021WR031575

Grace III, J. M. (2005). Forest operations and water quality in the south. *Transactions of the ASAE*, *48*(2), 871–880. https://doi.org/10.13031/2013.18295

Greenwell, B. M., & Schubert Kabban, C. M. (2014). investr: An R Package for Inverse Estimation. *The R Journal*, *6*(1), 90–100.

Guillemette, F., Plamondon, A. P., Prévost, M., & Lévesque, D. (2005). Rainfall generated stormflow response to clearcutting a boreal forest: peak flow comparison with 50 world-wide basin studies. *Journal of Hydrology*, *302*(1), 137–153. https://doi.org/10.1016/j.jhydrol.2004.06.043

Gupta, H. V., Kling, H., Yilmaz, K. K., & Martinez, G. F. (2009). Decomposition of the mean squared error and NSE performance criteria: Implications for improving hydrological modelling. *Journal of Hydrology*, *377*(1), 80–91. https://doi.org/10.1016/j.jhydrol.2009.08.003

Guswa, A. J., Tetzlaff, D., Selker, J. S., Carlyle-Moses, D. E., Boyer, E. W., Bruen, M., et al. (2020). Advancing ecohydrology in the 21st century: A convergence of opportunities. *Ecohydrology*, (n/a), e2208. https://doi.org/10.1002/eco.2208

Hallema, D. W., Sun, G., Caldwell, P. V., Norman, S. P., Cohen, E. C., Liu, Y., et al. (2017). Assessment of wildland fire impacts on watershed annual water yield: Analytical framework and case studies in the United States. *Ecohydrology*, *10*(2), e1794. https://doi.org/10.1002/eco.1794

Hallema, D. W., Sun, G., Bladon, K. D., Norman, S. P., Caldwell, P. V., Liu, Y., & McNulty, S. G. (2017). Regional patterns of postwildfire streamflow response in the Western United States: The importance of scale-specific connectivity. *Hydrological Processes*, *31*(14), 2582–2598. https://doi.org/10.1002/hyp.11208

Hallema, D. W., Sun, G., Caldwell, P. V., Norman, S. P., Cohen, E. C., Liu, Y., et al. (2018). Burned forests impact water supplies. *Nature Communications*, *9*(1). https://doi.org/10.1038/s41467-018-03735-6

Hallema, D. W., Robinne, F.-N., & Bladon, K. D. (2018). Reframing the Challenge of Global Wildfire Threats to Water Supplies. *Earth's Future*, *0*(0). https://doi.org/10.1029/2018EF000867

Hampton, T. B. (2020). budyko: Computes Budyko statistics, fits, and makes plots. (Version 1.0.0). Retrieved from https://github.com/tylerbhampton/budykoR

Hampton, T. B. (2022a). Accompanying Data to Hampton & Basu (2022) "Quantifying post-forest-

fire hydrologic response using the Budyko framework. *HydroShare*. Retrieved from http://www.hydroshare.org/resource/43280a7de6ef48b4b800ab5c12ae58cb

Hampton, T. B. (2022b). Accompanying Data to Hampton, Lin, and Basu (2022) "Wildfire effects on water quality at continental and global scales: A meta-analysis." *HydroShare*. Retrieved from https://www.hydroshare.org/resource/537dc5206d584625b0fd28ea6b6872de/

Hampton, T. B. (2022c). USGSreadR: Functions for pulling USGS NWIS Data (Version 0.1.0). Retrieved from https://github.com/tylerbhampton/USGSreadR

Hampton, T. B., & Basu, N. B. (2022). A novel Budyko-based approach to quantify post-forest-fire streamflow response and recovery timescales. *Journal of Hydrology*, 127685. https://doi.org/10.1016/j.jhydrol.2022.127685

Hampton, T. B., Lin, S., & Basu, N. B. (2022). Forest fire effects on stream water quality at continental scales: a meta-analysis. *Environmental Research Letters*, *17*(6), 064003. https://doi.org/10.1088/1748-9326/ac6a6c

Hanan, E. J., Tague, C. N., & Schimel, J. P. (2017). Nitrogen cycling and export in California chaparral: The role of climate in shaping ecosystem responses to fire. *Ecological Monographs*, *87*(1), 76–90. https://doi.org/10.1002/ecm.1234

Hannah, D. M., Sadler, J. P., & Wood, P. J. (2007). Hydroecology and ecohydrology: a potential route forward? *Hydrological Processes: An International Journal*, *21*(24), 3385–3390.

Hargreaves, G. H., & Samani, Z. A. (1985). Reference crop evapotranspiration from temperature. *Applied Engineering in Agriculture*, *1*(2), 96–99.

Harman, C. J., Troch, P. A., & Sivapalan, M. (2011). Functional model of water balance variability at the catchment scale: 2. Elasticity of fast and slow runoff components to precipitation change in the continental United States. *Water Resources Research*, *47*(2). https://doi.org/10.1029/2010WR009568

Harvey, B. J., Andrus, R. A., & Anderson, S. C. (2019). Incorporating biophysical gradients and uncertainty into burn severity maps in a temperate fire-prone forested region. *Ecosphere*, *10*(2). https://doi.org/10.1002/ecs2.2600

Hauer, F. R., & Spencer, C. N. (1998). Phosphorus and nitrogen dynamics in streams associated with wildfire: A study of immediate and longterm effects. *International Journal of Wildland Fire*, *8*(4), 183–198. https://doi.org/10.1071/WF9980183

Hazlett, P. W., Semkin, R. G., & Beall, F. D. (2001). Hydrologic Pathways during Snowmelt in First-order Stream Basins at the Turkey Lakes Watershed. *Ecosystems*, *4*(6), 527–535. https://doi.org/10.1007/s10021-001-0026-z

Heath, J. T., Chafer, C. J., van Ogtrop, F. F., & Bishop, T. F. A. (2014). Post-wildfire recovery of water yield in the Sydney Basin water supply catchments: An assessment of the 2001/2002 wildfires. *Journal of Hydrology*, *519*(PB), 1428–1440. https://doi.org/10.1016/j.jhydrol.2014.09.033

Hedges, L. V., Gurevitch, J., & Curtis, P. S. (1999). The meta-analysis of response ratios in experimental ecology. *Ecology*, *80*(4), 1150–1156. https://doi.org/10.1890/0012-9658(1999)080[1150:TMAORR]2.0.CO;2

Helvey, J. D. (1980). Effects of a north central Washington wildfire on runoff and sediment production. *JAWRA Journal of the American Water Resources Association*, *16*(4), 627–634. https://doi.org/10.1111/j.1752-1688.1980.tb02441.x

Hewlett, J. D., & Hibbert, A. R. (1961). Increases in water yield after several types of forest cutting. *Hydrological Sciences Journal*, *6*(3), 5–17.

Hewlett, J. D., & Hibbert, A. R. (1967). Factors affecting the response of small watersheds to precipitation in humid areas. *Forest Hydrology*, *1*, 275–290.

Hibbert, A. R. (1965). *Forest treatment effects on water yield*. (W. Sopper & H. Lull, Eds.) (Vol. 813). Oxford, UK: Pergamon.

Hijmans, R. J., Etten, J. van, Cheng, J., Mattiuzzi, M., Sumner, M., Greenberg, J. A., et al. (2018, October 16). raster: Geographic Data Analysis and Modeling (Version 2.7-15). Retrieved from https://CRAN.R-project.org/package=raster

Hinton, M. J., Schiff, S. L., & English, M. C. (1998). Sources and flowpaths of dissolved organic carbon during storms in two forested watersheds of the Precambrian Shield. *Biogeochemistry*, *41*(2), 175–197.

Hirsch, R. M., & De Cicco, L. A. (2015). *User guide to Exploration and Graphics for RivEr Trends (EGRET) and dataRetrieval: R packages for hydrologic data* (USGS Numbered Series No. 4-A10) (p. 104). Reston, VA: U.S. Geological Survey. Retrieved from http://pubs.er.usgs.gov/publication/tm4A10

Hirsch, R. M., & De Cicco, L. A. (2018, August 2). Guide to EGRET 3.0 enhancements. Retrieved from http://usgs-r.github.io/EGRET/articles/Enhancements.html

Hirsch, R. M., Moyer, D. L., & Archfield, S. A. (2010). Weighted Regressions on Time, Discharge, and Season (WRTDS), with an Application to Chesapeake Bay River Inputs. *JAWRA Journal of the American Water Resources Association*, *46*(5), 857–880. https://doi.org/10.1111/j.1752-1688.2010.00482.x

Hohner, A. K., Cawley, K., Oropeza, J., Summers, R. S., & Rosario-Ortiz, F. L. (2016). Drinking water treatment response following a Colorado wildfire. *Water Research*, *105*, 187–198. https://doi.org/10.1016/j.watres.2016.08.034

Hohner, A. K., Rhoades, C. C., Wilkerson, P., & Rosario-Ortiz, F. L. (2019). Wildfires Alter Forest Watersheds and Threaten Drinking Water Quality. *Accounts of Chemical Research*, *52*(5), 1234–1244. https://doi.org/10.1021/acs.accounts.8b00670

Hoover, M. D., & Hursh, C. R. (1943). Influence of topography and soil-depth on runoff from forest land. *Eos, Transactions American Geophysical Union*, *24*(2), 693–698.

Hothorn, T., Hornik, K., & Zeileis, A. (2006). Unbiased Recursive Partitioning: A Conditional Inference Framework. *Journal of Computational and Graphical Statistics*, *15*(3), 651–674.

Hrachowitz, M., Savenije, H. H. G., Blöschl, G., McDonnell, J. J., Sivapalan, M., Pomeroy, J. W., et al. (2013). A decade of Predictions in Ungauged Basins (PUB)—a review. *Hydrological Sciences Journal*, *58*(6), 1198–1255.

Hume, A. M., Chen, H. Y. H., & Taylor, A. R. (2018). Intensive forest harvesting increases susceptibility of northern forest soils to carbon, nitrogen and phosphorus loss. *Journal of*

Applied Ecology, *55*(1), 246–255. https://doi.org/10.1111/1365-2664.12942

Ice, G. G. (2004). History of Innovative Best Management Practice Development and its Role in Addressing Water Quality Limited Waterbodies. *Journal of Environmental Engineering*, *130*(6), 684–689. https://doi.org/10.1061/(ASCE)0733-9372(2004)130:6(684)

Ice, G. G., Neary, D. G., & Adams, P. W. (2004). Effects of Wildfire on Soils and Watershed Processes. *Journal of Forestry*, *102*(6), 16–20. https://doi.org/10.1093/jof/102.6.16

Inamdar, S. P., Christopher, S. F., & Mitchell, M. J. (2004). Export mechanisms for dissolved organic carbon and nitrate during summer storm events in a glaciated forested catchment in New York, USA. *Hydrological Processes*, *18*(14), 2651–2661. https://doi.org/10.1002/hyp.5572

Inamdar, S. P., Rupp, J., & Mitchell, M. (2008). Differences in Dissolved Organic Carbon and Nitrogen Responses to Storm-Event and Ground-Water Conditions in a Forested, Glaciated Watershed in Western New York. *JAWRA Journal of the American Water Resources Association*, *44*(6), 1458–1473. https://doi.org/10.1111/j.1752-1688.2008.00251.x

Jain, P., Castellanos-Acuna, D., Coogan, S., Abatzoglou, J., & Flannigan, M. (2021). Increased trends in global extreme fire weather driven predominantly by atmospheric humidity and temperature.

Jaramillo, F., Cory, N., Arheimer, B., Laudon, H., Van der Velde, Y., Hasper, T. B., et al. (2018). Dominant effect of increasing forest biomass on evapotranspiration: interpretations of movement in Budyko space. *Hydrology and Earth System Sciences*, *22*(1), 567–580. https://doi.org/10.5194/hess-22-567-2018

Jarvie, H. P., Jürgens, M. D., Williams, R. J., Neal, C., Davies, J. J. L., Barrett, C., & White, J. (2005). Role of river bed sediments as sources and sinks of phosphorus across two major eutrophic UK river basins: the Hampshire Avon and Herefordshire Wye. *Journal of Hydrology*, *304*(1), 51–74. https://doi.org/10.1016/j.jhydrol.2004.10.002

Jeffries, D. S., & Foster, N. W. (2001). The Turkey Lakes Watershed study: milestones and prospects. *Ecosystems*, *4*(6), 501–502.

Jeffries, D. S., Kelso, J. R. M., & Morrison, I. K. (1988). Physical, Chemical, and Biological Characteristics of the Turkey Lakes Watershed, Central Ontario, Canada. *Canadian Journal of Fisheries and Aquatic Sciences*, *45*(S1), s3–s13. https://doi.org/10.1139/f88-262

Jencso, K. G., McGlynn, B. L., Gooseff, M. N., Wondzell, S. M., Bencala, K. E., & Marshall, L. A. (2009). Hydrologic connectivity between landscapes and streams: Transferring reach-and plot-scale understanding to the catchment scale. *Water Resources Research*, *45*(4). Retrieved from http://onlinelibrary.wiley.com/doi/10.1029/2008WR007225/full

Johnsen, K., Samuelson, L., Teskey, R., McNulty, S. G., & Fox, T. (2001). Process models as tools in forestry research and management. *Forest Science*, *47*(1), 2–8.

Johnson, D. W., & Turner, J. (2014). Nitrogen budgets of forest ecosystems: A review. *Forest Ecology and Management*, *318*, 370–379. https://doi.org/10.1016/j.foreco.2013.08.028

Johnson, D. W., West, D. C., Todd, D. E., & Mann, L. K. (1982). Effects of Sawlog vs. Whole-Tree Harvesting on the Nitrogen, Phosphorus, Potassium, and Calcium Budgets of an Upland Mixed Oak Forest 1. *Soil Science Society of America Journal*, *46*(6), 1304–1309. https://doi.org/10.2136/sssaj1982.03615995004600060036x

Jones, J. A., & Grant, G. E. (1996). Peak flow responses to clear-cutting and roads in small and large basins, western Cascades, Oregon. *Water Resources Research*, *32*(4), 959–974.

Jones, J. A., Creed, I. F., Hatcher, K. L., Warren, R. J., Adams, M. B., Benson, M. H., et al. (2012). Ecosystem Processes and Human Influences Regulate Streamflow Response to Climate Change at Long-Term Ecological Research Sites. *BioScience*, *62*(4), 390–404. https://doi.org/10.1525/bio.2012.62.4.10

Jones, J. A., Wei, X., van Noordwijk, M., Creed, I. F., Gush, M., Ellison, D., et al. (2018). Forest Landscape Hydrology in a 'New Normal' Era of Climate and Land Use Change. In *Forest and Water on a Changing Planet: Vulnerability, Adaptation and Governance Opportunities. A Global Assessment Report.* (Vol. Volume 38, pp. 82–99). Vienna, Austria: International Union of Forest Research Organizations (IUFRO).

Jung, H. Y., Hogue, T. S., Rademacher, L. K., & Meixner, T. (2009). Impact of wildfire on source water contributions in Devil Creek, CA: evidence from end-member mixing analysis. *Hydrological Processes*, *23*(2), 183–200. https://doi.org/10.1002/hyp.7132

Kassambara, A., & Mundt, F. (2020). factoextra: Extract and Visualize the Results of Multivariate Data Analyses (Version 1.0.7). Retrieved from <https://CRAN.R-project.org/package=factoextra>

Keeley, J. E., & Fotheringham, C. J. (2001). Historic fire regime in southern California shrublands. *Conservation Biology*, *15*(6), 1536–1548. https://doi.org/10.1046/j.1523-1739.2001.00097.x

Kelly, R. H., Parton, W. J., Crocker, G. J., Graced, P. R., Klír, J., Körschens, M., et al. (1997). Simulating trends in soil organic carbon in long-term experiments using the century model. *Geoderma*, *81*(1), 75–90. https://doi.org/10.1016/S0016-7061(97)00082-7

Kennedy, M. C., McKenzie, D., Tague, C., & Dugger, A. L. (2017). Balancing uncertainty and complexity to incorporate fire spread in an eco-hydrological model. *International Journal of Wildland Fire*, *26*(8), 706. https://doi.org/10.1071/WF16169

Khorshidi, M. S., Dennison, P. E., Nikoo, M. R., AghaKouchak, A., Luce, C. H., & Sadegh, M. (2020). Increasing concurrence of wildfire drivers tripled megafire critical danger days in Southern California between1982 and 2018. *Environmental Research Letters*, *15*(10), 104002.

Kichigina, N. V., & Bilichenko, I. N. (2019). Specificity of the river flow formation of small mountain streams of the Baikal Natural Territory resulting from wildfires. *IOP Conference Series: Earth and Environmental Science*, *381*(1), 012042. https://doi.org/10.1088/1755-1315/381/1/012042

Kinoshita, A. M., & Hogue, T. S. (2011). Spatial and temporal controls on post-fire hydrologic recovery in Southern California watersheds. *Catena*, *87*(2), 240–252. https://doi.org/10.1016/j.catena.2011.06.005

Kinoshita, A. M., & Hogue, T. S. (2015). Increased dry season water yield in burned watersheds in Southern California. *Environmental Research Letters*, *10*(1), 014003. https://doi.org/10.1088/1748-9326/10/1/014003

Kinoshita, A. M., Chin, A., Simon, G. L., Briles, C., Hogue, T. S., O'Dowd, A. P., et al. (2016). Wildfire, water, and society: Toward integrative research in the "Anthropocene."

Anthropocene, *16*, 16–27. https://doi.org/10.1016/j.ancene.2016.09.001

Kirchner, J. W., Berghuijs, W. R., Allen, S. T., Hrachowitz, M., Hut, R., & Rizzo, D. M. (2020). Streamflow response to forest management. *Nature*, *578*(7794), E12–E15. https://doi.org/10.1038/s41586-020-1940-6

Knowles, J. D., Corne, D. W., & Fleischer, M. (2003). Bounded archiving using the lebesgue measure. In *The 2003 Congress on Evolutionary Computation, 2003. CEC '03.* (Vol. 4, pp. 2490-2497 Vol.4). https://doi.org/10.1109/CEC.2003.1299401

Kolden, C. A., Smith, A. M. S., & Abatzoglou, J. T. (2015). Limitations and utilisation of Monitoring Trends in Burn Severity products for assessing wildfire severity in the USA. *International Journal of Wildland Fire*, *24*(7), 1023–1028. https://doi.org/10.1071/WF15082

van Kraalingen, D. W. G., & Stol, W. (1997). *Evapotranspiration modules for crop growth simulation: implementation of the algorithms from Penman, Makkink and Priestley-Taylor*. Wageningen; Netherlands: DLO Research Institute for Agrobiology and Soil Fertility ; The C.T. de Wit Graduate School for Production Ecology. Retrieved from https://edepot.wur.nl/4413

Kreutzweiser, D. P., & Capell, S. S. (2001). Fine sediment deposition in streams after selective forest harvesting without riparian buffers. *Canadian Journal of Forest Research*, *31*(12), 2134–2142. https://doi.org/10.1139/x01-155

Kreutzweiser, D. P., Capell, S. S., & Good, K. P. (2005). Macroinvertebrate community responses to selection logging in riparian and upland areas of headwater catchments in a northern hardwood forest. *Journal of the North American Benthological Society*, *24*(1), 208–222.

Kreutzweiser, D. P., Hazlett, P. W., & Gunn, J. M. (2008). Logging impacts on the biogeochemistry of boreal forest soils and nutrient export to aquatic systems: A review. *Environmental Reviews*, *16*, 157–179.

Krysanova, V., & Arnold, J. G. (2008). Advances in ecohydrological modelling with SWAT—a review. *Hydrological Sciences Journal*, *53*(5), 939–947.

Kusaka, S., Nakane, K., & Mitsudera, M. (1983). Effect of fire on water and major nutrient budgets in forest ecosystems I. Water balance. *Japanese Journal of Ecology*, *33*(3), 323–332. https://doi.org/10.18960/seitai.33.3_323

Laio, F., Porporato, A., Ridolfi, L., & Rodriguez-Iturbe, I. (2001). Plants in water-controlled ecosystems: active role in hydrologic processes and response to water stress: II. Probabilistic soil moisture dynamics. *Advances in Water Resources*, *24*(7), 707–723. https://doi.org/10.1016/S0309-1708(01)00005-7

Lajtha, K., & Jones, J. A. (2018). Forest harvest legacies control dissolved organic carbon export in small watersheds, western Oregon. *Biogeochemistry*, *140*(3), 299–315. https://doi.org/10.1007/s10533-018-0493-3

Landsberg, J. J., & Waring, R. H. (1997). A generalised model of forest productivity using simplified concepts of radiation-use efficiency, carbon balance and partitioning. *Forest Ecology and Management*, *95*(3), 209–228. https://doi.org/10.1016/S0378-1127(97)00026-1

Lang, A. J., Aust, W. M., Bolding, M. C., McGuire, K. J., & Schilling, E. B. (2018). Best Management Practices Influence Sediment Delivery from Road Stream Crossings to

Mountain and Piedmont Streams. *Forest Science*, *64*(6), 682–695. https://doi.org/10.1093/forsci/fxy019

Leach, J. A., Buttle, J. M., Webster, K. L., Hazlett, P. W., & Jeffries, D. S. (2020). Travel times for snowmelt-dominated headwater catchments: Influences of wetlands and forest harvesting, and linkages to stream water quality. *Hydrological Processes*. https://doi.org/10.1002/hyp.13746

Leach, J. A., Hudson, D. T., & Moore, R. D. (2022). Assessing stream temperature response and recovery for different harvesting systems in northern hardwood forests using 40 years of spot measurements. *Hydrological Processes*, *36*(11), e14753. https://doi.org/10.1002/hyp.14753

Lee, W., Westerhoff, P., & Croué, J.-P. (2007). Dissolved organic nitrogen as a precursor for chloroform, dichloroacetonitrile, N-nitrosodimethylamine, and trichloronitromethane. *Environmental Science & Technology*, *41*(15), 5485–5490.

Leopardi, M., & Scorzini, A. R. (2015). Effects of wildfires on peak discharges in watersheds. *iForest-Biogeosciences and Forestry*, *8*(3), 302.

Levia, D. F., Carlyle-Moses, D., & Tanaka, T. (Eds.). (2011). *Forest Hydrology and Biogeochemistry: Synthesis of Past Research and Future Directions* (Vol. 216). Dordrecht, Netherlands: Springer. https://doi.org/10.1007/978-94-007-1363-5

Li, C., Wang, L., Wanrui, W., Qi, J., Linshan, Y., Zhang, Y., et al. (2018). An analytical approach to separate climate and human contributions to basin streamflow variability. *Journal of Hydrology*, *559*, 30–42. https://doi.org/10.1016/j.jhydrol.2018.02.019

Li, F., Lawrence, D. M., & Bond-Lamberty, B. (2018). Human impacts on 20th century fire dynamics and implications for global carbon and water trajectories. *Global and Planetary Change*, *162*, 18–27. https://doi.org/10.1016/j.gloplacha.2018.01.002

Li, X., Nour, M. H., Smith, D. W., Prepas, E. E., Putz, G., & Watson, B. M. (2008). Incorporating water quantity and quality modelling into forest management. *Forestry Chronicle*, *84*(3), 338–348. https://doi.org/10.5558/tfc84338-3

Likens, G. E., & Bormann, F. H. (1974). Linkages between Terrestrial and Aquatic Ecosystems. *BioScience*, *24*(8), 447–456. https://doi.org/10.2307/1296852

Likens, G. E., Bormann, F. H., Johnson, N. M., Fisher, D. W., & Pierce, R. S. (1970). Effects of Forest Cutting and Herbicide Treatment on Nutrient Budgets in the Hubbard Brook Watershed-Ecosystem. *Ecological Monographs*, *40*(1), 23–47. https://doi.org/10.2307/1942440

Likens, G. E., Bormann, F. H., Pierce, R. S., Eaton, J. S., & Johnson, N. M. (1977). *Biogeochemistry of a forested ecosystem*. NY: Springer-Verlag.

Likens, G. E., Buso, D. C., Bernhardt, E. S., & Rosi, E. (2021). A century of change: Reconstructing the biogeochemical history of Hubbard Brook. *Hydrological Processes*, *35*(6), e14256. https://doi.org/10.1002/hyp.14256

Lins, H. F., & Slack, J. R. (1999). Streamflow trends in the United States. *Geophysical Research Letters*, *26*(2), 227–230.

Loáiciga, H. A., Pedreros, D., & Roberts, D. (2001). Wildfire-streamflow interactions in a chaparral

watershed. *Advances in Environmental Research*, *5*(3), 295–305. https://doi.org/10.1016/S1093-0191(00)00064-2

Lohse, K. A., Brooks, P. D., McIntosh, J. C., Meixner, T., & Huxman, T. E. (2009). Interactions Between Biogeochemistry and Hydrologic Systems. *Annual Review of Environment and Resources*, *34*(1), 65–96. https://doi.org/10.1146/annurev.environ.33.031207.111141

Loucks, D. P., & Van Beek, E. (2017). *Water resource systems planning and management: An introduction to methods, models, and applications*. Springer. Retrieved from https://link.springer.com/book/10.1007%2F978-3-319-44234-1

Lowe, W. H., & Likens, G. E. (2005). Moving headwater streams to the head of the class. *BioScience*, *55*(3), 196–197.

Lu, J., Sun, G., McNulty, S. G., & Amatya, D. M. (2005). A comparison of six potential evapotranspiration methods for regional use in the southeastern United States. *Journal of the American Water Resources Association*, *41*(3), 621–633. https://doi.org/10.1111/j.1752-1688.2005.tb03759.x

Lynch, J. A., & Corbett, E. S. (1990). Evaluation of Best Management Practices for Controlling Nonpoint Pollution from Silvicultural Operations. *JAWRA Journal of the American Water Resources Association*, *26*(1), 41–52. https://doi.org/10.1111/j.1752-1688.1990.tb01349.x

Maina, F. Z., & Siirila-Woodburn, E. R. (2020). Watersheds dynamics following wildfires: Nonlinear feedbacks and implications on hydrologic responses. *Hydrological Processes*, *34*(1), 33–50. https://doi.org/10.1002/hyp.13568

Mäkelä, A., Landsberg, J., Ek, A. R., Burk, T. E., Ter-Mikaelian, M., \AAgren, G. I., et al. (2000). Process-based models for forest ecosystem management: current state of the art and challenges for practical implementation. *Tree Physiology*, *20*(5–6), 289–298.

Manzoni, S., & Porporato, A. (2007). A theoretical analysis of nonlinearities and feedbacks in soil carbon and nitrogen cycles. *Soil Biology and Biochemistry*, *39*(7), 1542–1556. https://doi.org/10.1016/j.soilbio.2007.01.006

Manzoni, S., Taylor, P., Richter, A., Porporato, A., & Ågren, G. I. (2012). Environmental and stoichiometric controls on microbial carbon-use efficiency in soils. *New Phytologist*, *196*(1), 79–91. https://doi.org/10.1111/j.1469-8137.2012.04225.x

Martin, C. W., Hornbeck, J. W., Likens, G. E., & Buso, D. C. (2000). Impacts of intensive harvesting on hydrology and nutrient dynamics of northern hardwood forests. *Canadian Journal of Fisheries and Aquatic Sciences*, *57*(S2), 19–29. https://doi.org/10.1139/f00-106

Martin, D. A. (2016). At the nexus of fire, water and society. *Philosophical Transactions of the Royal Society B: Biological Sciences*, *371*(1696), 20150172. https://doi.org/10.1098/rstb.2015.0172

Matott, L. S. (2017). OSTRICH: An optimization software tool: Documentation and users guide (Version Version 17.12.19). Buffalo, NY, USA: University of Buffalo Center for Computational Research. Retrieved from https://usbr.github.io/ostrich/index.html

McBroom, M. W., Beasley, R. S., Chang, M., & Ice, G. G. (2008). Water Quality Effects of Clearcut Harvesting and Forest Fertilization with Best Management Practices. *Journal of Environmental Quality*, *37*(1), 114–124. https://doi.org/10.2134/jeq2006.0552

McCullough, I. M., Cheruvelil, K. S., Lapierre, J.-F., Lottig, N. R., Moritz, M. A., Stachelek, J., & Soranno, P. A. (2019). Do lakes feel the burn? Ecological consequences of increasing exposure of lakes to fire in the continental United States. *Global Change Biology*, *0*(0). https://doi.org/10.1111/gcb.14732

McDowell, N. G., Allen, C. D., Anderson-Teixeira, K., Aukema, B. H., Bond-Lamberty, B., Chini, L., et al. (2020). Pervasive shifts in forest dynamics in a changing world. *Science*, *368*(6494), eaaz9463. https://doi.org/10.1126/science.aaz9463

McDowell, W. H., & Wood, T. (1984). Podzolization: soil processes control dissolved organic carbon concentrations in stream water. *Soil Science*, *137*(1), 23–32.

McGuffie, K., Henderson-Sellers, A., Holbrook, N., Kothavala, Z., Balachova, O., & Hoekstra, J. (1999). Assessing simulations of daily temperature and precipitation variability with global climate models for present and enhanced greenhouse climates. *International Journal of Climatology*, *19*(1), 1–26. https://doi.org/10.1002/(SICI)1097-0088(199901)19:1<1::AID-JOC348>3.0.CO;2-T

McGuire, K. J., & Likens, G. E. (2011). Historical Roots of Forest Hydrology and Biogeochemistry. In D. F. Levia, D. Carlyle-Moses, & T. Tanaka (Eds.), *Forest Hydrology and Biogeochemistry: Synthesis of Past Research and Future Directions* (pp. 3–26). Dordrecht, Netherlands: Springer. https://doi.org/10.1007/978-94-007-1363-5_1

McHale, M. R., Murdoch, P. S., Burns, D. A., & Baldigo, B. P. (2008). *Effects of forest harvesting on ecosystem health in the headwaters of the New York City water supply, Catskill mountains, New York* (Scientific Investigations Report No. 2008–5057) (p. 22). U.S. Geological Survey. Retrieved from https://pubs.usgs.gov/sir/2008/5057/SIR2008-5057.pdf

McKenzie, D., & Perera, A. H. (2015). Modeling Wildfire Regimes in Forest Landscapes: Abstracting a Complex Reality. In *Simulation Modeling of Forest Landscape Disturbances* (pp. 73–92). Springer, Cham. https://doi.org/10.1007/978-3-319-19809-5_4

McLauchlan, K. K., Higuera, P. E., Miesel, J., Rogers, B. M., Schweitzer, J., Shuman, J. K., et al. (2020). Fire as a fundamental ecological process: Research advances and frontiers. *Journal of Ecology*, *108*(5), 2047–2069. https://doi.org/10.1111/1365-2745.13403

McManamay, R. A., Bevelhimer, M. S., & Kao, S.-C. (2014). Updating the US hydrologic classification: an approach to clustering and stratifying ecohydrologic data. *Ecohydrology*, *7*(3), 903–926. https://doi.org/10.1002/eco.1410

Medema, G. J., Shaw, S., Waite, M., Snozzi, M., Morreau, A., & Grabow, W. (2003). *Catchment characterisation and source water quality* (Assessing Microbial Safety of Drinking Water) (p. 111). London, UK: WHO/OEDC.

van Meerveld, I. H. J., & McDonnell, J. J. (2006). Threshold relations in subsurface stormflow: 1. A 147-storm analysis of the Panola hillslope. *Water Resources Research*, *42*(2). https://doi.org/10.1029/2004WR003778

van Meerveld, I. H. J., & Weiler, M. (2008). Hillslope dynamics modeled with increasing complexity. *Journal of Hydrology*, *361*(1), 24–40. https://doi.org/10.1016/j.jhydrol.2008.07.019

Meixner, T., & Wohlgemuth, P. M. (2003). Climate variability, fire, vegetation recovery, and watershed hydrology. In *Proceedings of the First Interagency Conference on Research in the*

Watersheds (pp. 651–656). Benson, Arizona, USA.

Melo, F. P. L., Parry, L., Brancalion, P. H. S., Pinto, S. R. R., Freitas, J., Manhães, A. P., et al. (2021). Adding forests to the water–energy–food nexus. *Nature Sustainability*, *4*(2), 85–92. https://doi.org/10.1038/s41893-020-00608-z

Meybeck, M., & Moatar, F. (2012). Daily variability of river concentrations and fluxes: indicators based on the segmentation of the rating curve. *Hydrological Processes*, *26*(8), 1188–1207. https://doi.org/10.1002/hyp.8211

Millard, P. (1996). Ecophysiology of the internal cycling of nitrogen for tree growth. *Zeitschrift Für Pflanzenernährung Und Bodenkunde*, *159*(1), 1–10. https://doi.org/10.1002/jpln.1996.3581590102

Millard, P., & Grelet, G. -a. (2010). Nitrogen storage and remobilization by trees: ecophysiological relevance in a changing world. *Tree Physiology*, *30*(9), 1083–1095. https://doi.org/10.1093/treephys/tpq042

Milly, P. C. D. (1994). Climate, soil water storage, and the average annual water balance. *Water Resources Research*, *30*(7), 2143–2156. https://doi.org/10.1029/94WR00586

Milly, P. C. D., & Dunne, K. A. (2002). Macroscale water fluxes 2. Water and energy supply control of their interannual variability. *Water Resources Research*, *38*(10), 24-1-24–9. https://doi.org/10.1029/2001WR000760

Mishra, A., Alnahit, A., & Campbell, B. (2021). Impact of land uses, drought, flood, wildfire, and cascading events on water quality and microbial communities: A review and analysis. *Journal of Hydrology*, *596*, 125707. https://doi.org/10.1016/j.jhydrol.2020.125707

Mistick, E., & Johnson, M. S. (2020). High-frequency analysis of dissolved organic carbon storm responses in headwater streams of contrasting forest harvest history. *Journal of Hydrology*, *590*, 125371. https://doi.org/10.1016/j.jhydrol.2020.125371

Mitchell, M. J., Foster, N. W., Shepard, J. P., & Morrison, I. K. (1992). Nutrient cycling in Huntington Forest and Turkey Lakes deciduous stands: nitrogen and sulfur. *Canadian Journal of Forest Research*, *22*(4), 457–464.

Mo, S., Li, Z., Gou, K., Qin, L., & Shen, B. (2018). Quantifying the Effects of Climate Variability and Direct Human Activities on the Change in Mean Annual Runoff for the Bahe River (Northwest China). *Journal of Coastal Research*, 81–89. https://doi.org/10.2112/JCOASTRES-D-16-00159.1

Moatar, F., Abbott, B. W., Minaudo, C., Curie, F., & Pinay, G. (2017). Elemental properties, hydrology, and biology interact to shape concentration-discharge curves for carbon, nutrients, sediment, and major ions. *Water Resources Research*, *53*(2), 1270–1287.

Monserud, R. A. (2003). Evaluating forest models in a sustainable forest management context. *Forest Biometry, Modelling and Information Sciences*, *1*(1), 35–47.

Morales, D., Rostagno, C. M., & La Manna, L. (2013). Runoff and erosion from volcanic soils affected by fire: the case of Austrocedrus chilensis forests in Patagonia, Argentina. *Plant and Soil*, *370*(1), 367–380. https://doi.org/10.1007/s11104-013-1640-1

Moritz, M. A., Parisien, M.-A., Batllori, E., Krawchuk, M. A., Dorn, J. V., Ganz, D. J., & Hayhoe, K.

(2012). Climate change and disruptions to global fire activity. *Ecosphere*, *3*(6), art49. https://doi.org/10.1890/ES11-00345.1

Morrison, I. K. (1990). Organic matter and mineral distribution in an old-growth Acer saccharum forest near the northern limit of its range. *Canadian Journal of Forest Research*, *20*(9), 1332–1342.

Morrison, I. K. (1991). Addition of organic matter and elements to the forest floor of an old-growth Acersaccharum forest in the annual litter fall. *Canadian Journal of Forest Research*, *21*(4). https://doi.org/10.1139/x91-062

Morrison, I. K., Foster, N. W., & Nicolson, J. A. (1992). Influence of acid deposition on element cycling in mature sugar maple forest, Algoma, Canada. *Water, Air, & Soil Pollution*, *61*(3–4), 243–252. https://doi.org/10.1007/BF00482608

Morrison, I. K., Foster, N. W., & Hazlett, P. W. (1993). Carbon reserves, carbon cycling, and harvesting effects in three mature forest types in Canada. *New Zealand Journal of Forestry Science*, 14.

Morton, D. M., & Miller, F. K. (2006). *Geologic Map of the San Bernardino and Santa Ana 30' x 60' quadrangles, California* (No. Open-File Report 2006-1217). Riverside, CA, USA: U.S. Geological Survey. Retrieved from http://pubs.usgs.gov/of/2006/1217/

Mupepele, A.-C., & Dormann, C. F. (2017). Influence of Forest Harvest on Nitrate Concentration in Temperate Streams—A Meta-Analysis. *Forests*, *8*(1), 5. https://doi.org/10.3390/f8010005

Murphy, P. N. C., Castonguay, M., Ogilvie, J., Nasr, M., Hazlett, P., Bhatti, J., & Arp, P. A. (2009). A geospatial and temporal framework for modeling gaseous N and other N losses from forest soils and basins, with application to the Turkey Lakes Watershed Project, in Ontario, Canada. *Forest Ecology and Management*, *258*(10), 2304–2317. https://doi.org/10.1016/j.foreco.2008.12.006

Murphy, S. F., McClesky, R. B., & Writer, J. H. (2012). Effects of flow regime on stream turbidity and suspended solids after wildfire, Colorado Front Range (Vol. IAHS Publ. 354, p. 8). Presented at the Wildfire and Water Quality: Processes, Impacts and Challenges, Banff, Alberta, Canada. Retrieved from https://pdfs.semanticscholar.org/2c6e/599b85f4f1ba8021aca1a2d7087bebd70ace.pdf

Murphy, S. F., Writer, J. H., McCleskey, R. B., & Martin, D. A. (2015). The role of precipitation type, intensity, and spatial distribution in source water quality after wildfire. *Environmental Research Letters*, *10*(8), 084007. https://doi.org/10.1088/1748-9326/10/8/084007

Murphy, S. F., McCleskey, R. B., Martin, D. A., Writer, J. H., & Ebel, B. A. (2018). Fire, Flood, and Drought: Extreme Climate Events Alter Flow Paths and Stream Chemistry. *Journal of Geophysical Research: Biogeosciences*, *123*(8), 2513–2526. https://doi.org/10.1029/2017JG004349

Murray, C. D., & Buttle, J. M. (2005). Infiltration and soil water mixing on forested and harvested slopes during spring snowmelt, Turkey Lakes Watershed, central Ontario. *Journal of Hydrology*, *306*(1–4), 1–20. https://doi.org/10.1016/j.jhydrol.2004.08.032

Musolff, A., Schmidt, C., Selle, B., & Fleckenstein, J. H. (2015). Catchment controls on solute export. *Advances in Water Resources*, *86*, 133–146.

https://doi.org/10.1016/j.advwatres.2015.09.026

Musolff, A., Schmidt, C., Rode, M., Lischeid, G., Weise, S. M., & Fleckenstein, J. H. (2016). Groundwater head controls nitrate export from an agricultural lowland catchment. *Advances in Water Resources*, *96*, 95–107. https://doi.org/10.1016/j.advwatres.2016.07.003

Musolff, A., Fleckenstein, J. H., Rao, P. S. C., & Jawitz, J. W. (2017). Emergent archetype patterns of coupled hydrologic and biogeochemical responses in catchments. *Geophysical Research Letters*, *44*(9), 4143–4151. https://doi.org/10.1002/2017GL072630

Musolff, A., Zhan, Q., Dupas, R., Minaudo, C., Fleckenstein, J. H., Rode, M., et al. (2021). Spatial and Temporal Variability in Concentration-Discharge Relationships at the Event Scale. *Water Resources Research*, *57*(10), e2020WR029442. https://doi.org/10.1029/2020WR029442

Muwamba, A., Rau, B., Trettin, C. C., Amatya, D. M., Tollner, E. W., & Panda, S. (2019). Regional Differences in Stream Water Nitrogen, Phosphorus, and Sediment Responses to Forest Harvesting in the Conterminous USA. *Journal of Environmental Quality*, *48*(3), 634–644. https://doi.org/10.2134/jeq2018.04.0145

NASA. (2003, October 25). Grand Prix Fire and Piru Fire near Los Angeles. Greenbelt, MD, USA: NASA Goddard Space Flight Center, EOS Project Science Office, Visible Earth Catalog. Retrieved from https://visibleearth.nasa.gov/view.php?id=69159

Nearing, M. A. (2001). Potential changes in rainfall erosivity in the U.S. with climate change during the 21st century. *Journal of Soil and Water Conservation*, *56*(3), 229–232.

Neary, D. G., & Koestner, K. A. (2012). Forest bioenergy feedstock harvesting effects on water supply: Forest bioenergy feedstock harvesting. *Wiley Interdisciplinary Reviews: Energy and Environment*, *1*(3), 270–284. https://doi.org/10.1002/wene.26

Neary, D. G., Ice, G. G., & Jackson, C. R. (2009). Linkages between forest soils and water quality and quantity. *Forest Ecology and Management*, *258*(10), 2269–2281. https://doi.org/10.1016/j.foreco.2009.05.027

Newbold, J. D., Elwood, J. W., O'Neill, R. V., & Winkle, W. V. (1981). Measuring nutrient spiralling in streams. *Canadian Journal of Fisheries and Aquatic Sciences*, *38*(7), 860–863.

Nicolson, J. A. (1988). Water and Chemical Budgets for Terrestrial Basins at the Turkey Lakes Watershed. *Canadian Journal of Fisheries and Aquatic Sciences*, *45*(S1), s88–s95. https://doi.org/10.1139/f88-271

Niemeyer, R. J., Bladon, K. D., & Woodsmith, R. D. (2020). Long-term hydrologic recovery after wildfire and post-fire forest management in the interior Pacific Northwest. *Hydrological Processes*, *34*(5), 1182–1197. https://doi.org/10.1002/hyp.13665

Noske, P. J., Lane, P. N. J., & Sheridan, G. J. (2010). Stream exports of coarse matter and phosphorus following wildfire in NE Victoria, Australia. *Hydrological Processes*, *24*(11), 1514–1529. https://doi.org/10.1002/hyp.7616

Nunes, J. P., Doerr, S. H., Sheridan, G., Neris, J., Santín, C., Emelko, M. B., et al. (2018). Assessing water contamination risk from vegetation fires: Challenges, opportunities and a framework for progress. *Hydrological Processes*, *32*(5), 687–694. https://doi.org/10.1002/hyp.11434

Olden, J. D., Kennard, M. J., & Pusey, B. J. (2012). A framework for hydrologic classification with a

review of methodologies and applications in ecohydrology. *Ecohydrology*, *5*(4), 503–518. https://doi.org/10.1002/eco.251

Oliveira-Filho, E. C., Brito, D. Q., Dias, Z. M. B., Guarieiro, M. S., Carvalho, E. L., Fascineli, M. L., et al. (2018). Effects of ashes from a Brazilian savanna wildfire on water, soil and biota: An ecotoxicological approach. *Science of The Total Environment*, *618*, 101–111. https://doi.org/10.1016/j.scitotenv.2017.11.051

Paci, L., Gelfand, A. E., Beamonte, M. A., Rodrigues, M., & Pérez-Cabello, F. (2017). Space-time modeling for post-fire vegetation recovery. *Stochastic Environmental Research and Risk Assessment*, *31*(1), 171–183. https://doi.org/10.1007/s00477-015-1182-6

Parolari, A. J., & Porporato, A. (2016). Forest soil carbon and nitrogen cycles under biomass harvest: stability, transient response, and feedback. *Ecological Modelling*, *329*, 64–76. https://doi.org/10.1016/j.ecolmodel.2016.03.003

Parton, W. J., Schimel, D. S., Cole, C. V., & Ojima, D. S. (1987). Analysis of Factors Controlling Soil Organic Matter Levels in Great Plains Grasslands. *Soil Science Society of America Journal*, *51*(5), 1173–1179. https://doi.org/10.2136/sssaj1987.03615995005100050015x

Parton, W. J., Stewart, J. W. B., & Cole, C. V. (1988). Dynamics of C, N, P and S in grassland soils: a model. *Biogeochemistry*, *5*(1), 109–131. https://doi.org/10.1007/BF02180320

Pastor, J., & Post, W. M. (1986). Influence of climate, soil moisture, and succession on forest carbon and nitrogen cycles. *Biogeochemistry*, *2*(1), 3–27.

Pebesma, E. (2018). Simple Features for R: Standardized Support for Spatial Vector Data. *The R Journal*, *10*(1), 439–446. https://journal.r-project.org/archive/2018/RJ-2018-009/index.html

Pollock, M. M., Beechie, T. J., Liermann, M., & Bigley, R. E. (2009). Stream temperature relationships to forest harvest in Western Washington. *Journal of the American Water Resources Association*, *45*(1), 141–156. https://doi.org/10.1111/j.1752-1688.2008.00266.x

Poon, P. K., & Kinoshita, A. M. (2018). Estimating Evapotranspiration in a Post-Fire Environment Using Remote Sensing and Machine Learning. *Remote Sensing*, *10*(11), 1728. https://doi.org/10.3390/rs10111728

Porporato, A., Laio, F., Ridolfi, L., & Rodriguez-Iturbe, I. (2001). Plants in water-controlled ecosystems: active role in hydrologic processes and response to water stress: III. Vegetation water stress. *Advances in Water Resources*, *24*(7), 725–744.

Porporato, A., D'Odorico, P., Laio, F., & Rodriguez-Iturbe, I. (2003). Hydrologic controls on soil carbon and nitrogen cycles. I. Modeling scheme. *Advances in Water Resources*, *26*(1), 45–58. https://doi.org/10.1016/S0309-1708(02)00094-5

Potter, N. J., & Zhang, L. (2009). Interannual variability of catchment water balance in Australia. *Journal of Hydrology*, *369*(1–2), 120–129. https://doi.org/10.1016/j.jhydrol.2009.02.005

Pregitzer, K. S., Zak, D. R., Talhelm, A. F., Burton, A. J., & Eikenberry, J. R. (2010). Nitrogen turnover in the leaf litter and fine roots of sugar maple. *Ecology*, *91*(12), 3456–3462. https://doi.org/10.1890/10-0633.1

PRISM. (2018). PRISM Climate Group, Oregon State U. Retrieved October 1, 2018, from http://www.prism.oregonstate.edu/

Qian, Y., Miao, S. L., Gu, B., & Li, Y. C. (2009). Estimation of Postfire Nutrient Loss in the Florida Everglades. *Journal of Environmental Quality*, *38*(5), 1812–1820. https://doi.org/10.2134/jeq2008.0391

R Core Team. (2023). R: A language and environment for statistical computing. Vienna, Austria: R Foundation for Statistical Computing. Retrieved from https://www.R-project.org/

Ramsfield, T. D., Bentz, B. J., Faccoli, M., Jactel, H., & Brockerhoff, E. G. (2016). Forest health in a changing world: effects of globalization and climate change on forest insect and pathogen impacts. *Forestry: An International Journal of Forest Research*, *89*(3), 245–252. https://doi.org/10.1093/forestry/cpw018

Ranalli, A. J. (2004). *A Summary of the Scientific Literature on the Effects of Fire on the Concentration of Nutrients in Surface Waters* (Open-File Report No. 2004–1296). U.S. Geological Survey.

Raymond, P. A., Saiers, J. E., & Sobczak, W. V. (2016). Hydrological and biogeochemical controls on watershed dissolved organic matter transport: pulse-shunt concept. *Ecology*, *97*(1), 5–16. https://doi.org/10.1890/14-1684.1

Reddy, K. R., Kadlec, R. H., Flaig, E., & Gale, P. M. (1999). Phosphorus retention in streams and wetlands: a review. *Critical Reviews in Environmental Science and Technology*, *29*(1), 83–146.

Retallack, G. J. (2021). Soil, Soil Processes, and Paleosols. In D. Alderton & S. A. Elias (Eds.), *Encyclopedia of Geology (Second Edition)* (pp. 690–707). Oxford: Academic Press. https://doi.org/10.1016/B978-0-12-409548-9.12537-0

Revchuk, A. D., & Suffet, I. H. (Mel). (2014). Effect of Wildfires on Physicochemical Changes of Watershed Dissolved Organic Matter. *Water Environment Research*, *86*(4), 372–381. https://doi.org/10.2175/106143013X13736496909671

Rhoades, C. C., Entwistle, D., & Butler, D. (2011). The influence of wildfire extent and severity on streamwater chemistry, sediment and temperature following the Hayman Fire, ColoradoA. *International Journal of Wildland Fire*, *20*(3), 430–442. https://doi.org/10.1071/WF09086

Rhoades, C. C., Nunes, J. P., Silins, U., & Doerr, S. H. (2019). The influence of wildfire on water quality and watershed processes: new insights and remaining challenges. *International Journal of Wildland Fire*, *28*(10), 721. https://doi.org/10.1071/WFv28n10_FO

Rhoades, C. C., Chow, A. T., Covino, T. P., Fegel, T. S., Pierson, D. N., & Rhea, A. E. (2019). The Legacy of a Severe Wildfire on Stream Nitrogen and Carbon in Headwater Catchments. *Ecosystems*. https://doi.org/10.1007/s10021-018-0293-6

Rice, J. S., & Emanuel, R. E. (2019). Ecohydrology of Interannual Changes in Watershed Storage. *Water Resources Research*, *n/a*(n/a). https://doi.org/10.1029/2019WR025164

Richardson, J. S., & Béraud, S. (2014). Effects of riparian forest harvest on streams: a meta-analysis. *Journal of Applied Ecology*, *51*(6), 1712–1721. https://doi.org/10.1111/1365-2664.12332

Robichaud, P. R. (2000). Fire effects on infiltration rates after prescribed fire in Northern Rocky Mountain forests, USA. *Journal of Hydrology*, *231–232*, 220–229. https://doi.org/10.1016/S0022-1694(00)00196-7

Robinne, F.-N., Bladon, K. D., Miller, C., Parisien, M.-A., Mathieu, J., & Flannigan, M. D. (2018). A spatial evaluation of global wildfire-water risks to human and natural systems. *Science of the Total Environment*, *610*, 1193–1206. https://doi.org/10.1016/j.scitotenv.2017.08.112

Robinne, F.-N., Hallema, D. W., Bladon, K. D., Flannigan, M. D., Boisramé, G., Bréthaut, C. M., et al. (2021). Scientists' warning on extreme wildfire risks to water supply. *Hydrological Processes*, *35*(5), e14086. https://doi.org/10.1002/hyp.14086

Rockström, J., Falkenmark, M., Folke, C., Lannerstad, M., Barron, J., Enfors, E., et al. (2014). *Water resilience for human prosperity*. Cambridge University Press.

Roderick, M. L., & Farquhar, G. D. (2011). A simple framework for relating variations in runoff to variations in climatic conditions and catchment properties. *Water Resources Research*, *47*(12). https://doi.org/10.1029/2010WR009826

Rodríguez-Cardona, B. M., Coble, A. A., Wymore, A. S., Kolosov, R., Podgorski, D. C., Zito, P., et al. (2020). Wildfires lead to decreased carbon and increased nitrogen concentrations in upland arctic streams. *Scientific Reports*, *10*(1), 8722. https://doi.org/10.1038/s41598-020-65520-0

Rodriguez-Iturbe, I. (2000). Ecohydrology: A hydrologic perspective of climate-soil-vegetation dynamies. *Water Resources Research*, *36*(1), 3–9. https://doi.org/10.1029/1999WR900210

Rodriguez-Iturbe, I., D'Odorico, P., Porporato, A., & Ridolfi, L. (1999). On the spatial and temporal links between vegetation, climate, and soil moisture. *Water Resources Research*, *35*(12), 3709–3722. https://doi.org/10.1029/1999WR900255

Rodriguez-Iturbe, I., Porporato, A., Ridolfi, L., Isham, V., & Cox, D. (1999). Probabilistic modeling of water balance at a point: The role of climate, soil, and vegetation. *Proceedings of the Royal Society of London Series A-Mathematical Physical and Engineering Sciences*, *455*, 3789–3805. https://doi.org/10.1098/rspa.1999.0477

Rodriguez-Iturbe, I., Porporato, A., Laio, F., & Ridolfi, L. (2001). Plants in water-controlled ecosystems: active role in hydrologic processes and response to water stress: I. Scope and general outline. *Advances in Water Resources*, *24*(7), 695–705. https://doi.org/10.1016/S0309-1708(01)00004-5

Rohatgi, A. (2019, April). WebPlotDigitizer (Version 4.2). San Francisco, California, USA. Retrieved from https://automeris.io/WebPlotDigitizer

Romanya, J., Khanna, P. K., & Raison, R. J. (1994). Effects of slash burning on soil phosphorus fractions and sorption and desorption of phosphorus. *Forest Ecology and Management*, *65*(2–3), 89–103.

Rosén, K., & Lundmark-Thelin, A. (1987). Increased nitrogen leaching under piles of slash— a consequence of modern forest harvesting techniques. *Scandinavian Journal of Forest Research*, *2*(1–4), 21–29. https://doi.org/10.1080/02827588709382443

Rosenberg, M. S., Rothstein, H. R., & Gurevitch, J. (2013). Effect sizes: conventional choices and calculations. In *Handbook of Meta-analysis in Ecology and Evolution* (Vol. 61, pp. 61–71). Princeton, NJ, USA: Princeton University Press.

Roskoski, J. P. (1980). Nitrogen fixation in hardwood forests of the northeastern United States. *Plant and Soil*, *54*(1), 33–44.

Rousseeuw, P. J. (1987). Silhouettes: A graphical aid to the interpretation and validation of cluster analysis. *Journal of Computational and Applied Mathematics*, *20*, 53–65. https://doi.org/10.1016/0377-0427(87)90125-7

Running, S. W., & Coughlan, J. C. (1988). A general model of forest ecosystem processes for regional applications I. Hydrologic balance, canopy gas exchange and primary production processes. *Ecological Modelling*, *42*(2), 125–154. https://doi.org/10.1016/0304-3800(88)90112-3

Running, S. W., & Gower, S. T. (1991). FOREST-BGC, A general model of forest ecosystem processes for regional applications. II. Dynamic carbon allocation and nitrogen budgets. *Tree Physiology*, *9*(1–2), 147–160. https://doi.org/10.1093/treephys/9.1-2.147

Rust, A. J., Hogue, T. S., Saxe, S., & McCray, J. E. (2018). Post-fire water-quality response in the western United States. *International Journal of Wildland Fire*, *27*(3), 203. https://doi.org/10.1071/WF17115

Rust, A. J., Saxe, S., McCray, J. E., Rhoades, C. C., & Hogue, T. S. (2019). Evaluating the factors responsible for post-fire water quality response in forests of the western USA. *International Journal of Wildland Fire*, *28*(10), 769. https://doi.org/10.1071/WF18191

Rust, A. J., Randell, J., Todd, A. S., & Hogue, T. S. (2019). Wildfire impacts on water quality, macroinvertebrate, and trout populations in the Upper Rio Grande. *Forest Ecology and Management*, *453*, 117636. https://doi.org/10.1016/j.foreco.2019.117636

Ryan, S. E., Dwire, K. A., & Dixon, M. K. (2011). Impacts of wildfire on runoff and sediment loads at Little Granite Creek, western Wyoming. *Geomorphology*, *129*(1), 113–130. https://doi.org/10.1016/j.geomorph.2011.01.017

Sankarasubramanian, A., Vogel, R. M., & Limbrunner, J. F. (2001). Climate elasticity of streamflow in the United States. *Water Resources Research*, *37*(6), 1771–1781. https://doi.org/10.1029/2000WR900330

Saxe, S., Hogue, T. S., & Hay, L. (2018). Characterization and evaluation of controls on post-fire streamflow response across western US watersheds. *Hydrology and Earth System Sciences*, *22*(2), 1221–1237. https://doi.org/10.5194/hess-22-1221-2018

Schelker, J., Sponseller, R., Ring, E., Högbom, L., Löfgren, S., & Laudon, H. (2016). Nitrogen export from a boreal stream network following forest harvesting: Seasonal nitrate removal and conservative export of organic forms. *Biogeosciences*, *13*(1), 1–12. https://doi.org/10.5194/bg-13-1-2016

Schonher, T., & Nicholson, S. E. (1989). The Relationship between California Rainfall and ENSO Events. *Journal of Climate*, *2*(11), 1258–1269. https://doi.org/10.1175/1520-0442(1989)002<1258:TRBCRA>2.0.CO;2

Schumaker, D. (2003). *Old Fire burning in the San Bernardino Mountains. Looking west from Strawberry Peak.* Retrieved from https://commons.wikimedia.org/wiki/File:Old_fire.jpg

Segura, C., Sun, G., McNulty, S. G., & Zhang, Y. (2014). Potential impacts of climate change on soil erosion vulnerability across the conterminous United States. *Journal of Soil and Water Conservation*, *69*(2), 171–181. https://doi.org/10.2489/jswc.69.2.171

Seibert, J., & McDonnell, J. J. (2002). On the dialog between experimentalist and modeler in

catchment hydrology: Use of soft data for multicriteria model calibration. *Water Resources Research*, *38*(11), 23-1-23–14. https://doi.org/10.1029/2001WR000978

Seidl, R., Spies, T. A., Peterson, D. L., Stephens, S. L., & Hicke, J. A. (2016). Searching for resilience: addressing the impacts of changing disturbance regimes on forest ecosystem services. *Journal of Applied Ecology*, *53*(1), 120–129. https://doi.org/10.1111/1365-2664.12511

Seidl, R., Thom, D., Kautz, M., Martin-Benito, D., Peltoniemi, M., Vacchiano, G., et al. (2017). Forest disturbances under climate change. *Nature Climate Change*, *7*(6), 395–402. https://doi.org/10.1038/nclimate3303

Semkin, R. G., Jeffries, D. S., Neureuther, R., Lahaie, G., McAulay, M., Norouzian, F., & Franklyn, J. (2012). Summary of hydrological and meteorological measurements in the Turkey Lakes Watershed, Algoma, Ontario, 1980–2010, 85.

Shafii, M., Basu, N., Craig, J. R., Schiff, S. L., & Van Cappellen, P. (2017). A diagnostic approach to constraining flow partitioning in hydrologic models using a multiobjective optimization framework. *Water Resources Research*, *53*(4), 3279–3301. https://doi.org/10.1002/2016WR019736

Shahid, M., Cong, Z., & Zhang, D. (2018). Understanding the impacts of climate change and human activities on streamflow: a case study of the Soan River basin, Pakistan. *Theoretical and Applied Climatology*, *134*(1), 205–219. https://doi.org/10.1007/s00704-017-2269-4

Shakesby, R. A., & Doerr, S. H. (2006). Wildfire as a hydrological and geomorphological agent. *Earth-Science Reviews*, *74*(3–4), 269–307. https://doi.org/10.1016/j.earscirev.2005.10.006

Sham, C. H., Tuccillo, M. E., & Rooke, J. (2013). *Effects of Wildfire on Drinking Water Utilities and Best Practices for Wildfire Risk Reduction and Mitigation* (p. 119). Denver, CO: Water Research Foundation.

Shlisky, A., Waugh, J., Gonzalez, P., Gonzalez, M., Manta, M., Santoso, H., et al. (2007). *Fire, ecosystems and people: Threats and strategies for global biodiversity conservation* (No. GFI Technical Report 2007-2) (p. 18). Arlington, VA, USA: The Nature Conservancy. Retrieved from https://www.conservationgateway.org/Files/Documents/fire_ecosystems_and_people.pdf

Shlisky, A., Alencar, A., Manta, M., Curran, L., & Cochrane, M. (2009). Overview: Global fire regime conditions, threats, and opportunities for fire management in the tropics (pp. 65–83). Retrieved from DOI: 10.1007/978-3-540-77381-8_3

Shoda, M. E., Sprague, L. A., Murphy, J. C., & Riskin, M. L. (2019). Water-quality trends in U.S. rivers, 2002 to 2012: Relations to levels of concern. *Science of The Total Environment*, *650*, 2314–2324. https://doi.org/10.1016/j.scitotenv.2018.09.377

Sierra, C. A., Trumbore, S. E., Davidson, E. A., Vicca, S., & Janssens, I. (2015). Sensitivity of decomposition rates of soil organic matter with respect to simultaneous changes in temperature and moisture. *Journal of Advances in Modeling Earth Systems*, *7*(1), 335–356. https://doi.org/10.1002/2014MS000358

Silins, U., Stone, M., Emelko, M. B., & Bladon, K. D. (2009). Sediment production following severe wildfire and post-fire salvage logging in the Rocky Mountain headwaters of the Oldman

River Basin, Alberta. *Catena*, *79*(3), 189–197. https://doi.org/10.1016/j.catena.2009.04.001

Silins, U., Bladon, K. D., Kelly, E. N., Esch, E., Spence, J. R., Stone, M., et al. (2014). Five-year legacy of wildfire and salvage logging impacts on nutrient runoff and aquatic plant, invertebrate, and fish productivity. *Ecohydrology*, *7*(6), 1508–1523. https://doi.org/10.1002/eco.1474

Šimůnek, J., Šejna, M., & van Genuchten, M. Th. (2005). The HYDRUS-1D software package for simulating the one-dimensional movement of water, heat, and multiple solutes in variably-saturated media. *University of California-Riverside Research Reports*, *3*, 1–240.

Šimůnek, J., Šejna, M., Saito, H., Sakai, M., & van Genuchten, M. Th. (2013, June). The HYDRUS-1D Software Package for Simulating the One-Dimensional Movement of Water, Heat, and Multiple Solutes in Variably-Saturated Media (Version 4.17). University of California-Riverside.

Sirois, A., Vet, R., & MacTavish, D. (2001). Atmospheric Deposition to the Turkey Lakes Watershed: Temporal Variations and Characteristics. *Ecosystems*, *4*(6), 503–513. https://doi.org/10.1007/s10021-001-0024-1

Sivapalan, M. (2003). Process complexity at hillslope scale, process simplicity at the watershed scale: is there a connection? *Hydrological Processes*, *17*(5), 1037–1041. https://doi.org/10.1002/hyp.5109

Sivapalan, M., Blöschl, G., Zhang, L., & Vertessy, R. (2003). Downward approach to hydrological prediction. *Hydrological Processes*, *17*(11), 2101–2111. https://doi.org/10.1002/hyp.1425

Sivapalan, M., Takeuchi, K., Franks, S. W., Gupta, V. K., Karambiri, H., Lakshmi, V., et al. (2003). IAHS Decade on Predictions in Ungauged Basins (PUB), 2003–2012: Shaping an exciting future for the hydrological sciences. *Hydrological Sciences Journal*, *48*(6), 857–880. https://doi.org/10.1623/hysj.48.6.857.51421

Sivapalan, M., Yaeger, M. A., Harman, C. J., Xu, X., & Troch, P. A. (2011). Functional model of water balance variability at the catchment scale: 1. Evidence of hydrologic similarity and space-time symmetry. *Water Resources Research*, *47*(2). https://doi.org/10.1029/2010WR009568

Slowikowski, K. (2015, January 28). Quickly aggregate your data in R with data.table [Personal Blog]. Retrieved November 17, 2022, from https://slowkow.com/notes/data-table-aggregate/

Smith, H. G., Sheridan, G. J., Lane, P. N. J., & Sherwin, C. B. (2010). Paired Eucalyptus forest catchment study of prescribed fire effects on suspended sediment and nutrient exports in south-eastern Australia. *International Journal of Wildland Fire*, *19*(5), 624–636. https://doi.org/10.1071/WF08208

Smith, H. G., Sheridan, G. J., Lane, P. N. J., Nyman, P., & Haydon, S. (2011). Wildfire effects on water quality in forest catchments: A review with implications for water supply. *Journal of Hydrology*, *396*(1–2), 170–192. https://doi.org/10.1016/j.jhydrol.2010.10.043

Smith, H. G., Hopmans, P., Sheridan, G. J., Lane, P. N. J., Noske, P. J., & Bren, L. J. (2012). Impacts of wildfire and salvage harvesting on water quality and nutrient exports from radiata pine and eucalypt forest catchments in south-eastern Australia. *Forest Ecology and Management*, *263*, 160–169. https://doi.org/10.1016/j.foreco.2011.09.002

Soulis, K. X., Generali, K. A., Papadaki, C., Theodoropoulos, C., & Psomiadis, E. (2021). Hydrological Response of Natural Mediterranean Watersheds to Forest Fires. *Hydrology*, *8*(1), 15. https://doi.org/10.3390/hydrology8010015

Spencer, C. N., Gabel, K. O., & Hauer, F. R. (2003). Wildfire effects on stream food webs and nutrient dynamics in Glacier National Park, USA. *Forest Ecology and Management*, *178*(1–2), 141–153. https://doi.org/10.1016/S0378-1127(03)00058-6

Stednick, J. D. (2008). Long-term streamflow changes following timber harvesting. In *Hydrological and Biological Responses to Forest Practices* (pp. 139–155). Springer. Retrieved from https://doi.org/10.1007%2F978-0-387-69036-0_9

Steffen, W., Richardson, K., Rockström, J., Cornell, S. E., Fetzer, I., Bennett, E. M., et al. (2015). Planetary boundaries: Guiding human development on a changing planet. *Science*, *347*(6223), 1259855. https://doi.org/10.1126/science.1259855

Stevens, A. A., Moore, L. A., Slocum, C. J., Smith, B. L., Seeger, D. R., & Ireland, J. C. (1990). By-products of chlorination at ten operating utilities. In R. L. Jolley, *Water Chlorination: Chemistry, Environmental Impact and Health Effects* (Vol. 6, pp. 579–604). Chelsea, MI, USA: Lewis Publishers.

Stone, M., Emelko, M. B., Droppo, I. G., & Silins, U. (2011). Biostabilization and erodibility of cohesive sediment deposits in wildfire-affected streams. *Water Research*, *45*(2), 521–534. https://doi.org/10.1016/j.watres.2010.09.016

Subiza, E. A. W., Brand, C., Subiza, E. A. W., & Brand, C. (2018). Short-term effects of wildfire on Patagonian headwater streams. *International Journal of Wildland Fire*, *27*(7), 457–470. https://doi.org/10.1071/WF17164

Sutanto, S., Wenninger, J., Coenders-Gerrits, M., & Uhlenbrook, S. (2012). Partitioning of evaporation into transpiration, soil evaporation and interception: A comparison between isotope measurements and a HYDRUS-1D model. *Hydrology and Earth System Sciences*, *16*, 2605–2616. https://doi.org/10.5194/hess-16-2605-2012

Swanson, F. J., & Dyrness, C. T. (1975). Impact of clear-cutting and road construction on soil erosion by landslides in the western Cascade Range, Oregon. *Geology*, *3*(7), 393–396.

Tague, C. L., & Band, L. (2001). Simulating the impact of road construction and forest harvesting on hydrologic response. *Earth Surface Processes and Landforms*, *26*(2), 135–151. https://doi.org/10.1002/1096-9837(200102)26:2<135::AID-ESP167>3.0.CO;2-J

Tague, C. L., & Band, L. E. (2004). RHESSys: Regional Hydro-Ecologic Simulation System—An Object-Oriented Approach to Spatially Distributed Modeling of Carbon, Water, and Nutrient Cycling. *Earth Interactions*, *8*(19), 1–42. https://doi.org/10.1175/1087-3562(2004)8<1:RRHSSO>2.0.CO;2

Tague, C. L., Moritz, M., & Hanan, E. (2019). The changing water cycle: The eco-hydrologic impacts of forest density reduction in Mediterranean (seasonally dry) regions. *WIREs Water*, *6*(4), e1350. https://doi.org/10.1002/wat2.1350

Tarczyńska, M., Romanowska-Duda, Z., Jurczak, T., & Zalewski, M. (2001). Toxic cyanobacterial blooms in a drinking water reservoir-causes, consequences and management strategy. *Water Science and Technology: Water Supply*, *1*(2), 237–246.

Taylor, A. R., Chen, H. Y., & VanDamme, L. (2009). A review of forest succession models and their suitability for forest management planning. *Forest Science*, *55*(1), 23–36.

Teng, J., Chiew, F. H. S., Vaze, J., Marvanek, S., & Kirono, D. G. C. (2012). Estimation of climate change impact on mean annual runoff across continental Australia using Budyko and Fu equations and hydrological models. *Journal of Hydrometeorology*, *13*(3), 1094–1106. https://doi.org/10.1175/JHM-D-11-097.1

Teutschbein, C., Grabs, T., Laudon, H., Karlsen, R. H., & Bishop, K. (2018). Simulating streamflow in ungauged basins under a changing climate: The importance of landscape characteristics. *Journal of Hydrology*, *561*, 160–178. https://doi.org/10.1016/j.jhydrol.2018.03.060

Thompson, S. E., Basu, N. B., Lascurain, J., Aubeneau, A., & Rao, P. S. C. (2011). Relative dominance of hydrologic versus biogeochemical factors on solute export across impact gradients. *Water Resources Research*, *47*(10). https://doi.org/10.1029/2010WR009605

Thurton, D. (2017, February 9). Fort McMurray seeing big spike in water-treatment costs. Retrieved August 5, 2018, from http://www.cbc.ca/news/canada/edmonton/fort-mcmurray-wildfire-water-treatment-costs-contaminants-1.3973249

Tiegs, S. D., Chaloner, D. T., Levi, P., Rüegg, J., Tank, J. L., & Lamberti, G. A. (2008). Timber harvest transforms ecological roles of salmon in southeast Alaska rain forest streams. *Ecological Applications*, *18*(1), 4–11.

Tolson, B. A., & Shoemaker, C. A. (2007). Dynamically dimensioned search algorithm for computationally efficient watershed model calibration. *Water Resources Research*, *43*(1). https://doi.org/10.1029/2005WR004723

Trabucco, A., & Zomer, R. J. (2018). *Global Aridity Index and Potential Evapo-Transpiration (ET0) Climate Database v2*. CGIAR Consortium for Spatial Information (CGIAR-CSI). Retrieved from Published online, available from the CGIAR-CSI GeoPortal at https://cgiarcsi.community

Troch, P. A., Carrillo, G., Sivapalan, M., Wagener, T., & Sawicz, K. (2013). Climate-vegetation-soil interactions and long-term hydrologic partitioning: signatures of catchment co-evolution. *Hydrology and Earth System Sciences*, *17*(6), 2209–2217. https://doi.org/10.5194/hess-17-2209-2013

Turner, M. G. (2010). Disturbance and landscape dynamics in a changing world. *Ecology*, *91*(10), 2833–2849. https://doi.org/10.1890/10-0097.1

U.S. Forest Service. (2018). *S_USA.Activity_TimberHarvest*. Retrieved from https://data.fs.usda.gov/geodata/edw/edw_resources/meta/S_USA.Activity_TimberHarvest.xml

Valipour, M., Driscoll, C. T., Johnson, C. E., Battles, J. J., Campbell, J. L., & Fahey, T. J. (2018). The application of an integrated biogeochemical model to simulate dynamics of vegetation, hydrology and nutrients in soil and streamwater following a whole-tree harvest of a northern hardwood forest. *Science of the Total Environment*, *645*, 244–256. https://doi.org/10.1016/j.scitotenv.2018.07.066

Vannote, R. L., Minshall, G. W., Cummins, K. W., Sedell, J. R., & Cushing, C. E. (1980). The river continuum concept. *Canadian Journal of Fisheries and Aquatic Sciences*, *37*(1), 130–137.

Venable, N. B. H., Lockwood, R., DiMaria, J., Duda, J., Rhoades, C., & Mason, L. (2017). Forest management to protect Colorado's water resources: A synthesis report to support House Bill 16-1255, 20.

Vitousek, P. M., Menge, D. N. L., Reed, S. C., & Cleveland, C. C. (2013). Biological nitrogen fixation: rates, patterns and ecological controls in terrestrial ecosystems. *Philosophical Transactions of the Royal Society B: Biological Sciences*, *368*(1621), 20130119. https://doi.org/10.1098/rstb.2013.0119

Vörösmarty, C. J., & Sahagian, D. (2000). Anthropogenic disturbance of the terrestrial water cycle. *BioScience*, *50*(9), 753–765. https://doi.org/10.1641/0006-3568(2000)050[0753:ADOTTW]2.0.CO;2

Wade, A., White, I., Worthy, M., Gill, A., Mueller, N., Taylor, P., & Wasson, R. (2013). Land management impacts on water quality following fire in a major water supply catchment. *Australian Journal of Water Resources*, *16*(2). https://doi.org/10.7158/W10-841.2013.16.2

Wagenbrenner, J. W., Ebel, B. A., Bladon, K. D., & Kinoshita, A. M. (2021). Post-wildfire hydrologic recovery in Mediterranean climates: A systematic review and case study to identify current knowledge and opportunities. *Journal of Hydrology*, *602*, 126772. https://doi.org/10.1016/j.jhydrol.2021.126772

Wang, D., & Hejazi, M. (2011). Quantifying the relative contribution of the climate and direct human impacts on mean annual streamflow in the contiguous United States. *Water Resources Research*, *47*(10). https://doi.org/10.1029/2010WR010283

Wang, H., & Stephenson, S. R. (2018). Quantifying the impacts of climate change and land use/cover change on runoff in the lower Connecticut River Basin. *Hydrological Processes*, *32*(9), 1301–1312. https://doi.org/10.1002/hyp.11509

Wang, W. J., He, H. S., Spetich, M. A., Shifley, S. R., Thompson III, F. R., Larsen, D. R., et al. (2013). A large-scale forest landscape model incorporating multi-scale processes and utilizing forest inventory data. *Ecosphere*, *4*(9), art106. https://doi.org/10.1890/ES13-00040.1

Wattel- Koekkoek, E. J. W., Buurman, P., Van Der Plicht, J., Wattel, E., & Van Breemen, N. (2003). Mean residence time of soil organic matter associated with kaolinite and smectite. *European Journal of Soil Science*, *54*(2), 269–278. https://doi.org/10.1046/j.1365-2389.2003.00512.x

Webster, K. L., & Hazlett, P. W. (2015). Long-term ecological research at the Turkey Lakes Watershed: 35th anniversary of interdisciplinary, cooperative research, program booklet and workshop summary. GLC-X-13. Retrieved from https://cfs.nrcan.gc.ca/publications?id=36355

Webster, K. L., Leach, J. A., Houle, D., Hazlett, P. W., & Emilson, E. J. S. (2021). Acidification recovery in a changing climate: Observations from thirty-five years of stream chemistry monitoring in forested headwater catchments at the Turkey Lakes watershed, Ontario. *Hydrological Processes*, *35*(9), e14346. https://doi.org/10.1002/hyp.14346

Webster, K. L., Leach, J. A., Hazlett, P. W., Fleming, R. L., Emilson, E. J. S., Houle, D., et al. (2021). Turkey Lakes Watershed, Ontario, Canada: 40 years of interdisciplinary whole-ecosystem research. *Hydrological Processes*, (n/a), e14109. https://doi.org/10.1002/hyp.14109

Webster, K. L., Leach, J. A., Hazlett, P. W., Buttle, J. M., Emilson, E. J. S., & Creed, I. F. (2022).

Long-term stream chemistry response to harvesting in a northern hardwood forest watershed experiencing environmental change. *Forest Ecology and Management*, *519*, 120345. https://doi.org/10.1016/j.foreco.2022.120345

Weis, W., Rotter, V., & Göttlein, A. (2006). Water and element fluxes during the regeneration of Norway spruce with European beech: Effects of shelterwood-cut and clear-cut. *Forest Ecology and Management*, *224*(3), 304–317. https://doi.org/10.1016/j.foreco.2005.12.040

Wells, W. G. (1981). Some effects of brushfires on erosion process in coastal Southern California. *International Association of Hydrological Sciences*, *132*, 305–342.

Westerberg, I. K., Wagener, T., Coxon, G., McMillan, H. K., Castellarin, A., Montanari, A., & Freer, J. (2016). Uncertainty in hydrological signatures for gauged and ungauged catchments. *Water Resources Research*, *52*(3), 1847–1865. https://doi.org/10.1002/2015WR017635

Westerling, A., Brown, T., Schoennagel, T., Swetnam, T., Turner, M., & Veblen, T. (2014). Briefing: Climate and wildfire in western U.S. forests. *In: Sample, V. Alaric; Bixler, R. Patrick, Eds. Forest Conservation and Management in the Anthropocene: Conference Proceedings. Proceedings. RMRS-P-71. Fort Collins, CO: US Department of Agriculture, Forest Service. Rocky Mountain Research Station. p. 81-102.*, *71*, 81–102.

Westerling, A. L. (2006). Warming and Earlier Spring Increase Western U.S. Forest Wildfire Activity. *Science*, *313*(5789), 940–943. https://doi.org/10.1126/science.1128834

Westerling, A. L. (2016). Increasing western US forest wildfire activity: sensitivity to changes in the timing of spring. *Philosophical Transactions of the Royal Society B: Biological Sciences*, *371*(1696), 20150178. https://doi.org/10.1098/rstb.2015.0178

WHO. (1993). *Guidelines for Drinking Water Quality* (2nd ed., Vol. 1). Geneva, Switzerland: World Health Organization. Retrieved from https://www.who.int/water_sanitation_health/publications/gdwq2v1/en/

Wilkinson, S., Wallbrink, P. J., Blake, W., Doerr, S. H., & Shakesby, R. A. (2006). *Impacts on water quality by sediments and nutrients released during extreme bushfires: Report 3: Post-fire sediment and nutrient redistribution to downstream waterbodies,Nattai National Park, NSW* (Land and Water Science Report No. 64/06) (p. 39). Canberra, Australia: CSIRO. Retrieved from https://www.academia.edu/download/41606735/Impacts_on_water_quality_by_sediments_an20160126-14165-1shc96p.pdf

Wilkinson, S., Wallbrink, P., Hancock, G., Blake, W., & Farwig, V. (2007). *Impacts on water quality by sediments and nutrients released during extreme bushfires: Report 4: Impacts on Lake Burragorang* (Land and Water Science Report No. 6/07) (p. 24). Canberra, Australia: CSIRO.

Wine, M. L., & Cadol, D. (2016). Hydrologic effects of large southwestern USA wildfires significantly increase regional water supply: Fact or fiction? *Environmental Research Letters*, *11*(8). https://doi.org/10.1088/1748-9326/11/8/085006

Winter, C., Lutz, S. R., Musolff, A., Kumar, R., Weber, M., & Fleckenstein, J. H. (2021). Disentangling the Impact of Catchment Heterogeneity on Nitrate Export Dynamics From Event to Long-Term Time Scales. *Water Resources Research*, *57*(1), e2020WR027992. https://doi.org/10.1029/2020WR027992

Withers, P. J. A., & Jarvie, H. P. (2008). Delivery and cycling of phosphorus in rivers: A review. *Science of The Total Environment*, *400*(1), 379–395. https://doi.org/10.1016/j.scitotenv.2008.08.002

Wohl, E. (2013). Migration of channel heads following wildfire in the Colorado Front Range, USA. *Earth Surface Processes and Landforms*, *38*(9), 1049–1053. https://doi.org/10.1002/esp.3429

Wootton, J. T. (2012). Effects of Timber Harvest on River Food Webs: Physical, Chemical and Biological Responses. *PLOS ONE*, *7*(9), e43561. https://doi.org/10.1371/journal.pone.0043561

Writer, J. H., Hohner, A., Oropeza, J., Schmidt, A., Cawley, K. M., & Rosario-Ortiz, F. L. (2014). Water treatment implications after the high Park wildfire, Colorado. *Journal-American Water Works Association*, *106*(4), E189–E199. https://doi.org/10.5942/jawwa.2014.106.0055

Wu, P., Liang, S., Wang, X.-S., Feng, Y., & McKenzie, J. M. (2018). A New Assessment of Hydrological Change in the Source Region of the Yellow River. *Water*, *10*(7), 877. https://doi.org/10.3390/w10070877

Wymore, A. S., Yang, W. H., Silver, W. L., McDowell, W. H., & Chorover, J. (Eds.). (2022). *Biogeochemistry of the Critical Zone*. Cham: Springer International Publishing. https://doi.org/10.1007/978-3-030-95921-0

Wynn, T. M., Mostaghimi, S., Frazee, J. W., McClellan, P. W., Shaffer, R. M., & Aust, W. M. (2000). Effects of forest harvesting best management practices on surface water quality in the Virginia coastal plain. *Transactions of the ASAE*, *43*(4), 927–936. https://doi.org/10.13031/2013.2989

Xu, X., Thornton, P. E., & Post, W. M. (2013). A global analysis of soil microbial biomass carbon, nitrogen and phosphorus in terrestrial ecosystems. *Global Ecology and Biogeography*, *22*(6), 737–749. https://doi.org/10.1111/geb.12029

Yang, D., Sun, F., Liu, Z., Cong, Z., Ni, G., & Lei, Z. (2007). Analyzing spatial and temporal variability of annual water-energy balance in nonhumid regions of China using the Budyko hypothesis. *Water Resources Research*, *43*(4). https://doi.org/10.1029/2006WR005224

Ye, S., Yaeger, M., Coopersmith, E., Cheng, L., & Sivapalan, M. (2012). Exploring the physical controls of regional patterns of flow duration curves - Part 2: Role of seasonality, the regime curve, and associated process controls. *Hydrology and Earth System Sciences*, *16*(11), 4447–4465. https://doi.org/10.5194/hess-16-4447-2012

Yin, J., Porporato, A., D'Odorico, P., & Rodríguez-Iturbe, I. (2019). Ecohydrology. In *Encyclopedia of Water: Science, Technology, and Society*. https://doi.org/10.1002/9781119300762.wsts0026

Zarnetske, J. P., Bouda, M., Abbott, B. W., Saiers, J., & Raymond, P. A. (2018). Generality of Hydrologic Transport Limitation of Watershed Organic Carbon Flux Across Ecoregions of the United States. *Geophysical Research Letters*, *45*(21), 11,702-11,711. https://doi.org/10.1029/2018GL080005

Zhang, L., Dawes, W. R., & Walker, G. R. (2001). Response of mean annual evapotranspiration to vegetation changes at catchment scale. *Water Resources Research*, *37*(3), 701–708.

Zhang, L., Potter, N., Hickel, K., Zhang, Y., & Shao, Q. (2008). Water balance modeling over

variable time scales based on the Budyko framework – Model development and testing. *Journal of Hydrology*, *360*(1–4), 117–131.

Zhang, L., Zhao, F., Chen, Y., & Dixon, R. N. M. (2011). Estimating effects of plantation expansion and climate variability on streamflow for catchments in Australia. *Water Resources Research*, *47*(12). https://doi.org/10.1029/2011WR010711

Zhang, M., & Wei, X. (2012). The effects of cumulative forest disturbance on streamflow in a large watershed in the central interior of British Columbia, Canada. *Hydrology and Earth System Sciences*, *16*(7), 2021–2034. https://doi.org/10.5194/hess-16-2021-2012

Zhang, M., & Wei, X. (2014). Contrasted hydrological responses to forest harvesting in two large neighbouring watersheds in snow hydrology dominant environment: implications for forest management and future forest hydrology studies. *Hydrological Processes*, *28*(26), 6183–6195. https://doi.org/10.1002/hyp.10107

Zhi, W., & Li, L. (2020). The Shallow and Deep Hypothesis: Subsurface Vertical Chemical Contrasts Shape Nitrate Export Patterns from Different Land Uses. *Environmental Science & Technology*, *54*(19), 11915–11928. https://doi.org/10.1021/acs.est.0c01340

Appendix A
Supporting Information to Chapter 2

This Appendix is a mirror of the Supporting Information originally accompanying the following published article. References at the end of this Appendix are for the contained citations.

Hampton, Tyler B., and Nandita B. Basu. "A Novel Budyko-Based Approach to Quantify Post-Forest-Fire Streamflow Response and Recovery Timescales." *Journal of Hydrology*, March 4, 2022, 127685. https://doi.org/10.1016/j.jhydrol.2022.127685.

All data and codes are publicly available in the online Hydroshare repository: http://www.hydroshare.org/resource/43280a7de6ef48b4b800ab5c12ae58cb

A1 Supplemental Methods

A1.1 Catchment Selection

A sample of 7 burned catchments and 10 unburned catchments (Tables 2-1 and 2-2) were selected from a population of 112 stream gages in Southern California that had greater than 20% forested land (within the bounding box of 114-121°W 32-35°N, GAGES II dataset, Falcone, 2011). Of these, 89 watersheds had greater than 20% of the catchment burned over the period of the study (1982-2009), and 12 catchments had less than 5% burned over the period of record. Two were removed for missing flow data during the period of study. These 10 unburned catchments would go on to serve as our reference candidates. Sixty five of the 89 burned catchments satisfied the requirement of having a large fire (>20% burned) within the period of record surrounded by 10 years prior and 5 years following with no fires (none >5% burned). Amongst these burned watersheds, the period of 2002-2003 had the most fires. For those burned in 2003 (WY 2004), only 7 burned watersheds had at least 15% burned and 15 total years of hydrologic record, with 10 years before WY 2004 and 5 after. Finally, we arrived at a sample size of 7 burned and 10 reference catchments for our analysis. The USGS gage numbers are included in Tables 2-1 and 2-2. One of our burned study catchments (Devil Canyon, USGS gage 11063680) was also studied by Kinoshita & Hogue (2011, 2015), and they offer a more extensive analysis of seasonal flows and flow duration curves. We arrived at a narrow subset of catchments, but our criteria could have been relaxed, for example, to analyze all the catchments with appropriate periods of record surrounding large fires.

A1.2 Open-Source Datasets

We relied on the same datasets as those used by Hallema, Sun, et al. (2018) and Saxe et al. (2018) (see Table 2-3). We used streamflow data from the U.S. Geological Survey (USGS), and gridded monthly climatic datasets to complete our assessment of the water balance. Sites were selected from the USGS stream gaging network, accessed through the GAGES II dataset. These shapefiles were paired with shapefile outlines of fires from the MTBS dataset. In the statistical computing language R (R Core Team, 2023), the *sf* package (Pebesma, 2018) was used perform an intersection of these two datasets and identify years of fires affecting watersheds.. Data were sorted and averaged according to water-year (WY; starting October 1st). Gridded data for monthly temperature and precipitation were from the PRISM Dataset. The *raster* package in R (Hijmans et al., 2018) was used to clip and average the climate data for individual watersheds. The *raster* package was also used to clip burn severity raster data from MTBS and characterize percent burn for each category in each watershed.

A1.3 Estimation of PET using the Hargreaves-Samani Equation

Mean, minimum, and maximum monthly temperatures from PRISM were used to calculate potential evapotranspiration (PET) following the Hargreaves-Samani equation (Hargreaves & Samani, 1985):

$$PET_{WY} = 365 * \sum_{m=1}^{12} 0.0023 \times R_m \times {TD_m}^{0.5} \times (T_m + 17.8) \quad \text{(A-1)}$$

where PET_{WY} is WY summed potential evapotranspiration. R_m is the monthly extraterrestrial radiation at the top of the atmosphere converted to equivalent evaporation (mm day^{-1}), and is a function of latitude and date of the year. TD_m is the difference between maximum and minimum monthly temperature (°C), and, T_m is the mean monthly temperature (°C). Monthly values were calculated to take advantage of the temporal resolution of the PRISM data.

The calculations of extraterrestrial radiation (R) in Hargreaves equation are laid out in Allen et al. (1998), and are included here.

$$R = \frac{1}{\lambda} * \frac{1}{\pi} * \mathrm{G}_{sc} * d_r * (\omega_s * \sin(\varphi) * \sin(\alpha) + \cos(\varphi) * \cos(\alpha) * sin(\omega_s)) \quad \text{(A-2)}$$

where λ is the latent head of vaporization of water ($\frac{1}{\lambda}$=0.408 MJ^{-1} kg),

G_{sc} is the solar constant (118.08 MJ m^{-2} day^{-1}),

d_r is the inverse relative distance between the Earth and the Sun,

$$d_r = 1 + 0.033 * \cos\left(\frac{2\pi}{365}J\right) \quad \text{(A-3)}$$

where J is the Julian day of the year (1 – 365), and for monthly calculations are set to the 15th day of each month;

φ is the latitude (in radians),

α is the solar decimation (radians),

$$\alpha = 0.409 * \sin\left(\frac{2\pi}{365}J - 1.39\right) \quad \text{(A-4)}$$

and ω_s is the sunset hour angle (radians):

$$\omega_s = \arccos\left(-\tan(\varphi) * \tan(\alpha)\right) \quad \text{(A-5)}$$

A1.4 Analysis to Support Hydrologic Steady-state Assumption

We analyzed data from across the continental US provided by Rice & Emanuel (2019) to evaluate the effect of hydrologic storage change on the Budyko fit. Rice & Emanuel (2019) supplied data in their Supplementary Data Table 1 for mean ΔS (change in storage), precipitation (P), evapotranspiration (ET, MODIS estimate), and streamflow (Q). In our analysis we extracted data from the GAGES dataset corresponding to each USGS gage number to calculate annual mean potential evapotranspiration (PET) using the Hargreaves-Samani equation (Section A1.3). Budyko parameters (AET/P and PET/P) were calculated and points were colored by the calculated dS/P data from Rice & Emanuel. All data and code are provided in the online repository. The results show that catchments with higher values of interannual storage changes (ΔS/P) deviate more strongly from the Budyko curve.

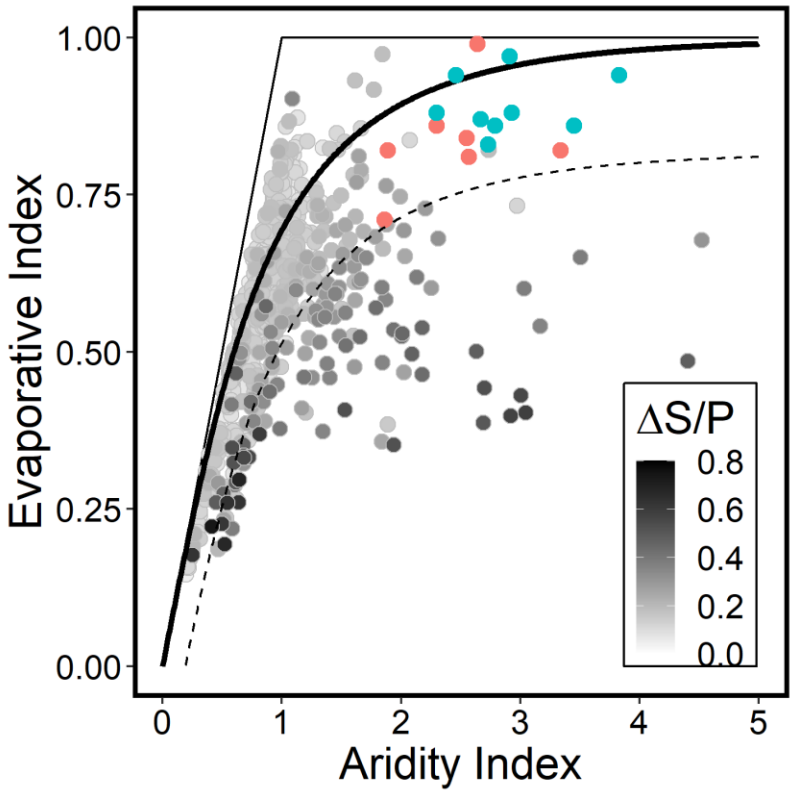

Figure A-1: Grayscale points are from Rice & Emanuel (2019), showing data from 953 catchments, averaged across approximately 20 years of data each. ΔS is the mean absolute change in storage, calculated between each water year. Where ΔS/P is low, the annual water budget is on average very closed, and where ΔS/P is high, there is strong interannual storage carryover between water years. High ΔS/P catchments to cluster lower in the plot (low EI) and away from the Budyko curve. Red points are our 7 burned catchments and blue points are our 10 unburned catchments, with data averaged from 1982–2003.

A2 Discussion of Method Choices

A2.1 Analyzing Effect of PET Estimation Method on Budyko Deviation

There are two groups of methods available for estimating PET: temperature-based methods (eg, Thornthwaite, Hamon, and Hargreaves-Samani) and radiation-based methods (e.g., Turc, Makkink, and Priestley-Taylor). We focused on the 6 listed methods to build off a previous comparison study by Lu et al. (2005). All equations can be found in that study. We did not have access to radiation data at our sites and thus used the temperature-based Hargreaves-Samani equation (Hargreaves & Samani, 1985). To ensure that this didn't bring bias into our results, we analyzed the choice of our PET calculation method by assessing agreement between the six PET methods (Section A2.2 and Figures

A-3,4). This was done using the CAMELS dataset (Addor et al., 2017), a dataset comprising of 671 catchments across the US that succeeded the MOPEX dataset (Duan et al., 2006). CAMELS contains daily climatological data including incoming short-wave radiation, temperature, and precipitation; and catchment attributes including ecozone, land cover, and topography.

Preliminary analysis of all 671 sites in the CAMELS dataset showed that annual (for 21 years) PET calculated using these six methods varied widely (Figure A2). We explored the results of linear regression of annual timeseries of PET between pairs of methods, denoted by the x-axis, and found that of the radiation-based Preistley-Taylor and Makkink agreed perfectly. Of the temperature-based methods, Hargreaves agreed most closely with the Preistley-Taylor and Makkink methods (red colors in Figure A3). Regression of Hargreaves against Makkink and Preistley-Taylor had a median Pearson's R^2 of about 0.75 and regression slope of 1 (Figure A3). In calculation of PET by the Preistley-Taylor method, we had to rely on an estimate of ground-level net radiation (incoming shortwave radiation plus incoming longwave radiation minus outgoing longwave radiation) because CAMELS only provided shortwave. Kraalingen & Stol (1997) outline that net radiation is generally around 50% of incoming shortwave radiation, so a factor of 0.5 was used in our calculations. Due to the uncertainty of this factor however, and the strong agreement of Hargreaves and another radiation-based method Makkink, we did not explore Preistley-Taylor further.

Next, we narrowed our analysis and explored the relationships of two methods (Hargreaves and Makkink) for seven watersheds from CAMELS within California. These watersheds were selected from the total population for proximity to our sites, with latitude less than 35 degrees N and longitude less than -133 degrees W. We examined how annual aridity index (AI=PET/P) varied if calculated according to Makkink or Hargreaves. Figure A3 shows that Hargreaves consistently underestimated AI relative to the Makkink method by about 26%. The average slope of the linear regression slopes for the 7 sites was 0.74.

If one assumed that radiation-based methods like Makkink more truly represent annual PET, we could say that the estimates from Hargreaves used in the manuscript are underestimates of the true values. To test whether this assumption affected our results and conclusions, all annual PET estimates calculated by the Hargreaves method were multiplied by a factor of 1.35 (1/0.74). We saw no change in our results (Figure A5), with only small changes in some vertical Budyko measurements at low AI,

and very small shifts in flow attributions between climate and fire (Figure A6). The results presented in the manuscript represent the original Hargreaves values.

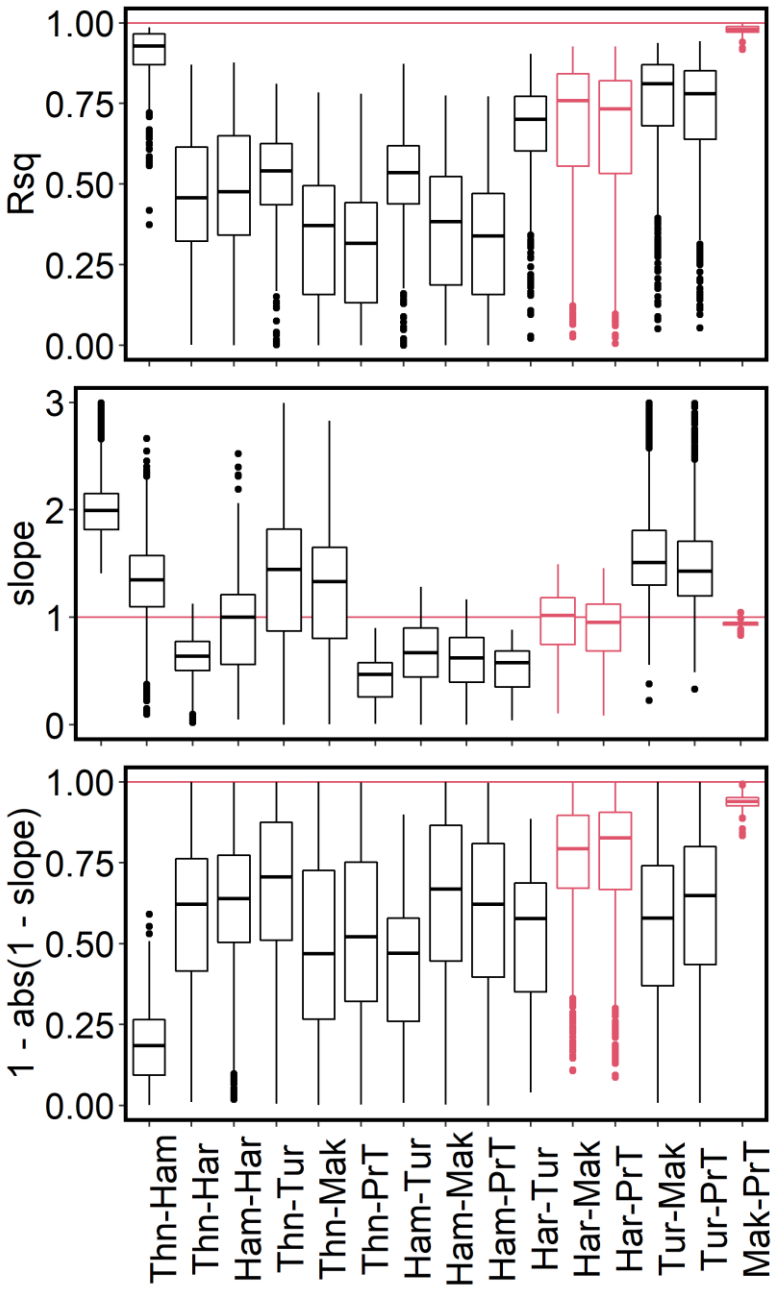

Figure A2: Comparison of the slope of the linear regressions in annual PET timeseries using six methods: Thornthwaite (Thn), Hamon (Ham), Hargreaves-Samani (Har), Turc (Tur), Makkink (Mak), and Priestley-Taylor (PrT). Points are for 671 watersheds in the CAMELS dataset. Boxes in red show comparison of Har to Mak and PrT. a) Pearson's R^2 of the regression slopes. b) The regression slopes. c) Absolute values of the regression slopes, where 1 is closest to a 1:1 slope (perfect agreement between methods) and 0 is farthest away from the 1:1 slope in either the positive or negative direction, and indicates no relationship between the methods.

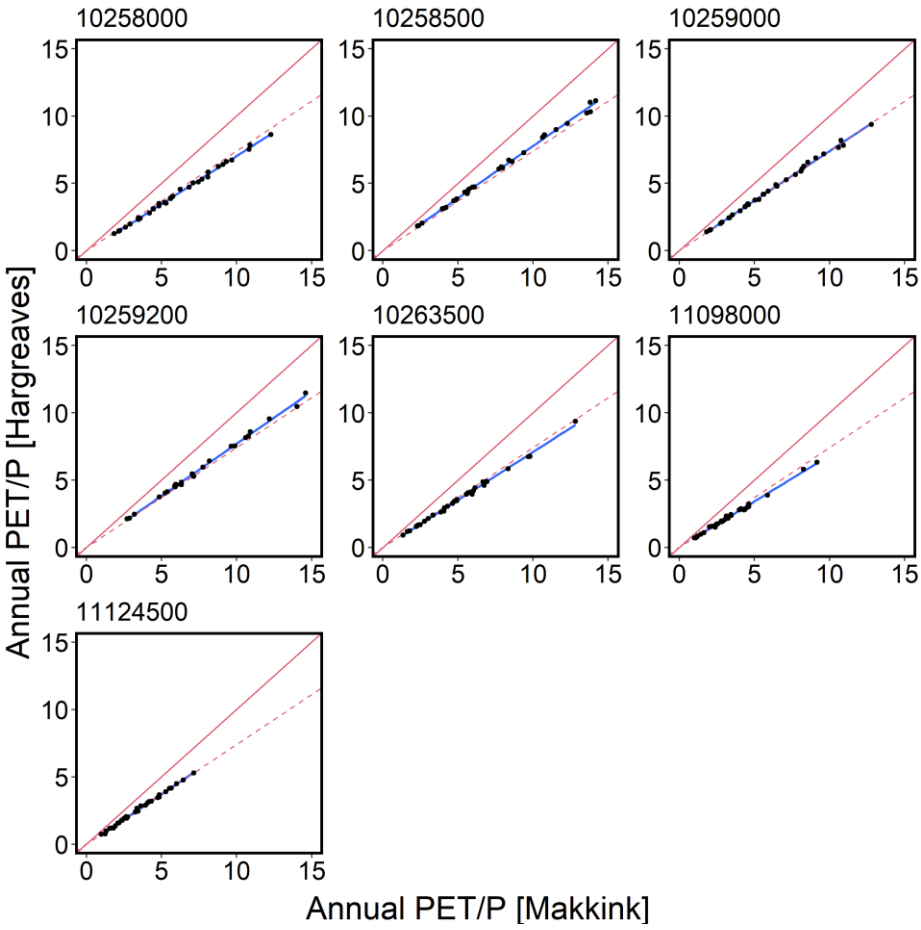

Figure A3: Comparison of annual aridity index between the Makkink and Hargreaves methods for 7 catchments from the CAMELS dataset. The solid red line has a slope of 1 and the dashed red line has a slope of 0.74. Blue lines are individual regression slopes.

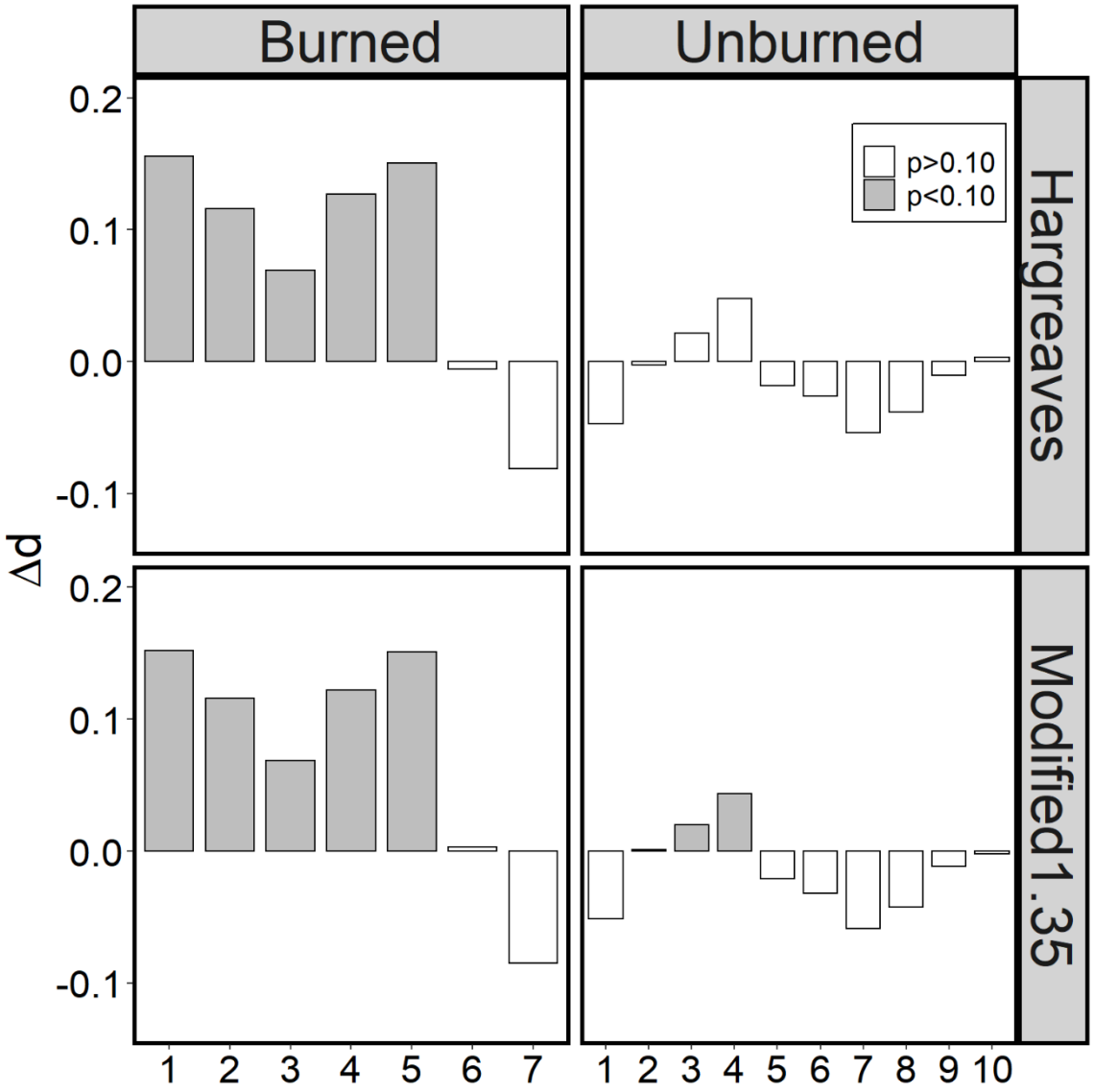

Figure A4: Boxplots of change in vertical Budyko deviations between two 10-year periods (pre- and post-fire). Box fill is shaded gray for p-value of less than 0.10 from a K-S test indicating a significant difference between the sample medians. Original “Hargreaves” method is compared (top) to the modified increased AI alternative (bottom), where AI was scaled up by 1.35.

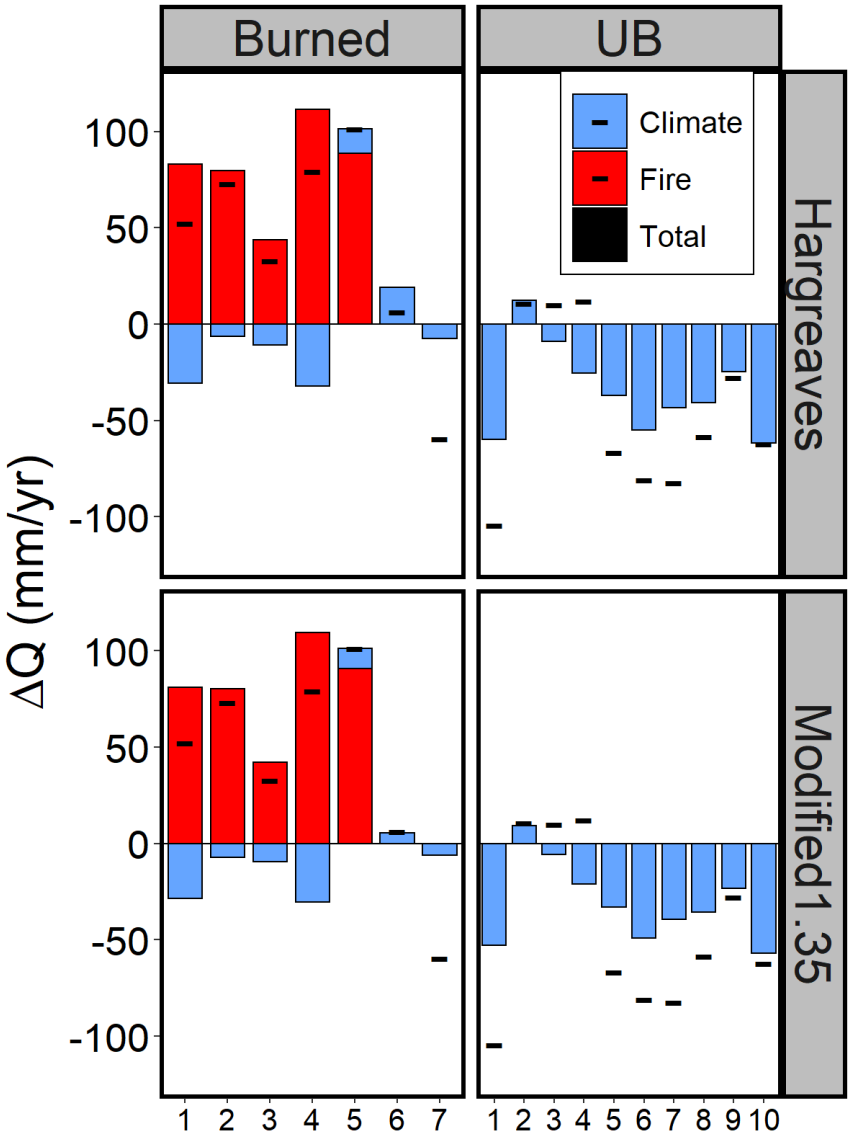

Figure A5: Mean Q changes between pre- and post-fire periods. Black horizontal bars are total Q change observed for each site between the 10-year averages. Blue bars are calculated is predicted Q change due solely to climate-induced horizontal movement along the fit Budyko curve for each site. Red bars are calculated as the contribution of vertical Budyko deviations to change in Q.

A2.2 Analysis of Choice of the Fu-type Budyko Curves

We chose the Fu-type Budyko curves to conduct our analysis. Wang & Hejazi (2011) conducted their analysis using both the Fu and Turc-Pike Budyko curves and found no differences in the interpretation of their results. Similarly, we also tested the Zhang (2001) and Wang-Tang (2014) curves and found no difference in the measurement of vertical Budyko deviations and the interpretation of our results. Figure A6 shows for one burned watershed in the pre-fire period how the different curves agree very closely when calibrated to the same data.

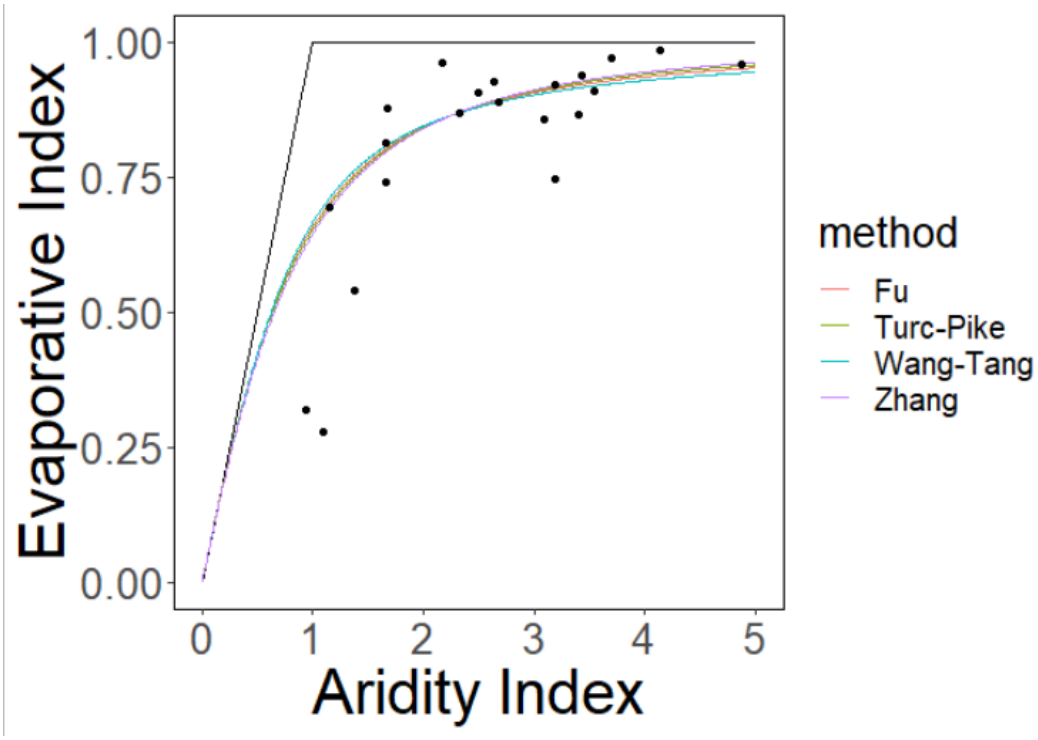

Figure A6: Data from site 10260950 between water years 1982 and 2003, with four Budyko-type curve fits.

A3 Figure A7

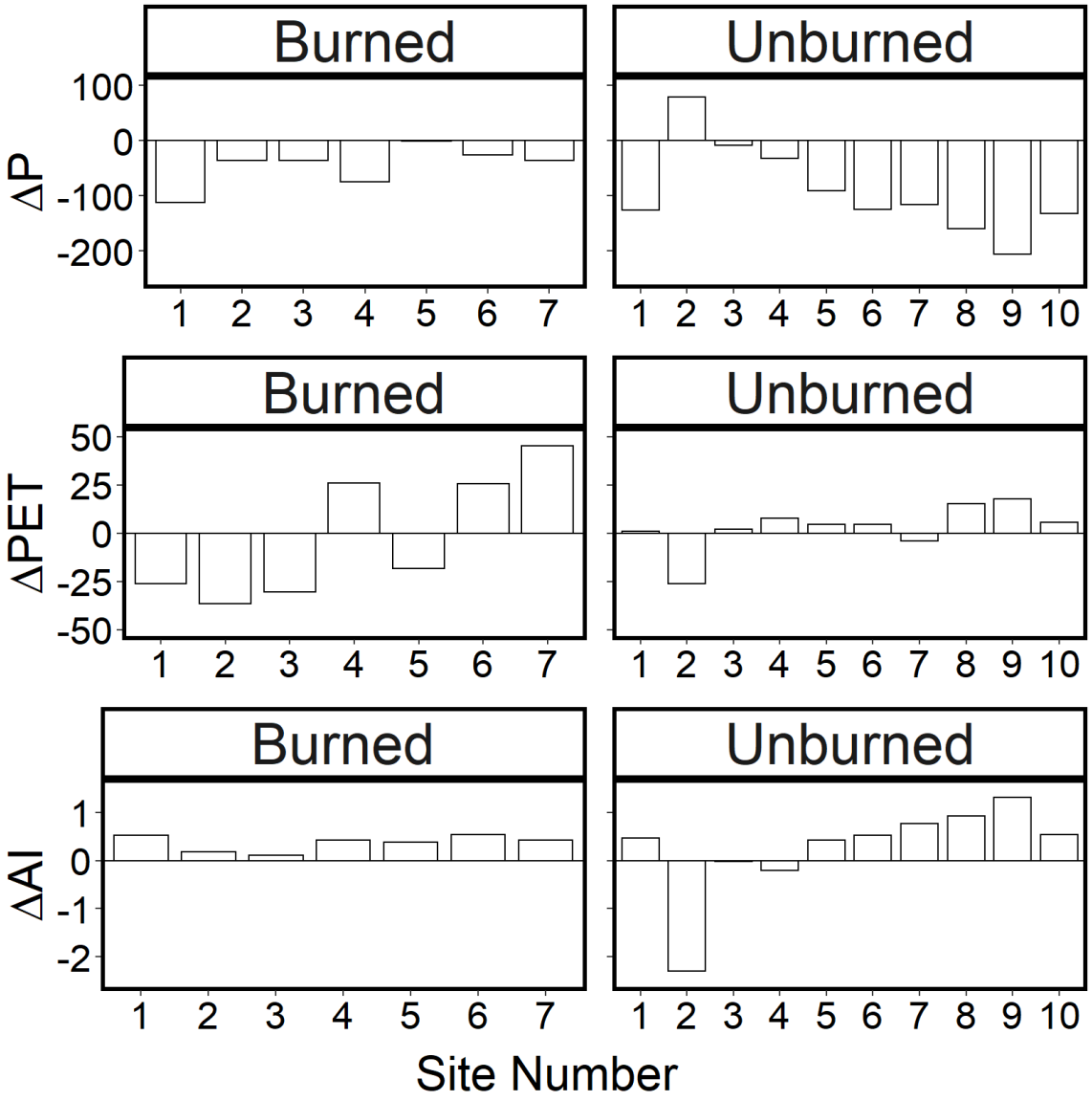

Figure A7: Change in climate parameters (precipitation, P; potential evapotranspiration, PET; aridity index, AI) between 10-year averages for the pre- and post-fire periods for 7 burned catchments and 10 unburned catchments.

Appendix B

Supporting Information to Chapter 3

This Appendix is a mirror of the Supporting Information originally accompanying the following published article. References at the end of this Appendix are for the contained citations.

Hampton, Tyler B., Lin Simon G.M. and Nandita B. Basu. “Forest fire effects on stream water quality at continental scales: A meta-analysis.” *Environmental Research Letters*, May 2022. https://doi.org/10.1088/1748-9326/ac6a6c.

All data and codes are publicly available in the online Hydroshare repository: https://www.hydroshare.org/resource/537dc5206d584625b0fd28ea6b6872de/

B1 Supplemental Figures

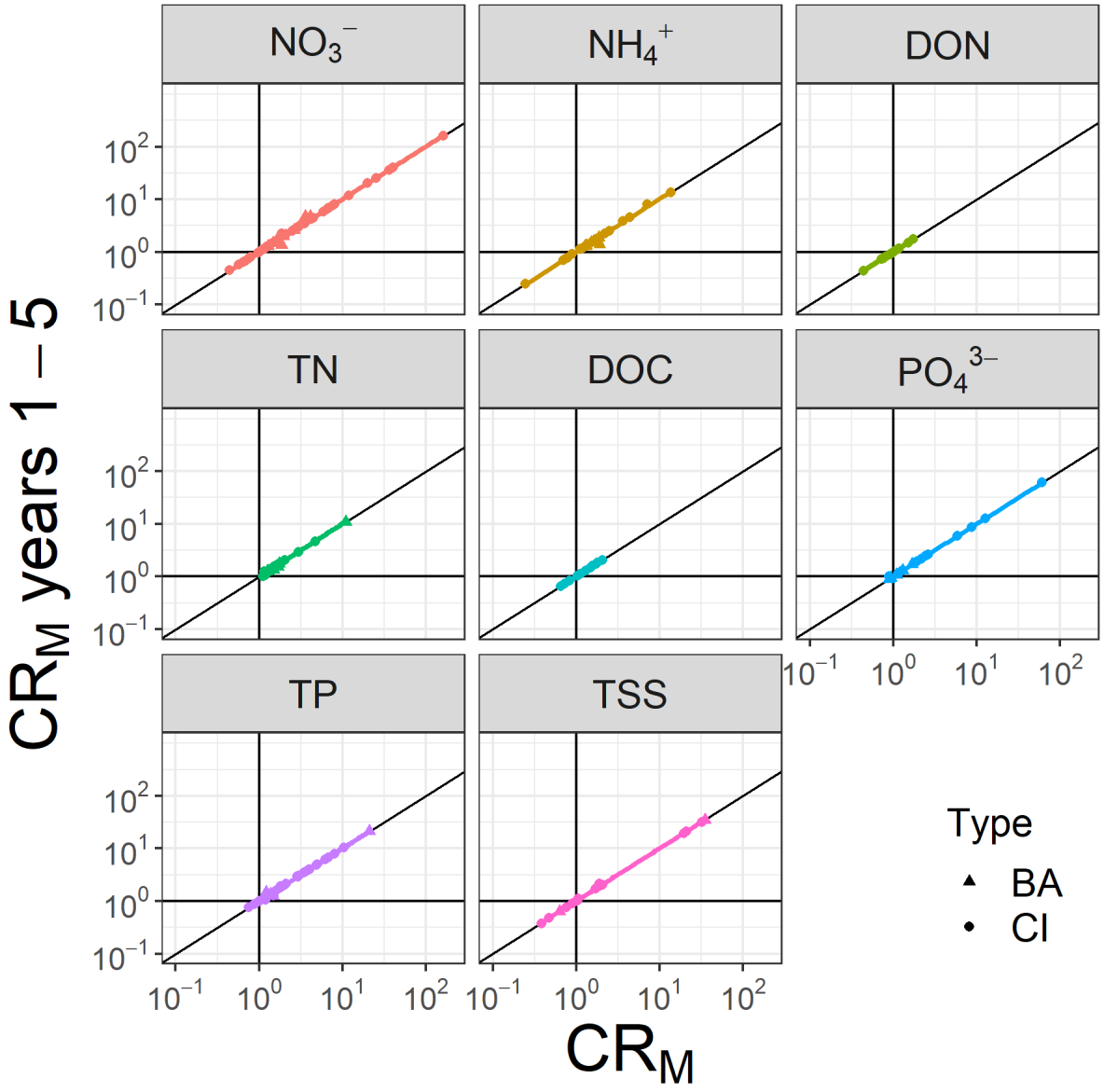

Figure B1: Comparison by site of change ratios. CR_M all-time compared to change ratio for the first five post-fire years. Points are sorted by shape, with triangles for BA (before-after) comparison and circles for CI (control-impact) comparison. A 1:1 line is drawn in black, with horizontal/vertical lines drawn at CR=1.

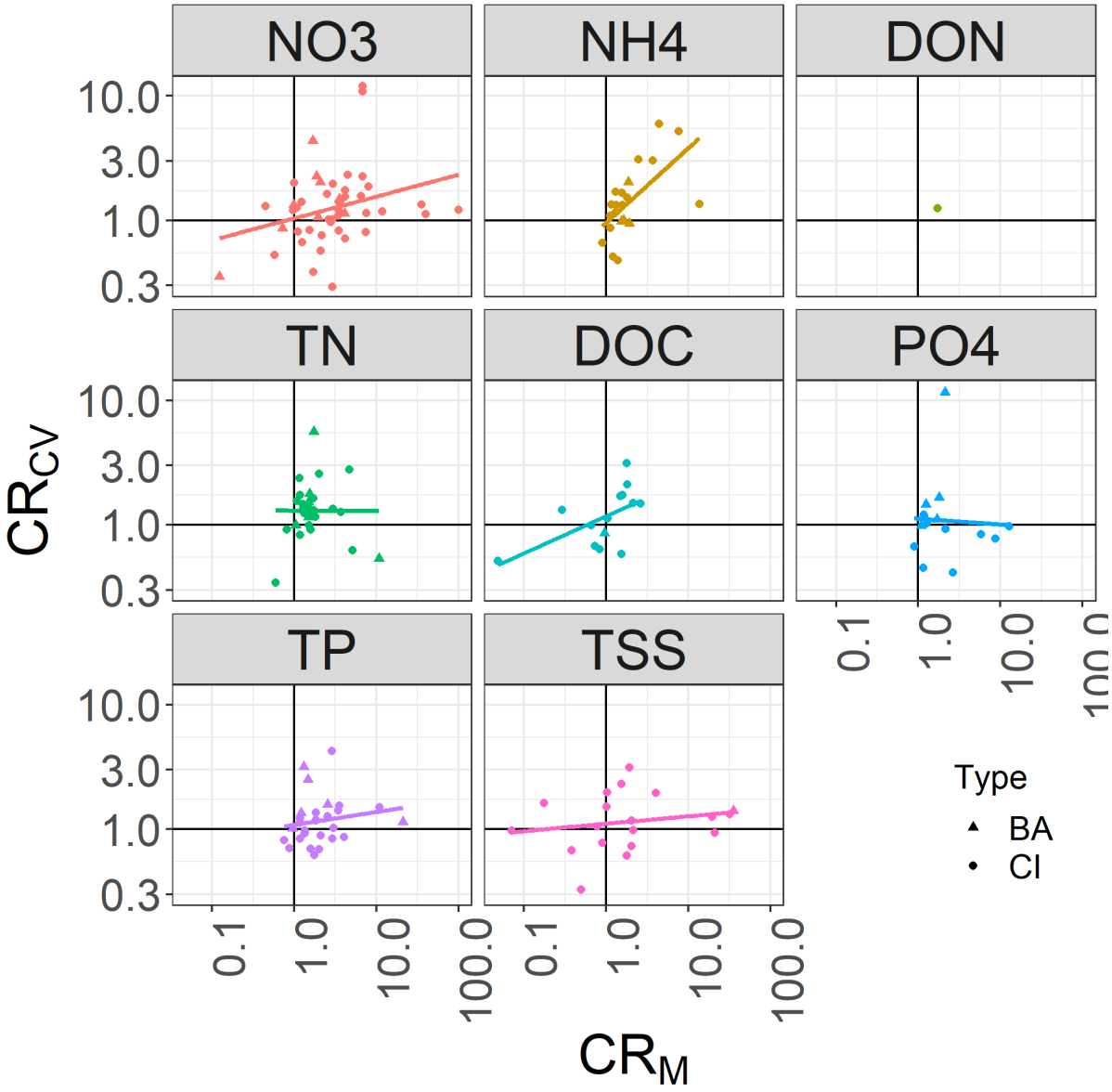

Figure B2: Comparison of CR_M (all-time) to CR_{CV}. Points are sorted by shape, with triangles for BA (before-after) comparison and circles for CI (control-impact) comparison. A linear regression in log-space is drawn for all points, with relationship only significant for NO_3^- ($p=0.05$, $R^2=0.08$), NH_4^+ ($p=0.003$, $R^2=0.38$), and DOC ($p=0.03$, $R^2=0.33$).

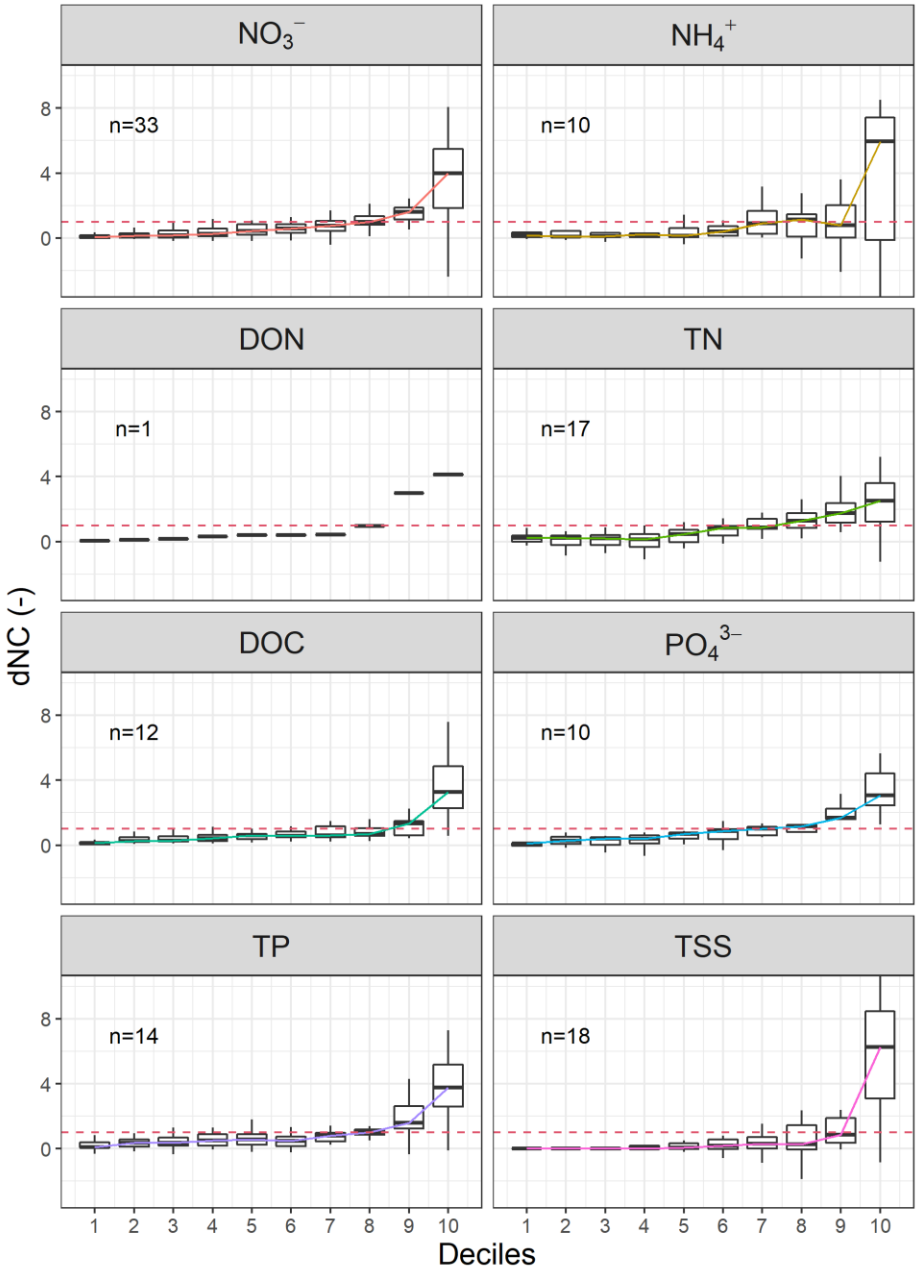

Figure B3: Following the example in Figure 3-2, for each burned site with sufficient data to calculate deciles, the decile normalized change (dNC) was calculated as the ratio of decile change (dAC) over total change (AC). Data from all sites are grouped by decile in boxplots, showing the median, interquartile range, and whiskers out to the 10th and 90th percentiles.

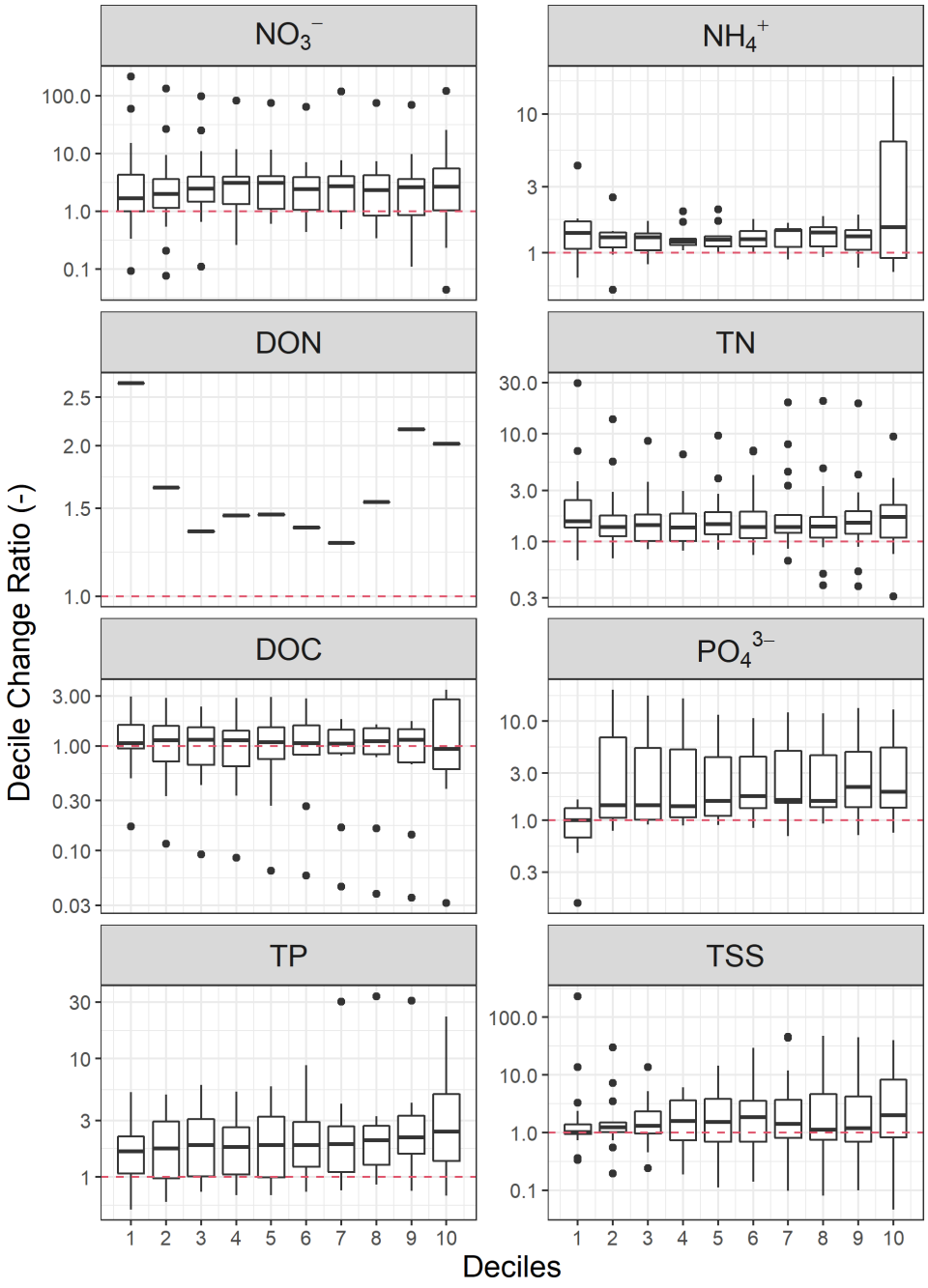

Figure B4: Following the example in Figure 3-2, for each burned site with sufficient data to calculate deciles, the decile change ratio (dCR) was calculated as the ratio of post-fire decile concentration over pre-fire decile concentration. Data from all sites are grouped by decile in boxplots, showing the median, interquartile range, and whiskers out to the 10th and 90th percentiles.

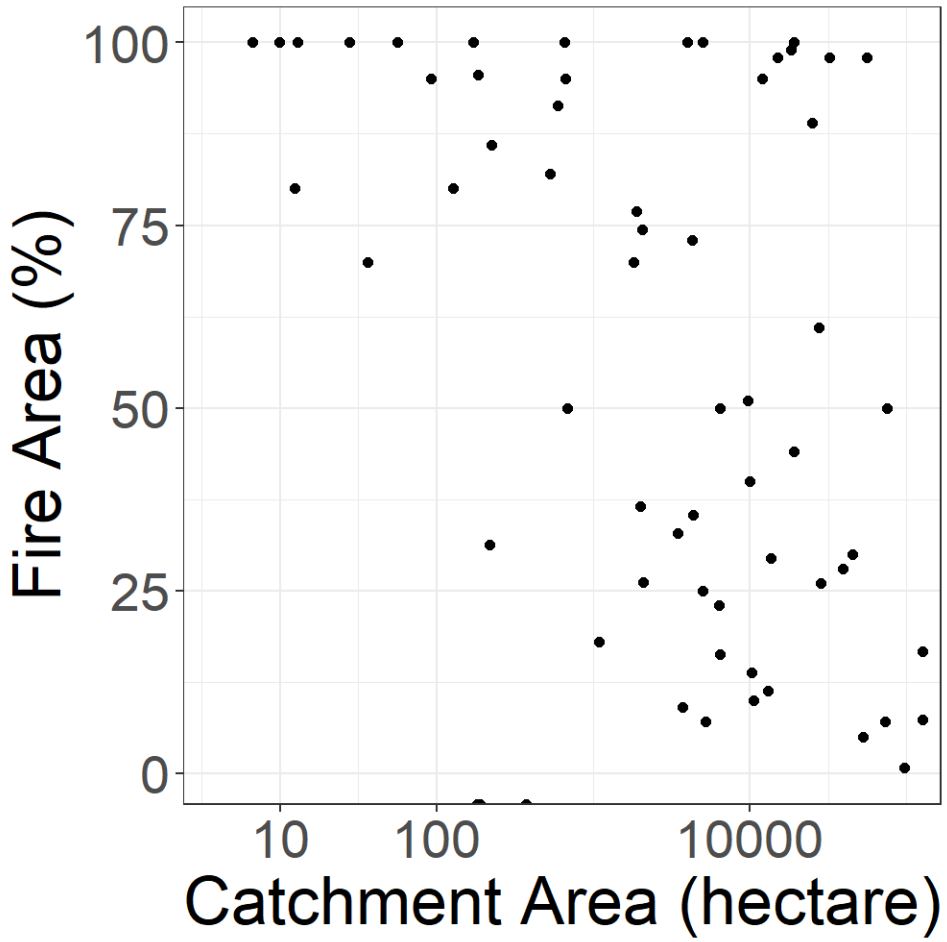

Figure B5: Comparison of site characteristics. Percent catchment burned is negatively correlated with catchment area. Note the log scale on the x axis.

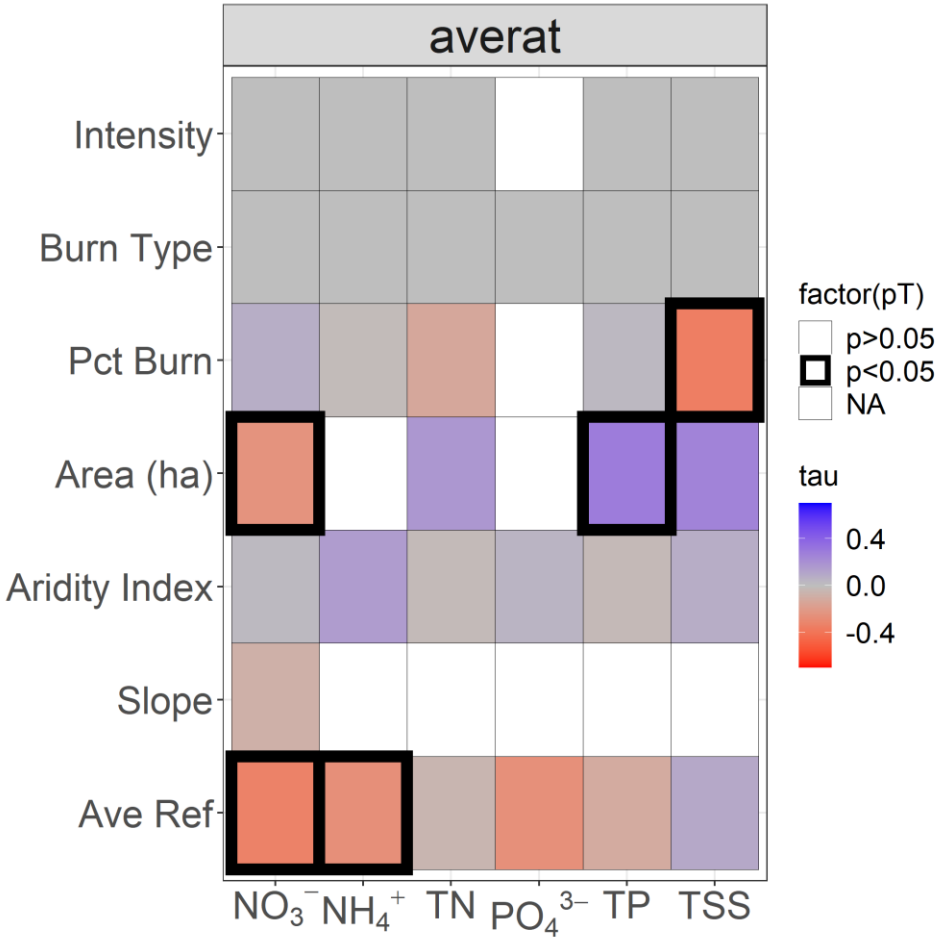

Figure B6: Grid comparing correlation of predictor and response variables (CR_M). The p value of correlation is shown as the box border if p<0.1. Intensity and Burn Type were categorical variables and correlation was tested with the Kruskal-Wallis test. No significant relationships were found with categorical variables. For continuous variables, Kendall's rank correlation tau is reported as the box color fill. Blue is positive correlation and red is negative correlation. White fill indicates insufficient data (<20 points).

B2 Supplemental Tables

Table B1: Studies (n=34) used in this Meta-Analysis

No	Study	Year	DOI	Title
1	Bayley et al.	1992	https://doi.org/10.1139/f92-068	Effects of multiple fires on nutrient yields from streams draining boreal forest and fen watersheds: nitrogen and phosphorus
2a	Bladon et al.	2008	https://doi.org/10.1139/X08-071	Wildfire impacts on nitrogen concentration and production from headwater streams in southern Alberta's Rocky Mountains
2b	Silins et al.	2009	https://doi.org/10.1016/j.catena.2009.04.001	Sediment production following severe wildfire and post-fire salvage logging in the Rocky Mountain headwaters of the Oldman River Basin, Alberta
3	Britton et al.	1991	https://doi.org/10.1007/BF00038834	Fire and the chemistry of a South African mountain stream
4	Chessman	1986	https://doi.org/10.1071/MF9860399	Impact of the 1983 wildfires on river water quality in east gippsland, victoria
5	Coombs and Melack	2013	https://doi.org/10.1002/hyp.9508	Initial impacts of a wildfire on hydrology and suspended sediment and nutrient export in California chaparral watersheds
6	Corbin	2012	https://doi.org/10.1071/WF11014	Short-term effects of a wildfire on the water quality and macroinvertebrate community of a saline stream
7	Crouch	2006	https://doi.org/10.1016/j.chemosphere.2005.05.031	Post-fire surface water quality: Comparison of fire retardant versus wildfire-related effects
8	Davis	1989	https://doi.org/10.1016/0378-1127(89)90120-5	Prescribed fire in Arizona chaparral: Effects on stream water quality
9	Earl and Blinn	2003	https://doi.org/10.1046/j.1365-2427.2003.01066.x	Effects of wildfire ash on water chemistry and biota in south-western U.S.A. streams
10	Fernandez et al.	2011	https://dialnet.unirioja.es/descarga/articulo/3735363.pdf	Effects of the sequence wildfire-clearcutting-thinning on nutrient export via streamflow in a small e. globulus watershed in galicia (NW spain)
11	Gerla and Galloway	1998	https://doi.org/10.1007/s002540050328	Water quality of two streams near Yellowstone Park, Wyoming, following the 1988 Clover-Mist wildfire
12	Gluns and Toews	1989	PDF available	Effect of a major wildfire on water quality in southeastern British Columbia
13	Hauer and Spencer	1998	https://doi.org/10.1071/WF9980183	Phosphorus and nitrogen dynamics in streams associated with wildfire: A study of immediate and longterm effects
14	Hohner et al.	2016	https://doi.org/10.1016/j.watres.2016.08.034	Drinking water treatment response following a Colorado wildfire
15	Klose et al.	2015	https://doi.org/10.1086/683431	Effects of wildfire on stream algal abundance, community structure, and nutrient limitation
16	Lotspeich et al.	1970	PDF available	Disturbances on a wooded raised bog—how windthrow, bark beetle and fire affect vegetation and soil water quality?
17	Loupe et al.	2009	https://doi.org/10.2134/jeq2007.0494	Effects of large scale forest fires on water quality in interior Alaska
18	MacKay and Robinson	1987	https://doi.org/10.1002/hyp.3360010405	Effects of mechanical harvest plus chipping and prescribed fire on Sierran Runoff water quality

19	Mast and Clow	2008	https://doi.org/10.1002/hyp.7121	Effects of wildfire and logging on streamwater chemistry and cation exports of small forested catchments in Southeastern New South Wales, Australia
20	Mast et al.	2016	https://doi.org/10.1002/hyp.10755	Effects of 2003 wildfires on stream chemistry in Glacier National Park, Montana
21	Murphy et al.	2015	https://doi.org/10.1088/1748-9326/10/8/084007	Water-quality response to a high-elevation wildfire in the Colorado Front Range
22	Neary and Currier	1982	https://doi.org/10.1093/sjaf/6.2.81	The role of precipitation type, intensity, and spatial distribution in source water quality after wildfire
23	Oliver et al.	2012	https://doi.org/10.1007/s10533-011-9657-0	Impact of wild fire and watershed restoration on water quality in South Carolina's Blue Ridge Mountains.
24	Prepas et al.	2003	https://doi.org/10.1139/s03-036	Water quality response to the Angora Fire, Lake Tahoe, California
25	Rhoades et al.	2019	https://doi.org/10.1007/s10021-018-0293-6	Impact of wildfire on discharge and phosphorus export from the Sakwatamau watershed in the Swan Hills, Alberta, during the first two years
26	Stephens et al.	2004	https://doi.org/10.1071/WF03002	Prescribed fire, soils, and stream water chemistry in a watershed in the Lake Tahoe Basin, California
27	Thomas et al.	2000	https://doi.org/10.1002/(SICI)1099-1085(20000415)14:5%3C971::AID-HYP4%3E3.0.CO;2-J	Solutes in overland flow following fire in eucalyptus and pine forests, northern Portugal
28	Tiedemann et al.	1973	https://www.fs.fed.us/pnw/pubs/journals/pnw_1973_tiedemann001.pdf	Stream chemistry following a forest fire and urea fertilization in north-central Washington
29	Townsend and Douglas	2000	https://doi.org/10.1016/S0022-1694(00)00165-7	The effect of a wildfire on stream water quality and catchment water yield in a tropical savanna excluded from fire for 10 years (Kakadu National Park, North Australia)
30	Townsend and Douglas	2004	https://doi.org/10.1016/j.watres.2004.04.009	The effect of three fire regimes on stream water quality, water yield and export coefficients in a tropical savanna (northern Australia)
31	Wilkinson et al.	2007	http://www.clw.csiro.au/publications/science/2006/sr64-06.pdf	Impacts on water quality by sediments and nutrients released during extreme bushfires: Report 3: Post-fire sediment and nutrient redistribution to downstream waterbodies,Nattai National Park, NSW
32	Williams and Melack	1997	https://doi.org/10.1023/A:1005858219050	Effects of prescribed burning and drought on the solute chemistry of mixed-conifer forest streams of the Sierra Nevada, California
33	Wright et al.	1976	https://doi.org/10.2307/1936180	The Impact of Forest Fire on the Nutrient Influxes to Small Lakes in Northeastern Minnesota
34	Writer et al.	2014	https://doi.org/10.5942/jawwa.2014.106.0055	Water treatment implications after the high Park wildfire, Colorado

Table B2: Summary of catchment characteristics showing distribution of variables, including minimum, maximum, and quartiles.

variable	0% (min)	25%	50%	75%	100% (max)
Slope (%)	0.5	8.5	20	37	70
Area (ha)	0.04	235	3580	13000	126000
Precip (cm/yr)	19	58	82	128	330
Runoff (cm/yr)	1.15E-05	9.6	24	81	116
Aridity Index	0.68	1.4	1.8	2.9	11

Table B3: Count of sites with data for CR_M, CR_{CV} (see Figure 3-4), and decile-specific data (see Figure 3-7, Figure B4).

Param	CR_M	CR_MYr1-5	CR_{CV}	Deciles
NO3	67	65	49	33
NH4	30	30	21	10
DON	14	14	1	1
TN	31	27	29	17
DOC	17	13	14	12
PO4	20	20	15	15
PP	8	8	0	0
TP	41	41	28	14
TSS	27	23	20	19
NO3:TN	27	23	0	0
PO4:TP	8	8	0	0
PP:TP	8	8	0	0
TN:TP	23	23	0	0
DOC:NO3	17	13	0	0
DOC:PO4	6	6	0	0
TP:TSS	17	17	0	0
PO4:TSS	5	5	0	0

Table B4: Mean and median values of CR_M and CR_{CV}, comparison to Rust et al. (2018). P-values are for a t-test performed on the population of log of change ratios. Missing table cells represent either insufficient data to calculate values, or not reported variables for Rust.

Param	This study							Rust et al. (2018)	
	site n	mean CR_M	median CR_M	CR_M p-value	mean CR_{CV}	median CR_{CV}	CR_{CV} p-value	mean CR_M	site n
NO3	67	2.84	2.63	0.00	1.42	1.27	0.00	1.76	39
NH4	30	1.75	1.54	0.00	1.43	1.33	0.02	1.03	46
DON	14	1.00	0.98	0.96	1.25	1.25			
TN	31	1.66	1.50	0.00	1.38	1.34	0.00	0.94	7
DOC	17	1.04	1.48	0.87	1.16	1.22	0.32	1.23	4
PO4	20	2.37	1.76	0.00	0.89	0.97	0.33	1.32	40
PP	8	2.24	2.10	0.08					
TP	41	2.31	1.85	0.00	1.14	1.11	0.13	1.06	18
TSS	27	1.63	1.54	0.11	1.16	1.22	0.22	3.45	3
NO3:TN	27	1.54	1.44	0.00					
PO4:TP	8	1.16	1.54	0.73					
PP:TP	8	0.78	0.60	0.60					
TN:TP	23	0.82	0.89	0.05					
DOC:NO3	17	0.33	0.39	0.00					
DOC:PO4	6	0.30	0.29	0.00					
TP:TSS	17	1.42	1.40	0.07					
PO4:TSS	5	0.64	1.23						

Table B5: Correlation information from Figure 3-5. Number is the number of sites. Kendall Rank correlation shows the parameter tau and p-value.

x	y	Number	P-value	Kendall Tau
NO3	NH4	26	0.24	0.17
NO3	DON	14	1.00	0.01
NO3	TN	27	0.01	0.36
NO3	DOC	17	0.13	0.28
NO3	PO4	16	0.27	0.22
NO3	PP	6	1.00	-0.07
NO3	TP	30	0.03	-0.29
NO3	TSS	23	0.40	0.13
NO3	NO3:TN	27	0.00	0.62
NO3	PO4:TP	6	1.00	0.07
NO3	PP:TP	6	1.00	-0.07
NH4	DON	4	0.75	0.33
NH4	TN	17	0.03	0.38
NH4	DOC	3	0.33	1
NH4	PO4	10	0.16	-0.38
NH4	PP	3	1.00	-0.33
NH4	TP	18	0.37	-0.16
NH4	TSS	12	1.00	0
NH4	NO3:TN	17	0.97	0.01
NH4	PO4:TP	3	0.33	1
NH4	PP:TP	3	0.33	-1
DON	TP	10	0.00	0.69
TN	DOC	13	0.00	0.69
TN	PO4	7	0.77	0.14
TN	PP	7	0.24	0.43
TN	TP	23	0.14	0.23
TN	TSS	22	0.14	0.23
TN	NO3:TN	27	0.93	-0.01
TN	PO4:TP	7	0.77	0.14
TN	PP:TP	7	0.77	-0.14
DOC	PO4	6	0.06	0.73
DOC	PP	6	0.27	0.47
DOC	TP	6	0.27	0.47
DOC	TSS	11	0.06	0.45
DOC	NO3:TN	13	0.25	-0.26

DOC	PO4:TP	6	0.14	0.6
DOC	PP:TP	6	0.14	-0.6
PO4	PP	8	0.72	0.14
PO4	TP	7	0.07	0.62
PO4	TSS	5	1.00	0.00
PO4	NO3:TN	6	1.00	-0.07
PO4	PO4:TP	8	0.01	0.79
PO4	PP:TP	8	0.01	-0.79
PP	TP	8	0.01	0.79
PP	TSS	4	0.75	0.33
PP	NO3:TN	6	1.00	-0.07
PP	PO4:TP	8	0.90	-0.07
PP	PP:TP	8	0.90	0.07
TP	TSS	17	0.60	0.10
TP	NO3:TN	19	1.00	-0.01
TP	PO4:TP	8	0.72	0.14
TP	PP:TP	8	0.72	-0.14
TSS	NO3:TN	18	0.07	-0.32
TSS	PO4:TP	4	0.33	-0.67
TSS	PP:TP	4	0.33	0.67
NO3:TN	PO4:TP	6	1.00	0.07
NO3:TN	PP:TP	6	1.00	-0.07
PO4:TP	PP:TP	8	0.00	-1.00

Appendix C

Supporting Information to Chapter 4

C1 Supplemental Table

Table C1: Number of time series datasets (from unique pairings of site, fire and year, and hydrochemical variable) between this study and other recent syntheses of water quality response to wildfire.

This study				Rust et al. 2018 Synthesis (same dataset)		Hampton et al. 2022 Meta-analysis
Subgroup	Subgroup Count	Group	Group Count	Subgroup Count	Group Count	Group Count
TN	24	TN	24	36	36	31
Org N	27	NH3 plus Org N	61	46	140	44
NH3	15			59		
NH3 plus Org N	19			35		
NO3	7	NO3 plus NO2	31	26	94	67
NO2	4			25		
NO3 plus NO2	20			43		
OP	28	OP	28	40	40	0
P	25	P	25	103	103	61
OC	13	OC	13	9	9	17

C2 Supplemental Figures

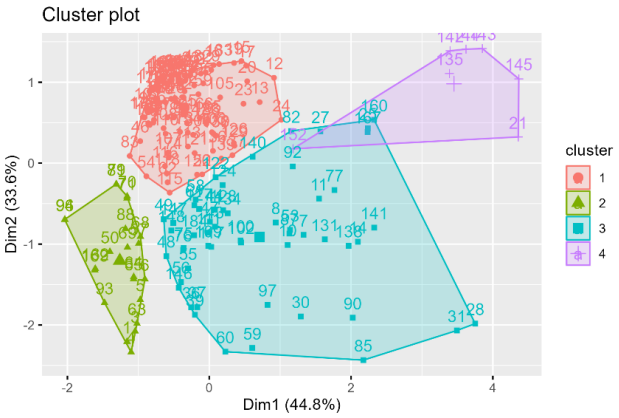

Figure C1: Output of Clustering analysis

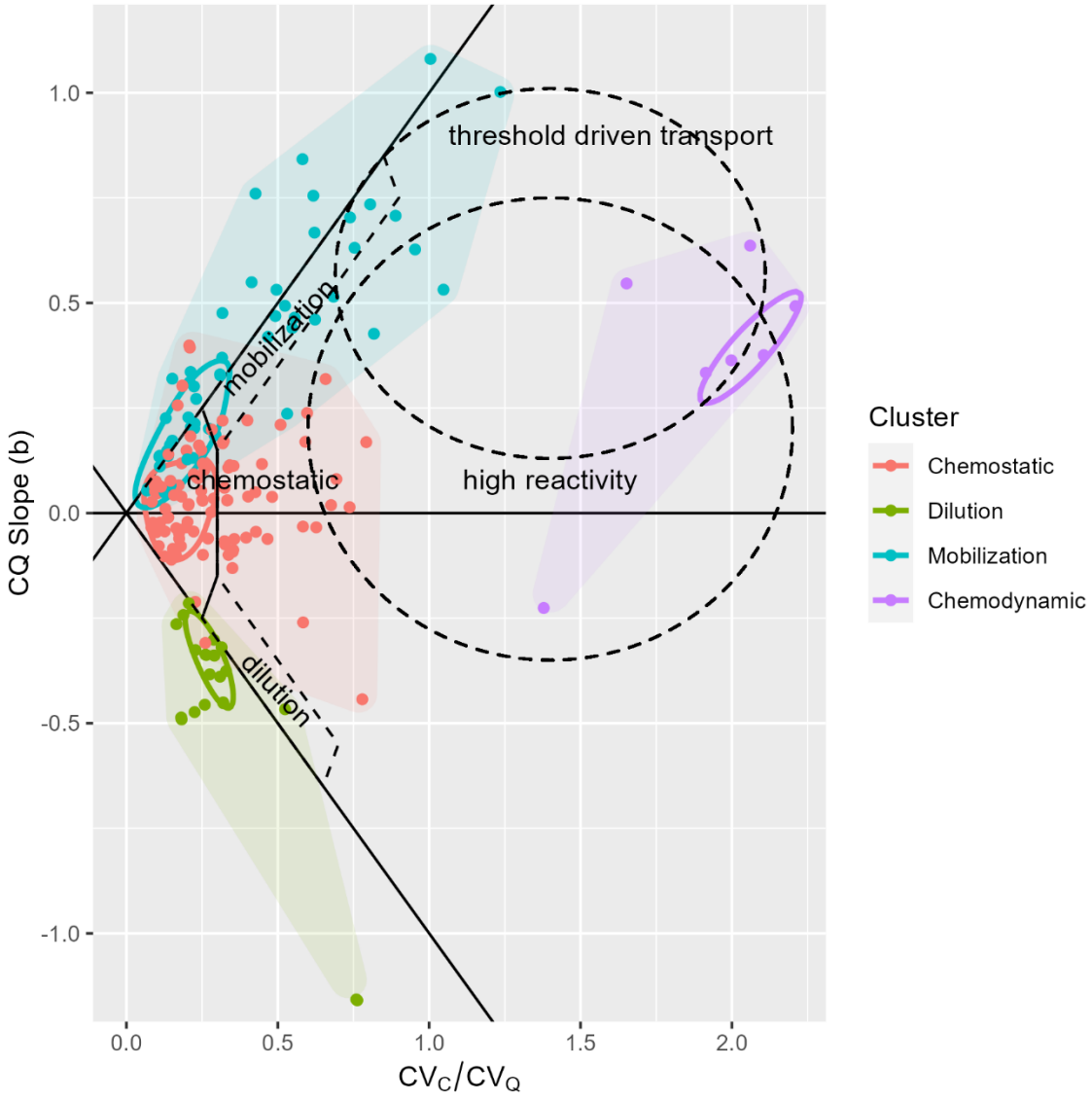

Figure C2: Following the format of Figure 3a, points from clusters are shown with dark outline (50% Kernel density) and semi-transparent colored convex hulls. Dashed black lines and labels outline CQ typologies proposed by Musolff et al. (2015; Fig. 4).

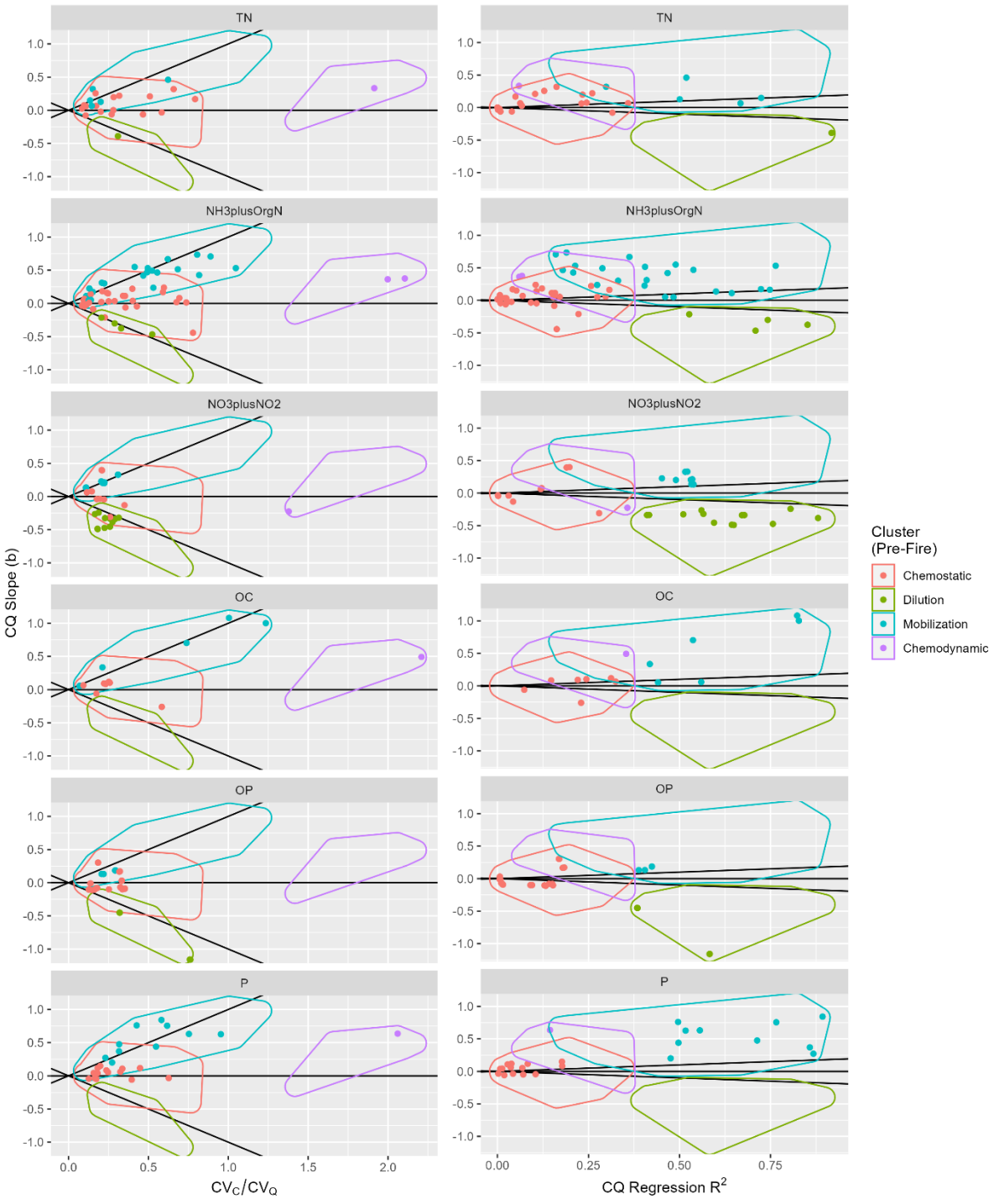

Figure C3: Following the format of Figure 3, broken out by element groupings. The convex hulls show the overall cluster domains from Figure 3, while points show behavior for each element group.

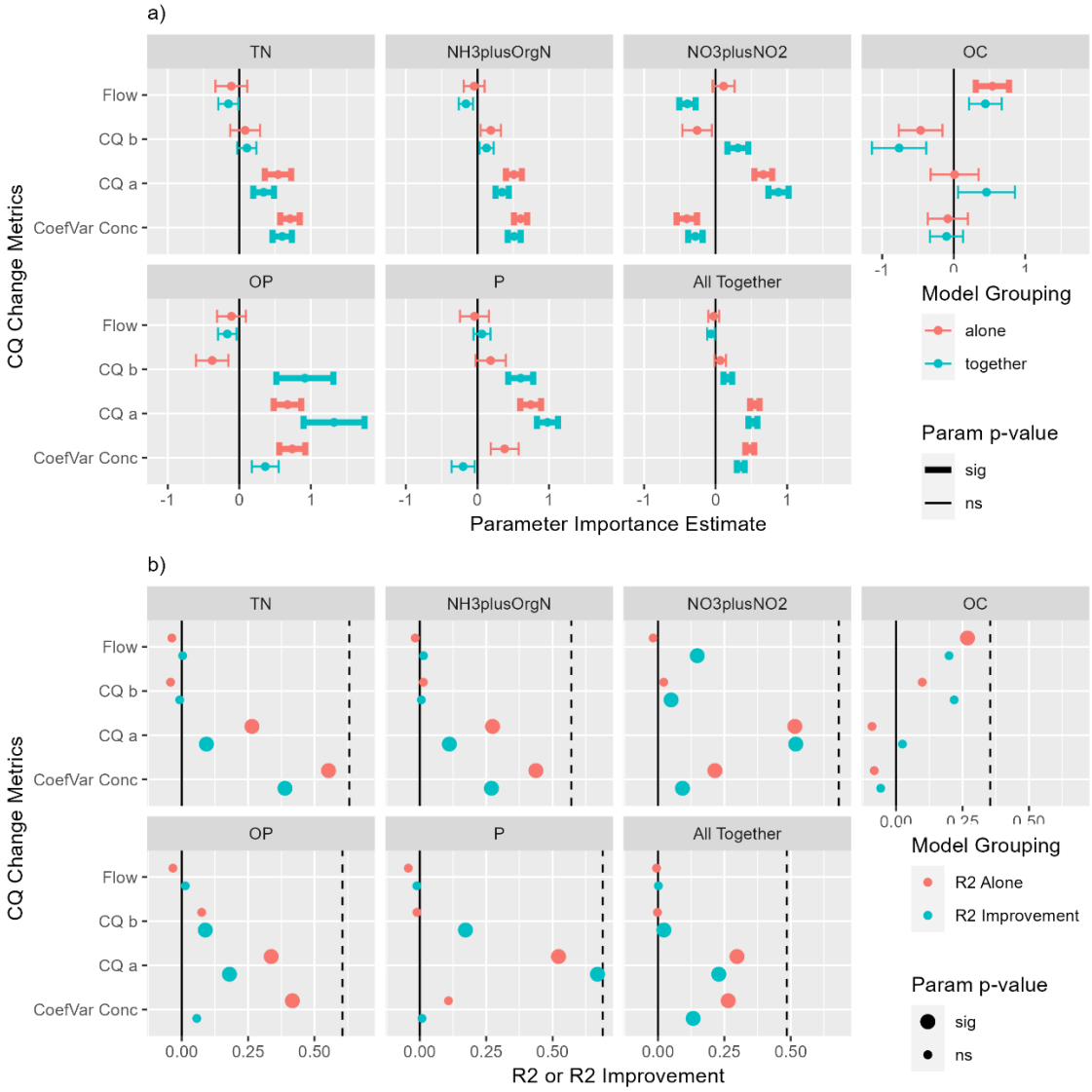

Figure C4: Standardized multiple linear regression output. The linear model sought to predict the 5-year change ratio of concentration (CR-C) after fire (5 years pre and 5 years post). For the regression, Change ratios were log transformed, and then all variables were divided by their respective standard deviations. Regression variables were changes in flow, concentration variability (as the coefficient of variation), b slope (absolute change), and intercept parameter a (absolute change). Significance was measured with an alpha of 0.05, and is shown with bold lines or points. Model "alone" (red color) was each variable independently against CR-C. Model "together" (blue color) was CR-C against all four variables. R2 improvement (blue) was measured during "leave one out" analysis as the R2

improvement after the inclusion of each variable back into the model against CR-C and the remaining 3 not “left out”.

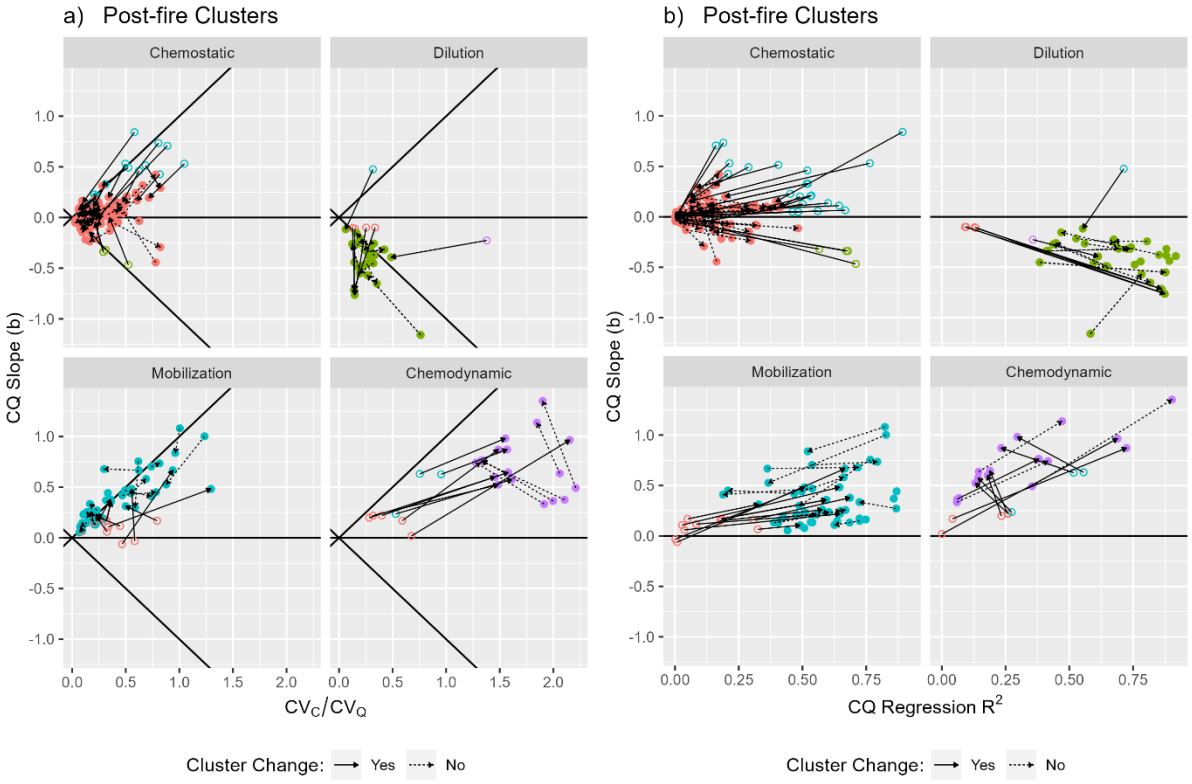

Figure C5: Following the format of Figure 3, points are plotted with coordinates from pre-fire and post-fire CQ conditions. Arrows connect pre- and post-fire points and are styled to indicate cluster change (change: solid line; no change: dashed line). Points are separated into 4 subplots (each post-fire cluster). Solid points indicate no change in cluster classification between pre- and post-fire, whereas points that did change cluster have the pre-fire point (beginning of arrow) styles as empty, with the color indicating the pre-fire cluster. For example, dashed lines will only connect like-colored points, whereas solid lines will connect one empty point to a different colored solid point.

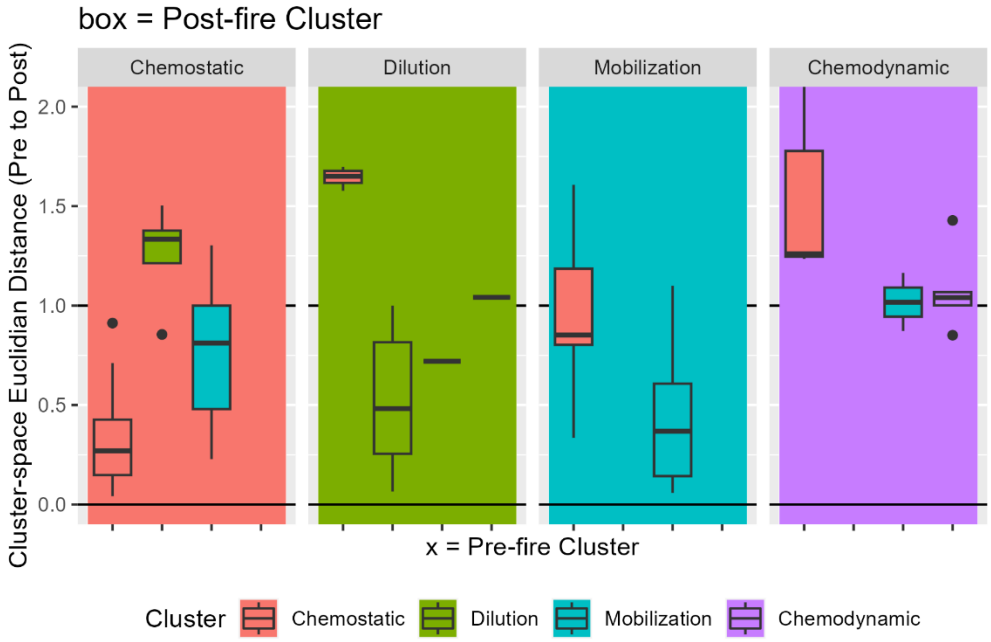

Figure C6: Euclidean distance, calculated in 3-dimensional space (coordinates of b slope, CVC/CVQ, and R2) between pre- and post-fire CQ conditions. The plot is separated into 4 panels, indicating the post-fire cluster, and each of 4 divisions on the x axis indicates the pre-fire cluster. Boxplot fill indicates pre-fire cluster, while panel fill indicates post-fire cluster. Like-colors indicate no change in cluster. Mis-matched color indicates the "to" and "from" of changing clusters.

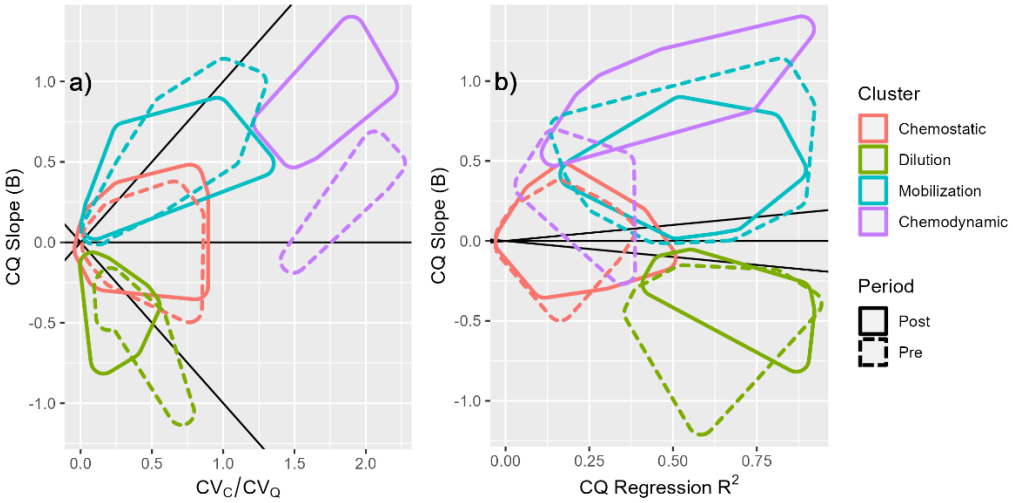

Figure C7: Convex hulls for pre- and post-fire clusters. Following the format of Figure 3, the hulls outline points from pre-fire (dashed hull) and post-fire (solid hull) CQ conditions.

Appendix D
Model Description for Chapter 5

This appendix describes the model state variables (D1.1), formulation (D2), calibration (D1.4), and initial conditions (D1.1) for the coupled model presented in Chapter 5 of this dissertation. Additional information provided includes data from literature supporting decisions in model formulation or parameterization (D3), supporting figures for the results section (D4), and a derivation of the annual steady-state behavior of the soil carbon and nitrogen cycle (D5).

For description of the coupled model, Sections D1 and D2 should be examined alongside the model description in Chapter 5.2 and Figure 5-1 and Table 5-1.

D1. Key for Variables and Parameters

D1.1. Model State Variables

Symbol	Name	Model Initial Condition	Units
S_1	Subsurface water box 1	60% * $Sb1$	mm
S_2	Subsurface water box 2	60% * $Sb2$	mm
S_n	Snow water storage	150	mm

Vegetation Pools			
C_p	Plant Carbon pool	11000	$g\ C\ m^{-2}$
C_{pl}	Plant leaf Carbon pool	0	$g\ C\ m^{-2}$
N_{stem}	Number of stems	1000	$stems\ ha^{-1}$
N_{store}	Overwinter N storage pool for leaf-out	5	$g\ N\ m^{-2}$

Soil Biogeochemistry Model Pools			
N_{Sn+}	Snow Ammonium pool	0	$g\ N\ m^{-2}$
N_{Sn-}	Snow Nitrate pool	0	$g\ N\ m^{-2}$
C_l	Litter C pool	1610	$g\ C\ m^{-2}$
N_l	Litter N pool	89.4	$g\ N\ m^{-2}$
C_h	Humus C pool	21400	$g\ C\ m^{-2}$
C_b	Biomass C pool	300	$g\ C\ m^{-2}$
$N_{m+,1}$	Mineral Ammonium Pool (Box 1)	0.05	$g\ N\ m^{-2}$
$N_{m+,2}$	Mineral Ammonium Pool (Box 2)	0.01	$g\ N\ m^{-2}$
$N_{m-,1}$	Mineral Nitrate Pool (Box 1)	0.04	$g\ N\ m^{-2}$
$N_{m-,2}$	Mineral Nitrate Pool (Box 2)	0.01	$g\ N\ m^{-2}$
C_{d1}	Dissolved organic carbon (Box 1)	0	$g\ C\ m^{-2}$
C_{d2}	Dissolved organic carbon (Box 2)	0	$g\ C\ m^{-2}$

D1.2. Model Forcing Functions

Symbol	Name	Units	Parameters	Affects
Hydrology Forcing Functions				
$sm1$	Soil moisture percentage for pool 1	-	$Sb1$	
$sm2$	Soil moisture percentage for pool 2	-	$Sb2$	
T	Daily mean temperature	$°C$		Q_n, PET
PET	Potential Evapotranspiration	$mm\ d^{-1}$		$Trans$, $Evap$
LAI	Leaf Area Index	-		$Trans$, $Evap$

Vegetation Forcing Functions				
dbh	Season-start Diameter Breast Height	cm	dbh_a, dbh_n	C_{pl-max}
N_{stemS}	Season-start Nstem	$stems\ ha^{-1}$		C_{pl-max}
SLA	Specific Leaf Area	$m^2\ g^{-1}$	$SLA_l, SLA_h,$ $SLA_m,$ ref_N, ref_M	LAI
C_{pl-max}	Maximum seasonal plant leaf C pool	$g\ C\ m^{-2}$	$leaf_a, leaf_n$	LAI, fr_{leaf}
fr_{leaf}	Fraction of growth allocated to leaves	-	$leaf_{pct}$	NPP_l, NPP_s
$N_{thin-line}$	Thinning threshold	$stems\ ha^{-1}$	$ref_N, ref_M,$ $thin_n$	$N_{close},$ N_{max}, N_{thin}
N_{close}	"Closer" stem threshold	$stems\ ha^{-1}$	$stem_c$	N_{grow}
N_{max}	"Maximum" stem threshold	$stems\ ha^{-1}$	$stem_m$	N_{grow}
λ_{age}	Stem mortality age rate	-	$mort_l, mort_h,$ $mort_m, mort_a$ ref_N, ref_M	$N_{mort-age}$
Soil Biogeochemistry Forcing Functions				
CN_l	Litter carbon to nitrogen ratio	-		φ
φ	(phi) N limited inhibition of decomposition	-	r_r, r_h, k_h, k_l CN_h, CN_b	Φ, DEC
Φ	(PHI) Absolute value of immobilization or mineralization flux	-		MIN, IMM
f_{STemp}	Temperature-dependent process function	-	x_T, k_{temp}	$DEC, MIN,$ IMM, NIT
f_{deC}	Moisture-dependent decomposition inhibition	-	s_{fc}	$DEC, MIN,$ IMM

f_{NIT}	Moisture-dependent nitrification inhibition	-	s_{fc}	NIT
f_{deN}	Moisture-dependent denitrification inhibition	-	den_i, den_{exp}	DEN
f_{UpN}	Moisture-dependent N uptake inhibition	-	$sDif, ndd, k_{Up}$	UP_{act}

D1.3. Model Fluxes

Symbol	Name	Units	Parameters
Hydrology Model Fluxes			
P	Precipitation flux	$mm\ d^{-1}$	
Pr	Precipitation flux as rain	$mm\ d^{-1}$	T_{snow}
Ps	Precipitation flux as snow	$mm\ d^{-1}$	T_{snow}
Qn	Snow melt flux	$mm\ d^{-1}$	T_{melt}, ddf
$INTr$	Precipitation interception (rain)	$mm\ d^{-1}$	α, K_{Ie}
In	Infiltration flux	$mm\ d^{-1}$	β_I
$Q1f$	Infiltration excess quickflow (pool 1)	$mm\ d^{-1}$	β_I
$Qperc$	Percolation flux (pool 1 to pool 2)	$mm\ d^{-1}$	K_{perc}, β_{b1}
$Q2u$	Water leakage from pool 2	$mm\ d^{-1}$	K_{q2u}, β_{b2}
$Q2f$	Quickflow from pool 2	$mm\ d^{-1}$	
$Trans$	Total Plant-driven transpiration	$mm\ d^{-1}$	K_{Ie}, s^*
$T1$	Plant-driven transpiration from pool 1	$mm\ d^{-1}$	$Sb1$
$T2$	Plant-driven transpiration from pool 2	$mm\ d^{-1}$	$Sb2$
$Evap$	Total soil evaporation	$mm\ d^{-1}$	$K_{Ie}, Evap_{max}$

Vegetation Fluxes			6.3.1.1
NPP	Net primary productivity (CO_2 fixation)	$g\ C\ m^{-2}d^{-1}$	g, K_{Ie}
NPP_p	NPP allocated to stem growth	$g\ C\ m^{-2}d^{-1}$	
NPP_l	NPP allocated to leaf growth	$g\ C\ m^{-2}d^{-1}$	
$sprout$	Carbohydrate transfer from stems to leaf sprouting	$g\ C\ m^{-2}d^{-1}$	$sprout_r, leaf_{pct}$
$N_{store-withd}$	Sprout withdrawal from N store	$g\ N\ m^{-2}d^{-1}$	
$N_{store-depos}$	Senescence N storage	$g\ N\ m^{-2}d^{-1}$	$fsprout_{Nstore}$
LF_p	Plant stem and root turnover	$g\ C\ m^{-2}d^{-1}$	$mort_{p-l}, mort_{p-h}, mort_{p-m}, mort_{p-a}, ref_N, ref_M$
LF_l	Plant leaf litterfall	$g\ C\ m^{-2}d^{-1}$	$turn_l$
H	Harvest flux	$g\ C\ m^{-2}d^{-1}$	
UP	Plant uptake of N	$g\ N\ m^{-2}d^{-1}$	$k_{LeN-}, k_{LeN+}, k_{UpN}, sDif, ndd, k_{Nfix}$
N_{mort}	Stem mortality	$stems\ ha^{-1}\ d^{-1}$	$mort_l, mort_h, mort_m, mort_a, ref_N, ref_M, thin_d, thin_n,$
N_{grow}	Stem reproduction	$stems\ ha^{-1}\ d^{-1}$	$stem_c, stem_m, stem_r, thin_n, ref_N, ref_M,$

Soil Biogeochemistry Model Fluxes			
$ADDC$	Litter influx	$g\ C\ m^{-2}d^{-1}$	

$ADDN$	Litter influx minus N translocation	$g\ N\ m^{-2}d^{-1}$	
DEC_l	Litter decomposition	$g\ C\ m^{-2}d^{-1}$	k_l
DEC_h	Humus decomposition	$g\ C\ m^{-2}d^{-1}$	k_h
BD	Biomass Death	$g\ C\ m^{-2}d^{-1}$	k_d
DEP	Atmospheric N deposition	$g\ N\ m^{-2}d^{-1}$	
NIT	Nitrification of NH_4^+ to NO_3^-	$g\ N\ m^{-2}d^{-1}$	k_{NIT}
IMM	N immobilization of NO_3^- to litter	$g\ N\ m^{-2}d^{-1}$	
MIN	N mineralization of litter to NO_3^-	$g\ N\ m^{-2}d^{-1}$	
LEN	Mineral N leaching from the soil pool	$g\ N\ m^{-2}d^{-1}$	k_{LeN-}, k_{LeN+}
DEN	Denitrification flux (N_2 release)	$g\ N\ m^{-2}d^{-1}$	k_{den}
$Cdissolve$	Dissolved organic C production	$g\ C\ m^{-2}d^{-1}$	k_{dc}

D1.4. Model Parameters

Justifications for model parameters or calibrated ranges are included in Chapter 5 Section 5.3.3. The "Source" column seen in the remainder of this section refers to how the bounds of calibration ranges in the "Value (Range)" column were determined, which may refer to either the upper or lower bound, or both; or if it refers to the single value of a parameter, if it was not calibrated. Table 5-2 outlines the sequences of different parameter calibration steps, which are indicated in the "Calibr." column.

D1.4.1. Hydrology Model

Symbol	Name	Value (Range)	Units	Calibr	Source
ddf	Degree-day factor	2.77 (1-4.5)	mm day^{-1} $°K^{-1}$	CalH	Ye et al. (2012)
T_{snow}	Snow transition temp	-0.34 (-1 - 1)	$°C$	CalH	"Ye"
T_{melt}	Melting transition temp	-1.14 (-1.5 - 1)	$°C$	CalH	"Ye"

$Sb1$	Soil water pool size 1	314 (50-350)	mm	CalH	Murray & Buttle (2005)
$Sb2$	Soil water pool size 2	28.2 (5-100)	mm	CalH	Estimate
s_h	Hygroscopic Point	0.2 (0.11-0.25)	-	-	Laio et al. (2001)
s^*	Plant Stress Threshold	0.45 (0.25-0.45)	-	-	"Laio"
s_{fc}	Field Capacity	0.55 (0.5-0.65)	-	-	"Laio"
α	Canopy Interception fraction	0.24 (0.05-1)	mm day^{-1}	CalH	Buttle & Farnsworth (2012)
K_{Ie}	Canopy extinction rate	0.35 (0.25-1)	-	CalH	"Buttle & Farnsworth"
β_I	Infiltration exponent	4.46 (2-5)	-	CalH	Estimate
K_{perc}	Percolation constant (pool 1 to pool 2)	41 (0-80)	mm day^{-1}	CalH	"Murray & Buttle"
β_{B1}	Percolation exponent	8.5 (7-17)	-	CalH	"Laio"
K_{q2u}	Leakage constant	5.67 (0-30)	mm day^{-1}	CalH	"Murray & Buttle"
β_{B2}	Leakage exponent	11.3 (7-17)	-	CalH	"Laio"
$Evap_{max}$	Maximum daily evap rate	1.5	mm day^{-1}	-	Porporato et al. (2003)
LAI_{max}	Maximum LAI	4.5	-	-	Han (2022), "Buttle & Farnsworth"

D1.4.2. Vegetation Model

Symbol	Name	Value	Units	Calibr	Source
CN_p	C/N ratio: Plant stems	200	-	-	Table D2
CN_{pl}	C/N ratio: Plant stems	20	-	-	Table D2
K	Plant carrying capacity	11000	$g\ C\ m^{-2}$	-	Table D2
g	Plant growth rate (transpiration factor)	0.868 (0.5-5)	$g\ N\ m^{-2}\ mm^{-1}$	CalPre	Estimate

$mort_{p-l}$	Plant turnover rate (low)	2.2×10^{-5} (1×10^{-6} - 1×10^{-4})	d^{-1}	CalPre	Estimate
$mort_{p-h}$	Plant turnover rate (high)	2.85×10^{-5} (1×10^{-5} - 1×10^{-4})	d^{-1}	CalPre	Estimate
$mort_{p-m}$	Plant turnover rate (fractional midpoint)	0.9	-	-	Estimate
$mort_{p-a}$	Plant turnover rate (alpha exponent)	-10	-	-	Estimate
$leaf_{pct}$	Threshold of seasonal maximum leaf to stop maximum growth	0.9	-	-	Estimate
$turn_l$	Leaf turnover rate (senescence)	0.15	d^{-1}	-	Estimate
$sprout_r$	Rate percent of leaf-out sprouting	0.1	d^{-1}	-	Estimate
$sprout_s$	Percent of leaf-N during senescence that is stored per timestep	0.66	-	-	Morrison (1991)
ref_N	thinning line reference Nstem	1000	$stem\ ha^{-1}$	-	Estimate
ref_M	thinning line reference Mass	124	$kg\ C\ stem^{-}$	-	Estimate
dbh_a	dbh multiplier	0.0197 (0.01-0.1)	-	CalA	Estimate
dbh_n	dbh exponent	2.10 (1-3)	-	CalA	Estimate
$leaf_a$	leaf max multiplier	0.0636 (0.01-0.08)	-	CalA	Estimate
$leaf_n$	leaf max exponent	0.346 (0.1-0.8)	-	CalA	Estimate
SLA_l	Specific Leaf Area value low	245 (150-300)	$m^2\ g^{-1}$	CalA	Estimate
SLA_h	Specific Leaf Area value high	318 (300-400)	$m^2\ g^{-1}$	CalA	Estimate
SLA_m	Specific Leaf Area value midpoint	0.5	-	CalA	Estimate
$thin_n$	thinning threshold exponent	-0.1	-	-	Estimate
$thin_d$	thinning delay throttle	0.05 (0.001-0.5)	-	CalR	Estimate

$mort_l$	Stem mortality rate low	5×10^{-5} (1×10^{-5} - 1×10^{-4})	d^{-1}	CalR	Estimate
$mort_h$	Stem mortality rate high	3×10^{-3} (1×10^{-4} - 1×10^{-3})	d^{-1}	CalR	Estimate
$mort_m$	Stem mortality rate midpoint	0.5	-	-	Estimate
$mort_a$	Stem mortality rate exponent	-3	-	-	Estimate
$stem_c$	Stem close threshold	0.9 (0.1-0.9)	-	CalR	Estimate
$stem_m$	Stem maximum threshold	1.15 (1-1.5)	-	CalR	Estimate
$stem_r$	Stem reproduction rate	3.5×10^{-4} (1×10^{-4} - 5×10^{-3})	d^{-1}	CalR	Estimate

D1.4.3. Soil Biogeochemistry Model

Symbol	Name	Value	Units	Calibr	Source
CN_b	C/N ratio: Soil biomass	10	-	-	Manzoni & Porporato (2007)
CN_h	C/N ratio: Humus	22	-	-	Table D2
k_{Nfix}	Maximum direct plant N fixation rate	1.06×10^{-1} (1×10^{-3}-1×10^{-1})	$g\ N\ m^{-2}d^{-1}$	CalPre	Estimate
r_h	Decomposition humification fraction	0.1	-	CalSS	Section 5.3.3.5
r_r	Decomposition respired fraction	0.47 (0.3-0.7)	-	CalSS	Section 5.3.3.5
x_T	Soil temperature process switch	0 (0-1)	-	CalPre	Estimate
k_{temp}	Soil temperature process correction factor	4	-	-	Estimate
k_l	Litter decomposition rate	3.75×10^{-6} (1×10^{-6}-4×10^{-6})	d^{-1}	CalPre	Estimate
k_h	Humus decomposition rate	2.8×10^{-8} (1.5×10^{-8}-1×10^{-7})	d^{-1}	CalPre	Estimate

k_d	Biomass death rate	2.35×10^{-3} (7×10^{-4}-2×10^{-3})	d^{-1}	CalPre	Estimate
k_{NIT}	Nitrification Rate	7.35×10^{-4} (1×10^{-4}-1×10^{-2})	d^{-1}	CalPre	Estimate
k_{den}	Denitrification rate	2.70×10^{-4} (1×10^{-5}-1×10^{-2})	d^{-1}	CalPre	Estimate
den_i	Denitrification inhibition moisture threshold	0.4 (0.4-1)	-	CalPre	Porporato et al. (2003)
den_{exp}	Denitrification-moisture exponent	2 (1-4)	-	CalPre	Estimate
k_{UpN}	Plant nitrate demand	0.168 (1×10^{-2}-2×10^{-1})	-	CalPre	Estimate
k_{LeN-}	Nitrate solubility coefficient	1.0	-	-	"Porporato"
k_{LeN+}	Ammonium solubility coefficient	0.05	-	-	"Porporato"
$sDif$	Scaled diffusion coefficient	0.1	-	-	Estimate
ndd	Nonlinear diffusion factor	3	-	-	"Porporato"
k_{dC}	Dissolved organic carbon production rate	1.20×10^{-3} (1×10^{-4}-1×10^{-2})	d^{-1}	CalPre	Estimate
$pulse_C$	Post-harvesting "pulse" of biologic material to the litter pool	348 (100-800)	$g\ C\ m^{-2}$	CalPost	Estimate
$pulse_{rati}$	Post-harvesting "pulse" C/N ratio	10 (10-50)	-	CalPost	Estimate

D2. Model Equations

Explanation of equation format:

- In the following equations, multiplication is indicated by two variables next to one another, without any operation sign (e.g. addition or subtraction signs). A space is added to help differentiate variables with multiple characters for a name, and to differentiate functions (e.g. *sin*, *cos*, *exp*)
- Several equations take the form of IF-ELSE. These will take the following format:
    - {} brackets surround each case of the IF statement
    - IF statement, followed by colon:
        - IF statements may use Boolean language, including *and*, *or*, less than <, or greater than >
    - Following the colon is the function value in the case that the statement is TRUE
- Common functions are used such as *sin* or *cos*, which will not be followed by parentheses unless needed. Functions like *exp*, *min*, or *max* will be followed by parentheses. Inside the *min* or *max* functions, multiple input values are separated by commas.

D2.1. Environmental Variables and Forcings

D2.1.1. Climate

Mean, minimum, and maximum monthly temperatures were used to calculate potential evapotranspiration (PET) following the Hargreaves-Samani equation (Hargreaves & Samani, 1985):

$$PET = 0.0023\ R\ \ TD^{0.5}\ \ (T + 17.8) \quad \text{(D2-1)}$$

where:

PET is daily potential evapotranspiration,

TD is the difference between maximum and minimum daily temperature (°C),

T is the mean daily temperature (°C), and

R is extraterrestrial radiation at the top of the atmosphere, a function of latitude and date of the year, converted to mm d^{-1} (calculated following Allen et al., 1998):

where

$$R = \frac{0.408}{\pi} G\ D(\omega\ sin\theta\ sin\delta\ + cos\theta\ cos\delta\ sin\omega\ ) \quad \text{(D2-2)}$$

where

G is the solar constant (118.08 MJ m^{-2} day^{-1}),

D is the inverse relative distance between the Earth and Sun,

$$D = 1 + 0.033\ cos\ \left(2\pi \frac{yday}{366}\right) \quad \text{(D2-3)}$$

where $yday$ is the year day (1 through 366)

δ is the solar decimation by day of the year,

$$\delta = 0.409\ sin\ \left(\left(2\pi \frac{yday}{366}\right) - 1.39\right) \quad \text{(D2-4)}$$

θ is the latitude in units of radians,

$$\theta = lat \frac{\pi}{180} \quad \text{(D2-5)}$$

and

$$\omega = cos^{-1}(-tan\ \theta\ tan\ \delta\ ) \quad \text{(D2-6)}$$

D2.2. Hydrology and Soil Moisture Dynamics

The hydrology model had three state variables (all with units of water in millimeters): the snow water equivalent pool (S_n) and the two vertically stacked water boxes (S_1 and S_2). Refer to Section D1.1 and D1.3 for a key for variable names. In the next section, the equations for all fluxes are described.

D2.2.1. Model Stock Differential Equations

The snow pool receives water as snow precipitation (Ps) and loses water through melting (Qn).

$$\frac{dS_n}{dt} = Ps - Qn \tag{D2-7}$$

The first water pool (S_1) receives water through infiltration ($Qinf$), and loses water through fast flow ($Q1f$), downward percolation to the second pool ($Qperc$), evaporation ($Evap$), and transpiration ($Trans_1$).

$$\frac{dS_1}{dt} = Qinf - Q1f - Qperc - Evap - Trans_1 \tag{D2-8}$$

The second water pool (S_2) receives water through percolation ($Qperc$), and loses water through fast flow ($Q2f$), base flow ($Q2u$), and transpiration ($Trans_2$).

$$\frac{dS_2}{dt} = Qperc - Q2f - Q2u - Trans_2 \tag{D2-9}$$

D2.2.2. Snow and Melting Routine

Following the parsimonious model experiments of (Ye et al., 2012), we added a simple snowfall and snow melt routine. We added one level of complexity by calibrating two rather than one transition temperatures: one for the rain-to-snow transition (T_{snow}: Precip P allocated to rain Pr or snow Ps), and one for snow melting (T_{melt}).

$$Ps = \{if\ T \leq T_{snow}: P\ \}\{\ if\ T > T_{snow}: 0\ \} \tag{D2-10}$$

$$Pr = \{if\ T \leq T_{snow}: 0\ \}\{\ if\ T > T_{snow}: P\ \} \tag{D2-11}$$

Daily snow melt (Q_n) was calculated as a function of the degree day factor (ddf) and the positive temperature heating (H_{pos}), the difference between the daily temperature (T) and the transition temperature.

$$Qn = min\{ H_{pos}\, ddf, S_n \} \quad \text{(D2-12)}$$

where

$$H_{pos} = \{if\ T > T_{melt}\colon\ T - T_{melt}\}\{if\ T < T_{melt}\colon\ 0\} \quad \text{(D2-13)}$$

D2.2.3. Interception Routine

Interception of the rainfall ($INTr$) by the tree canopy was calculated following the HYDRUS formulation (Šimůnek et al., 2005, 2013), as used by (Sutanto et al., 2012), as a function of the daily leaf area index (LAI), and two parameters: α and K_{Ie}.

$$INTr = \alpha\ LAI\ \left(1 - \frac{1}{1+\frac{b\ Pr}{\alpha\ LAI}}\right) \quad \text{(D2-14)}$$

where

$$b\ =\ 1 - e^{(-K_{Ie}\ LAI)} \quad \text{(D2-15)}$$

We assumed that interception of snowfall was negligible, due to low LAI in the cold seasons. The parameter b represents the soil cover fraction (SCF), and varies between values of 0 and 1 as a function of the LAI and the extinction coefficient.

D2.2.4. Subsurface Flow Equations

The water that could potentially infiltrate ($pQinf$) was estimated as the sum of the snowmelt (Qn) and the difference between rainfall (Pr) and interception $INTr$.

$$pQinf = Q_n + (Pr - INTr) \quad \text{(D2-16)}$$

Actual infiltration (Qinf) was rate-limited by an exponential factor (β_I), following formulations used by the HBV model (Bergström, 1995). The infiltrated volume is the least of the two infiltration rates, driven by saturation excess (limited by the available space in pool 1, with maximum capacity $Sb1$) or infiltration excess processes (decreasing with increasing fractional soil moisture $sm1$).

$$\text{Qi}nf = min\big(max(Sb1 - S1{,}0)\ , pQinf(1 - sm1^{\beta_I})\big) \quad \text{(D2-17)}$$

where

$sm1$ is the saturation fraction of Pool 1: $sm1 = S1/Sb1$

Infiltration-excess runoff ($Q1f$) is then calculated as the difference between available water and rate-limited infiltration.

$$Q1f = pQinf - Qinf \quad \text{(D2-18)}$$

Percolation ($Qperc$) moves water "downward" from pool 1 to pool 2, and follows the formulation by Porporato et al. (2003). Percolation occurs if $sm1$ exceeds field capacity (s_{fc}). Increasing from field capacity, percolation increases exponentially (shape determined by β_{b1}) to a maximum value of the saturated hydraulic conductivity (K_{perc}) at full saturation ($sm1 = 1$).

$$Qperc = \{if\ sm1 < s_{fc}: 0\ \}$$
$$\{if\ sm1 > s_{fc}: K_{perc}\left(e^{\beta_{b1}(sm1-s_{fc})} - 1\right)\left(e^{\beta_{b1}(1-s_{fc})} - 1\right)^{-1}\ \} \quad \text{(D2-19)}$$

Base flow ($Q2u$) leaves pool 2, as a non-linear process.

$$Q2u = \{if\ sm2 < s_{fc}: 0\ \}$$
$$\{if\ sm2 > s_{fc}: K_{q2u}\left(e^{\beta_{b2}(sm2-s_{fc})} - 1\right)\left(e^{\beta_{b2}(1-s_{fc})} - 1\right)^{-1}\ \} \quad \text{(D2-20)}$$

In the case that box 2 was full (maximum capacity $Sb2$), fast flow also occurred from pool 2. In the case that box 2 was full and $Qperc$ was greater than 0, the total volume of $Qperc$ is diverted to fast flow.

$$Q2f = \{if\ sm2 < 1: 0\ \}$$
$$\{if\ sm2 > 1: \frac{S2-Sb2}{dt} + Qperc\ \} \quad \text{(D2-21)}$$

where

$sm2$ is the saturation fraction of Pool 2: $sm2 = S2/Sb2$

D2.2.5. Evapotranspiration

The final hydrologic process is evapotranspiration. Evapotranspiration was modeled as two components: evaporation and transpiration, generally following the implementation by (Porporato et al., 2003). Following Sutanto et al. (2012), Beer's law was used to partition PET to potential plant transpiration (PET_{Trans}) or potential soil evaporation (PET_{Evap}), according to the canopy cover fraction (b). When canopy cover is higher, the majority of PET is allocated to the leaf surface. This allows for interannual and seasonal variation in allocation.

$$PET_{Trans} = b\ PET \quad \text{(D2-22)}$$
$$PET_{Evap} = (1 - b)\ PET \quad \text{(D2-23)}$$

where

$$b = 1 - e^{(-K_{Ie}\, LAI)} \quad \text{(D2-24)}$$

Transpiration was withdrawn from both pools ($y = 1{,}2$) as a function of evaporate-able soil moisture ($sm1$ and $sm2$ as sm_y) above the hygroscopic point (s_h) according to the fraction $PET_{f,y}$:

$$PET_{f,y} = \{if\ sm, y < s_h : 0\}\{if\ sm, y > s_h : \frac{Sy - Sby\, s_h}{(S1 - Sb1\, s_h)(S2 - Sb2\, s_h)}\} \quad \text{(D2-25)}$$

Transpiration was highest above the plant stress point (s^*), and zero below the hygroscopic point (s_h). For the two pools, transpiration was allocated as follows:

$$\begin{aligned} Trans_y = {} & \{if\ sm_y < s_h : 0\} \\ & \{if\ sm_y > s^* : PET_{Trans}\, PET_{f,y}\} \\ & \{if\ sm_y < s^* : PET_{Trans}\, min(PET_{fy}, \frac{sm_y - s_h}{s^* - s_h}\} \end{aligned} \quad \text{(D2-26)}$$

Evaporation was withdrawn only from the first box.

$$Evap = \{if\ sm1 < s_h : 0\}\{if\ sm1 > s_h : PET_{Evap}\} \quad \text{(D2-27)}$$

D2.3. Vegetation Model.

The vegetation model captured carbon and nitrogen dynamics of biomass, as well as associated allometric equations. Plants have two components—stems (C_p) and leaves (C_{pl})—which are modelled only as carbon, because they have constant C/N ratios. The number of stems (N_{stem}) is a state variable that drives several allometric equations. The only nitrogen explicitly modeled in the plant system is overwinter N storage ($N_{pl-store}$).

D2.3.1. Model Stock Differential Equations

Stem carbon (C_p) grows at the rate of stem-allocated net primary productivity (NPP_p), and experiences litter fall turnover at a rate of LF_p. Leaf sprouting allocation of carbon ($sprout$) is withdrawn from the stems. During harvest, the harvest removal rate is withdrawn (H).

$$\frac{dC_p}{dt} = NPP_p - sprout - LF_p - H \quad \text{(D2-28)}$$

Leaf carbon (C_l) grows at the rate of leaf-allocated net primary productivity (NPP_l) plus sprouting ($sprout$), and experiences litter fall turnover at a rate of LF_l.

$$\frac{dC_{pl}}{dt} = NPP_l + sprout - LF_l \quad \text{(D2-29)}$$

The over-winter nitrogen store ($N_{pl-store}$) has deposit ($N_{store-deposit}$) and withdrawal ($N_{store-withdrawal}$) fluxes, and also receives excess passive nitrogen uptake ($N_{store-deposit}$).

$$\frac{dN_{pl-store}}{dt} = N_{store-deposit} + UP_{pas,excess} - N_{store-withdrawal} \quad \text{(D2-30)}$$

The number of stems state variable (N_{stem}) has growth (N_{grow}) and mortality (N_{mort}) fluxes.

$$\frac{dN_{stem}}{dt} = N_{grow} - N_{mort} \quad \text{(D2-31)}$$

D2.3.2. Net Primary Productivity, N uptake, and Growth Allocation

Daily net primary productivity (NPP) was modeled with daily "potential" NPP (NPP_{max}) a single growth multiplier (g) to the Transpiration flux.

$$NPP_{max} = g\ Trans \quad \text{(D2-32)}$$

The actual daily NPP will then be allocated to leaves (NPP_l) and stem (NPP_s), according to the growth stage, and any nutrient limitation. NPP allocation is largely governed by a preference to allocate growth to leaf biomass during the leaf-out period, until the leaf biomass approaches the fraction of the seasonal maximum leaf biomass ($leaf_p$).

The timestep growth fraction (fr_{leaf}) allocated to leaves is calculated as:

$$\begin{aligned} fr_{leaf} = \{&if\ NPP = 0\ or\ yday \geq sd[1]: 0\} \\ &\{if\ NPP > 0\ and\ yday < sd[1]\ \&\ \ldots \\ &\ldots C_{pl} < C_{pl-max}\ leaf_{pct}: 1\} \\ &\ldots C_{pl} \geq C_{pl-max}\ leaf_{pct}: \frac{C_{pl-max} - C_{pl}}{C_{pl} - C_{pl-max}\ leaf_{pct}}\} \end{aligned} \quad \text{(D2-33)}$$

where

sd is a vector of length two, corresponding to the long term average senescence period beginning- and ending-dates (in Julian days)

where

C_{pl-max} is the seasonal maximum leaf carbon store

The C_{pl-max} is calculated with an allometric equation based on the season-start number of stems (N_{stemS}) and season-start stand average diameter at breast height (dbh, See Appendix D2.3.4.):

$$C_{pl-max} = N_{stemS}\ leaf_a\ dbh^{leaf_n} \quad \text{(D2-34)}$$

Non-structural carbohydrate reserves are used to initiate leaf out, with a constant fractional growth rate ($sprout_r$) .

$$\begin{aligned} sprout_{max} = \{&if\ yday < gd[1] or\ yday > gd[2]\ or\ \dots \\ &\dots\ C_{pl} \geq C_{pl-max}\ leaf_{pct}: 0\} \\ &\{if\ yday \geq gd[1] and\ yday \leq gd[2]\ and\ \dots \\ &\dots\ C_{pl} < C_{pl-max}\ leaf_{pct}: \left(C_{pl-max} - C_{pl}\right) sprout_r\ \} \end{aligned} \quad \text{(D2-35)}$$

where

gd is a vector of length two, corresponding to the long term average leaf out period beginning- and ending-dates (in Julian days)

Before calculating the potential uptake of nitrogen, the demand for nitrogen from the two processes (NPP and $sprout$) are calculated.

The carbon to nitrogen ratios (C/N) or plant stems and leaves have very different values. As such, timestep N demand (NPP_N_{demand}) will depend on where C is allocated.

$$C/N_{demand} = fr_{leaf}\ C/N_{leaf} + (1 - fr_{leaf})\ C/N_{stem} \quad \text{(D2-36)}$$

$$NPP\_N_{demand} = \frac{NPP_{max}}{C/N_{demand}} \quad \text{(D2-37)}$$

The sprouting routine contributes solely to leaf growth, but at the expense of stem carbon. A storage pool (N_{store}) was incorporated into the model, to account for overwinter N storage solely for leaf growth. During the leaf-out period, the allocation of plant stem tissue to leaves comes with a small amount of "free" nitrogen, according to the C/N ratio of stem tissue. The remaining N required to produce the more N-rich foliage must come from the winter storage pool (N_{store}), and from the soil.

$$sprout\_N_{free} = \frac{sprout_{max}}{C/N_{stem}} \quad \text{(D2-38)}$$

The timestep inputs and outputs from the N storage pool are $N_{store-withdrawal}$ and $N_{store-deposit}$.

$$N_{store-withdrawal} = min\left(\frac{sprout_{max}}{C/N_{leaf}} - sprout\_N_{free}\ , N_{store}\ \right) \quad \text{(D2-39)}$$

$$sprout\_N_{demand} = max\left(\frac{sprout_{max}}{C/N_{leaf}} - N_{store-withdrawal} - sprout\_N_{free}\ , 0\ \right) \quad \text{(D2-40)}$$

Nutrition stress is incorporated following the methods of Parolari and Porporato (2016). In the paragraph above, maximum N demand was calculated, and next it will be throttled down if necessary to account for nitrogen limitation.

$$UP_{Nmax} = NPP\_N_{demand} + sprout\_N_{demand} \quad \text{(D2-41)}$$

Passive uptake is calculated for each N specie (ammonium, +; or nitrate, –), and each pool (y 1 or 2) as proportional to the solubility coefficient ($k_{LeN\pm}$), the N pool size ($N_{m\pm,y}$), and the fraction of transpiration from pool y ($Trans_y$) relative to the pool size (Sy).

$$UP_{pas,\pm,y} = k_{LeN\pm} N_{m\pm,y} \frac{Trans_y}{Sy} \quad \text{(D2-42)}$$

$$UP_{pas\sum} = \sum_{y=1}^{2} \sum_{+}^{-} UP_{pas,\pm,y} \quad \text{(D2-43)}$$

Excess passive uptake contributes to N storage in plant tissues, although it is not expected that this is a large contributor to the N budget during the growing season.

$$UP_{pas,excess} = \{if\ UP_{pas\sum} > UP_{Nmax}: UP_{Nmax} - UP_{pas\sum}\} \quad \text{(D2-44)}$$

Active N uptake is also related to soil moisture. Following the methods of Porporato et al. (2003), the moisture dependency of active uptake for pool y ($f_{UpN,y}$) decreases with the total moisture, due to dilution of the existing N within the soil pool, but increases relative to the fractional moisture due to nonlinear poor connectivity (ndd, nonlinear dependence of the diffusion process on soil moisture).

$$f_{UpN,y} = k_{UpN}\, sDif \left(\frac{sm,y^{ndd}}{Sy}\right) \quad \text{(D2-45)}$$

$$UP_{act,\pm,y} = \{if\ UP_{Nmax} > UP_{pas}: min\big((UP_{Nmax} - UP_{pas}) , f_{UpN,y}\ k_{LeN\pm} N_{m\pm,y}\big)\}$$
$$\{if\ UP_{Nmax} < UP_{pas}: 0\} \quad \text{(D2-46)}$$

A nitrogen fixation component was added to the model to allow a small amount of supplemental N directly for uptake.

$$UP_{fix} = \{if\ UP_{Nmax} > \big(UP_{pas} + UP_{act}\big): min\big((UP_{Nmax} - UP_{pas} - UP_{act}) , k_{Nfix}\big)\}$$
$$\{if\ UP_{Nmax} = \big(UP_{pas} + UP_{act}\big): 0\} \quad \text{(D2-47)}$$

Total potential nitrogen uptake is summed:

$$UP_N = UP_{pas} + UP_{act} + UP_{fix} \quad \text{(D2-48)}$$

Priority in N uptake is given to leaf sprouting. Recall that N demand for leaf sprouting can be met first with the small "free" stem re-allocation ($sprout\_N_{free}$), followed by storage withdrawal ($N_{store-withdrawal}$), and then by soil uptake ($sprout\_N_{UP}$).

$$sprout\_N_{UP} = min(sprout\_N_{demand}, UP_N) \quad \text{(D2-49)}$$

$$sprout\_N = sprout\_N_{free} + N_{store-withdrawal} + sprout\_N_{UP} \quad \text{(D2-50)}$$

Timestep sprout carbon allocation ($sprout$) is calculated based on available N ($sprout\_N$).

$$sprout = sprout\_N \; C/N_{leaf} \quad \text{(D2-51)}$$

The remaining portion of UP_N is allocated to NPP:

$$NPP\_N = UP_N - sprout\_N \quad \text{(D2-52)}$$

Finally, NPP is throttled by the term ch to account for nitrogen availability:

$$ch = \{if\ UP_{Nmax} = 0\text{: } 0\}$$
$$\{if\ UP_{Nmax} > 0\text{: } \frac{NPP\_N}{NPP\_N_{demand}}\} \quad \text{(D2-53)}$$

$$NPP = NPP_{max}\ ch \quad \text{(D2-54)}$$

NPP (N corrected) is then allocated to leaf and stem growth:

$$NPP_l = NPP\ fr_{leaf} \quad \text{(D2-55)}$$

$$NPP_s = NPP\left(1 - fr_{leaf}\right) \quad \text{(D2-56)}$$

D2.3.3. Plant Turnover

As part of the integration of the 3PG model, Plant biomass was modeled as two living pools: stem and leaves. Each pool also experienced turnover.

Leaf turnover (LF_l) was assumed to occur during the senescence period (See Section 5.2.2).

$$LF_l = \{if\ yday \geq sd[1]\text{: } turn_l\ C_{pl}\ \}\{if\ yday < sd[1]\text{: } 0\ \} \quad \text{(D2-57)}$$

$$N_{store-deposit} = \left(\frac{LF_l}{C/N_{pl}}\right) fsprout_{Nstore} \quad \text{(D2-58)}$$

In this model, the stem pool was assumed to also represent roots. Stem turnover (LF_p) was modeled as a function of the forest age, or the total stem biomass C_p relative to the carrying capacity.

$$LF_p = mort_{p-l} + \left(mort_{p-h} - mort_{p-l}\right) exp\left(-ln2 * \left(\frac{C_p}{ref_N\ ref_M}\frac{1}{mort_{p-m}}\right)^{mort_{p-a}}\right) \quad \text{(D2-59)}$$

The harvesting of trees also resulted in a loss of stem biomass, and was characterized as the flux H.

D2.3.4. Allometric Equations

The diameter at breast height (dbh) is calculated from the tree biomass per stem and two calibrated parameters:

$$dbh = \left(\frac{C_p}{N_{stem}} * \frac{1}{dbh_a}\right)^{\left(\frac{1}{dbh_n}\right)} \quad \text{(D2-60)}$$

Specific Leaf Area (SLA, units $m^2\ g^{-1}$) represents leaf area per leaf mass, which varies with total forest biomass. The SLA function ranges from low to high values (SLA_l and SLA_h, respectively) for high and low values (respectively) of C_p, relative to the reference values.

$$SLA = SLA_l + (SLA_h - SLA_l)\ exp\left(-ln2 * \left(\frac{C_p}{ref_N\ ref_M}\frac{1}{SLA_m}\right)^2\right) \quad \text{(D2-61)}$$

where ref_N is the reference number of stems from the pre-disturbance forest, and ref_M is the reference mass per stem density ($10^4 * g\ stem^{-1}$)

The Leaf Area Index (LAI) is a function of SLA and timestep leaf biomass.

$$LAI = SLA\ C_{pl}\ 0.0001 \quad \text{(D2-62)}$$

The Basal Area is a simple geometric function of N_{stem} and mean dbh.

$$Basal\ Area = N_{stem}\ \pi\ \left(0.01\ \frac{dbh}{2}\right)^2 \quad \text{(D2-63)}$$

D2.3.5. Stem Modelling

The number of stems state variable is modeled through time as a balance between growth and mortality. Mortality occurs via density-induced self-thinning and age-induced mortality. Growth occurs in two stages: (1) maximum growth, where N_{stem} is smaller than a "canopy closer" threshold (N_{close}; (W. J. Wang et al., 2013), and (2), where N_{stem} is greater than N_{close} and less than a maximum density threshold (N_{max}). Both of these two density thresholds change over time as a function of the self thinning threshold ($N_{thin-line}$). The thinning threshold is calibrated to a "reference" stem (ref_N) and mass (ref_M) density (as in Appendix D2.3.4.).

$$N_{thin-line} = ref_N\ \left(\frac{C_p}{N_{stem}}\frac{1}{ref_M}\right)^{thin_n} \quad \text{(D2-64)}$$

where

$thin_n$ is the thinning threshold exponent

The thresholds N_{close} and N_{max} were calculated as fractions ($stem_c$ and $stem_m$, respectively) of $N_{thin-line}$.

$$N_{close} = N_{thin-line}\ stem_c \tag{D2-65}$$

$$N_{max} = N_{thin-line}\ stem_m \tag{D2-66}$$

Stem growth is then calculated with a fractional reproduction rate ($stem_r$) of the current number of stems (N_{stem}):

$$N_{grow} = \{if\ N_{stem} < N_{close}: N_{stem}\ stem_r\ \} \\ \left\{if\ N_{stem} \geq N_{close}: N_{stem}\ stem_r\ \left(\frac{N_{max}-N_{stem}}{N_{max}-N_{close}}\right)\right\} \tag{D2-67}$$

Self-thinning occurred when N_{stem} exceeded $N_{thin-line}$, and was throttled by a delay coefficient ($thin_d$):

$$N_{mort-thin} = \{if\ N_{stem} \leq N_{thin-line}: 0\} \\ \{if\ N_{stem} > N_{thin-line}: (N_{stem} - N_{thin-line})\ thin_d\ \} \tag{D2-68}$$

Age-induced mortality occurred when forest biomass exceeded a threshold of stem biomass (calculated as ref_N times ref_M). The mortality rate was calculated as the function λ_{age}:

$$\lambda_{age} = mort_l + (mort_h - mort_l)\ exp\left(-ln2 * \left(\frac{C_p}{ref_N\ ref_M}\frac{1}{mort_m}\right)^{mort_a}\right) \tag{D2-69}$$

where

$mort_l$ and $mort_h$ are the low and high mortality rates, respectively,

$mort_m$ is the function midpoint of 0.5, and

$mort_a$ is the function exponent

The mortality rate function has a value close to $mort_l$ when C_p is small, and a value approaching $mort_h$ as C_p approaches the reference threshold.

$$N_{mort-age} = N_{stem}\ \lambda_{age} \tag{D2-70}$$

Harvesting also resulted in a decrease in number of stems, and was characterized as a model flux: $N_{mort-harv}$.

$$N_{mort} = N_{mort-thin} + N_{mort-age} + N_{mort-harv} \tag{D2-71}$$

D2.4. Soil Biogeochemistry Model

The soil biogeochemical model had three components: organic soil pools, mineral nitrogen pools, and dissolved carbon. Organic carbon and nitrogen in the soil was represented in the soil litter (with carbon C_l and nitrogen N_l pools), the soil humus (C_h), and the soil biomass (C_b). Mineral nitrogen (as ammonium $+$ and nitrate $-$) was represented in the snowpack (NSn_+ and NSn_-) and both soil water pools ($N_{m+,1}$ and $N_{m-,1}$ for pool 1, and $N_{m+,2}$ and $N_{m-,2}$ for pool 2). Dissolved organic carbon was represented in both soil water pools (C_{d1} and C_{d2}).

D2.4.1. Model Stock Differential Equations

The litter carbon pool (C_l) has additions of litter fall turnover and harvesting residue ($ADDC$) and soil biomass death (BD), and decomposition of litter (DEC_l) moves mass out of the pool.

$$\frac{dC_l}{dt} = ADDC + BD - DEC_l \quad \text{(D2-72)}$$

The litter nitrogen pool (N_l) has the same fluxes as for carbon, but accounting for different carbon to nitrogen ratios (for example, for soil biomass C/N_b or the litter pool itself C/N_l).

$$\frac{dN_l}{dt} = ADDN + \left(\frac{BD}{C/N_b}\right) - \left(\frac{DEC_l}{C/N_l}\right) \quad \text{(D2-73)}$$

The humus carbon pool (C_h) receives mass from litter decomposition (DEC_l), and humus decomposition (DEC_h) moves mass out of the pool.

$$\frac{dC_h}{dt} = r_h\, DEC_l - DEC_h \quad \text{(D2-74)}$$

The soil biomass carbon pool (C_b) receives mass from both litter and humus decomposition (DEC_l and DEC_h), and soil biomass death (BD) returns mass back to the litter pool.

$$\frac{dC_b}{dt} = (1 - r_r - r_h)\, DEC_l + (1 - r_r)\, DEC_h\ - BD \quad \text{(D2-75)}$$

The snow pool stores ammonium (NSn_+) and nitrate (NSn_-), and receives mass through snow N deposition ($DEPS_{n,+}$ and $DEPS_{n,-}$) and loses mass through snowmelt loss ($NQ_{n,+}$ and $NQ_{n,-}$).

$$\frac{dNSn_+}{dt} = DEPS_{n,+} - NQ_{n,+} \quad \text{(D2-76)}$$

$$\frac{dNSn_-}{dt} = DEPS_{n,-} - NQ_{n,-} \quad \text{(D2-77)}$$

Likewise, the mineral nitrogen pool stores ammonium and nitrogen in pools 1 and 2 ($N_{m+,1}$ and $N_{m+,2}$; $N_{m-,1}$ and $N_{m-,2}$). N is added to the soil pool 1 through deposition as dry deposition (DEP_{d+}

and $DEP_{d\_}$) or via the hydrologic infiltration pathway ($NQinf_{+}$ and $NQinf\_$). Hydrologic transport redistributes N from pool 1 to pool 2 through percolation ($Nperc_{+}$ and $Nperc\_$), and from pool 2 to baseflow ($Nq2u_{+}$ and $Nq2u\_$). Plant uptake removes N from both pools through both passive and active pathways (e.g. $UP_{pas,+,1}$ and $UP_{act,+,1}$). Nitrification (NIT) transforms ammonium to nitrate in pool 1, and immobilization (IMM_{+} and $IMM\_$) transfers mineral N to organic N to supplement N-poor conditions of decomposition. Inversely, mineralization (MIN_{+}) transforms excess organic N during N-rich conditions of decomposition into ammonium. Finally, denitrification serves as a sink of nitrate from both pools ($DEN1$ and $DEN2$)

$$\frac{dN_{m+,1}}{dt} = DEP_{d+} + NQinf_{+} - Nperc_{+} - UP_{pas,+,1} - UP_{act,+,1} - NIT + MIN_{+} - IMM_{+} \quad \text{(D2-78)}$$

$$\frac{dN_{m-,1}}{dt} = DEP_{d-} + NQinf_{-} - Nperc_{-} - UP_{pas,-,1} - UP_{act,-,1} + NIT - IMM_{-} - DEN1 \quad \text{(D2-79)}$$

$$\frac{dN_{m+,2}}{dt} = Nperc_{+} - Nq2u_{+} - UP_{pas,+,2} - UP_{act,+,2} \quad \text{(D2-80)}$$

$$\frac{dN_{m-,2}}{dt} = Nperc_{-} - Nq2u_{-} - UP_{pas,-,2} - UP_{act,-,2} - DEN2 \quad \text{(D2-81)}$$

Dissolved organic carbon is stored in pools 1 and 2 (C_{d1} and C_{d2}, respectively), and experiences only production ($Cdissolve$) and transport ($Cperc$ and $Cq2u$).

$$\frac{dC_{d1}}{dt} = Cdissolve - Cperc \quad \text{(D2-82)}$$

$$\frac{dC_{d2}}{dt} = Cperc - Cq2u \quad \text{(D2-83)}$$

D2.4.2. Nitrogen Deposition

If there was snow, then deposition ($DEPS_{n,\pm}$) was allocated entirely to the snowpack N pool (NS_n). If there was no snow, then deposition was fell as dry ($DEP_{d,\pm}$) or wet ($DEP_{w,\pm}$) deposition depending on if there was precipitation. Dry deposition was added directly to the soil.

For each day with snowmelt, N flux from the snowpack ($NQ_{n,\pm}$) was calculated:

$$NQ_{n,\pm} = \{if\ S_n = 0{:}\ 0\}\left\{if\ S_n > 0{:}\ NS_{n,\pm}\frac{Q_n}{S_n}\right\} \quad \text{(D2-84)}$$

On any day with snowmelt or precipitation, any nitrogen in the snowmelt or wet deposition pathways was allocated to infiltration and quickflow:

$$NQf_{\pm} = \{if\ Qf = 0: 0\}\left\{if\ Qf > 0: (NQ_{n,\pm} + DEP_{w,\pm})\frac{Qf}{Qinf+Qf}\right\} \quad \text{(D2-85)}$$

$$NQinf_{\pm} = \{if\ Qinf = 0: 0\}\left\{if\ Qf > 0: (NQ_{n,\pm} + DEP_{w,\pm})\frac{Qinf}{Qinf+Qf}\right\} \quad \text{(D2-86)}$$

D2.4.3. Decomposition Model

Fluxes from plant turnover (leaves and stem) are added to the litter pool

$$ADDC = LF_l + LF_p \quad \text{(D2-87)}$$

$$ADDN = \left(\frac{LF_l}{C/N_{pl}}\right)(1 - fsprout_{Nstore}) + \left(\frac{LF_p}{C/N_p}\right) \quad \text{(D2-88)}$$

Biomass death is also added to the litter pool.

$$BD = k_d\ C_b \quad \text{(D2-89)}$$

The term φ (phi) was developed by Porporato et al. (2003) and determines whether decomposition requires mineralization or immobilization to deal with excess or deficit N (respectively).

Functionally, φ_{bottom} calculates the moisture-normalized and biomass-normalized net-nitrogen from decomposition. If φ_{bottom} is negative, then mineralization will occur, and if φ_{bottom} is positive, then immobilization will occur.

$$\varphi_{bottom} = k_h\ C_h\left(\frac{1}{CN_h} - \frac{1-r_r}{CN_b}\right) + k_l\ C_l\left(\frac{1}{CN_l} - \frac{r_h}{CN_h} - \frac{1-r_h-r_r}{CN_b}\right) \quad \text{(D2-90)}$$

$$\varphi_{top} = -N_{m\Sigma} \quad \text{(D2-91)}$$

where

$$N_{m\Sigma} = \sum_{+}^{-} N_{m,\pm,y=1} \quad \text{(D2-92)}$$

$$\varphi = \{if\ \varphi_{bottom} \geq 0: 1\}\{if\ \varphi_{bottom} < 0\ \&\ \varphi_{bottom} < |\varphi_{top}|: 1\}$$
$$\left\{if\ \varphi_{bottom} < 0\ \&\ \varphi_{bottom} > |\varphi_{top}|: \frac{\varphi_{top}}{\varphi_{bottom}}\right\} \quad \text{(D2-93)}$$

After assessing nitrogen limitation of decomposition, a forcing function for moisture regulation (f_{deC}) was calculated as in Porporato et al. (2003).

$$f_{deC} = \left\{if\ sm > s_{fc}: \frac{s_{fc}}{sm}\right\}\left\{if\ sm \leq s_{fc}: \frac{sm}{s_{fc}}\right\} \quad \text{(D2-94)}$$

Following the influence of soil temperature on decomposition in RHYSSys (Tague & Band, 2004), a forcing function to temperature regulation (f_{STemp}) was calculated:

$$f_{STemp} = (1 - x_T) + x_T\ k_{temp}\ exp\left[308.56\left(\frac{1}{71.02} - \frac{1}{Tsoil-227.13}\right)\right] \quad \text{(D2-95)}$$

where

exp is the exponential function,

x_T is a "switch" parameter calibrated between zero and one to regulate the effect of temperature on decomposition,

k_{temp} is a correction factor added to the RHYSSys equation to make the temperature-driven equation ($x_T = 1$) compatible with the isothermal equation ($x_T = 0$), and

$Tsoil$ is in degrees Kelvin (°K) and is a buffered time series of air temperature (°K) where for each time $[t+1]$ it is correlated to Tsoil at time $[t]$:

$$Tsoil[t+1] = 0.9\,Tsoil[t] + (1-0.9)(Tair[t+1] + 273.15) \quad \text{(D2-96)}$$

Decomposition of litter (DEC_l) and humus (DEC_h) are re-calculated, accounting for moisture, temperature, biomass, and N limitation:

$$DEC_l = \varphi\, f_{deC}\, f_{STemp}\, k_l\, C_l \quad \text{(D2-97)}$$

$$DEC_h = \varphi\, f_{deC}\, f_{STemp}\, k_h\, C_h \quad \text{(D2-98)}$$

As described earlier, the nitrogen accounting must be completed to account for immobilization or mineralization conditions. The same governing functions applied to decomposition regulate immobilization and mineralization. The function Φ (PHI) has the same sign as φ_{bottom} and directs the value of immobilization (IMM) and mineralization (MIN).

$$\Phi = \varphi\ f_{deC}\, f_{STemp}\, \varphi_{bottom} \quad \text{(D2-99)}$$

$$MIN = \{if\ \Phi > 0: \Phi\}\{if\ \Phi \le 0: 0\} \quad \text{(D2-100)}$$

Importantly, Mineralization will equal the excess N produced in decomposition, minus soil biotic uptake:

$$MIN = DEC_h\ \left(\frac{1}{CN_h} - \frac{1-r_r}{CN_b}\right) + DEC_l\ \left(\frac{1}{CN_l} - \frac{r_h}{CN_h} - \frac{1-r_h-r_r}{CN_b}\right) \quad \text{(D2-101)}$$

Immobilization will occur if there is an N deficit from decomposition.

$$IMM_{max} =\ f_{deC}\, f_{STemp}\, C_b\, N_m \quad \text{(D2-102)}$$

$$IMM = \{if\ \Phi < 0: min(-\Phi, IMM_{max})\}\{if\ \Phi \ge 0: 0\} \quad \text{(D2-103)}$$

The inflow to the soil biomass pool regulates much of the decomposition. As seen in Equation D2-89, the soil humification and respiration fractions in the φ equation determines the carbon and nitrogen flow to biomass, and ensures that biomass receives the appropriate C/N ratio.

D2.4.4. Nitrification and Denitrification

Nitrification and denitrification was calculated according to Porporato et al. (2003). Nitrification moisture inhibition was the same as decomposition below field capacity, but reduced to zero as moisture approached 100%.

$$f_{NIT} = \left\{if\ sm > s_{fc}: \frac{1-sm}{1-s_{fc}}\right\}\left\{if\ sm \leq s_{fc}: \frac{sm}{s_{fc}}\right\} \quad \text{(D2-104)}$$

The nitrification rate (NIT) was also governed by a rate constant (k_{NIT}), and the amount of soil biomass (C_b).

$$NIT = f_{NIT}\ f_{STemp}\ k_{NIT}\ N_{m,+,1}\ C_b \quad \text{(D2-105)}$$

The denitrification forcing function (f_{deN}) inhibited denitrification (DEN) below a threshold soil moisture (den_i), after which denitrification increased exponentially (with a variable exponent rate: den_{exp}).

$$f_{deN,y} = \{if\ sm_y \leq d_i: 0\}\left\{if\ sm_y > den_i: \left(\frac{sm,y-den_i}{1-den_i}\right)^{den.exp}\right\} \quad \text{(D2-106)}$$

The denitrification rate (DEN) was also governed by a rate constant (k_{den}).

$$DEN_y = f_{deN,y}\ f_{STemp}\ k_{den}\ N_{m,-,y} \quad \text{(D2-107)}$$

D2.4.5. Dissolved Organic C Production

The DOC production rate ($Cdissolve$) was governed by a rate constant (k_{dc}).

$$Cdissolve = k_{dc}\ C_l \quad \text{(D2-108)}$$

D2.4.6. Subsurface N and C Leaching

Subsurface leaching was assumed to be proportional to the pool size of N or C (X) times the fraction of soil water leaching for each time step times the solubility term (k_{LeX}).

$$Xperc_{\pm} = k_{LeX}\ X\ \frac{Qperc}{S1} \quad \text{(D2-109)}$$

$$Xq2u_{\pm} = k_{LeX}\ X\ \frac{Q2u+Q2f}{S2} \quad \text{(D2-110)}$$

D3. Site Measurements and Data from Turkey Lakes

Table D2: Carbon and Nitrogen stores and ratios from Turkey Lakes Forest. Pool description references my model (see Table 5-5), with description from authors in parentheses. Measurements are from Morrison et al. ("Mo92", 1992), Morrison et al. ("Mo93", 1993), or Mitchell et al. ("Mi92", 1992). Measurement methods also reference (Foster et al., 1992; Morrison, 1990, 1991).

Pool Description	Carbon ($g\ C\ m^{-2}$)	Source	Nitrogen ($g\ C\ m^{-2}$)	Source	C/N Ratio
Plant Leaf Biomass (Foliage)	180	Mo93	9.4	Mo92	19
Plant Stem Biomass (Woody: branches, stem, bark, roots, alive and dead)	10980	Mo93	42	Mi92	260
Vegetation (sum)	11760	Mi92	58.1	Mi92	200
Litter Pool (Forest Floor)	1610	Mo93	88.8	Mo92	18
Humus Pool (Mineral Soil)	21430	Mo93	971	Mi92	22

Table D3: Carbon and Nitrogen fluxes from Turkey Lakes Forest. Measurements as in Table D2. *Litter fall carbon measurement from (Morrison, 1991).

Pool Description	Carbon ($g\ C\ m^{-2}\ y^{-1}$)	Nitrogen ($g\ C\ m^{-2}\ y^{-1}$)	C/N Ratio
Atmospheric Deposition		0.68	
Leaf Litter Fall	186.5*	2.86	65.2
Net Fixation/Uptake	558	3.22	173
Leaching from Upper Soil		1.86	

Table D4: Forest measurements from TLW pre- and post-harvest. Catchment c32 is a control (unharvested catchment), and catchment c31 was clear-cut harvested in the fall of 1997 (beginning of water-year 1998). Data directly from Buttle et al. (2018) include number of stems, basal area, and volume. Diameter at Breast Height (DBH) is calculated from Buttle's data using Equation D2-56. Stem biomass is calculated assuming a constant ratio of carbon per wood volume, and using reference values from Table D2. Leaf area index (LAI) is from Han (2022).

Measurement:	Number of Stems (stems/ha)		DBH (cm)		Wood Volume (m3/ha)		Stem Biomass (10^3 g C/m2)		Leaf Area Index (LAI) (m2/m2)	
Source:	Buttle		Calculated from Buttle		Buttle		Calculated from Buttle		Han (2022)	
Catchment (right): Year (down):	c32	c32	c32	c31	c32	c31	c32	c31	c32	c31
Pre-harvest 1997	1060	905	17.6	20	206	237	9.6	11	4.5	4.5
Post-harvest 1997	NA	200	NA	20	206	53	9.6	2.5	4.5	0.83
2003	1000	265	19.1	18.2	233	55	10.8	2.5	4.5	3.23
2008	1035	615	19.3	13.7	249	67	11.5	3.1	4.5	4.17
2013	1005	1085	19.3	10.6	238	60	11	2.8	4.5	4.5

Table D5: Forest measurements from two forest stands of *Acer saccharum* (sugar maple) within TLW. Measurements taken in 1980 and 1982. Retrieved from Table 1 from (Morrison, 1990). Note: Means ± standard deviation of measurements are from trees ≥ 5cm DBH, plus smaller vegetation in the case of total phytomass. Units are in parentheses.

Site (right): Measurement (down):	Norberg Creek, TLW	Wishart Lake, TLW
Number of Stems (stems/ha)	682 ± 200	787 ± 233
Mean DBH (cm)	19.5 ± 3.6	16.8 ± 2.9
Basal area (m2/ha)	28.6 ± 0.7	24.7 ± 1.4
Total volume (m3/ha)	238.2 ± 9.6	199.4 ± 14.7
Total phytomass (tons/ha)	245.3 ± 5.2	210.3 ± 17.2

Table D6: Nitrogen deposition from TLW. Data from 1981 to 1997 are from (Sirois et al., 2001). *Asterisks next to years 1998 to 2011 represent interpolated data (detailed in Appendix D2.1).

Year	Precipitation (mm yr^{-1})	N wet deposition (g m^{-2} yr^{-1})	N dry deposition (g m^{-2} yr^{-1})	N total deposition (g m^{-2} yr^{-1})	Percent wet N dep. (%)
1981	1183.9	0.48	0.26	0.74	65
1982	1336.7	0.47	0.21	0.68	69
1983	1113.2	0.38	0.20	0.58	65
1984	1217.3	0.49	0.20	0.69	71
1985	1296.5	0.55	0.16	0.70	78
1986	1271.0	0.39	0.16	0.56	71
1987	1066.4	0.36	0.20	0.57	64
1988	1543.2	0.63	0.22	0.85	75
1989	1176.6	0.49	0.27	0.76	64
1990	1247.9	0.54	0.26	0.81	67
1991	1374.4	0.50	0.26	0.76	65
1992	1290.5	0.46	0.27	0.73	63
1993	1407.1	0.48	0.21	0.69	70
1994	1058.2	0.42	0.31	0.73	58
1995	1323.0	0.51	0.24	0.75	68
1996	1307.1	0.44	0.27	0.71	62
1997	908.0	0.36	0.28	0.64	57
1998*	1088.0	0.41	0.24	0.65	63
1999*	1180.3	0.44	0.24	0.68	65
2000*	1103.5	0.41	0.24	0.66	63
2001*	1233.0	0.46	0.24	0.70	66
2002*	1288.1	0.48	0.23	0.72	68

2003*	1168.9	0.44	0.24	0.68	65
2004*	1225.2	0.46	0.24	0.70	66
2005*	930.1	0.35	0.25	0.59	59
2006*	1005.6	0.38	0.25	0.62	61
2007*	1158.3	0.44	0.24	0.68	64
2008*	1178.3	0.44	0.24	0.68	65
2009*	1116.2	0.42	0.24	0.66	63
2010*	1023.9	0.38	0.25	0.63	61
2011*	1163.1	0.44	0.24	0.68	64

D4. Supporting Figures

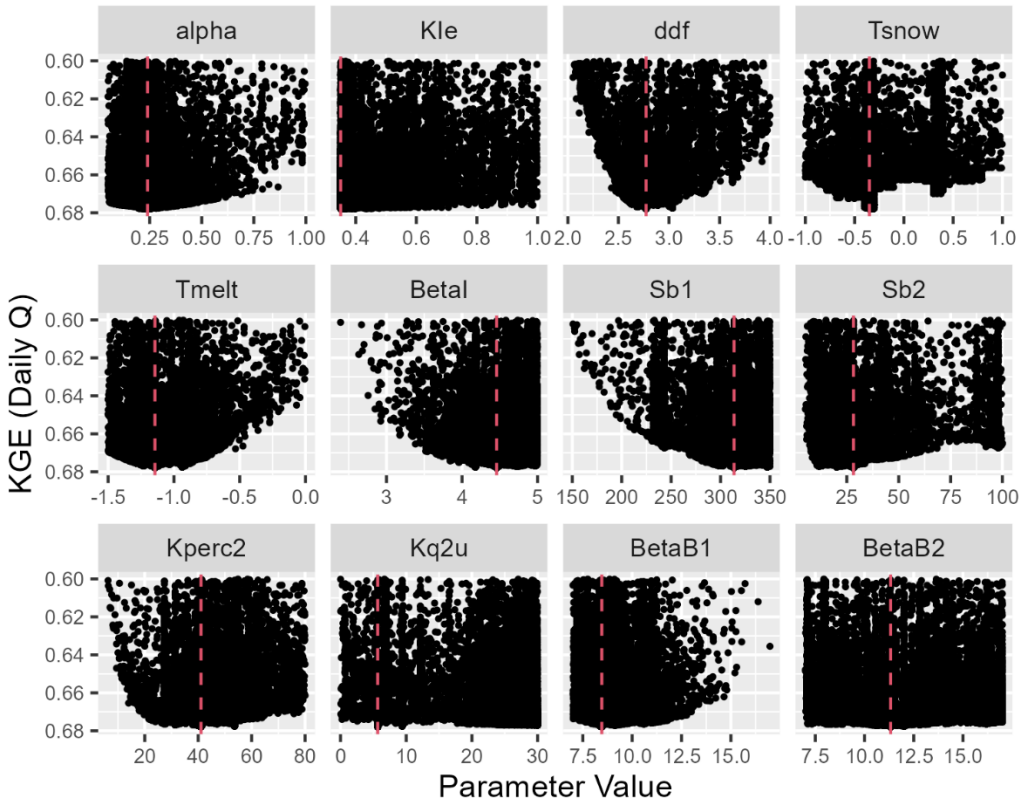

Figure D1: Parameter influence on model fit for the hydrology model (without vegetation). Y axis (reversed) is daily discharge Kling Gupta Efficiencies (KGE) for a 13 year model-run (1982-1994). Ostrich was run in parallel (10 cores) for 2,000 runs, producing 20,000 parameter sets. The data in the figure is subsetted to KGE>0.6, with 96% of sets shown on this graph. Dashed vertical red lines show parameter values for the best KGE set.

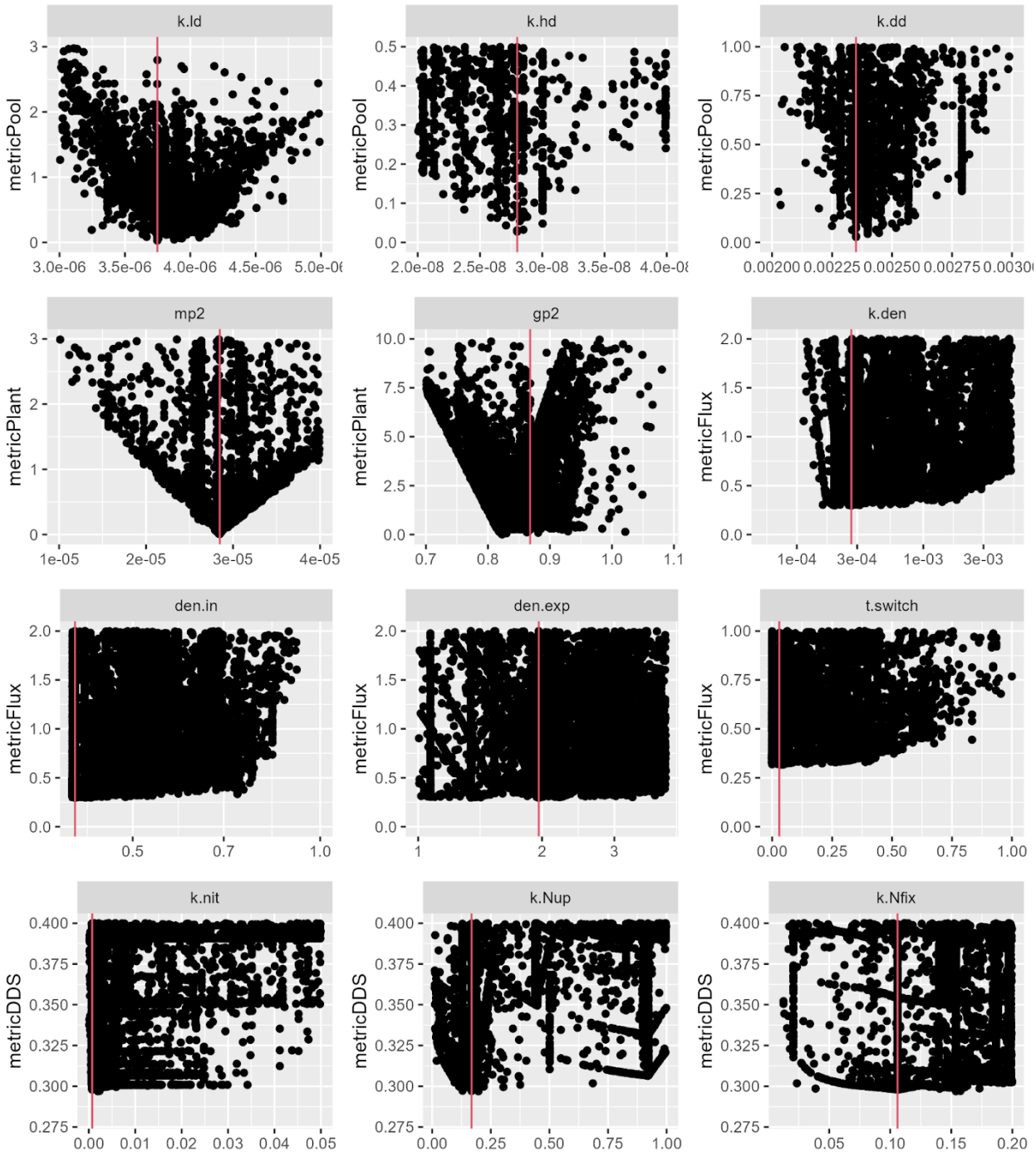

Figure D2: Parameter influence on model fit for the coupled model. The model run was for catchment c32 for 60 years (climate data 1981–2011 30 years duplicated). Ostrich had a budget of 2,000 runs. Y axis is the calibration metric: a combination of metrics for pool stability and nitrogen export. Note log axis on Y axis. The data in the figure is subsetted to <1, with 92% of sets shown on this graph. Dashed vertical red lines show parameter values for the best set.

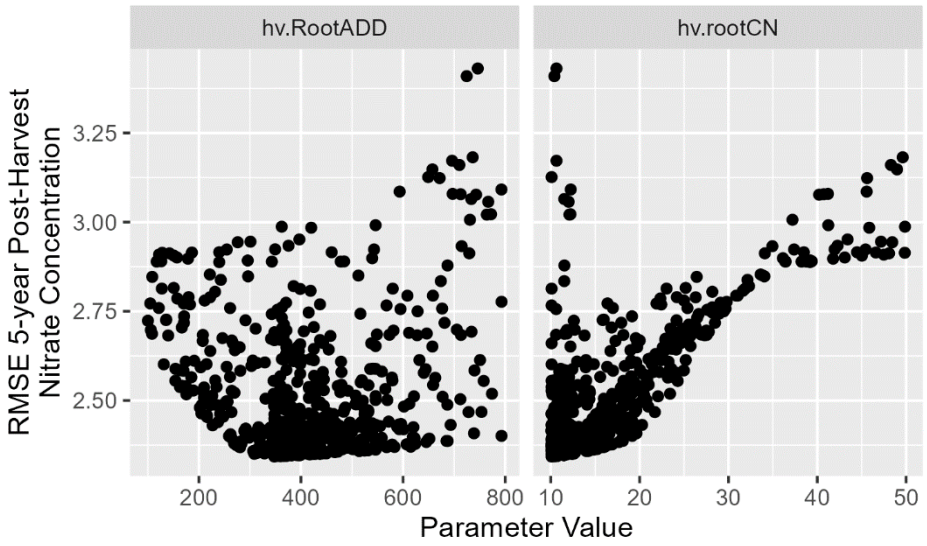

Figure D3: Calibration of RMSE of nitrate concentration. Calibration in first 5 post-harvest years (1998-2002) for two parameters: "Pulse" addition to the litter pool at time of harvest: left is the pulse size in g C m^{-2}, right is the pulse C/N ratio.

D5. Steady State Equations

D5.1. Model C/N Litter Steady State

The steady state equation for the C/N ratio of the litter pool can be calculated as the ratio of C to N outputs from the pool ($DECl$ and $DENl$, respectively). Refer to Figure 5-1, Table 5-5, and Appendix D3.

$$CN_l = DECl\ DENl^{-1} \tag{D5-1}$$

Under the steady state assumption, the pool inputs should equal the outputs. Thus, $DECl$ should equal the litter pool inputs, which include turnover of the plant stem (LFp) and leaf (LFl) and death of soil biomass (BD).

$$DECl = (LFp\ +\ LFl\ +\ BD) \tag{D5-2}$$

The biomass turnover is highly dependent on the litter pool turnover. Refer to the pool differential equations in Appendix D2.3.7.

$$BD = DECl(1 - rr - rh) + DECh(1 - rr) \tag{D5-3}$$

where

$DECl$ and $DECh$ are the turnover fluxes of the litter and humus pools

rh is the humification ratio and rr is the respired carbon ratio

The humus pool turnover is itself entirely dependent on the litter pool turnover and the humification ratio, and can be substituted as:

$$DECh = DECl \times rh \tag{D5-4}$$

Thus:

$$BD = DECl(1 - rr - rh) + DECl \times rh(1 - rr)$$

$$BD = DECl\big((1 - rr - rh) + rh(1 - rr)\big) \tag{D5-5}$$

We will define a term ϵ such that:

$$\epsilon = rh(1 - rr) + (1 - rr - rh) \tag{5-3}$$

Thus:

$$BD = DECl(\epsilon) \tag{D5-6}$$

We can substitute Equation D5-6 into Equation D5-2:

$$DECl = LFp + LFl + DECl(\epsilon)$$

Factoring by $DECl$:

$$DECl - DECl(\epsilon) = LFp + LFl$$
$$DECl(1 - \epsilon) = LFp + LFl$$
$$DECl = (LFp + LFl)(1 - \epsilon)^{-1} \quad \text{(D5-7)}$$

Referring back Equation D5-1, $DENl$ needs to be calculated. The corresponding N flux for each input to the litter pool can be converted by the pool C/N ratio, except for the leaf pool, where a fraction of nitrogen is retained by the tree during leaf-fall for the next year's leaf-out.

$$DENl = \frac{LFp}{CN_p} + \frac{LFl}{CN_{pl}}(1 - Nstore) + \frac{BD}{CN_b} \quad \text{(D5-8)}$$

$CNp, CNpl, CNb$ are the the plant stem, leaf, and soil biomass C/N ratios

$Nstore$ is the fraction of reintegrated leaf nitrogen during leaf-fall

Following Parolari & Porporato (2016), the difference between litter fall N ratios of stem to leaf can be corrected by the factor fN:

$$fN = CNp \times CNpl^{-1} \times (1 - Nstore) \quad \text{(5-2)}$$

Substituting Equation 5-2 into Equation D5-8 and factoring by CNp:

$$DENl = \frac{LFp}{CN_p} + \frac{fN \times LFl}{CN_p} + \frac{BD}{CN_b}$$
$$DENl = \frac{LFp + fN \times LFl}{CNp} + \frac{BD}{CN_b} \quad \text{(D5-9)}$$

Substituting Equation D5-6 for BD into Equation D5-9:

$$DENl = \frac{LFp + fN \times LFl}{CNp} + \frac{DECl(\epsilon)}{CN_b} \quad \text{(D5-10)}$$

Substituting Equation D5-7 for $DECl$ into Equation D5-10:

$$DENl = \frac{LFp + fN \times LFl}{CNp} + \frac{(LFp + LFl)(1-\epsilon)^{-1}(\epsilon)}{CN_b} \quad \text{(D5-11)}$$

Referring back to Equation D5-1, and substituting in Equations D5-7 and D5-11:

$$CN_l = DECl \ DENl^{-1} \quad \text{(D5-1)}$$

The generalized solution for CN_l is seen in Equation 5-1:

$$CN_l = \frac{LFp + LFl}{1-\epsilon} \times \left[\frac{LFp + fN \times LFl}{CNp} + \frac{LFp + LFl}{CNb}\left(\frac{\epsilon}{1-\epsilon}\right)\right]^{-1} \quad \text{(5-1)}$$

D5.2. Proof of Equivalency to Parolari & Porporato (2016)

The steady state equation from Parolari & Porporato (2016) is as follows:

$$CN_l = \left[\frac{mp(1-e)(1+rh)}{mp+a*fv}\left(\frac{fN\,mp+fv}{CN_p} - \frac{(1-a)fv}{CN_{hv}}\right) + \frac{e-(1-e)rh}{CN_b}\right]^{-1} \quad \text{(D5-12)}$$

where

mp is the annual plant turnover fraction

e is the microbial C use efficiency, equivalent to $(1 - rr)$

fv is the constant fraction of standing biomass removed per unit time

a is the residual fraction of harvested biomass returned to the litter pool

Under my model's steady state, no harvesting takes place: both a and fv are set equal to zero. Parolari's equation can be simplified to:

$$CN_l = \left[\frac{mp(1-e)(1+rh)}{mp}\left(\frac{fN\,mp}{CN_p}\right) + \frac{e-(1-e)rh}{CN_b}\right]^{-1} \quad \text{(D5-13)}$$

Further, if it is assumed that all biomass added to the litter is from the leaf pool, which experiences 100% turnover (mp=1) on an annual basis, then the equation simplifies to:

$$CN_l = \left[(1-e)(1+rh)\left(\frac{fN}{CN_p}\right) + \frac{e(1-e)rh}{CN_b}\right]^{-1} \quad \text{(D5-14)}$$

Substituting $e = (1 - rr)$, $rr = (1 - e)$,

$$CN_l = \left[rr(1+rh)\left(\frac{fN}{CN_p}\right) + \frac{(1-rr)-(rr)rh}{CN_b}\right]^{-1} \quad \text{(D5-15)}$$

Equation 5-3, $\epsilon = rh(1 - rr) + (1 - rr - rh)$, can be factored to equal: $\epsilon = 1 - (rr(1 + rh))$ or $\epsilon = 1 - rr - rr(rh)$.

Substituting in ϵ, Equation D5-15 simplifies to:

$$CN_l = \left[(1-\epsilon)\left(\frac{fN}{CN_p}\right) + \frac{\epsilon}{CN_b}\right]^{-1} \quad \text{(D5-16)}$$

Now, starting with my Steady State Equation 5-1, I mirror Parolari and Porporato's model, in that all litter contributions are assumed to come from leaf turnover and soil biomass death. By setting LFp=0, Equation 5-1 simplifies to

$$CN_l = \frac{LFl}{1-\epsilon} \times \left[\frac{fN \times LFl}{CNp} + \frac{LFl}{CNb}\left(\frac{\epsilon}{1-\epsilon}\right)\right]^{-1} \quad \text{(D5-17)}$$

The term LFl can be factored:

$$CN_l = \frac{LFl}{1-\epsilon} \times \left[LFl \left(\frac{fN}{CNp} + \frac{1}{CNb} \left(\frac{\epsilon}{1-\epsilon} \right) \right) \right]^{-1} \quad \text{(D5-18)}$$

The term LFl then cancels, and $(1-\epsilon)$ can be factored into the denominator:

$$CN_l = \left[(1-\epsilon) \left(\frac{fN}{CN_p} + \frac{1}{CN_b} \left(\frac{\epsilon}{1-\epsilon} \right) \right) \right]^{-1}$$

or

$$CN_l = \left[(1-\epsilon) \left(\frac{fN}{CN_p} \right) + \frac{\epsilon}{CN_b} \right]^{-1} \quad \text{(D5-19)}$$

The simplified version of my Equation 5-1 is Equation D5-19, which is equivalent to Parolari & Porporato's simplified Equation D5-16. The two equations are equivalent when no stem turnover or harvest occurs, and for complete turnover of the leaf pool each year.